UNIVERSITÄT ZU LÜBECK

From the Institute of Nutritional Medicine
of the University of Lübeck
Director: Prof. Dr. Christian Sina

"Paneth cells and azathioprine in Crohn's disease: revisiting an old drug"

Dissertation
for Fulfillment of
Requirements
for the Doctoral Degree
of the University of Lübeck

from the Department of Natural Sciences

Submitted by
Mohab Ragab
From Alexandria

Lübeck 2023

First referee: Prof. Dr. Stefanie Derer-Petersen

Second referee: Prof. Dr. Peter König

Date of oral examination: 23.06.2023

Approved for printing. Lübeck, 2023

Experiments were either performed by the author or by the technical assistants Maren Hicken, Heidi Schlichting from the Institute of Nutritional Medicine, University Hospital Schleswig-Holstein, Campus Lubeck, Germany and Daniel Margis during his internship at the Institute of Nutritional Medicine under the author's guidance unless otherwise stated.

Table of Contents

List of Figures

List of Tables

Abbreviations

1H-NMR: Proton nuclear magnetic resonance
6-MeMP: 6-methyl mercaptopurine
6-MP: 6-mercaptopurine
6-TG: Thioguanine
6-TGDP: 6-thioguanine diphosphate
6-TGMP: 6-thioguanine monophosphate
6-TGTP: 6-thio¬guanine triphosphate
6-TIMP: 6-thioinosine monophosphate
6-TUA: 6-thiouric acid
AIEC: Adherent-invasive *E. coli*
WAT: White adipose tissue
ALPI: Intestinal alkaline phosphatase
AMP: Anti-microbial peptide
Apo: Apolipoprotein
ATG16L1: Autophagy related 16 like 1
ATOH1: Atonal BHLH Transcription Factor 1
ATP: Adenosine triphosphate
a.u: arbitrary unit
AZA: Azathioprine
CBir1: Anti-flagellin antibody
CD: Crohn's disease
Chol: Cholesterol
DC: Dendritic cell
Defa3: alpha-defensin 3
DLB: Denaturing lysis buffer
DMSO: Dimethyl sulfoxide
DNP: 2,4-Dinitrophenol
EGF: Epidermal growth factor
EIMs: Extraintestinal manifestations
eWAT: Epididymal white adipose tissue
fB: Factor B
FC: Free cholesterol

GALT: Gut associated lymphoid tissue

Gfi1: Growth Factor Independent 1 Transcriptional Repressor

GIT: Gastrointestinal tract

Glut1: Glucose transporter 1

GP2: Glycoprotein 2

GSTs: Glutathione s-transferase

GWAS: Genome-wide association study

HD5: Human alpha defensin 5

HD6: Human alpha defensin 6

HDL: High density lipoprotein

Hes1: Hairy and enhancer of split-1

HFD: High fat diet

HPRT: Hypoxanthine-guanine phosphoribosyltransferase

IBD: Inflammatory bowel disease

IDL: Intermediate lipoprotein

IEC: Intestinal epithelial cell

IFN-γ: Interferon gamma

IRE1α: Inositol-requiring transmembrane kinase endoribonuclease-1α

iWAT: Inguinal adipose tissue

LDL: Low density lipoprotein

LGR5: leucine rich repeat containing G protein-coupled receptor 5

LYZ: Lysozyme

MAMP: Microbe-associated molecular pattern

Mist1: Muscle, intestine and stomach expression 1

Muc2: Mucin 2

NLR: NOD-like receptor

NRG1: Neuregulin 1

OXHPOS: Oxidative phosphorylation

PC: Paneth cell

PL: Phospholipids

PPs: Peyer Patches

Rac1: Rac Family Small GTPase 1

RFU: relative fluorescence unit

SNP: Single nucleotide polymorphism

SOX9: SRY-Box Transcription Factor 9

STAT4: signal transducer and activator of transcription 4

Tcf1: T cell factor 1

TFF3: Trefoil Factor 3

TG: Triglyceride

T_H1: T helper 1 cell

TNF: Tumor necrosis factor

TOM20: Translocase of outer membrane

TORC1: Target of rapamycin complex 1

TPM: Transcripts per million

TPMT: Thiopurine S-methyltransferase

UPR: Unfolded protein response

VDAC-1: Voltage-dependent anion-selective channel 1

VLDL: Very low density lipoprotein

Wnt: Wingless-related integration site

XBP1: X-box binding protein 1

XDH: Xanthine dehydrogenase

Abstract

The small intestinal lumen is lined with various types of epithelial cells that vary in their functions and metabolic characteristics. Paneth cells (PCs) are one of these cells that are found at the base of small intestinal crypts and play an important role in maintaining intestinal homeostasis. Functions of PCs range from the support of intestinal stem cells (ISCs) to the release of anti-microbial peptides (AMPs). Therefore, dysfunctional PCs have been reported to be associated with intestinal pathologies such as Crohn's disease (CD) and necrotizing enterocolitis. Patients with CD with ileal involvement displayed impairment in PCs and decreased levels of AMPs. There is a wide range of drugs used in the therapy of CD patients, with Azathioprine (AZA) being a widely used immunosuppressive drug for the treatment of CD. Nonetheless, despite the critical contribution of PCs to the pathogenesis of CD, the impact of medications on these cells is largely unrecognized.

In the present study, it was hypothesized that the orally administered drug AZA exerts its effect through modulation of the intestinal epithelium, specifically PCs. Of note, AZA-treated CD patients exhibited an ileal upregulation of AMPs on both mRNA and protein levels compared to non-AZA treated patients. These observations were corroborated by *in vitro* assessment. Intestinal epithelial cell lines, MODE-K and HT-29 exhibited heightened expression levels of PC markers and diminished cell proliferation upon AZA stimulation. Moreover, differentiation to secretory cells, such as PCs was boosted in AZA-treated murine small intestinal 3D-organoids.

These alterations were accompanied by metabolic changes. Specifically, increased mitochondrial oxidative phosphorylation activity and dampened lactate production were the major metabolic characteristics associated with AZA treatment. Additionally, the dyslipidemia found in CD patients, which is linked to PC dysfunction, was reduced in the sera of AZA-treated CD patients. Specifically, nuclear magnetic resonance (NMR) analysis demonstrated decreased levels of lipid moieties attached to low-density lipoprotein subfraction 6 (LDL-6) in AZA-treated patients.

In conclusion, AZA has been shown to inhibit proliferation of intestinal epithelial cells (IECs) that is accompanied by boosted mitochondria function and IEC differentiation into PC.

Zusammenfassung

Das Lumen des Dünndarms ist mit verschiedenen Arten von Epithelzellen ausgekleidet, die sich in ihren Funktionen und metabolischen Eigenschaften unterscheiden. Paneth-Zellen (PZ) sind eine dieser Zellen. PZ befinden sich am Grund der Dünndarmkrypten und spielen eine wichtige Rolle bei der Aufrechterhaltung der intestinalen Homöostase. Die Funktionen der PZ reichen von der Unterstützung intestinaler Stammzellen (ISZ) bis zur Freisetzung antimikrobieller Peptide (AMPs). Daher wurde berichtet, dass dysfunktionale PZ mit Darmpathologien wie Morbus Crohn (CD) und nekrotisierender Enterokolitis in Verbindung gebracht werden. Bei CD-Patienten mit Entzündung des Ileums wurden Beeinträchtigungen der PZ und verminderte AMP-Spiegel festgestellt. Für die Therapie von CD-Patienten gibt es eine breite Palette von Medikamenten, wobei insbesondere Azathioprin (AZA) als Immunsuppressivum bei der Behandlung von CD weit verbreitet ist. Trotz des entscheidenden Beitrags der PZ zur Pathogenese der CD sind die Auswirkungen von Medikamenten auf diese Zellen noch weitgehend unbekannt.

In der vorliegenden Studie wurde die Hypothese aufgestellt, dass oral verabreichtes AZA seine Wirkung über eine Modulation des Darmepithels, insbesondere der PZs, entfaltet. Bemerkenswert ist, dass AZA-behandelte CD-Patienten im Vergleich zu nicht mit AZA-behandelten Patienten eine ileale Hochregulierung von AMPs sowohl auf mRNA- als auch auf Proteinebene aufwiesen. Diese Beobachtungen wurden durch *In-vitro*-Untersuchungen bestätigt. Intestinale Epithelzelllinien, MODE-K und HT-29, zeigten nach AZA-Stimulation eine erhöhte Expression von PZ-Markern und eine verringerte Zellproliferation. Darüber hinaus wurde die Differenzierung zu sekretorischen Zellen, wie z.B. PZ, in mit AZA behandelten 3D-Organoiden des Mausdünndarms gefördert.

Diese Veränderungen wurden von metabolischen Veränderungen begleitet. Insbesondere waren eine erhöhte mitochondriale oxidative Phosphorylierungsaktivität und eine gedämpfte Laktatproduktion die wichtigsten metabolischen Merkmale, die mit der AZA-Behandlung einhergingen. Außerdem wurde festgestellt, dass die bei CD-Patienten festgestellte Dyslipidämie, die mit einer PZ-Dysfunktion verbunden ist, in den Seren der CD-Patienten minimiert wurde. Insbesondere zeigte die kernmagnetische Resonanz (NMR)-Analyse bei AZA-behandelten Patienten eine

Verringerung der an die Low-Density-Lipoprotein-Subfraktion 6 (LDL-6) gebundenen Lipidanteile.

Zusammenfassend lässt sich sagen, dass AZA nachweislich die Proliferation von intestinalen Epithelzellen (IEZs) hemmt, was mit einer gesteigerten Mitochondrienfunktion und einer Differenzierung der IEZ in PZ einhergeht.

1. Introduction

1.1 Paneth cells (PCs)

In 1872, Gustav Schwalbe briefly mentioned the presence of highly eosinophilic cells at the base of Lieberkühn crypts in the small intestine, which he described as similar to pancreatic glandular cells (Schwalbe, 1872). Fifteen years later, Josef Paneth, an Austrian physician, built on Schwalbe`s observation and concluded that these "*Körnchenzellen"* or granular cells, as he named them, are unique secretory population with no similarities to goblet cells or pancreatic cells (Paneth, 1887). Eventually, these cells carried the name of Josef Paneth, and the very granules that attracted the attention to these cells would turn out to be a trove of various factors that govern intestinal homeostasis.

1.1.1 Development and maintenance

It is not known when PCs first appear in the small intestine exactly. Antimicrobial peptides were detected at various prenatal time points. For example, human small intestinal α-Defensin 5 and 6 (HD5,6) were detectable at 13.5-17 weeks of gestation, while lysozyme is appearing around 20 weeks (Mallow et al., 1996; Rumbo and Schiffrin, 2005). An increase in the number of mature PCs was observed at a postmenstrual age of 29 weeks (Heida et al., 2016). In contrast, terminally differentiated PCs appear postnatally in mice (Bry et al., 1994).

PCs originate from ISCs, but unlike other differentiated intestinal epithelial cells, they migrate to the base of the crypts to intermingle with ISCs (Stappenbeck, 2009). PCs tend to have a longer lifespan (>30 days) than other intestinal epithelial lineages (3-5 days) (Stappenbeck, 2009). The cell fate to secretory (including PCs) or absorptive lineage is influenced by various interacting factors. Specifically, Wingless-related integration site (Wnt) signaling pathway is the major driver of secretory lineage commitment (Beumer and Clevers, 2020). Atonal BHLH Transcription Factor 1 (Atoh1), an essential basic helix-loop-helix transcription factor, is one of the Wnt pathway targets (Cray et al., 2021). Genetic deletion of *Atoh1* resulted in the loss of PCs and a rise in absorptive enterocyte population (Durand et al., 2012; Shroyer et al., 2007). In addition, other transcription factors such as SRY-Box transcription factor 9 (Sox9) and Growth factor independent 1 transcriptional repressor (Gfi1) are involved

in PC specification (Bastide et al., 2007; Shroyer et al., 2005). Further, Dekaney *et al.* showed that PC function is regulated by muscle, intestine and stomach expression 1 (Mist1). On the other hand, Notch signaling directs toward absorptive cell fate through the induction of the Hairy and enhancer of split 1 gene (Hes1), which in turn inhibits Atoh1 (Suzuki et al., 2005). Canonical Wnt/β-catenin signaling is essential not only for PC development but also for its maintenance and proper functionality. WNT can activate the Frizzled-Lrp5/6 receptor complex, which is present on the surface of the PC. The subsequent result is the accumulation of β-catenin, which in turn enters the nucleus and boosts transcription of T cell factor (TCF) targets (Armbruster et al., 2017). Beisner *et al.* suggested the involvement of TCF1 in the activation of HD 5 and 6 promotors (Beisner et al., 2014). Additionally, ileal samples from Crohn's disease (CD) patients showed a reduction in TCF1 and HD5 (Beisner et al., 2014). Non-canonical Wnt/ planar cell polarity (PCP) pathway is reported to contribute to secretory cell fate (Böttcher et al., 2021). Wnt/PCP-activated Leucine-rich repeat containing G protein-coupled receptor 5 (Lgr5) + ISCs are set to differentiate into Paneth cell or enteroendocrine lineage.

1.1.2 PCs and ISCs

The link between ISC and PC is not exclusive to PC development but rather extends bilaterally to involve ISC maintenance (Fig. 1). For decades, PCs were hypothesized to be involved in ISC sustainment (Garabedian et al., 1997). Nonetheless, efforts came to fruition in 2011 when Sato *et al.* showed that the combination of PCs with ISCs improved the growth of *in vitro* intestinal organoids, unlike PC-free cultures (Sato et al., 2011). Various niche factors are involved in ISCs' maintenance and regulation of the balance between self-renewal and differentiation (Beumer and Clevers, 2020). The mechanism by which PCs exert effect was revealed by secreting a wide range of niche factors such as epidermal growth factor (EGF), Wnt3a, and the Notch ligands DLL1, DLL4 (Sato et al., 2011). Supplying ISCs with such factors induced the same effect observed in co-culture experiments (Farin et al., 2012). The use of EGF is widely used in the maintenance of organoid culture, as it induces proliferation through the activation of ERBB1, a highly abundant EGF receptor in ISC (Beumer and Clevers, 2020; Sato et al., 2009). Recently, an EGF ligand called neuregulin 1 (NRG1) was found to be expressed in PCs and induced an effect on ISCs *via* ErbB2 and ErbB3 receptors (Jardé et al., 2020). Notch signaling, which relies on the close contact

between cells, is pivotal for stemness (Nakata et al., 2017; Pellegrinet et al., 2011). Transmissible gastroenteritis virus (TGEV) is reported to cause ISCs loss by invading PCs and thus cutting down Notch ligands needed for ISCs self-renewal (Wu et al., 2020). PCs were shown to acquire plastic properties upon injury. RNA sequencing showed that PCs from irradiated mice exhibited a stem cell signature (Yu et al., 2018). Additionally, organoids developed from pure irradiated PCs while non-irradiated cells failed (Yu et al., 2018). Rodríguez-Colman *et al.* explored the metabolic aspect of the connection between PC and ISC (Rodríguez-Colman et al., 2017). They proposed that PCs provide stem cells with lactate, which is later converted to pyruvate to boost mitochondrial oxidative phosphorylation. In turn, nutritional modification, such as caloric restriction, influences ISCs through modulation of mTORC1, a critical metabolic regulator, in PCs (Yilmaz et al., 2012). On the other hand, Khaloian et al., 2020 emphasized the role of mitochondria in the development of functional PCs. Inhibition of mitochondrial respiration in ISC resulted in the appearance of aberrant PCs, which is associated with CD-like inflammation. Similarly, mitochondrial dysfunction induced by loss of prohibitin 1 in PCs was accompanied by ileitis (Jackson et al., 2020).

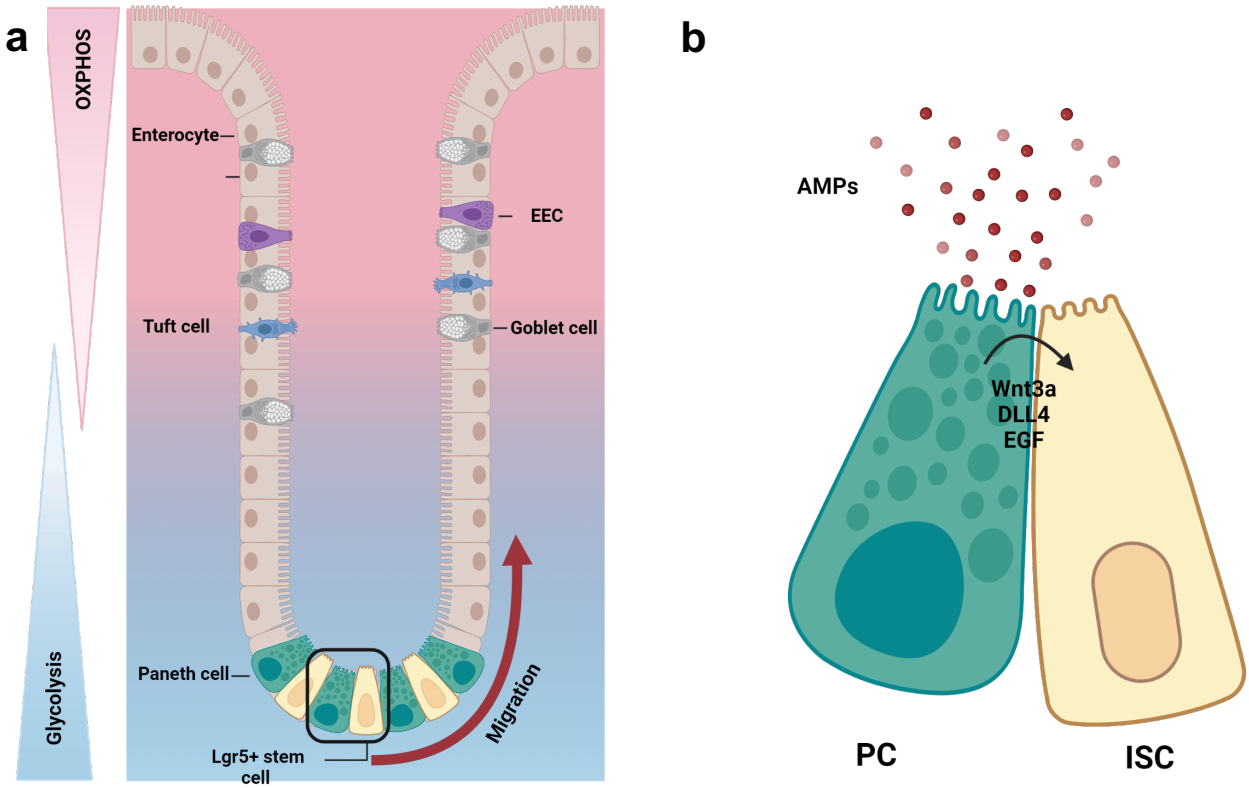

Figure 1. Intestinal epithelium zonation and metabolic gradient along the intestinal crypt-villus axis. (a) Lgr5+ cells continuously replenish intestinal epithelium with mature differentiated cells. Unlike the other types of IECs that migrate towards to villus tip, mature PCs tend to settle next to ISCs. Proliferation and differentiation are governed by metabolic gradient that regulates intestinal homeostasis with higher mitochondrial content in the upper compartment. (b) Beside the release of AMPs, PCs provide niche to support ISCs by producing factors such as Wnt3a, EGF and DLL4. EEC: enteroendocrine cell; PC: Paneth cell; ISC: intestinal stem cell; AMPs: anti-microbial peptides; Wnt3a: Wingless-related integration site 3a; EGF: epidermal growth factor; DLL4: Delta-like 4; OXPHOS: mitochondrial oxidative phosphorylation; EEC: enteroendocrine cells. Designed with Biorender.com

1.1.3 Antimicrobial peptides (AMPs)

The second major function attributed to PCs is the ability to produce a wide spectrum of peptides with microbial-modulating properties. AMPs include α-defensins, lysozyme, angiogenin, and secretory phospholipase A2 (Gassler, 2017). Enteric α-defensins are exclusive major elements of PC secretory granules. Six different isoforms of α-defensins were detected in the small intestine of adult mice, which are known as cryptidins, yet only two major Paneth cell α-defensins, HD5 and HD6, appear in humans (Ouellette, 2006).

The expression levels of α-defensins are not comparable along different segments of the small intestine (Nakamura et al., 2020). The ileal compartment has the highest levels of different cryptidin isoforms compared to the jejunum and duodenum (Nakamura et al., 2020). Similarly, HD5 and 6 are highly abundant in the ileum (Wehkamp et al., 2006). The bactericidal activity of human enteric α-defensins varies greatly. While HD5 exhibited broad activity against gram-positive and negative bacteria *in vitro*, HD6 showed a modest bactericidal effect (Ericksen et al., 2005). Different mechanisms have been proposed to explain defensins' mechanism of action. For example, HD5 has been shown to induce morphological changes in *Escherichia coli* in the form of bulges and elongation (Chileveru et al., 2015). On the other hand, HD6 forms structures known as nanonets, entangling *Salmonella* Typhimurium and thus preventing bacterial dislocation into host cells (Chu et al., 2012). Besides, enteric α-defensins possess antiviral properties. Recently, SARS-CoV-2 viral entry has been reported to be abrogated by HD5 (Xu et al., 2021). In addition, Wiens *et al.* investigated the mechanism by which HD5 inhibits human papillomavirus through accelerating lysosomal degradation (Wiens and Smith, 2017). Phospholipase A2 is among AMPs that influence the growth of bacteria such as *Listeria monocytogenes* and *E. coli*

(Harwig et al., 1995). In conclusion, enteric AMPs can shape and regulate gut microbiota since they possess microbial modulating capacity. Namely, transgenic *HD5*-expressing mice exhibited a lower Firmicutes/Bacteroidetes ratio compared to wild-type counterparts. Moreover, a significant loss of segmented filamentous bacteria was observed in *HD5*-expressing mice (Salzman et al., 2010). Lysozyme deficiency led to alterations in ileal luminal bacteria in mice (Yu et al., 2020). Matrix metalloproteinase-7 (MMP-7) is required to activate pro-α-defensins into fully functional defensins (Gassler, 2017). The absence of the proteolytic activation process as in the case of genetically modified mice, renders PCs dysfunctional (Wilson et al., 1999). Furthermore, *Mmp-7* knockout mice exhibited changes in gut microbiota composition and increased susceptibility to bacterial infections (Mastroianni et al., 2012; Salzman et al., 2010). Nucleotide-binding oligomerization domain 2 (NOD2), a member of the NOD-like receptor (NLR) family, is involved in the upregulation of α-defensins expression (Yang and Shen, 2021). Bel *et al.* proposed that lysozyme release is mediated by secretory autophagy upon bacterial infection (Bel et al., 2017). *Salmonella* Typhimurium-invaded PCs resort to package lysozyme into double-membraned vesicles, which are secreted into the intestinal lumen (Bel et al., 2017).

1.1.4 PCs and Crohn`s disease

Dysfunctional PCs were long theorized as a major contributor to the pathogenesis of CD (Klockars et al., 1977; Lewin, 1969). Nonetheless, this hypothesis was substantiated in 2003 when NOD2, an exclusive small intestinal protein, was found to be highly expressed in metaplastic PCs in colonic biopsies from CD patients (Lala et al., 2003; Ogura et al., 2003). Subsequently, it was reported that *NOD2* mutations are associated with downregulation of enteric defensins in patients with CD (Wehkamp et al., 2004). In another study, CD patients with ileal involvement exhibited a significant reduction in HD5 and 6 in comparison with non- inflammatory bowel disease (IBD) controls (Wehkamp et al., 2005). This reduction was correlated with diminished antimicrobial activity (Wehkamp et al., 2005). Peripheral blood mononuclear cells (PBMCs) isolated from CD patients homozygous for *NOD2* mutations failed to induce TLR9 activation upon treatment with CpG DNA, a TLR9 ligand (Van Heel et al., 2005).

Genome-wide association studies have pointed out the correlation between mutations in other PC genes such as autophagy related 16 like 1 (*ATG16L1*), inositol-requiring transmembrane kinase endoribonuclease-1α (*IRE1α*) and X-box binding protein 1 (*XBP1)* and CD pathogenesis (Cray et al., 2021) (Fig. 2). Partial loss of autophagy gene, *Atg16L1* resulted in impaired PC function in mice (Deretic et al., 2008). In addition, CD patients homozygous for ATG16L1 displayed similar PC abnormalities (Cadwell et al., 2009). Inducing endoplasmic reticulum (ER) stress in PCs via deletion of unfolded protein response (UPR) transcription factor XBP1 exacerbated CD-like ileitis in *Atg16l1*$^{\Delta IEC}$ mice (Tschurtschenthaler et al., 2017).

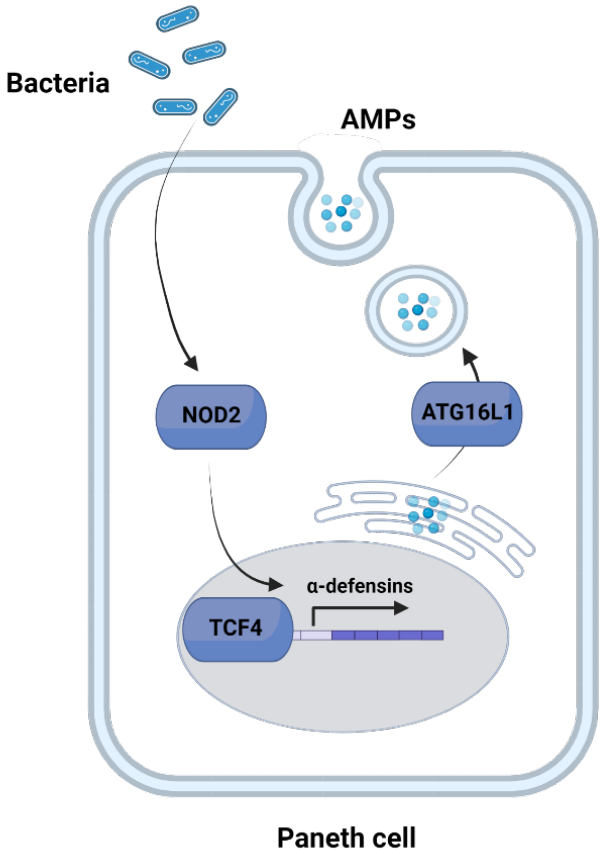

Figure 2. Polymorphisms associated with PC dysfunction in Crohn's disease. Multiple proteins such as, NOD2, TCF4 and ATG16L1 regulate expression, secretion and release of AMPs. CD patients with PC dysfunction display mutations in the genes that encode these proteins. AMPs: anti-microbial peptides; NOD2: nucleotide-binding oligomerization domain-containing protein 2; TCF4: T-cell factor 4; ATG16L1: autophagy related 16 like 1. Modified from Mukherjee and Hooper, 2015. Designed with Biorender.com.

Genetic deletion of XBP1 eradicated PC presence in the small intestine and exposed mice to oral infection with *Listeria monocytogenes* (Kaser et al., 2008). As previously mentioned, Wnt pathway is crucial for PC development and function. Mutations in *TCF-4*, a Wnt transcription factor, were found to be frequently present in CD patients with ileal involvement (Koslowski et al., 2009; Mukherjee and Hooper, 2015).

1.1.5 Impact of Dietary modifications on PCs

The intestinal epithelium plays a major role in the absorption of nutrients and on the other side, these nutrients influence intestinal permeability, barrier integrity and epithelial cells (Guzman et al., 2013). Several studies have shown that dietary modifications affect PC development and function. Mice fed a high-fat, low-fiber diet showed elevated expression of PC markers in villus cells on both mRNA and protein levels (Wang et al., 2011). On the contrary, cells at the bottom of the crypts exhibited a reduction in the levels of defensins, indicating a disturbance in epithelial cell differentiation (Wang et al., 2011). Similarly, decreased numbers of PCs and goblet cells were observed in mice fed diet containing 60% fat (Lee et al., 2017). These changes in epithelial cell populations, along with intestinal microbiota alteration, are believed to exacerbate experimental colitis in mice fed a high-fat diet (HFD) (Lee et al., 2017). Todrov *et al.* showed that α-linolenic acid (ALA), a poly unsaturated fatty acid, negatively influenced the numbers of intestinal secretory cells similar to the effect of high-fat diet (Todorov et al., 2020). Additionally, Liu *et al.* emphasized the mechanism behind western diet (WD)-induced PC dysfunction (Liu et al., 2021). Activation of farnesoid X receptor (FXR) signaling was associated with western diet intake and was evident at the crypt base where PCs are present(Liu et al., 2021). WD-fed mice treated with FXR agonist have higher mortality rates upon *Salmonella* infection, pointing out to PC malfunction (Liu et al., 2021). Nonetheless, caloric restriction (CR) enriched the intestine with ISCs and PC populations through mTORC1 (Yilmaz et al., 2012). Organoid-forming capacity was enhanced when CR-PCs were co-cultured with ISCs (Yilmaz et al., 2012). Zhou *et al.* proposed another mechanism by which HFD induces a negative impact on PCs (Zhou et al., 2020). An increased bile acid secretion because of fatty diet intake enhanced the expression of G protein–coupled receptor TGR5 present in PCs (Zhou et al., 2020). This effect was abrogated when cholestyramine, a bile acid sequestrant, was introduced with HFD. On the other hand, other compounds are necessary for proper PC development and function. For

example, vitamin D deficiency leads to diminished defensins secretion and an increased abundance of pathogenic bacteria like *Helicobacter hepaticus* (Lu et al., 2021; Su et al., 2016).

1.2 Crohn`s disease

1.2.1 Epidemiology

CD belongs to the spectrum of IBD, which also includes ulcerative colitis (UC). A chronic transmural inflammation that usually affects ileum and colon but could still target any part of the gastrointestinal tract (GIT) is one of the distinct features of CD (Peppercorn and Cheifetz, 2022). The global prevalence of IBD has been rising in the last few decades. The age-standardized prevalence rate increased from 79.5 per 100,000 population in 1990 to 84.3 per 100 000 population in 2017 (Alatab et al., 2020). However, there is a high geographical variability in incidence and prevalence. A significant number of studies are investigating populations from western countries where the highest prevalence was recorded in North America and Northern Europe (Roda et al., 2020). For example, in Canada, the prevalence of CD has risen up from 282 in 2008 to 352 cases per 100,000 population in 2018 and is expected to reach 482 by 2030 (Coward et al., 2019). Despite that prevalence rates in Asian countries are lower than that in the western counterparts, numbers are still high, most probably due to drastic environmental and socioeconomic changes (Burisch and Munkholm, 2015). In Japan, the prevalence of CD has jumped in the last three decades, making it the highest country in East Asia in the incidence and prevalence of IBD(Park and Cheon, 2021). The Caribbean, Latin America and sub-Saharan Africa constitute the lowest regions in the numbers of IBD cases (Alatab et al., 2020). Nonetheless, similar to Asia, some countries in these regions have registered a rise in the number of cases, such as Brazil and Ghana (Hodges and Kelly, 2020; Zaltman et al., 2021). There is high variability in CD prevalence among people from different ethnicities. CD is predominant in patients of western ancestry (Edward L Barnes et al., 2021). However, increasing reports are showing high incidence rates in non-White populations. For example, the incidence rate of IBD in non-Whites reached 60% of the white incidence rate in the period between 2000 and 2010, while it was only 35% between 1970 and 1984 (Aniwan et al., 2019). Further, there is a high diversity in disease patterns and phenotypes among different societies. African American, Asian and Hispanic patients displayed widespread intestinal inflammation compared to White patients (Barnes et

al., 2021). Nonetheless, these variations could be attributed to the availability and quality of treatment.

1.2.2 Age and sex differences

Although CD can occur at any age, onset is usually reported between 20-30 years of age (Peppercorn and Cheifetz, 2022). Some studies have pointed out that a second incidence peak occurs between 50-80 years of age (Duricova et al., 2014). Studies that focus on gender distribution are often inconsistent and different based on geographical location. The prevalence of CD has been reported to be higher in females among US population, while it is more common in males in Asia (Betteridge et al., 2013; Greuter et al., 2020). In addition, sex differences were reported in disease distribution. A cohort study conducted on Dutch CD patients revealed that ileum was commonly affected in males while females exhibited the colonic phenotype (Severs et al., 2018).

1.2.3 Disease phenotype

CD has various phenotypes that can come in the form of transmural inflammation, stricturing or fistulizing disease (Feuerstein and Cheifetz, 2017). The majority of CD patients display inflammation in the small intestine, mainly in the distal ileum. Around 50% of patients have both ileum and colon affected by the inflammation and 20% of the cases have only colonic involvement (Feuerstein and Cheifetz, 2017; Peppercorn and Kane, 2022). On the other hand, the perianal area is affected in approximately one-third of patients (Peppercorn and Kane, 2022). Increasing studies have pointed out to the rising incidence of upper GIT involvement which includes oesophagus, stomach, duodenum and jejunum (Roda et al., 2020). Chronic inflammation can lead to fibrosis which eventually will cause structuring disease. Complications may also include the formation of fistulas, tracts that connect the intestine to organs with epithelial lining such as the urinary bladder, skin or vagina (Roda et al., 2020). It has been reported that 35% of CD patients developed fistulas with high incidence in the perianal region (Schwartz et al., 2002). Montreal classification is widely used to categorize CD patients based on three factors, (A) age at diagnosis, (L) location and (B) behavior (Table. 1) (Satsangi et al., 2006).

Table 1. Montreal classification for Crohn´s disease (Satsangi et al., 2006)

Age at diagnosis	A1 below 16 years A2 between 17 and 40 years A3 above 40 years
Location	L1 ileal L2 colonic L3 ileocolonic L4 isolated upper disease*
Behavior	B1 nonstricturing, nonpenetrating B2 stricturing B3 penetrating p perianal disease modifier

* L4 is a modifier that can be added to L1-L3 when concomitant upper gastrointestinal disease is present.
¶ "p" is added to B1-B3 when concomitant perianal disease is present.

1.2.4 Clinical features

CD manifestations are quite variable according to the disease phenotype. The most common symptoms are abdominal pain, diarrhea and systemic manifestations such as fatigue, anemia and weight loss (Lichtenstein et al., 2018). Chronic pain in the right lower abdominal quadrant is often reported by patients with ileal involvement. Stricturing disease due to fibrosis usually leads to frequent abdominal pain and small bowel obstruction. Fistulas can cause a wide range of signs and symptoms that depend on their locations. Perianal swelling, fever and fecal incontinence are the most common symptoms associated with perianal fistula (Marzo et al., 2015). Enterovesical fistulas (connections between intestine and urinary bladder) lead to increased susceptibility to urinary tract infections, while fistulas to the peritoneum can result in the development of peritonitis (Peppercorn and Kane, 2022). Extraintestinal manifestations (EIMs) are commonly associated with IBD, particularly CD(Harbord et al., 2016) (Fig. 3). Approximately 6-47% of IBD patients have reported at least one EIM(Ott et al., 2013). Moreover, in a cohort study, EIMs were present in 43% of CD patients (Vavricka et al., 2011). Asymmetrical peripheral arthritis is reported in 10-20% of CD patients (Harbord et al., 2016). Iritis, episcleritis and anterior uveitis are the most commonly reported ocular manifestations (Roda et al., 2020).

Mucocutaneous manifestations can include erythema nodosum (5-15% of CD cases) which is characterized by the appearance of subcutaneous nodules on the extensor surfaces of the lower extremities(Ott et al., 2013). There is a variation in the prevalence of such nodules based on disease activity with higher prevalence in patients with inactive CD reaching 6.8% and 2.4% of patients with active CD (Rogler et al., 2021). Rapidly developing ulcer which is frequently seen in the lower extremities known as pyoderma gangrenosum is another dermatological manifestation that appears in 0.4 to 2.6% of IBD cases (Rogler et al., 2021). Primary sclerosing cholangitis could be seen in CD patients but less frequently in comparison with UC patients (Roda et al., 2020; Rogler et al., 2021). Other EIMs can include renal and urological manifestations (Nephritis and urolithiasis), cardiac disorders (myocarditis and pericarditis) and in rare cases pancreatitis and pneumonitis (Ott et al., 2013).

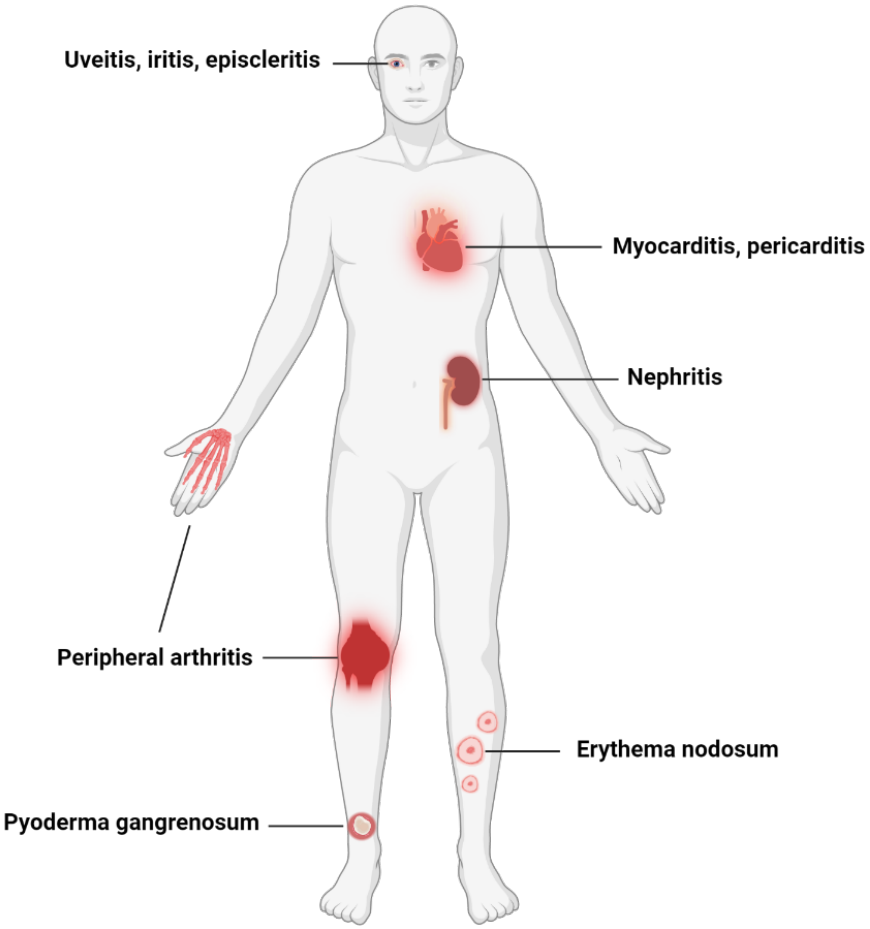

Figure 3. Extraintestinal manifestations of Crohn`s disease. Modified from (Baumgart and Sandborn, 2012). Designed with Biorender.com

1.2.5 Risk factors

A combination of environmental and genetic factors works in tandem in the development of CD. Twin studies have confirmed the role of heredity in IBD, reaching a concordance rate between 20–50% in monozygotic twins and 10% for dizygotic ones (Ananthakrishnan, 2015). Moreover, susceptibility to IBD is higher in first-degree relatives of CD patients compared with UC relatives (Moller et al., 2015). Genome-wide association studies (GWAS) have provided a deep insight into how genetics are implicated in the pathogenesis of IBD. GWAS led to the identification of 200 IBD-associated genetic loci. Ogura *et al.* identified *NOD2* as the first susceptibility gene to be associated with CD and involved in innate immunity (Ogura et al., 2001). It has been reported that 30-50% of European CD patients carry mutations in *Nod2* gene (Yamamoto and Ma, 2009). NOD2 is a sensor of bacterial muramyl dipeptides (LD-MDP) leading to the activation of NF-κB pathway and the release of pro-inflammatory cytokines (Yamamoto and Ma, 2009). Other risk genes such as *ATG16L1, IRGM* and *IL23R* were found to be influencing various immunological pathways like autophagy and IL17 signaling (Lees et al., 2011). Susceptibility to ileal CD was reported to be approximately three times higher in individuals with a genetic variant in *ATG16L1* (Fowler et al., 2008).

Smoking is one of the most studied environmental risk factors in IBD patients. In a meta-analysis, an association between CD and smoking was examined in the period between 1980 and 2006, concluding that there is a strong relationship (OR, 1.76; 95% confidence interval [CI], 1.40-2.22) (Mahid et al., 2006). A large-scale statistical analysis described how smoking increased the susceptibility to CD through the modulation of the NOD2 1007fs polymorphism (Helbig et al., 2012). In another study, smoking was reported to induce dysfunction in PCs in CD patients with $ATG16L1^{T300A}$ genotype (Liu et al., 2018). Additionally, smoking can alter microbiota composition leading to an increased level of adherent invasive *Escherichia coli* and a decrease in bacteria with anti-inflammatory properties, such as *Faecalibacterium prausnitzii* (Parkes et al., 2014).

Industrialization has massively affected dietary lifestyles such as the increased consumption of western diet with high fat and low fiber content. However, data on the exact role of diet in the growing incidence of IBD remains inconsistent most probably due to limited number of studies. High intake of trans-unsaturated fatty acids was

positively correlated with the incidence of UC but not CD (Ananthakrishnan et al., 2014). In contrast, a recent cohort of 328 CD patients and 428 cases of UC found a strong association between Western diet and ileal CD but not UC (Lo et al., 2020). Further, Disease activity and pro-inflammatory cytokines positively correlated with serum % n-3 fatty acids and inversely correlated with serum % n-6 fatty acids (Scoville et al., 2019). In another study, increased intake of polyunsaturated fatty acids induced endoplasmic reticulum (ER) stress and aggravated intestinal inflammation (Schwärzler et al., 2022). Other reports highlighted the altered lipid profile that can distinguish between IBD subsets. A cohort study, that included 20 CD patients, 20 UC patients and 20 healthy controls detected 286 metabolites to be differentially present in the sera of CD patients compared to healthy individuals (Scoville et al., 2018). Specifically, pathways related to fatty acid metabolism were significantly distinct in CD patients compared to UC patients. A Korean study population revealed low serum levels of total cholesterol (TC) and HDL-C in CD (Soh et al., 2020). In another study, CD patients exhibited similar findings and disease activity negatively correlated with TC, HDL-C and LDL-C concentrations (D Wang et al., 2021). Hypocholesterolemia was also associated with pediatric CD patients (Levy et al., 2000). On the other hand, serum triglycerides were found to be increased in CD patients, an observation that might explain the heightened cardiovascular risk in IBD patients (Levy et al., 2000; Ripollés Piquer et al., 2006; Van Leuven et al., 2007).

High consumption of fermentable carbohydrates such as glucose, sucrose and lactose exacerbated intestinal inflammation by increasing gut permeability and inducing dysbiosis (Rizzello et al., 2019). Sugar intake but not the total carbohydrate intake was found to be directly correlated with the risk of CD in a meta-analysis study that combined the data from 4 cohort studies (Khademi et al., 2021). In another meta-analysis, strong association was reported to be between sucrose intake and the development of CD (Zeng et al., 2017).

1.2.6 Pathophysiology

The pathogenesis of CD is an extremely complex process that involves innate and adaptive immunity dysregulation along with dysbiosis (Roda et al., 2020) (Fig. 4).

1.2.6.1 Gut microbiota

Several studies pointed out that changes in gut bacterial composition were associated with several intestinal pathologies including IBD with loss of α-diversity (Imhann et al., 2018; Vich Vila et al., 2018). However, it is not known whether these changes act as a trigger or they are secondary outcomes of inflammation, medication, and mucosal immunity dysregulation. The Firmicutes/Bacteroidetes ratio is widely used as a marker of microbial imbalance. CD patients displayed a reduction in the abundance of Firmicutes, specifically *Faecalibacterium prausnitzii* and an increase in *Proteobacteria* such as adherent-invasive *E. coli* (AIEC) (Caruso et al., 2020). It was reported that AIEC from CD patients induced the development of granulomatous colitis (Meconi et al., 2007; Palmela et al., 2018; Simpson et al., 2006). These alterations are more pronounced in ileal CD with severe phenotype (Vester-Andersen et al., 2019). A recent study emphasized the role of autoantibodies against glycoprotein 2 (GP2) in the accumulation of AIEC and the aggravation of intestinal inflammation (Derer et al., 2020). GP2-splicing variant 4 possessed a high binding capacity to FimH, a bacterial adhesin that helps bacteria to bind to intestinal microfold (M) cells (Derer et al., 2020). Chevalier et al., 2021 designed a FimH- blocker which was found to abrogate bacterial adhesion. Colonic CD has a different microbiota signature from CD patients with ileal involvement (Atreya and Siegmund, 2021; Erickson et al., 2012; Imhann et al., 2018). A twin study revealed that colonic CD was associated with opposite changes in several bacterial species compared to ileal CD (Willing et al., 2010). Specifically, an increased abundance of four bacterial families was observed in colonic CD in comparison with healthy controls: Firmicutes (*Ruminoccocaceae*), Actinobacteria (*Bifidobacteriaceae*,*Coriobacteriaceae*) and Tenericutes (*Anaeroplasmataceae*) (Willing et al., 2010). Variations in viral and fungal communities were also detected in IBD patients (Roda et al., 2020). Dysregulated IgA antibody responses were correlated with an increase in granular fungal morphologies in CD mucosal washings (Doron et al., 2021). Wagner *et al.* investigated bacteriophage levels in pediatric CD patients and found an increased phage DNA in ileal biopsies from CD patients (Wagner et al., 2013).

1.2.6.2 Intestinal barrier function

Indirect data revealed that impaired barrier function contributed to intestinal inflammation. Abnormal barrier integrity serves as an indicator of CD onset (Gibson,

2004; Irvine and Marshall, 2000; Turpin et al., 2020). However, the question remains if these changes are primary or come as a result of the pro-inflammatory status. Despite not showing apparent signs of intestinal inflammation, relatives of CD patients displayed increased intestinal permeability (Martini et al., 2017). IBD animal models show signs of increased paracellular permeability. For instance, improved recovery from colitis was achieved by reducing enteric permeability in *Il10* deficient mice (Arrieta et al., 2009). Further, disrupted barrier integrity associated with TNBS colitis model was restored upon sodium butyrate treatment (Chen et al., 2018). Some reports pointed out that TNF-α is involved in leaky gut by inducing alterations in tight junctions(Gibson, 2004). Incubation of Caco-2 cysts with plasma from CD patients increased paracellular permeability which was reversed by the addition of a TNF-α inhibitor (Xu et al., 2019). Tissue-specific knocking out occludin, a tight junction protein, resulted in the amelioration of DSS-induced colitis (Kuo et al., 2019).

1.2.6.3 Mitochondrial dysfunction

Intact mitochondrial function significantly contributes to intestinal homeostasis (Novak and Mollen, 2015; Sünderhauf et al., 2021). Hence, there is no wonder that IBD is associated with mitochondrial dysregulation (Rath and Haller, 2022). While growing evidence supports mitochondrial involvement in UC pathogenesis, the numbers of studies addressing the issue in CD is still quite limited. ATP (Adenosine triphosphate) levels negatively correlated with CD-like inflammation in ileal compartment of $TNF^{\Delta ARE}$ mice (Khaloian et al., 2020). Blockage of glycolysis with dichloroacetate forced $TNF^{\Delta ARE}$ intestinal organoids to rely on OXPHOS and restored IEC composition (Khaloian et al., 2020). Treating DSS-receiving mice with Mito-Tempo, a mitochondria-targeted antioxidant significantly reduced colitis severity. (Wang et al., 2014). Voltage-dependent anion channel 1 (VDAC1), a major mitochondrial regulator, was found to be overexpressed and oligomerized in CD patients (Verma et al., 2022). Interestingly, the usage of VDAC1-targeting molecules abolished apoptosis and alleviated DSS-induced colitis (Verma et al., 2022). Proteomic analysis of pediatric CD patients revealed downregulation of different proteins involved in mitochondrial metabolism, namely the sulfur dioxygenase (ETHE1 and mitochondrial complexes III and IV (Mottawea et al., 2016).

1.2.6.4 Innate immunity

Various innate immune cells such as macrophages and dendritic cells (DCs) take part in the first response towards accumulated microbe-associated molecular patterns (MAMPs) such as lipopolysaccharide, peptidoglycan-derived muramyl dipeptide and lipoteichoic acid (Torres et al., 2017). Sensing of microbial antigens is accomplished through the activation of pattern recognition receptors (PRRs) such as Toll-like receptors (TLR) and NOD-like receptors (NLR) (Geremia et al., 2014). Under normal conditions, dendritic cells maintain intestinal homeostasis through antigen-presentation (Geremia et al., 2014). Heightened levels of TLR2, TLR4 and cytokines were found in mucosal DCs from CD patients indicating a functional dysregulation that drives inflammation (De Souza and Fiocchi, 2016). Furthermore, the recruitment of monocytes to lamina propria and the increased levels of macrophage-derived IL-12 were observed under CD, thus exacerbating the inflammatory response (Gren and Grip, 2016). Interestingly, Dharmasiri *et al.* revealed that CD macrophages do not exclusively belong to inflammatory M1 subset but they also express M2-related genes, explaining the development of granulosis and fibrosis in CD (Dharmasiri et al., 2021).

A powerful innate immune response is also processed by the complement system which orchestrates the interplay between bacteria and innate immune cells. Several studies highlighted the role of intestinal complement factors in the pathogenesis of IBD (Jain et al., 2014; Sina et al., 2018). C3a contributes to ISC regeneration and proliferation as demonstrated in intestinal organoids (Matsumoto et al., 2017). C3 and C4 were reported to accumulate significantly in the sera of CD patients (Richens et al., 1982). Similarly, the metabolism of C3 and C1q was heightened in CD patients compared to healthy and UC individuals (Hodgson et al., 1977; Potter et al., 1979; Preisker et al., 2019). Ohno *et al.* confirmed the contribution of C3 in intestinal inflammation by C3 depletion in DSS-colitis model (Ohno et al., 2020). Specifically, protection from colitis induced by colonization with mutant *E. coli* lacking polysaccharide layer was abrogated in the absence of C3. Beside liver, intestinal epithelium have its share of local complement molecules` production (Andoh et al., 1996; Colten et al., 1966). Nonetheless, direct *in vivo* evidence on whether IECs are the source of accumulated mucosal complement molecules is still lacking. Several IEC lines, such as Caco2 were found to express C3, C4 and factor B (fB) (Andoh et al.,

1993). Treating PCs with exogenous C3 *in vitro* resulted in enhanced secretory activity during the early stage of acute intestinal injury (Zhang et al., 2018).

1.2.6.5 Adaptive immunity

Recruitment of activated lymphocytes from gut-associated lymphoid tissue (GALT) comes secondary to intestinal barrier dysfunction and the accumulation of luminal antigen in lamina propria (De Souza and Fiocchi, 2016). Peyer's patches (PPs) are one of the densely populated GALT that are exclusively present in the small intestine, particularly in the terminal ileum (Caprilli, 2008). B cells along with T cells are the major constituents of PPs (Gullberg and Söderholm, 2006). M cells which are mainly present on the top PPs coordinate antigen presentation by taking up luminal antigens, triggering adaptive immune response (Derer et al., 2020). An imbalance of T helper cells and T regulatory cells is an important aspect of CD pathogenesis (Baumgart and Sandborn, 2012). Specifically, T helper subset such as T helper 1 (T_H1) and T_H17 cells which secretes pro-inflammatory cytokines such as IL-17, TNF and IFN-γ is massively contributing to intestinal inflammation (Baumgart and Sandborn, 2012). Mice overexpressing T_H1 cell-associated transcription factor, signal transducer and activator of transcription 4 (STAT4) exhibited exacerbated experimental colitis, highlighting the role of T_H1 cells in pro-inflammatory condition (Neurath, 2014). Mucosal IL-17 levels were reported to be significantly increased in active CD patients compared to inactive CD and active UC (Fujino et al., 2003). These cytokines induce the production of IL-1, IL-6 and IL-8, by other immune cells and the recruitment of neutrophils (Neurath, 2014; Roda et al., 2020). Additionally, T_H17 cells influence gut barrier functions through the release of IL-22, that control the development of PCs, release of AMPs and mucosal wound healing (Gaudino et al., 2021; Sun et al., 2012). *Nod2* knockout mice exhibited increased numbers of CD4+ cells in their PPs which was accompanied by a rise in IFN-γ levels (Barreau et al., 2010). On the other hand, dysregulation in anti-inflammatory cytokines such as IL-10 is implicated in IBD pathogenesis. Several single nucleotide polymorphisms (SNPs) in *IL-10* gene were found to be associated with pediatric CD (Amre et al., 2009).

The role of B cells in PPs has not fully elucidated. Increased $CD127^-$ memory B cell population was reported in IBD patients (Pararasa et al., 2019; Preisker et al., 2019). Further, activated humoral immune response is found in IBD. Serum antimicrobial antibodies such as anti- *Saccharomyces cerevisiae* antibody, anti-outer membrane

porin C antibody, anti flagellin antibody (CBir1), and antiglycan antibodies, are often reported in CD patients (De Souza and Fiocchi, 2016; Torres et al., 2017).

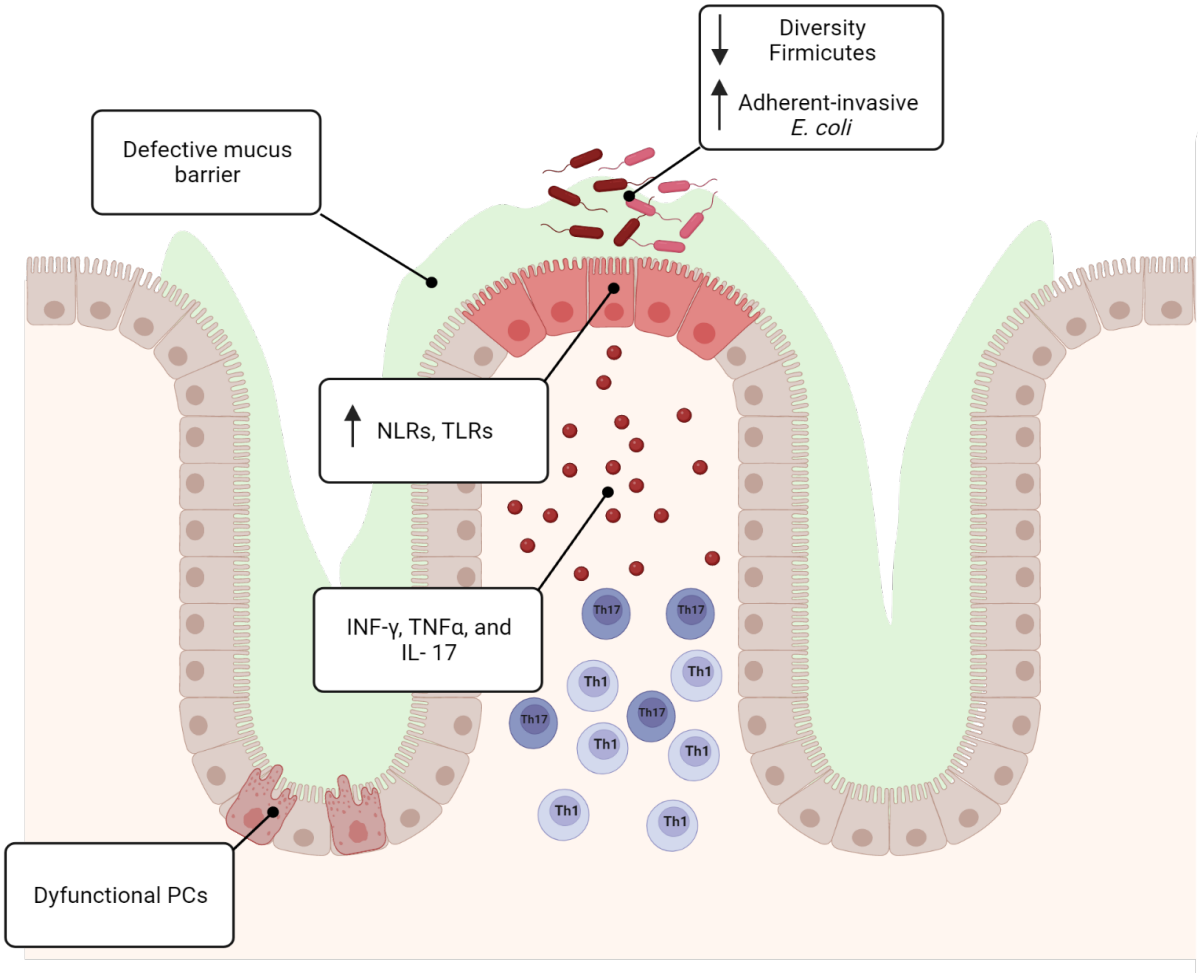

Figure 4. Intestinal pathogenesis in Crohn's disease. Inflamed intestinal tissue in CD is characterized by an increased abundance of invasive bacteria like AIEC and impaired barrier functions. These alterations cause the accumulation of Th1 and Th17 in the lamina propria and the production of pro-inflammatory cytokines such as TNFα and IFN-γ. PC: Paneth cell; NLRs: NOD-like receptors; TLRs: Toll-like receptors; IFN-γ, interferon-gamma; TNFα: tumor necrosis factor alpha; Th cells: T helper cells; IL-17: interleukin 17. Designed with Biorender.com.

1.3 Azathioprine

Azathioprine (AZA) has been extensively prescribed over the past five decades in the maintenance of a wide range of inflammatory disorders such as IBD (A-Rahim, Yousif I; Farrell, 2021; Brooke et al., 1969). AZA was first developed by Gertrude Elion and George Hitchings in 1961 as an alternative to 6-mercaptopurine (6-MP) (Elion, 1989; ELION et al., 1960).

1.3.1 Pharmacology and metabolism

Along with 6-mercaptopurine (6-MP) and thioguanine (6-TG), AZA belongs to the family of thiopurines which are known as *de novo* purine synthesis suppressors (Winkelstein, 1979). Chemically, AZA is a modified version of 6-MP with the addition of imidazole side chain to prolong the duration of action (Winkelstein, 1979). Oral intake is the most common form of AZA administration ("Azathioprine: Drug information - UpToDate," n.d.). However, other routes such as intravenous and rectal delivery have been reported (El-Yazigi and Wahab, 1993; Os et al., 1996). Os *et al.* have demonstrated that colonic delivery of AZA resulted in reduction of bioavailability in comparison with oral intake (Os et al., 1996). AZA is superior to 6-MP when it comes to oral bioavailability. Intestinal absorption of the former ranges from 50-72% whereas 22% of the 6-MP is found unabsorbed in stool (Cuffari et al., 2000; Winkelstein, 1979). In addition, AZA has a longer half-life between 4-5 hours, while 6-MP is only 0.3 to 0.8 hours (Pollard et al., 2005). Upon absorption, the majority of AZA is non-enzymatically converted to 6-MP within a short time (Fig. 5) (Os et al., 1996). Sulfhydryl-containing compounds such as cysteine and glutathione in red blood cells cleave AZA causing an increased release of 6-MP (Elion, 1989; Kundu and Khare, 1999). Afterwards, three enzymes are competitively targeting 6-MP, xanthine dehydrogenase (XDH), thiopurine S-methyltransferase (TPMT), and hypoxanthine guanine phosphoribosyl transferase (HPRT). The latter enzyme plays an important role in the activity of AZA through the formation of 6-MP nucleotides and eventually the active metabolites, thioguanine nucleotides (TGNs) (Van Scoik et al., 1985). Alternatively, 6-MP can be converted to inactive metabolites such as 6-thiouric acid (6-TU) or 6-methylmercaptopurine (6-MMP) by XDH or TPMT, respectively (Sahasranaman et al., 2008). The inactive metabolites and their catalyzing enzymes influence drug activity and toxicity. For example, it has been reported that XDH-inhibitors, namely allopurinol can boost the efficacy of AZA and increase the levels of the active TGNs (Gearry et al., 2010). On

the other hand, patients with TPMT genetic mutations develop severe complications after treatment with standard doses of AZA (Mhanna et al., 2019; Park et al., 2009; Steponaitiene et al., 2016; Yang et al., 2019). Therefore, determination of TPMT genotype and activity is recommended to determine safe dose (Dean, 2020). Additionally, polymorphisms in nudix hydrolase 15 (*NUDT15*) gene which catalyzes the conversion of cytotoxic thioguanine triphosphate (TGTP) to the non-toxic thioguanine monophosphate (TGMP) are associated with AZA-induced leukopenia (Miao et al., 2021).

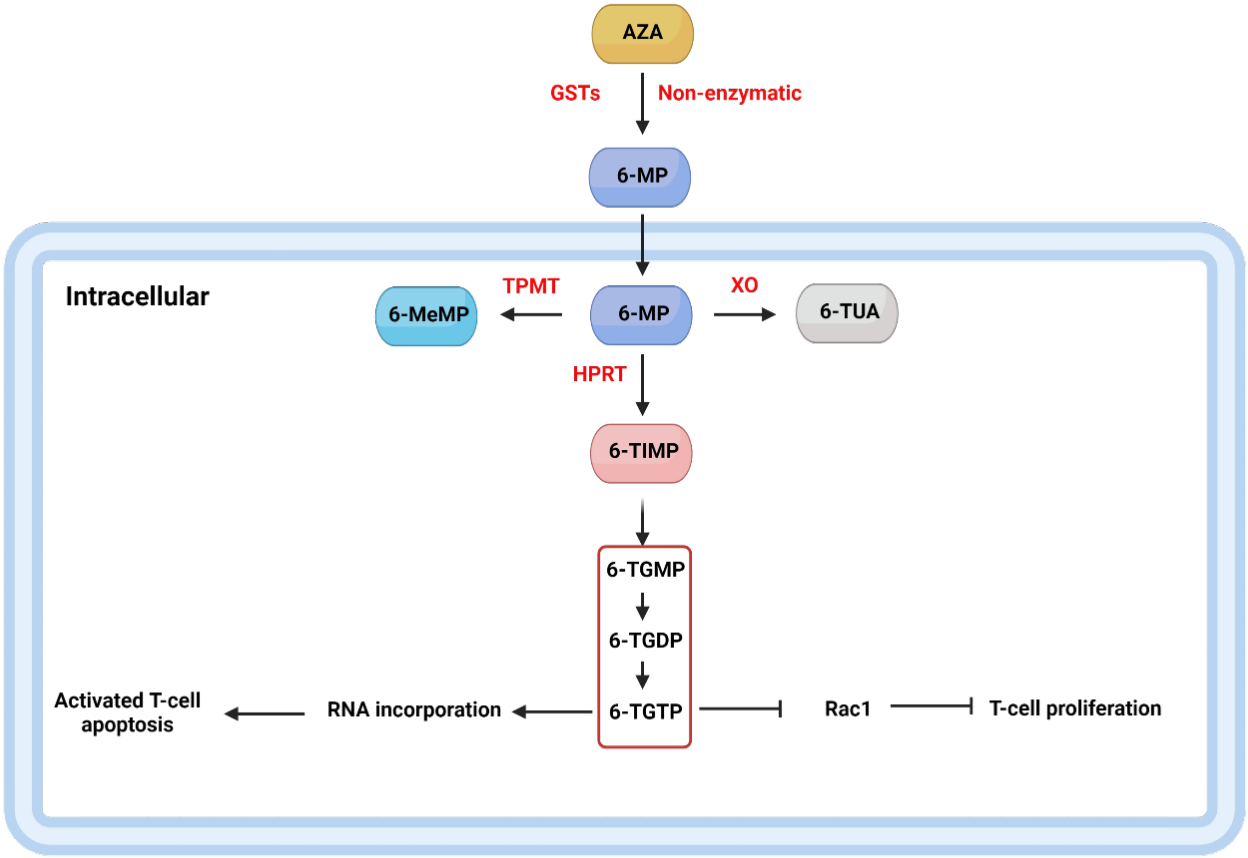

Figure 5. Azathioprine metabolism. After the rapid conversion of AZA to 6-MP, 3 major enzymes target 6-MP. First, HPRT catalyzes the formation of TIMP which is further metabolized to form active thioguanine nucleotides. Immunosuppressive effects of AZA are largely due to thioguanine nucleotides. The second enzyme is TPMT which drives the formation of MeMP. The conversion into TUA is catalyzed by the thirde enzyme XO. AZA: azathioprine; 6-MP: 6-mercaptopurine; 6-TUA: 6-thiouric acid; 6-TIMP: 6-thioinosine monophosphate; 6-TGMP: 6-thioguanine monophosphate; 6-TGDP: 6-thioguanine diphosphate; 6-TGTP: 6-thioguanine triphosphate; 6-MeMP: 6-methyl mercaptopurine; GSTs: glutathione S-transferases; HPRT: hypoxanthine phosphoribosyltransferase; TPMT: thiopurine S-methyltransferase; XO: xanthine oxidase. Designed with Biorender.com

1.3.2 Mechanism of action

The impact of AZA on immune cells has been extensively investigated. Several studies have highlighted the strong cytotoxic effects of AZA metabolites, thioinosine monophosphate (6-TIMP) and its methylated form (MeTIMP) by inhibiting purine *de novo* synthesis (PDNS) (MCCOLLISTER et al., 1964; Tay et al., 1969). The aforementioned metabolites target phosphoribosyl pyrophosphate amidotransferase (PRPP) which catalyzes the first reaction in PDNS. Phosphoribosylamine generated from the first step of PDNS will eventually yield inosine monophosphate (IMP), a crucial compound which is believed to be at the center of PDNS (Winkelstein, 1979). In addition, 6-TIMP inhibits the conversion of IMP to adenylosuccinic acid and xanthylic acid, the precursors of adenine monophosphate (AMP) and guanine monophosphate (GMP) (SALSER et al., 1960). Cara *et al* suggested that AZA acts through creating a balance between anti-metabolic and pro-apoptotic effects (Cara CJ, Pena AS, Sans M, Rodrigo L, Guerrero-Esteo M, Hinojosa J, García-Paredes J, 2004). 6-thioguanine nucleotides (6-TGNs), the end products of 6-TIMP, enters the nucleus and incorporates mainly into DNA as fraudulent bases (Karran, 2006). As a result of this incorporation, DNA mismatch repair (MMR) system is activated leading to cell death (Brem and Karran, 2012). Moreover, van Furth et al showed that AZA is interfering with mitotic activity by arresting cells at S and G_2 phases (van Furth et al., 1975). Cell cycle of AZA-treated premonocytes was 5.5 h longer than untreated cells (van Furth et al., 1975). Targeting Rac1 has been reported to be another facet of Azathioprine-induced apoptosis (Tiede et al., 2003). Specifically, AZA metabolite, 6-thioguanine triphosphate (6-TGTP) binds to Rac1, an important modulator of T-cell proliferation, and abrogates anti-apoptotic signal generated by bcl-xl (Tiede et al., 2003). Furthermore, this coupling leads to the accumulation of 6-thioguanine diphosphate (6TGDP)- inactive Rac complex which in turn represses T cell–APC conjugation (Poppe et al., 2006).

1.3.3 Azathioprine and Crohn`s disease

Utilizing AZA against Crohn`s disease was first mentioned in 1969 (Brooke et al., 1969). Six CD patients who were resistant to conventional therapy showed significant improvement and remarkable healing upon 10-day course of AZA (4 mg/kg daily), followed by a daily maintenance dose of 2 mg/kg (Brooke et al., 1969). Nowadays, there are two major indications of AZA in CD treatment; remission and postoperative

maintenance ("Azathioprine: Drug information - UpToDate," n.d.). Despite the extensive use of thiopurines in IBD, available studies are inconclusive. Several guidelines recommend the induction of remission by combination therapy of AZA (1.5-2.5 mg/kg/day) and an anti-TNF drug (eg, infliximab) (Lichtenstein et al., 2018; Mayberry et al., 2013). Recently, a meta-analysis showed the low ability of AZA to induce remission alone when compared to infliximab, and the superiority of combination therapy over infliximab monotherapy (Chande et al., 2016). On the other hand, 48% (95/197) of purine analogues treated patients achieved remission compared to 37% (68/183) of placebo patients (RR 1.23, 95% CI 0.97-1.55). The same study also indicated the strong glucocorticoid-sparing effect of AZA. Sixty-four percent (47/163) of AZA-treated CD patients were able to maintain remission while tapering prednisone dose to < 10 mg/day compared to 46% (32/70) of placebo patients (RR 1.34, 95% CI 1.02 to 1.77) (Chande et al., 2016). Further, 60% (116/194) of patients received combination therapy of AZA and infliximab reached steroid-free remission compared to 48% (91/189) of infliximab only patients (2 studies, 383 patients; RR 1.23, 95% CI 1.02 to 1.47) (Chande et al., 2016). In another meta-analysis, AZA is shown to be superior over placebo in the induction and maintenance of remission (OR, 3.5; 95% Crl, 1.4-8.9) (Rui et al., 2021). However, similar to what was reported by Chande *et al*, AZA + infliximab is more powerful than AZA alone (OR, 7.0; 95% Crl, 1.2-41.0) (Rui et al., 2021). Furthermore, a Cochrane review of 10 randomized controlled trials (RCTs) with a total of 928 participants suggested that AZA and 6-MP are effective in the maintenance of surgically-induced remission (Gjuladin-Hellon et al., 2019). Clinical relapse was registered in 51% (109/215) of AZA/6-MP group while it reached 64% (124/193) of the placebo group (RR 0.79; 95% CI 0.67 to 0.92). However, these data are based on moderate certainty evidence. Data from one trial indicated the decrease in endoscopic relapse upon AZA treatment in comparison with mesalazine (65% (11/17) of AZA group vs. 83% (15/18) of mesalazine group, RR 0.78; 95% CI 0.52 to 1.17) (Savarino et al., 2013).

1.3.4 Azathioprine and intestinal epithelial cells

The number of studies focusing on the effect of AZA on intestinal epithelial cells differentiation and proliferation is scarce. Schroll *et al* demonstrated the anti-proliferative activity of AZA in intestinal epithelial cells *in vitro* (Schroll et al., 2005). AZA-treated Caco-2 and IEC-6 cell lines showed a dose-dependent decrease in their

proliferation rate after 24h incubation (Schroll et al., 2005). Nevertheless, AZA-induced apoptosis varied in different cell lines. Specifically, AZA induced apoptosis in jejunal non-malignant IEC-6, while no effect was observed in colonic cancerous cell lines (Caco-2, HT29 and T-84). Additionally, cell cycle arrest occurred in AZA-treated HT29 but not in the other treated cell lines indicating a cell type specific response. In another study, gene expression of AZA-treated Caco-2 was compared to tissue harvested from CD patients (Dooley et al., 2004). Investigators identified metallothioneins (MTs) to be regulated in CD patients as well as AZA-treated Caco-2 cells in an anti-correlation manner (Dooley et al., 2004). MTs are involved in controlling inflammation and the protein level of MT-2, for example, was reported to be correlated with CD severity (Socha-Banasiak et al., 2021; Starr et al., 2017).

Swidsinski *et al.* explored the effect of AZA on intestinal mucosal barrier (Swidsinski et al., 2007). AZA-treated colitis patients showed a drastic decrease in the number of mucosal leukocytes in comparison with other colitis groups (Swidsinski et al., 2007). Further, investigators in this study revealed that AZA also influenced the number of mucosal bacteria. A significant rise in bacteria present in the mucus layer was reported in AZA-treated patients. Nevertheless, this effect was dampened when patients were treated with combination therapy of mesalamine and AZA or mesalamine alone. The mucus layer thickness was not altered in AZA-treated group (Swidsinski et al., 2007).

Since Paneth cell dysfunction is thought to trigger CD, the effect of AZA on PC's secretions was examined (Kübler et al., 2009). Ileal α-defensins (HD 5,6) were not affected by AZA therapy on mRNA levels. However, the total number of AZA-treated patients included in this study was only 10 patients compared to 43 controls, making the conclusion difficult to finalize.

Efficient mitochondrial function is crucial to guard against inflammatory disorders like IBD. Sünderhauf *et al*. demonstrated the colonic downregulation of p32 in UC patients, an important gene for mitochondrial energy maintenance (Sünderhauf et al., 2021). Surprisingly, this negative effect was overcome by AZA treatment. Treating T84 cells, a human carcinoma cell line, with AZA restored epithelial barrier integrity compromised by pro-inflammatory cytokines (Khare et al., 2019). This effect was demonstrated by a significant decrease in paracellular permeability and a rise in transepithelial electrical

resistance. Additionally, it has been shown that AZA can restore epithelial barrier function by influencing genes involved in tight junctions' regulation.

2. Objective

In recent years, the global burden of IBD has been increasing which creates the necessity for a better understanding of its pathogenesis and improving drug therapy. Growing evidence underlines the pivotal role of PCs in the regulation of intestinal homeostasis. Therefore, dysfunctional PCs were reported to be linked to the propagation of CD. The IBD drug market is full of different sorts of medications with various targets. Nonetheless, a comprehensive investigation of the effect of these drugs is still needed. The aim of this study is to examine the effect of one of the earliest existing IBD drugs, AZA. The intestinal epithelium is in a constant state of renewal due to its great capacity for proliferation. It was hypothesized that since AZA possesses a strong anti-proliferative activity, it is capable of improving differentiation while lowering IEC proliferation and hence enhances differentiation or function.

To address this hypothesis, the following aims were generated:

Aim I: Investigating the effect of AZA on IEC proliferation and differentiation by utilizing various intestinal cell lines and 3D-SI organoids

Aim II: Studying the expression pattern of PC markers in ileal tissue from AZA-treated CD patients compared to non-AZA treated CD patients.

Aim III: Unravelling the relationship between PC differentiation and mitochondrial function and the influence of AZA in murine 3D-SI organoids with defective respiratory chain complex V activity.

Aim IV: Examining the influence of dyslipidemia on PC development and function in diet-induced obesity model and assessing the impact of AZA on lipid metabolism by looking into serum samples from AZA-treated CD patients.

3. Materials and Methods

3.1 Materials

Table 2. List of kits

Kit	*Vendor*
Fluitest GLU kit	Analyticon Diagnostics (Lichtenfels, Germany)
Fluitest Triglyceride kit	Analyticon Diagnostics (Lichtenfels, Germany)
Human Lysozyme ELISA Kit (ab267798)	Abcam, Cambridge, UK
InnuPREP RNA Mini Kit 2.0	Analytik Jena AG (Jena, Germany)
L-Lactic Acid (L-Lactate) Assay Kit	Megazyme (Bray, Ireland)
MitoXpress Xtra Oxygen Consumption Assay	Agilent Technologies Inc. (Santa Clara, California, USA)
MycoAlert Mycoplasma Detection Kit	LONZA (Basel, Switzerland)

Table 3. Media composition of cell lines

Cell line	*Medium (Vendor)*
MODE-K	DMEM medium (Thermo Fisher Scientific Inc., Waltham, Massachusetts, USA) + 10% (v/v) FCS + 1: 100,000 (v/v) β-mercaptoethanol + 100 U/ml penicillin, and 100 µg/ml streptomycin
HT-29, Caco-2	DMEM medium (Thermo Fisher Scientific Inc., Waltham, Massachusetts, USA) + 10% (v/v) FCS + 100 U/ml penicillin, and 100 µg/ml streptomycin

Table 4. Media used for intestinal organoids

Medium	*Composition*
Standard medium	IntestiCult™ Organoid Growth Medium (Mouse), STEMCELL Technologies (Vancouver, Canada)

Table 5. List of chemicals

Compound	*Vendor*
2,4-Dinitrophenol (DNP)	Sigma-Aldrich Inc. (St. Louis, Missouri, USA)
2-Mercaptoethanol (≥ 99.0%)	Sigma-Aldrich Inc. (St. Louis, Missouri, USA)
2-Propanol (≥ 99.5%, for synthesis)	Carl Roth GmbH + Co. KG (Karlsruhe, Germany)
3,3′,5,5′-Tetramethylbenzidine (TMB) single solution	Thermo Fisher Scientific Inc. (Waltham, Massachusetts, USA)
4′,6-diamidino-2-phenylindole (DAPI)	Sigma-Aldrich Inc. (St. Louis, Missouri, USA)
Acetic acid (100%, extra pure)	Carl Roth GmbH + Co. KG (Karlsruhe, Germany)
Agarose LE	Biozym Scientific GmbH (Hessisch Oldendorf, Germany)
Aquatex® mounting solution	Merck KGaA (Darmstadt, Germany)

B-27™ Supplement (50x), serum-free	Gibco, Thermo Fisher Scientific Inc. (Waltham, Massachusetts, USA)
Bacto™ Agar	BD Biosciences (San José, California, USA)
Blocking solution with goat serum	GeneTex (Irvine, California, USA)
Bovine Serum Albumin (BSA) Fraction V	AppliChem GmbH (Darmstadt, Germany)
Casein	Carl Roth GmbH + Co. KG (Karlsruhe, Germany)
CHIR99021	STEMCELL Technologies (Vancouver, Canada)
Chloroform	Carl Roth GmbH + Co. KG (Karlsruhe, Germany)
Citrate Buffer, pH 6.0, 10x	Sigma-Aldrich Inc. (St. Louis, Missouri, USA)
CryoStor® CS10	STEMCELL Technologies (Vancouver, Canada)
DAB+ chromogen substrate system	Dako (Jena, Germany)
Dimethyl sulfoxide (DMSO)	Sigma-Aldrich Inc. (St. Louis, Missouri, USA)
DNA Gel Loading Dye (6x)	Thermo Fisher Scientific Inc. (Waltham, Massachusetts, USA)
dNTP-Set peqGOLD (dATP, dCTP, dGTP, dTTP, 100 mM)	VWR International LLC. (Radnor, Pennsylvania, USA)
Dual endogenous enzyme block	Dako (Jena, Germany)
Dulbecco's Phosphate Buffered Saline (DPBS) (without calcium and magnesium)	Sigma-Aldrich Inc. (St. Louis, Missouri, USA)
Epidermal Growth Factor from murine submaxillary gland (mEGF)	Merck KGaA (Darmstadt, Germany)
Ethanol absolute, EMPLURA®	Merck KGaA (Darmstadt, Germany)
Ethanol denatured (≥ 99.8%)	Carl Roth GmbH + Co. KG (Karlsruhe, Germany)
Fetal bovine serum (FBS)	Thermo Fisher Scientific Inc. (Waltham, Massachusetts, USA)
Fibrinogen, Human Plasma	Merck KGaA (Darmstadt, Germany)
Fixable viability dye eFluor 780	Thermo Fisher Scientific Inc. (Waltham, Massachusetts, USA)
Formaldehyde solution 4.5%	Th. Geyer GmbH & Co. KG (Renningen, Germany)
Geltrex™ LDEV-free basement membrane matrix with reduced growth factor	Gibco, Thermo Fisher Scientific Inc. (Waltham, Massachusetts, USA)
GeneRuler 100 bp DNA Ladder	Thermo Fisher Scientific Inc. (Waltham, Massachusetts, USA)
Gentle Cell Dissociation Reagent (GCDR)	STEMCELL Technologies (Vancouver, Canada)
Glucose Solution (D-Glucose at 200 g/l)	Thermo Fisher Scientific Inc. (Waltham, Massachusetts, USA)
Glycerine (anhydrous puriss., ≥ 99.0%)	Th. Geyer GmbH & Co. KG (Renningen, Germany)

HEPES (N-2-hydroxyethylpiperazine-N-2-ethane sulfonic acid), 1M	Gibco, Thermo Fisher Scientific Inc. (Waltham, Massachusetts, USA)
Carl Zeiss™ Immersion Oil Immersols	Carl Zeiss AG (Jena, Germany)
Lipoproteins, Low Density, Human Plasma	Calbiochem, Merck KGaA (Darmstadt, Germany)
Matrigel® Basement Membrane Matrix, LDEV-free, Phenol Red-Free	Corning Inc. (Corning, New York, USA)
Mayer's hemalum solution	Merck KGaA (Darmstadt, Germany)
MEM Non-Essential Amino Acids Solution (100X)	Thermo Fisher Scientific Inc. (Waltham, Massachusetts, USA)
Methanol (≥ 99%)	Carl Roth GmbH + Co. KG (Karlsruhe, Germany)
Midori Green Advance	Nippon Genetics Europe GmbH (Düren, Germany)
Millipore Immobilon® Western Chemiluminescent HRP Substrate	Merck KGaA (Darmstadt, Germany)
Mowiol 4-88	Carl Roth GmbH + Co. KG (Karlsruhe, Germany)
Mouse serum (fraction)	Dako (Jena, Germany)
N-2 Supplement (100X)	Gibco, Thermo Fisher Scientific Inc. (Waltham, Massachusetts, USA)
N-Acetylcysteine	Sigma-Aldrich Inc. (St. Louis, Missouri, USA)
Neutral Red (≥ 90%)	Sigma-Aldrich Inc. (St. Louis, Missouri, USA)
Non-fat dried milk powder	AppliChem GmbH (Darmstadt, Germany)
Palmitic acid	Sigma-Aldrich Inc. (St. Louis, Missouri, USA)
Paraplast Plus® (Paraffin)	Carl Roth GmbH + Co. KG (Karlsruhe, Germany)
Paraformaldehyde	Merck KGaA (Darmstadt, Germany)
Penicillin/Streptomycin (100x)	Th. Geyer GmbH & Co. KG (Renningen, Germany)
PerfeCTa SYBR Green FastMix	Quanta BioSciences Inc. (Gaithersburg, Maryland, USA)
Phosphatase Inhibitor Cocktail III (DMSO solution)	Sigma-Aldrich Inc. (St. Louis, Missouri, USA)
Phosphatase Inhibitor Cocktail II	Th. Geyer GmbH & Co. KG (Renningen, Germany)
Precision Plus Protein™ Dual Color Standards	Bio-Rad Laboratories Inc. (Hercules, California, USA)
Protease Inhibitor Cocktail (DMSO solution)	Sigma-Aldrich Inc. (St. Louis, Missouri, USA)
Restore™ Plus Western Blot Stripping Buffer	Thermo Fisher Scientific Inc. (Waltham, Massachusetts, USA)
RiboLock RNase Inhibitor (40 U/µl)	Thermo Fisher Scientific Inc. (Waltham, Massachusetts, USA)
Roti®-Quant universal (reagents 1 and 2)	Carl Roth GmbH + Co. KG (Karlsruhe, Germany)

Sodium azide (NaN_3) (≥ 99.5%)	Sigma-Aldrich Inc. (St. Louis, Missouri, USA)
Thrombin, Human Plasma	Merck KGaA (Darmstadt, Germany)
Tris	Merck KGaA (Darmstadt, Germany)
Tris ultrapure	AppliChem GmbH (Darmstadt, Germany)
Trypan Blue solution (0.4%)	Sigma-Aldrich Inc. (St. Louis, Missouri, USA)
Tween® 20	AppliChem GmbH (Darmstadt, Germany)
UltraPureTM DNase/RNase-free distilled water	Thermo Fisher Scientific Inc. (Waltham, Massachusetts, USA)

Table 6. List of buffers

Buffer	***Composition***
Blotting buffer (10x)	0.25 M Tris 1.92 M Glycine
Blotting buffer (1x) + Methanol	10% Blotting buffer (10x) 20% Methanol *ad* ddH_2O
Citrate buffer, pH 6.0	2.1% *w/v* Citric acid *ad* ddH_2O
Denaturing lysis buffer (DLB) (2x), pH 7.4	20 mM Tris 2% SDS *ad* ddH_2O
Electrophoresis buffer (5x)	1.25 mM Tris 960 mM Glycine 0.5% SDS *ad* ddH_2O
Embedding medium	75 µl thrombin 375 µl Casein 200 µl fibrinogen (25 mg/ml)
Mowiol mounting media, pH 8.5	0.2 M Tris-HCL buffer, pH 8.5 12 g Mowiol in 30 ml ddH_2O Mix Mowiol solution and Tris-HCL buffer 1:2 Stear 45 min at 90°C, cool to 50°C 26,7% fluorescent free glycerin
Native lysis buffer (NLB) (1x), pH 7.4	1 mM EDTA 20 mM Tris 150 mM NaCl
Neutral Red destain solution	50% Ethanol (≥ 99.8%) 1% Acetic acid (100%) *ad* ddH_2O
Neutral Red stock solution (0.4%)	40 mg Neutral Red 10 ml 1x PBS
Paraformaldehyde (PFA) fixation buffer, pH 7,4	4% PFA *ad* ddH_2O, 60°C until dissolved
PEN buffer	20 mM Na2HPO4 650 mM NaCl 1 mM EDTA 1mM PMSF
RSB Buffer	10 mM Tris, pH 7.4 10 mM NaCl

	1.5 mM MgCl2 10 mM Sodium fluoride (NaF) 1:100 Phosphatase Inhibitor Cocktail II
SDS buffer (5x) + 10% 2-Mercaptoethanol	1563 µl Tris (1 M, pH 6.8) 2500 µl Glycerine (≥ 99.0%) 500 µl 2-Mercaptoethanol 0.5 g SDS 437 µl ddH_2O Bromophenol blue sodium salt (spatula tip)
Stripping buffer with 2-Mercaptoethanol	2% SDS 62.5 mM Tris 0.5% 2-Mercaptoethanol *ad* ddH_2O
TAE buffer (50x), pH 8	1M Tris 5.7% v/v Acetic acid (100%) 0.5 M EDTA *ad* ddH_2O
TBS buffer (10x)	200 mM Tris 1.4 M NaCl *ad* ddH_2O
T-TBS buffer (1x)	TBS (10x) *ad* ddH_2O 0.1% Tween 20

Table 7. List of instruments

Instrument	***Vendor***
Accu-jet® pro pipetting aid	BRAND GmbH + Co. KG (Wertheim, Germany)
Accurpette pipetting aid	VWR International LLC. (Radnor, Pennsylvania, USA)
Attune NxT Flow Cytometer	Thermo Fisher Scientific Inc. (Waltham, Massachusetts, USA)
Autoclave VX-75	Systec GmbH (Linden, Germany)
Axio Scope.A1 microscope Axiocam 503 color microscope camera	Carl Zeiss AG (Oberkochen, Germany)
BarnsteadTM GenPureTM Pro UV/UF – TOC system for bidistilled water	Thermo Fisher Scientific Inc. (Waltham, Massachusetts, USA)
Bottle-top dispenser CalibrexTM 520 (10 ml)	Socorex Isba S.A. (Ecublens, Switzerland)
Centrifuge MC 6	Sarstedt AG & Co. KG (Nümbrecht, Germany)
Centrifuge Sigma 2K 15	Sigma Laborzentrifugen GmbH (Osterode am Harz, Germany)
ChemiDocTM XRS+ Imaging System	Bio-Rad Laboratories Inc. (Hercules, California, USA)
CriterionTM Cell 135BR gel electrophoresis system	Bio-Rad Laboratories Inc. (Hercules, California, USA)
Electrophoresis power supply 3000Xi	Bio-Rad Laboratories Inc. (Hercules, California, USA)
Film sealing device FS 3604	SEVERIN Elektrogeräte GmbH (Sundern, Germany)
Fluorometer Quibit 2.0	Thermo Fisher Scientific Inc. (Waltham, Massachusetts, USA)
FormaTM Steri-CycleTM i160 CO2 Incubator	Thermo Fisher Scientific Inc. (Waltham, Massachusetts, USA)
Freezers (- 20 °C)	Liebherr-International AG (Bulle, Switzerland) Robert Bosch GmbH (Gerlingen, Germany) Siemens (München, Germany)

Freezers (- 80 °C)	Liebherr-International AG (Bulle, Switzerland) Sanyo Electric Co. Ltd. (Watford, United Kingdom)
Gel documentation system Quantum ST4	Vilber Lourmat Deutschland GmbH (Eberhardzell, Germany)
Glassware (bottles, Erlenmeyer flasks)	DWK Life Sciences GmbH (Wertheim, Germany)
Gyratory rocker SSL3	Cole-Parmer Instrument Company, LLC. (Vernon, Illinois, USA)
Heraeus Multifuge X3 FR	Thermo Fisher Scientific Inc. (Waltham, Massachusetts, USA)
Hotplate Stirrer RT2 Basic	Thermo Fisher Scientific Inc. (Waltham, Massachusetts, USA)
Ice Machine UFF-0350A	Manitowoc Ice Inc. (Manitowoc, Wisconsin, USA)
Incubator Heracell™ VIOS 160i	Thermo Fisher Scientific Inc. (Waltham, Massachusetts, USA)
Incubator INCU-Line®	VWR International LLC. (Radnor, Pennsylvania, USA)
Incubator Heratherm	Thermo Fisher Scientific Inc. (Waltham, Massachusetts, USA)
Inverted microscope Primovert	Carl Zeiss AG (Oberkochen, Germany)
Laminar flow cabinet NU-425-600E (Class II Type A/B3)	NuAire Inc. (Plymouth, Minnesota, USA)
Liquid nitrogen tank LocatorTM 8 Plus	Thermo Fisher Scientific Inc. (Waltham, Massachusetts, USA)
Microcentrifuge, MiniStar silverline	VWR International LLC. (Radnor, Pennsylvania, USA)
Microplate Reader SpectraMax® iD3	Molecular Devices, LLC. (San José, California, USA)
Microtome Hn-40	Jung (Heidelberg, Germany)
Microwave HMT702C	Robert Bosch GmbH (Gerlingen, Germany)
Minishaker MS1 and MS2	IKA Werke GmbH & Co. KG (Staufen im Breisgau, Germany)
MiSeq™-System	Illumina (San Diego, California, USA)
Multifuge X3R	Thermo Fisher Scientific Inc. (Waltham, Massachusetts, USA)
Multipette® M4	Eppendorf AG (Hamburg, Germany)
Multipette® plus repetitive pipette	Eppendorf AG (Hamburg, Germany)
Multi-Tube Vortexer	SMI
NalgeneTM Cryo 1 °C Freezing Container	Thermo Fisher Scientific Inc. (Waltham, Massachusetts, USA)
NalgeneTM Cryogenic Storage Boxes	Thermo Fisher Scientific Inc. (Waltham, Massachusetts, USA)
NanoDropTM 2000c Spectrophotometer	Thermo Fisher Scientific Inc. (Waltham, Massachusetts, USA)
Neubauer-improved counting chamber	Paul Marienfeld GmbH & Co. KG (Lauda-Königshofen, Germany)
NucleoBondTM Xtra Combi Rack	Macherey-Nagel GmbH & Co. KG (Düren, Germany)
Orbital microplate shaker Type HKS 250	Behring Shaker Optoelectronic Control (Germany)
Orbital shaker TCR 170	Heidolph Instruments GmbH & Co. KG (Schwabach, Germany)
OwlTM EasyCastTM horizontal electrophoresis system (models B1A and B2) with trays and combs	Thermo Fisher Scientific Inc. (Waltham, Massachusetts, USA)
pH meter pH3110	WTW GmbH (Weilheim, Germany)

+ pH electrode SenTix® 41	
Piston-operated pipettes Research® plus (0.5 – 10 µl, 10 – 100 µl, 100 – 1,000 µl)	Eppendorf AG (Hamburg, Germany)
PowerPacTM Basic Power Supply	Bio-Rad Laboratories Inc. (Hercules, California, USA)
Precellis® 24 homogenizer	Bertin Instruments (Montigny-le-Bretonneux, France)
Precision scales ABS 120-4	KERN & SOHN GmbH (Balingen, Germany)
Precision scales PFB 200-3	KERN & SOHN GmbH (Balingen, Germany)
Refrigerators	Liebherr-International AG (Bulle, Switzerland) Robert Bosch GmbH (Gerlingen, Germany)
Rocking platform Mini Rocker	Bio-Rad Laboratories Inc. (Hercules, California, USA)
Seahorse XF24 analyzer	Agilent (Santa Clara, California, USA)
Shaking incubator MaxQTM 4000	Thermo Fisher Scientific Inc. (Waltham, Massachusetts, USA)
Sigma 1-14 centrifuge	Sigma Laborzentrifugen GmbH (Osterode am Harz, Germany)
Single channel pipettes, Ultra High-Performance (0.5 – 10 µl, 10 – 100 µl, 100 – 1,000 µl)	VWR International LLC. (Radnor, Pennsylvania, USA)
Sonorex RK 102 Transistor	BANDELIN electronic GmbH & Co. KG (Berlin, Germany)
Standard Power Pack P25 Power Supply	Biometra GmbH (Göttingen, Germany)
Steamer	Braun (Kronberg in Taunus, Germany)
StepOnePlus Real-Time PCR System	Thermo Fisher Scientific Inc. (Waltham, Massachusetts, USA)
Stereo microscope Leica S6 E + Leica KL300 LED fiber optic light source	Leica Microsystems GmbH (Wetzlar, Germany)
Thermoblock Biometra® TB1	Biometra GmbH (Göttingen, Germany)
Thermocycler T1	Biometra GmbH (Göttingen, Germany)
Thermocycler TGradient	Biometra GmbH (Göttingen, Germany)
Thermomixer Compact	Eppendorf AG (Hamburg, Germany)
Trans-Blot® SD Semi-Dry Transfer Cell	Bio-Rad Laboratories Inc. (Hercules, California, USA)
Transferpette® -8 (30 – 300 µl)	BRAND GmbH + Co. KG (Wertheim, Germany)
Vortex Mixer Advanced ZX3	VELP Scientifica Srl (Usmate, Italy)
Vortex mixer REAX 2000	Heidolph Instruments GmbH & Co. KG (Schwabach, Germany)
Vortex-Genie 2	Scientific Industries Inc. (Bohemia, New York, USA)
Waterbath Type 1007	Gesellschaft für Labortechnik (GFL) mbH (Burgwedel, Germany)
Waterbath Type 3048	Köttermann GmbH & Co. KG (Uetze, Germany)
Waterbath WNB 29	Memmert GmbH & Co. KG (Schwabach, Germany)

Table 8. List of consumables

Product	***Vendor***
96 fast PCR Plate half skirt	Sarstedt AG & Co. KG (Nümbrecht, Germany)
96-Well Assay Plates Costar® (black, clear bottom, with lid, tissue culture treated)	Corning Inc. (Corning, New York, USA)
Acetate Foils for 96-Well Plates	Sarstedt AG & Co. KG (Nümbrecht, Germany)
AmershamTM HybondTM PVDF blotting membrane (0.2 µm)	GE Healthcare (Chicago, Illinois, USA)

Bacillol® AF surface disinfectant	Bode Chemie GmbH (Hamburg, Germany)
Biosphere® Filter Tips (0.1 – 20 µl, 2 – 100 µl, 100 – 1000 µl)	Sarstedt AG & Co. KG (Nümbrecht, Germany)
Blot filter paper (extra thick, 19.0 x 18.5 cm)	Bio-Rad Laboratories Inc. (Hercules, California, USA)
Cannulae Sterican® (20 G, 24 G, 26 G)	B. Braun Melsungen AG (Melsungen, Germany)
CELLSTAR® Cell Culture Multiwell, 24-well	Greiner Bio-One (Frickenhausen, Germany)
Combitips advanced® (5 ml, 1 ml, 0.2 ml)	Eppendorf AG (Hamburg, Germany)
Combitips advanced® Eppendorf Biopur® (sterile) (5 ml)	Eppendorf AG (Hamburg, Germany)
Costar® 24-well Clear TC-treated Multiple Well Plates, Individually Wrapped, Sterile	Corning Inc. (Corning, New York, USA)
Cover glasses, 24x32 mm	Th. Geyer GmbH & Co. KG (Renningen, Germany)
Cover glasses, Haemacytometer	Th. Geyer GmbH & Co. KG (Renningen, Germany)
CriterionTM TGXTM 4 – 15% Precast Midi Protein Gel (18 well, 30 µl and 26 well, 15 µl)	Bio-Rad Laboratories Inc. (Hercules, California, USA)
CryoPure tubes (1.0 ml, white)	Sarstedt AG & Co. KG (Nümbrecht, Germany)
Falcon® 70 µm Cell Strainer	Corning Inc. (Corning, New York, USA)
Filtropur S 0.2 syringe filtration unit (pore size 0.2 µm)	Sarstedt AG & Co. KG (Nümbrecht, Germany)
Gel Releaser	Bio-Rad Laboratories Inc. (Hercules, California, USA)
Injekt®-F single-use syringes (1 ml)	B. Braun Melsungen AG (Melsungen, Germany)
Micro tubes (1.5 ml, 2.0 ml)	Sarstedt AG & Co. KG (Nümbrecht, Germany)
Micro tubes (1.5 ml, 2.0 ml) (Sterile, DNase/RNase free)	Sarstedt AG & Co. KG (Nümbrecht, Germany)
MicroAmpTM Optical Adhesive Film (for 384- or 96-Well Plates)	Thermo Fisher Scientific Inc. (Waltham, Massachusetts, USA)
Microtest plate (96 Well, canonical bottom)	Sarstedt AG & Co. KG (Nümbrecht, Germany)
Microtest Plates 96 Well, F	Sarstedt AG & Co. KG (Nümbrecht, Germany)
MICRO-TOUCH® Nitra-Tex® nitrile gloves (powder-free)	Ansell Ltd. (Yarra City, Australia)
Mini-Protean® Cassette Opening Lever	Bio-Rad Laboratories Inc. (Hercules, California, USA)
Multiply®-µStrip Pro 4-strips (0.2 ml tubes, DNase/RNase free)	Sarstedt AG & Co. KG (Nümbrecht, Germany)
Multitex® Wipes	Zellstoff-Vertriebs-GmbH & Co. KG (Troisdorf, Germany)
Parafilm® M	Carl Roth GmbH + Co. KG (Karlsruhe, Germany)
Pipette tips with microcapillary for loading gels (1 – 200 µl)	VWR International LLC. (Radnor, Pennsylvania, USA)
Pellet Pestle™	Kimble Chase, Life Science (Vineland, New Jersey, USA)
Pipette tips without filter (10 – 200 µl)	Th. Geyer GmbH & Co. KG (Renningen, Germany)
Pipette tips without filter (10 µl, 1000 µl)	Sarstedt AG & Co. KG (Nümbrecht, Germany)
Plastic film (transparent, 0.1 mm)	Th. Geyer GmbH & Co. KG (Renningen, Germany)
Protran® BA83 nitrocellulose membrane (0.2 µm)	Whatman GmbH (Dassel, Germany)
RNaseZapTM RNase Decontamination Wipes	Thermo Fisher Scientific Inc. (Waltham, Massachusetts, USA)
Rodent Diet With 60 kcal% Fat (D12492i)	Research Diets, Inc. (NJ, USA)
Serological pipettes (sterile) (5 ml, 10 ml, 25 ml, 50 ml)	Sarstedt AG & Co. KG (Nümbrecht, Germany)
Slides, Menzel Superfrost®	Thermo Fisher Scientific Inc. (Waltham, Massachusetts, USA)

Staining Jars	Carl Roth GmbH + Co. KG (Karlsruhe, Germany)
Sterillium® classic pure hand disinfectant	Bode Chemie GmbH (Hamburg, Germany)
Syringe with BD Luer-LokTM Tip	Becton, Dickinson & Company (Franklin Lakes, New Jersey, USA)
TC dishes 100 (standard)	Sarstedt AG & Co. KG (Nümbrecht, Germany)
Tissue culture flasks (T25, T75) (Cell+, Vented Cap)	Sarstedt AG & Co. KG (Nümbrecht, Germany)
Tissue culture plates (96 Well, Cell+, F)	Sarstedt AG & Co. KG (Nümbrecht, Germany)
Tissue embedding cassettes	Carl Roth GmbH + Co. KG (Karlsruhe, Germany)
Transfer pipettes (3 ml)	Sarstedt AG & Co. KG (Nümbrecht, Germany)
Tubes (15 ml, 50 ml)	Sarstedt AG & Co. KG (Nümbrecht, Germany)

Table 9. List of software

Software	***Vendor***
ImageJ	National Institutes of Health (NIH) (Bethesda, Maryland, USA)
ImageLab™	Bio-Rad Laboratories Inc. (Hercules, California, USA)
NanoDrop 2000/2000c	Thermo Fisher Scientific Inc. (Waltham, Massachusetts, USA)
Quantum-Capt software for gel imaging	Vilber Lourmat Deutschland GmbH (Eberhardzell, Germany)
GraphPad Prism 9.0	GraphPad Software Inc. (San Diego, California, USA)
StepOne™ S v2.3	Thermo Fisher Scientific Inc. (Waltham, Massachusetts, USA)
ZEN 2.3 lite	Carl Zeiss AG (Oberkochen, Germany)
FlowJo™ v10	BD Biosciences (Newjersey, USA)
Biorender (https://biorender.com/)	Biorender (Toronto, Canada)

Table 10. List of Databases

Database	***Website***
NCBI (National Center for Biotechnology Information)	https://www.ncbi.nlm.nih.gov/
The human protein atlas	https://www.proteinatlas.org/
Primer BLAST	https://www.ncbi.nlm.nih.gov/tools/primer-blast/

Table 11. List of cell lines

Cell line	***Vendor***
MODE-K	Generated based on the method described by (Vidal et al., 1993)
HT-29	Deutsche Sammlung von Mikroorganismen und Zellkulturen (DSMZ) (Braunschweig, Germany)
Caco-2	Deutsche Sammlung von Mikroorganismen und Zellkulturen (DSMZ) (Braunschweig, Germany)

Table 12. List of oligonucleotides

Target gene (Human)	***Forward primer (5'-3')***	***Reverse primer (5'-3')***
ACTB	ACATCCGCAAAGACCTGTACG	TTGCTGATCCACATCTGCTGG
DEFA5	GGCTACAACCCAGAAGCAGT	CAGCGACAGCAGAGTCTGTA
DEFA6	CACCATCCTCACTGCTGTTCT	GCAATGGCAAGTGAAAGCCC
LYZ	GCCTAGCAAACTGGATGTGT	ATGCCTTGTGGATCACGGAC
UBC	CCGGGATTTGGGTCGCAG	TCACGAAGATCTGCATTGTCAAG
Target gene (Mouse)	***Forward primer (5'-3')***	***Reverse primer (5'-3')***
Atoh1	GTGGGGTTGTAGTGGACGAG	GTTGCTCTCCGACATTGGG
Defa3	CCAGGCTGATCCTATCCAAA	GTCCCATTCATGCGTTCTCT
Glut2	GTCCAGAAAGCCCCAGATACC	GTGACATCCTCAGTTCCTCTTAG
Hes1	CAAACCAAAGACGGCCTCT	GTCACCTCGTTCATGCACTC
Ki67	CCTGCCCGACCCTACAAAAT	TTGCTCACACTCGATGCAGT
Lgr5	CGGCAACAGTGTGGACGACCT	GCGAGCACTGCACCGAGTGA
Muc2	GCTGACGAGTGGTTGGTGAATG	GATGAGGTGGCAGACAGGAGAC
Ubc	GAGCCCAGTGTTACCACCAA	CACACCCAAGAACAAGCACA

Primers were purchased from Metabion international AG (Planegg, Germany)

Table 13. List of primary and secondary antibodies

Primary antibodies	**Host Species**	**Company**	**Working concentration**
Anti-α-Tubulin (#2125)	Rabbit	Cell Signaling (Danvers, Massachusetts, USA)	1:1000 (WB)
Lysozyme (GT1123)	Rabbit	Genetex (Irvine, California, United States)	1:100 (WB) 1:500 (IHC)
Tom20 (D8T4N)	Rabbit	Cell Signaling (Danvers, Massachusetts, USA)	1:1000 (WB)
Mucin 2 (C3)	Rabbit	Genetex (Irvine, California, United States)	1:500 (IHC)
Isotype control	Goat	R&D Systems (Minneapolis, Minnesota, USA)	
Isotype control	Mouse	Biotech (Onsala, Sweden)	

Fluorophore conjugated antibodies	**Species**	**Company**	**Working concentration**
Anti-mouse Pacific Blue™ CD24	Rat	Biolegend (San Diego, USA)	1:100
Pacific Blue™ IgG2b, κ Isotype Ctrl Antibody	Rat	Biolegend (San Diego, USA)	1:100

Secondary antibodies/ labelled polymers	Company	Working concentration
Anti-mouse IgG HRP	Cell Signalling (Danvers, Massachusetts, USA)	1:4000 (WB)
Anti-rabbit IgG HRP	Cell Signalling (Danvers, Massachusetts, USA)	1:4000 (WB)
Anti-goat IgG HRP	Agilent (Santa Clara, California, USA)	1 µg/ml (IHC); 0.5 µg/ml (WB)

3.2 Methods

3.2.1 Study cohort

Tissue biopsies from the terminal ileum were collected by endoscopy from CD patients in the period between 2004-2022 from the medical department I, University Hospital Schleswig-Holstein Campus Lübeck and Clinic and Polyclinic for Internal Medicine I, University Hospital Regensburg. Blood and stool samples were obtained from the University Hospital Schleswig-Holstein Campus Lübeck, the University Hospital Münster, North Rhine-Westphalia, Germany and the University Hospital Rostock, Mecklenburg-Vorpommern. Clinical characteristics of patients included in this cohort are listed in tables 14-18. Samples were collected upon receiving informed consent from each patient. Protocols were approved by the ethics committees of the University of Lübeck (0-073; 03-043; AZ 13/084A; AZ 05-112), the University of Münster (AZ 2016-305-b-S) and the University of Rostock (A 2017-0137).

3.2.2 Cell culture

MODE-K cells, a murine small intestinal cell line (generated based on the method described by Vidal et al., 1993, kindly provided by Prof. Mathias Hornef, Institute of Medical Microbiology, University Hospital RWTH Aachen) were cultured in DMEM medium supplemented with 10% (v/v) heat-inactivated FCS, 0.000001% (v/v) β-mercaptoethanol, 100 U/ml penicillin, and 100 µg/ml streptomycin. Human colonic HT-29 (first derived in 1964 from a 44-year-old White female with colorectal adenocarcinoma, DSMZ, Braunschweig, Germany) and Caco-2 (derived from a 72-year-old White male with colorectal adenocarcinoma, DSMZ) cells were kept in the same medium as MODE-K cells but without the addition of β -mercaptoethanol. Cells were incubated at 37^{o}C, 5% CO_2. Cells were passaged twice weekly and checked monthly for mycoplasma contaminants using MycoAlert Mycoplasma Detection Kit.

For AZA treatment experiments, cells were first treated with a range between 0.1 and 1,000 µM with 1:10 (v/v) dilution for 3 days. DMSO-treated cells were used as controls by mixing the same volume used for AZA-treated cells. DMSO concentration was between 0.0001 and 1% (v/v). Cell viability was determined by neutral red assay. MODE-K cells were treated with 1 µM AZA, and HT-29 and Caco-2 were treated with 10 µM AZA or DMSO (0.001%, v/v) for MODE-K and 0.01% (v/v) for HT-29 and Caco-2) for 3 days after 24h incubation with no treatment. Then, cells and supernatants were

collected and stored at -20°C for further analysis. In another set of experiments, MODE-K were treated with 10 µM 2,4-Dinitrophenol (DNP) in the presence or absence of 1 µM AZA for 2 days. Cells were either seeded in 96-well plates (5,000 cells/well) or 24-well plates at a density of 100,000 cells/well.

3.2.3 Intestinal 3D-organoid culture

Intestinal crypts were generated from the small intestine of *ATP8*-mutant and wild-type C57BL6/J mice (kindly provided by Prof. Saleh Ibrahim, The Lübeck Institute of Experimental Dermatology (LIED), University of Lübeck) using the protocol provided by STEMCELL Technologies. In short, small intestinal fragments from both genotypes were washed several times in cold 1x PBS and then incubated in 25 mL of Gentle Cell Dissociation Reagent (GCDR) at room temperature for 15 min. Several fractions were generated by passing supernatants through 70 µm filters. The quality of each fraction was evaluated using an inverted microscope and fractions with high crypts numbers were selected and centrifuged at 290 x *g* and 4°C for 5 min. Crypts were then resuspended in cold DMEM/F-12 medium, counted and aliquoted into 15 mL tubes in volumes containing 500 – 3,000 crypts and centrifuged at 200 x *g* and 4°C for 5 min. Crypts were resuspended in a 150 µl : 150 µl mixture of complete IntestiCult Organoid Growth Medium and Geltrex reduced growth factor basement membrane matrix or Corning Matrigel Growth Factor Reduced Basement Membrane Matrix. Domes were formed upon adding 50 µL per well of the suspension into pre-warmed 24-well plates. Consequently, domes were solidified by incubating the plate at 37°C for 10 minutes. Domes were overlaid with IntestiCult Organoid Growth Medium and incubated at 37°C, 5% CO_2 for 7 days with medium changes every 2 - 3 days.

3.2.3.1 AZA treatment experiments

B6 and *ATP8*-mutant SI organoids were maintained on IntestiCult Organoid Growth Medium for 4 days. Consequently, medium was exchanged with fresh medium supplemented with DMSO (0.001% v/v) or AZA (1 µM). Organoids were incubated at 37°C, 5% CO_2 for 3 days.

3.2.3.2 Lipid experiments

For lipid treatment experiments, B6 SI organoids were treated with either DMSO (0.3% v/v) or 30 µM palmitic acid (PA) dissolved in IntestiCult Organoid Growth Medium for 7 days with medium exchange on day 2 and 4. On the final day, organoids were counted, harvested and frozen at -20°C until further analysis. In another set of experiments, B6 SI organoids were treated with human LDL-cholesterol (0.5, 1 and 2 µg/ml) or 150mM NaCl, pH 7.4, 0.01% EDTA as a control for 7 days.

3.2.4 Molecular biology methods

3.2.4.1 RNA extraction

Total RNA was isolated from tissue biopsies, cell pellets or organoids using innuPREP RNA Mini Kit according to the manufacturer's protocol. Samples were homogenized in lysis buffer with the addition of 1% (v/v) β-mercaptoethanol. RNA column was incubated with 4 units DNase, 4 µl 10x DNase reaction buffer and 32 µl nuclease-free H_2O for 20 minutes at RT. RNA was eluted with 40 µl nuclease-free H_2O and RNA concentration and quality were determined by Microplate Reader SpectraMax® iD3. Samples were stored at -80 °C until cDNA synthesis.

3.2.4.2 cDNA synthesis

Reaction mixture for cDNA synthesis consisted of the following: 500-1,000 ng RNA, 100 pmol Oligo(dt)18, dNTP Mix (0.2 mM each), 20 U RiboLock RNase inhibitor, and 200 U RevertAid H Minus reverse transcriptase. Mixture was incubated at 42°C for 60 min followed by 70°C for 10 min. samples were diluted 1:5 (v/v) with nuclease free H_2O and stored at -20°C until further analysis.

3.2.4.3 Primer design, PCR and agarose gel electrophoresis

Primers were designed using NCBI primer blast tool based on the following criteria: melting temperature between 57-62 °C, a guanidine and cytosine percentage of 50-60%, a primer size of 18-23 nucleotides and a product size range of 250-500 nucleotides. To test primer specificity, RT-PCR and gel electrophoresis were performed.

cDNA (2 µl) was mixed with 10 µl 2x Dream Taq Master Mix and 0.5 µM primer each in a total volume of 20 µl on ice. PCR conditions consisted of an initial denaturation of

95 °C for 5 min, followed by 35 cycles of 95 °C for 30 sec, 55 °C for 30 sec and 72 °C for 1 min, with final extension of 72 °C for 5 min using TGradient thermocycler.

PCR amplicons were separated at 80 V for 30 min on a 2% (w/v) agarose gel containing 0.004% (v/v) Midori green advanced DNA stain in 1x TAE running buffer. Samples were mixed with 6x Tritrack DNA loading buffer and loaded into the wells. The first well was reserved for Generuler 100 bp DNA ladder. Bands were visualized using ChemiDoc XRS+ Imaging System.

3.2.4.4 Quantitative Polymerase Chain Reaction (qPCR)

Target genes were amplified on StepOne real-time system by mixing cDNA (2 µl) with 18 µl reaction mixture containing 10 µl Perfecta SYBR Green Supermix and 0.5 µM forward and reverse primer (Table.12) and 7.5 µl PCR water. Cycling conditions were in the following order using StepOnePlus Real-Time PCR System: an initial denaturation of 95°C for 5 min, followed by 40 cycles of 95°C for 45 sec, 55°C for 30 sec and elongation at 72°C for 30 sec. Consequently, melting curves were obtained by the following cycling conditions: 95°C for 15 sec, 60°C for 20 sec and 95°C for 15 sec. Ct values of targets were normalized to β-actin or ubiquitin C (UBC) expression.

3.2.5 Biochemical methods

3.2.5.1 Protein isolation

Human stool samples (0.01-0.1 g) were mixed in PEN buffer (Table. 6). Mixture was then centrifuged at 15,000 x *g* and 4°C for 10 min. Sodium azide was added to the supernatants (0.045%, v/v). Proteins were extracted from cell pellets by resuspension in 100-150 µl of denaturing lysis buffer (DLB) with the addition of 1% (v/v) protease inhibitor and 2% (v/v) phosphatase inhibitor II and III, each. Samples were heated at 100°C for 5 min, shortly cooled on ice followed by two times ultrasound sonication step for 20 sec. Suspensions were spun down for 15 min at 12,000 x *g* at 4°C. Protein concentration in supernatants was quantified according to Bradford by rotiquant assay. OD was measured at 490 nm against a reference wavelength of 690 nm on a microplate reader and concentrations were calculated using a BSA standard curve. Protein samples were stored at - 20°C until further analysis.

3.2.5.2 SDS-PAGE and immunoblotting

Protein samples (15-40 µg) were mixed with a reducing 5x SDS buffer containing 10% β-mercaptoethanol, heated for 5 min at 95°C and shortly cooled on ice. Then, samples were loaded onto a 4-15% precast polyacrylamide gel. Proteins were separated according to size by gel electrophoresis in 1x TAE buffer at 230 V for 30 min. Prior to assembly of transfer, methanol-activated 0.2 µm polyvinylidene difluoride (PVDF) membranes as well as blotting paper were soaked in blotting buffer for 10 min. Membrane transfer was performed in a semi-dry blotting system for 1 hour at 100 mA at RT. Layers of the transfer sandwich were assembled in the following order from the cathode: 2 sheets of blotting paper, followed by the polyacrylamide gel, PVDF membrane and another two layers of blotting paper. After blotting, membranes were blocked in 5% w/v non-fat milk in Tween-TBS (T-TBS) for 1 hour at RT. Diluted primary antibodies (Table 13) in 5% non-fat milk or 5% BSA in T-TBS were applied to membranes and incubated at 4°C overnight. Membranes were washed two times for 20 min in T-TBS buffer. Membranes were incubated with horse-radish peroxidase (HRP) conjugated secondary antibodies (Table 13) for 1 hour at RT. Another 2 rounds of washing with T-TBS were performed. Finally, HRP substrate solution was evenly distributed on membranes and chemiluminescence was detected under UV light in the ChemiDocTM XRS+ imaging system using the ImageLab™ software.

For stripping and reprobing, membranes were either incubated with a self-made stripping buffer, containing β-mercaptoethanol, for 20 min at 56°C or with a ready-to-use buffer for 15 min at RT. Membranes were washed for 1 hour and subsequently stored at - 20°C until further analysis. Intensity of chemiluminescence was quantified via the Fiji plugin of ImageJ software and expression levels of proteins of interest were normalized to housekeeper proteins.

3.2.5.3 Human lysozyme enzyme-linked immunosorbent assay

Lysozyme concentration in protein extracts from human stool samples (1:100 v/v) was measured using Human Lysozyme ELISA Kit (Abcam, ab267798) according to the manufacturer's instructions. Samples or standard (50 µl) were mixed with 50 µl of antibody cocktail and added to coated 96-well plates (provided by the manufacturer). Plates were incubated at RT for 1 hour. Mixture was aspirated and wells were washed three times with 350 µl 1X Wash buffer PT (provided by the manufacturer). Each well

was incubated with 100 µl TMB Development Solution for 10 min. Finally, 100 µl stop solution (provided by the manufacturer) was added. OD was measured by Microplate Reader SpectraMax® iD3 at 450 nm. Concentrations were calculated based on the standard curve and values were eventually normalized to total protein concentration.

3.2.6 Fixation, paraffin embedding and immunohistochemistry

For intestinal organoid preparation, media was removed from organoid culture and wells were gently washed twice with 1ml 1x PBS/well. Subsequently, organoids were fixed with 4% (w/v) PFA for 30-60 min, RT. Organoid suspension was centrifuged 500 x *g,* 3 min, pellet was washed twice with 1x PBS and centrifuged 500 x *g,* 3 min. Next, organoids were incubated overnight in 50-100 µl of embedding medium (Table. 5) at 4°C. Samples were dehydrated by successively immersing through a series of increasing concentrations of alcohol, 70% (v/v), 80%, 90% 100% isopropanol for 6 to 24 hours at RT. Then, samples were embedded in 1:1 paraffin/ 100% isopropanol mixture, followed by three times in paraffin for 6 to 24 h each at 56°C.

Ileal tissue samples were thoroughly rinsed with 1x PBS, placed in embedding cassettes, and fixed in 4% (w/v) PFA fixative or ready-to-use formalin solution for 24 hours at RT. After washing with tap water for 2-4 hours, samples were dehydrated and paraffinized as previously mentioned with organoids.

Microtome sections were generated from paraffin blocks precooled to -20°C with a thickness of 4-6 µm. Sections were first collected in a 20°C water bath and then transferred to a 45°C water bath for flat mounting on slides. Finally, mounted slides were dried at 37°C before proceeding with histochemical staining.

For deparaffinization and rehydration, slides were sequentially immersed in the following: three times xylene for 5-10 min each, two times 100% (v/v) ethanol, 96% (v/v) ethanol, 80% (v/v) ethanol and two times 70% (v/v) ethanol for 3 min each followed by two times rinsing in ddH2O. Antigen retrieval was performed for 30 min in citrate buffer utilizing a steamer. Slides were then washed twice with 1x PBS for 10 min followed by blockage with 2% (w/v) BSA in 1x PBS. Specific primary antibodies or isotype control antibodies diluted in 2% (w/v) BSA in 1x PBS were applied and incubated in wet chambers for 45 min at RT. After washing with 1x PBS, slides were incubated with HRP-conjugated secondary antibodies or HRP-labelled polymers for 45 min at RT in wet chambers. Tissue slides were incubated for 10 min at RT with

DAB substrate solution. Finally, samples were counterstained with Mayer's hemalum solution and mounted with Aquatex® solution. Staining was evaluated using Axio Scope.A1 microscope and analyzed using the color deconvolution plugin in ImageJ software (Ross, 2014).

3.2.7 Cell biology methods

3.2.7.1 Extracellular oxygen consumption assay

Respiration rates of AZA-treated cells were measured using MitoXpress Xtra Oxygen Consumption Assay. The principle of the assay is based on fluorescent oxygen-sensitive probe which is quenched in the presence of oxygen. After 3 days of treatment, 80.000 cells/well were seeded in 96-well plate in triplicates. Next, fluorescent reagent was added (1:10) and wells were sealed with 2 drops of mineral oil to prevent diffusion of ambient oxygen. Plate was kinetically measured over 90 min in SpectraMax iD3 microplate reader at 37°C, excitation/emission: 380/650 nm.

3.2.7.2 D-Glucose assay

Glucose level was measured using Fluitest GLU kit according to manufacturer`s protocol. Organoids` supernatants (10 µl, 1:50 dilution) were incubated for 15 min at 37 °C with 100 µl of R1 solution which consists of a mixture of glucose oxidase and peroxidase. Glucose is oxidized by glucose oxidase in hydrogen peroxide which is later converted by peroxidase to colored product which could be detected at 540 nm.

3.2.7.3 L-Lactate assay

Lactate level was measured according to the manufacturer`s instructions. The assay is based on two enzymatic reactions. First, lactic acid is oxidized to pyruvate by nicotinamide-adenine dinucleotide (NAD^+) in the presence of L-lactate dehydrogenase (L-LDH). Second, D-glutamate-pyruvate transaminase (D-GPT) catalyzes the conversion of pyruvate to D-alanine and 2-oxoglutarate. The amount of NADH generated from these reactions is measured at 340 nm. Organoids` supernatants (10 µl, 1:10 dilution) were mixed with NAD^+ and D-GPT. Absorbance (A1) was measured after 3 min by Microplate Reader SpectraMax® iD3. Subsequently, L-LDH was added to the mixture and absorbance (A2) was measured after 10 min. Lactate concentration was calculated by subtracting A1 from A2 and determined using the standard curve provided by the manufacturer.

3.2.7.4 Triglyceride assay

Triglyceride levels were detected with Fluitest TG according to the manufacturer's instructions. Serum samples from CD patients and healthy subjects were diluted 1:5 with PBS/NaCl (0.9%, w/v). OD was measured by Microplate Reader SpectraMax® iD3 at 550 nm. Concentrations were calculated *via* the standard curve.

3.2.7.5 Neutral red assay

Cell viability was measured by the neutral red uptake assay using the protocol by (Repetto et al., 2008). In brief, neutral red medium was centrifuged for 10 min at 400 x *g* to remove any precipitated dye crystals. Medium was removed from cells and 100 µl of neutral red medium/well was added. Plate was incubated at 37°C, 5% CO_2 for 2 hours. Next, neutral red medium was discarded, and wells were washed with 150 µl 1x PBS. After decanting PBS, 150 µl of neutral red destain solution was added and plate was placed on a microtiter plate shaker for 10 min at RT. OD was measured at 540 nm against a reference wavelength of 690 nm on a spectrophotometer.

3.2.7.6 Flow cytometry of intestinal organoids

To generate single cell suspension, organoids were collected in 15 ml Falcon tubes and incubated with cold GCDR on ice for 10 min with frequent tapping. Then, organoids were pelleted by centrifuging for 5 min at 200 x *g* at 4°C. Pellet was resuspended in 5 ml of cold DMEM/F12 + 15 mM HEPES. Samples were centrifuged for 5 min at 200 x *g* at 4°C and warm Trypsin-EDTA (0.05%) was added to the pellets and vigorously resuspended. Cell suspension was incubated at 37 °C for 5-8 min. Samples were briefly vortexed and DMEM/F12 + 10% (v/v) FCS was added and vigorously mixed. Subsequently, cells were pelleted and washed with 1% (w/v) BSA in 1x PBS. Cells were pelleted and incubated with viability dye efluor 780 (1:1,500) and pacific blue anti-mouse CD24 (1:100) or pacific blue isotype control in 1% (w/v) BSA/PBS for 20 min on ice away from light. Cells were washed 1% (w/v) BSA in 1x PBS and pellets were eventually resuspended in 1% (w/v) BSA in 1x PBS. Events were measured using Attune NxT flow cytometer and analyzed by FlowJo software.

3.2.8 Diet-induced obesity model

Male 8-week-old C57BL6/J mice were fed regular chow diet (kcal/gm: 4.14, autoclavable rodent diet 5010, LabDiet, St. Louis, USA) *ad libitum* or high-fat diet with 60 kcal% fat (kcal/gm: 5.24, D12492i, Research Diets Inc, New Brunswick, USA).

Animals were randomly placed either at RT (22°C) or 30°C with 3 animals per IVC cage. Food pellets were exchanged, and weight was monitored on a regular weekly basis for a period of 6 weeks. All mice were sacrificed at the end of the 6th week according to the Guide for the Care and Use of Laboratory Animals and with the approval of CCHMC IACUC (Animal proposal number: IACUC2020-0034). Euthanasia was carried out by placing the animals in a closed container containing 5% isoflurane. Blood, ileal tissue, white adipose tissue (inguinal and epididymal) and stool samples were collected from each mouse. Experiments were performed during my internship at Cincinnati Children's Hospital Medical Center.

3.2.9 NMR sample Preparation and Measurement

Serum samples were analyzed by 1H-NMR (Proton nuclear magnetic resonance) spectroscopy using Bruker's standardized and certified in-vitro diagnostic research (IVDr) procedure (Bruker BioSpin). In brief, frozen aliquots were thawed at room temperature for several minutes. Serum was homogenized with phosphate buffer (75 mM, pH 7.4; incl. 2 mM NaN3 and 4.6 mM sodium trimethylsilyl propionate-[2,2,3,3-2H4] (TSP) in D2O). 600 µL were transferred to a 5 mm NMR tube. Tubes were cooled at 279 K in an automated SampleJet™ (Bruker) until measurement and were analyzed at a 600 MHz Avance III HD NMR spectrometer with TXI probe at 310 K. Daily, a strict standard operating procedure (SOP) was performed and optimized if necessary, including the checking of temperature calibration, quantification, and water suppression performance. One-dimensional (1D) NOESY experiment (pulse program: noesygppr1d) and 1D Carr–Purcell–Meiboom–Gill spin-echo experiment (CPMG) (pulse program: cpmgpr1d) for the suppression of proteins and other macromolecular signals were recorded per sample. Bruker Quantification in plasma/serum (B.I.Quant-PS 2.0.0) and Bruker IVDr Lipoprotein Subclass Analysis (B.I.-LISA) were used to automatically quantify 39 metabolites (+ 2 technical additives) and 112 lipoprotein parameters (Bruker BioSpin). Lipoprotein parameters contain several subfractions of cholesterol (Chol), free cholesterol (FC), phospholipids (PL), triglycerides (TG), and apolipoproteins (Apo).

Multivariate principal component analysis (PCA) and partial least square discriminant analysis (PLS-DA) were calculated using PLS toolbox (Eigenvector Research, Inc.) in Matlab. Targeted IVDr data were variance-scaled and mean-centered. In addition, for PLS-DA an orthogonal signal correction (OSC) was performed, followed by cross-

validation using venetian blinds and the area under the receiver operating characteristic (AUROC) curve was computed.

3.2.10 Statistical analysis

Data are presented as mean ± SD, mean ± SEM, or median with range. Statistical analysis was performed with GraphPad Prism software. Statistical tests were selected based on data distribution. For comparisons between two groups, unpaired, paired t-test or Mann-Whitney test was performed. Difference between more than two groups was detected by Two-Way ANOVA unless stated otherwise. Differences between groups were considered to be significant at a *p*-value of * <0.05, ** <0.01, *** <0.001, or **** <0.0001.

4. Results

AZA's impact on the immune system is well-known, but its effects on IECs have not been extensively researched. This study aims to investigate how AZA affects proliferation, differentiation, and metabolism in IECs.

4.1 Expression of azathioprine metabolizing enzymes is positively correlated with IEC markers

As shown in Fig. 3, after the rapid conversion of AZA to 6-MP, 3 major enzymes (HPRT, TPMT and XDH) target 6-MP. Several studies indicated that these enzymes are highly present in the intestine and the liver. However, little is known whether there are variations in their expression levels among different cell types. RNA-seq data, generated by the genotype-tissue expression (GTEx) project which are publicly available on proteinatlas.org, were used to examine whether these enzymes are differentially expressed in different parts of the intestine. *HPRT1*, which catalyzes the formation of AZA active metabolites, was highly expressed in the terminal ileum and transverse colon at nearly comparable levels (median: 3.82, 3.79 with range: 2, 2.23, respectively) (Fig. 6a).

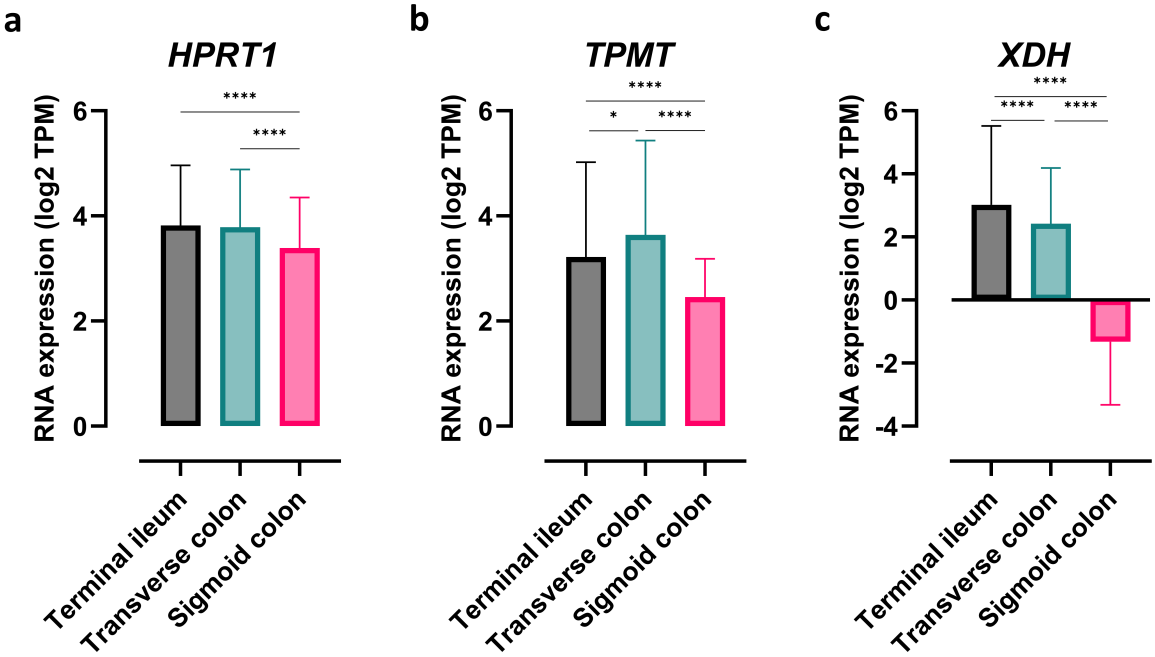

Figure 6. Transcript profile of AZA-metabolizing enzymes along human ileum and colon. Violin box represents transcripts per million (TPM) of *HPRT1* (a), *TPMT* (b) and *XDH* (c) in terminal ileum (n=187, 183 and 172 for each gene respectively), transverse (n=399, 397 and 286 for each gene respectively), and sigmoid colon (n=357, 354 and 76 for each gene respectively). Dunn´s multiple comparison test was performed to compare expression differences. Data are median with range. *p < 0.05, ****p < 0.0001. Data are obtained from proteinatlas.org. *HPRT1*: hypoxanthine phosphoribosyltransferase 1; *TPMT*: thiopurine S-methyltransferase; *XDH*: xanthine dehydrogenase.

On the other hand, sigmoid colon significantly showed the lowest expression of *HPRT1* when compared to terminal ileum and transverse colon (median: 3.39 with range: 1.89) (Fig. 6a). A similar profile was observed in *TPMT* expression levels (Fig. 6b). Nonetheless, *TPMT* expression was significantly elevated in transverse colon in comparison to terminal ileum (**p*-value: 0.0214) (Fig. 6b). Conversely, terminal ileum exhibited the highest expression levels of *XDH* (median: 3.03 with range: 8.84) substantially surpassing both transverse and sigmoid colon (median: 2.42, -1.32 with range: 7.52, 7.27, respectively) (Fig. 6c).

Next, correlation analyses were performed using RNA-Seq data from human terminal ileum. The relationship between the transcripts encoding AZA-metabolizing enzymes (*HPRT1, TPMT* and *XDH*) on one side and IEC markers was explored by Spearman`s correlation analysis. The correlation coefficient between *HPRT1* and IECs markers ranged between 0.16 and 0.48 (Fig. 7a-g). Expression levels of *HPRT1* and LYZ registered the highest positive correlation (r=0.48, $p \leq 0.0001$) (Fig.7c). Additionally, other PC markers such as *DEFA5*,*6* exhibited a similar positive correlation with *HPRT1* (r=0.39, r=0.42) (Fig. 7d,e). The results indicated that there was a positive correlation between the goblet cell marker *TFF3* (Trefoil Factor 3), and *HPRT1* expression (r=0.38, $p<0.0001$) (Fig. 7f). Similarly, ISC markers, *LGR5*, *OLFM4* and *HPRT1* were moderately correlated (*LGR5*: r=0.43, $p \leq 0.0001$, *OLFM4*: r=0.34, $p=0.0013$) (Fig. 7a,b). Surprisingly, absorptive enterocyte marker intestinal alkaline phosphatase (*ALPI*) was weakly correlated with *HPRT1* expression (r=0.16, $p=0.027$) (Fig. 7g). Interestingly, no correlation was found between *HPRT1* and T cell marker *CD3E* and B cell marker *CD19* (*CD3E*: r=0.0942, $p=0.1977$, *CD19*: r=-0.039, $p=0.6008$) (Fig. 7h,i).

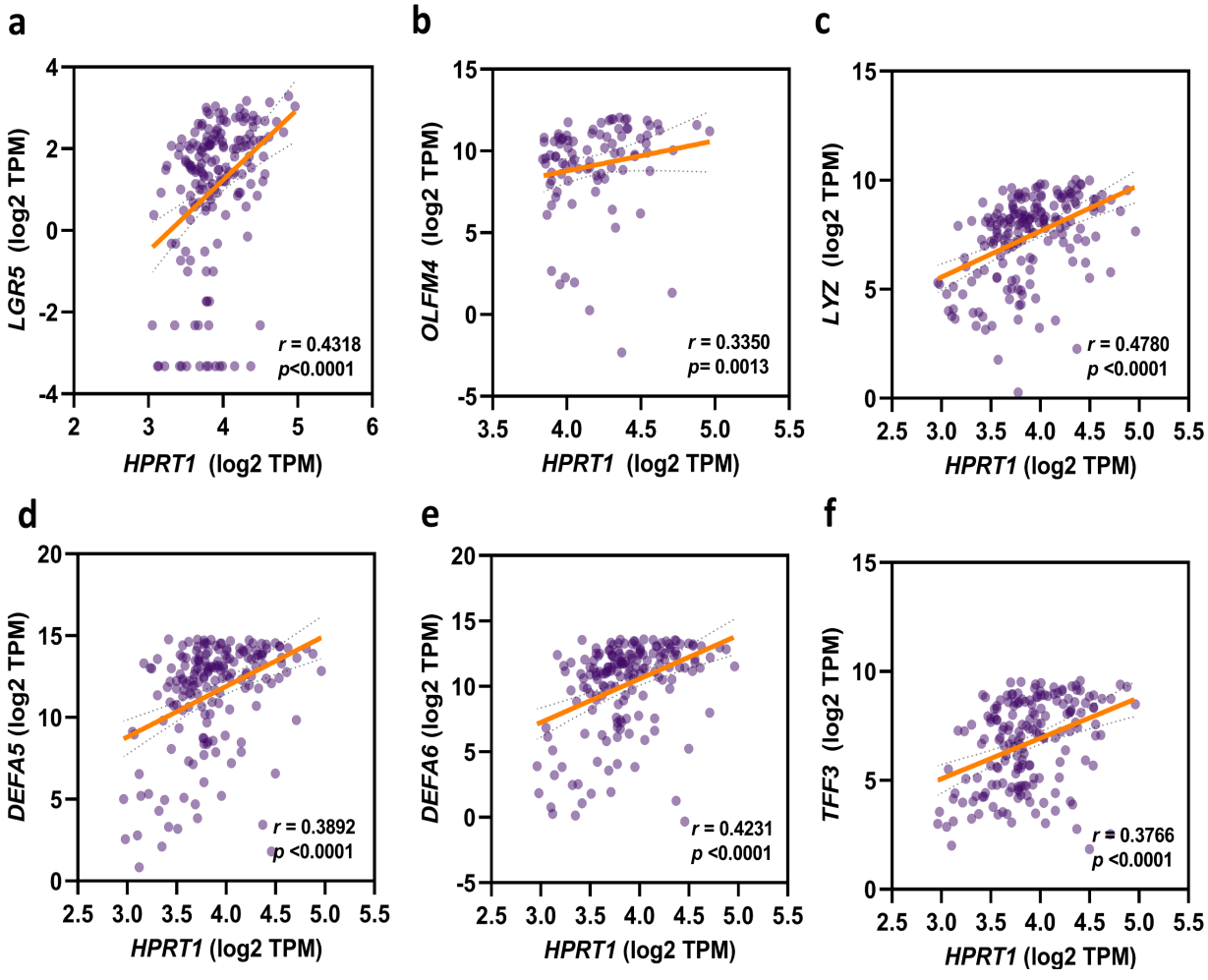

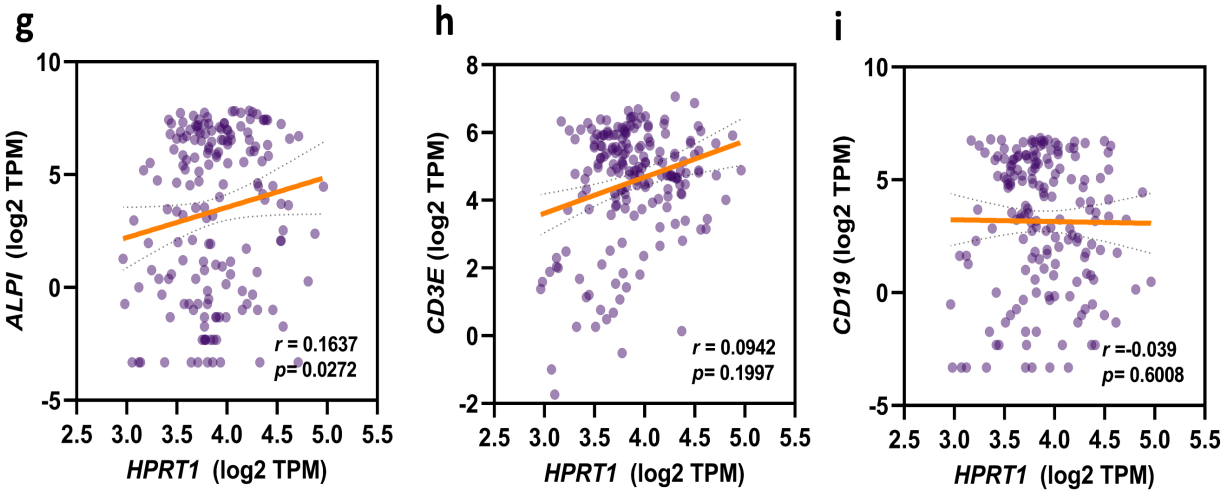

Figure 7. Correlation analysis between transcripts of cell markers and *HPRT1* in terminal ileum. The scatter plot shows the Spearman's correlation of *HPRT1* expression with the expression of (a) *LGR5*, (b) *OLFM4*, (c) *LYZ*, (d) *DEFA5*, (e) *DEFA6*, (f) *TFF3* and (g) *ALPI* (h) *CD3E and* (i) *CD19*. Data are obtained from proteinatlas.org. *HPRT1*: hypoxanthine phosphoribosyltransferase 1; *OLfM4*: olfactomedin 4; *LYZ*: lysozyme; *DEFA5, 6*: alpha-defensin 5, 6; *TFF3*: Trefoil Factor 3; *ALPI*: intestinal alkaline phosphatase.

The correlation coefficient between IEC markers and *TPMT* was higher than *HPRT1*, ranging from 0.59 to 0.88 (Fig. 8a-g). The strongest positive correlation was observed between *TPMT* and *ALPI* (r=0.88, p<0.0001) (Fig. 8g). The correlation between *TFF3* and *TPMT* recorded the second highest coefficient reaching 0.8560, p<0.0001 (Fig. 8f). Similar to *HPRT1*, *CD3E* did not correlate with *TPMT* (r=0.0807, p=2773) (Fig. 8h). Nevertheless, *CD19* moderately showed negative correlation with *TPMT* (r=-0.2951, p<0.0001) (Fig. 8i).

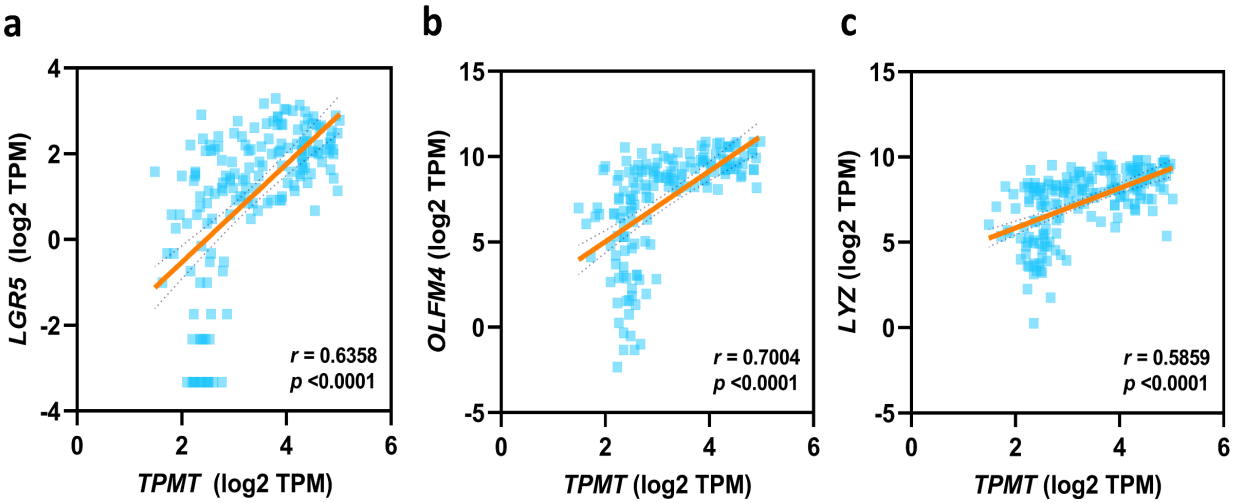

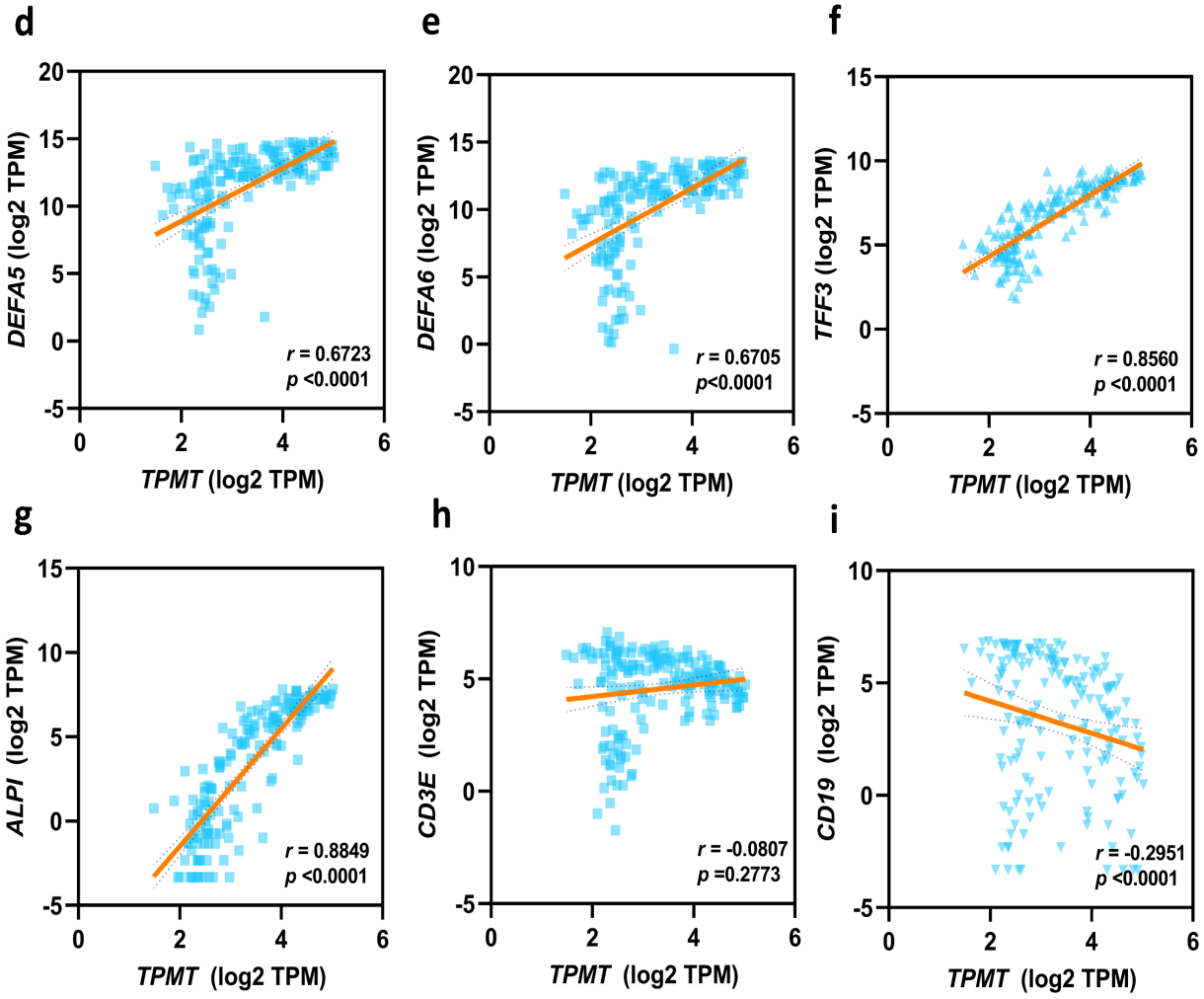

Figure 8. Correlation analysis between transcripts of cell markers and *TPMT* in terminal ileum. The scatter plot shows the Spearman's correlation of *HPRT1* expression with the expression of (a) *LGR5*, (b) *OLFM4*, (c) *LYZ*, (d) *DEFA5*, (e) *DEFA6*, (f) *TFF3* and (g) *ALPI* (h) *CD3E and* (i) *CD19*. Data are obtained from proteinatlas.org. *TPMT*: thiopurine S-methyltransferase; *OLfM4*: olfactomedin 4; *LYZ*: lysozyme; *DEFA5, 6*: alpha-defensin 5, 6; *TFF3*: Trefoil Factor 3; *ALPI*: intestinal alkaline phosphatase.

A similar correlation was seen between epithelial cell markers and *XDH* (Fig. 9a-g). Overall, the positive correlation was strong with most of IEC markers ranging from 0.62 to 0.93. The correlation between *XDH* and PC markers (*LYZ, DEFA5, DEFA6*) varied between 0.62 and 0.74 (Fig. 9c-e). In addition, the expression of ISC markers was positively correlated with *XDH* levels (r=0.69, 0.79 for *LGR5* and *OLFM4*, respectively $p<0.0001$) (Fig. 9a,b). Comparable to *TPMT* analysis, the strongest correlation was found between XDH and both *TFF3* and *ALPI* (r=0.88, 0.93, respectively $p<0.0001$) (Fig. 9f,g). While *CD3E* was not significantly correlated with *XDH*, transcripts of *CD19* was significantly decreased with increasing *XDH* (*CD3E*: r=0.0205, $p=0.7823$, *CD19*: r=-0.2113, *p<0.0001*) (Fig. 9h,i).

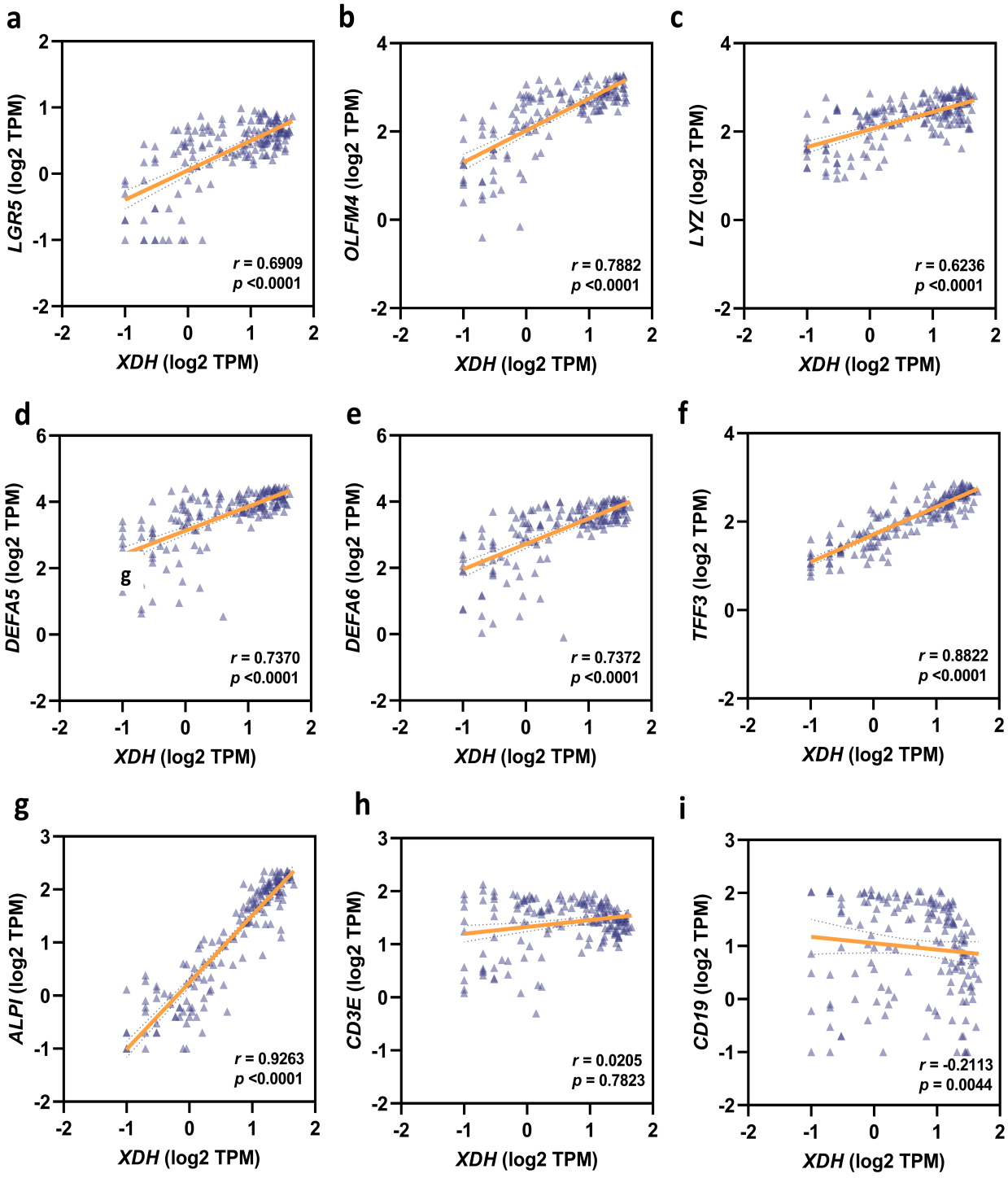

Figure 9. Correlation analysis between transcripts of cell markers and *XDH* in terminal ileum. The scatter plot shows the Spearman's correlation of *HPRT1* expression with the expression of (a) *LGR5*, (b) *OLFM4*, (c) *LYZ*, (d) *DEFA5*, (e) *DEFA6*, (f) *TFF3* and (g) *ALPI* (h) *CD3E and* (i) *CD19*. Data are obtained from proteinatlas.org. *XDH:* xanthine dehydrogenase; *OLfM4*: olfactomedin 4; *LYZ*: lysozyme; *DEFA5, 6*: alpha-defensin 5, 6; *TFF3*: Trefoil Factor 3; *ALPI*: intestinal alkaline phosphatase.

These findings suggest that IECs, especially in the terminal ileum, have the capacity to metabolize AZA. In contrast to the previous notion that absorptive enterocytes solely interact with AZA metabolites, other differentiated cells such as PCs and goblet cells might also be involved. Moreover, these observations trigger the question of whether this ability is unidirectional or AZA also induces effects on IECs.

4.2 Paneth cells' function is rescued in CD patients treated with azathioprine

AZA has proven effective in treating active CD and also in maintaining remission (French et al., 2011; Timmer et al., 2016). Considering that PCs dysfunction is hypothesized to trigger CD, we examined the effect of AZA on PC function in CD patients. AZA-treated patients displayed an upregulation of *LYZ* mRNA expression in ileal biopsies compared to patients who did not receive the drug (Fig. 10a). Human PCs secrete diverse anti-microbial peptides, mainly alpha-defensins such as *DEFA5* and 6 (Sankaran-Walters et al., 2017). Similar to *LYZ* expression, increased expression of *DEFA5* and *DEFA6* was observed in AZA-treated patients (Fig. 10b). Immunohistochemical staining of ileal biopsies and ELISA of stool samples revealed comparable findings to mRNA expression with high LYZ levels in patients who received AZA (Fig. 10d-f).

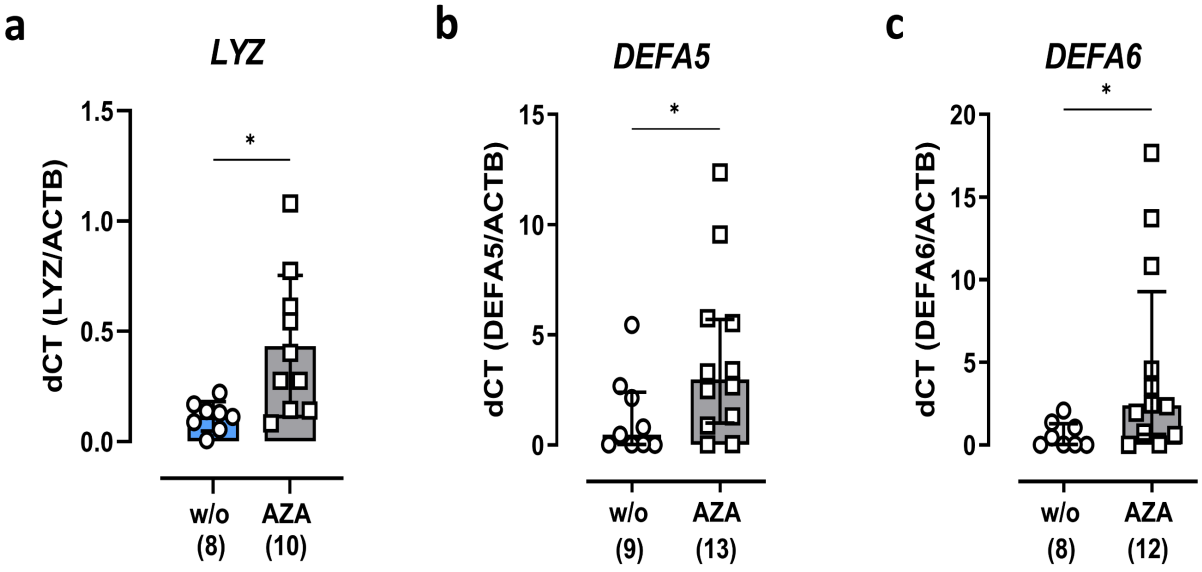

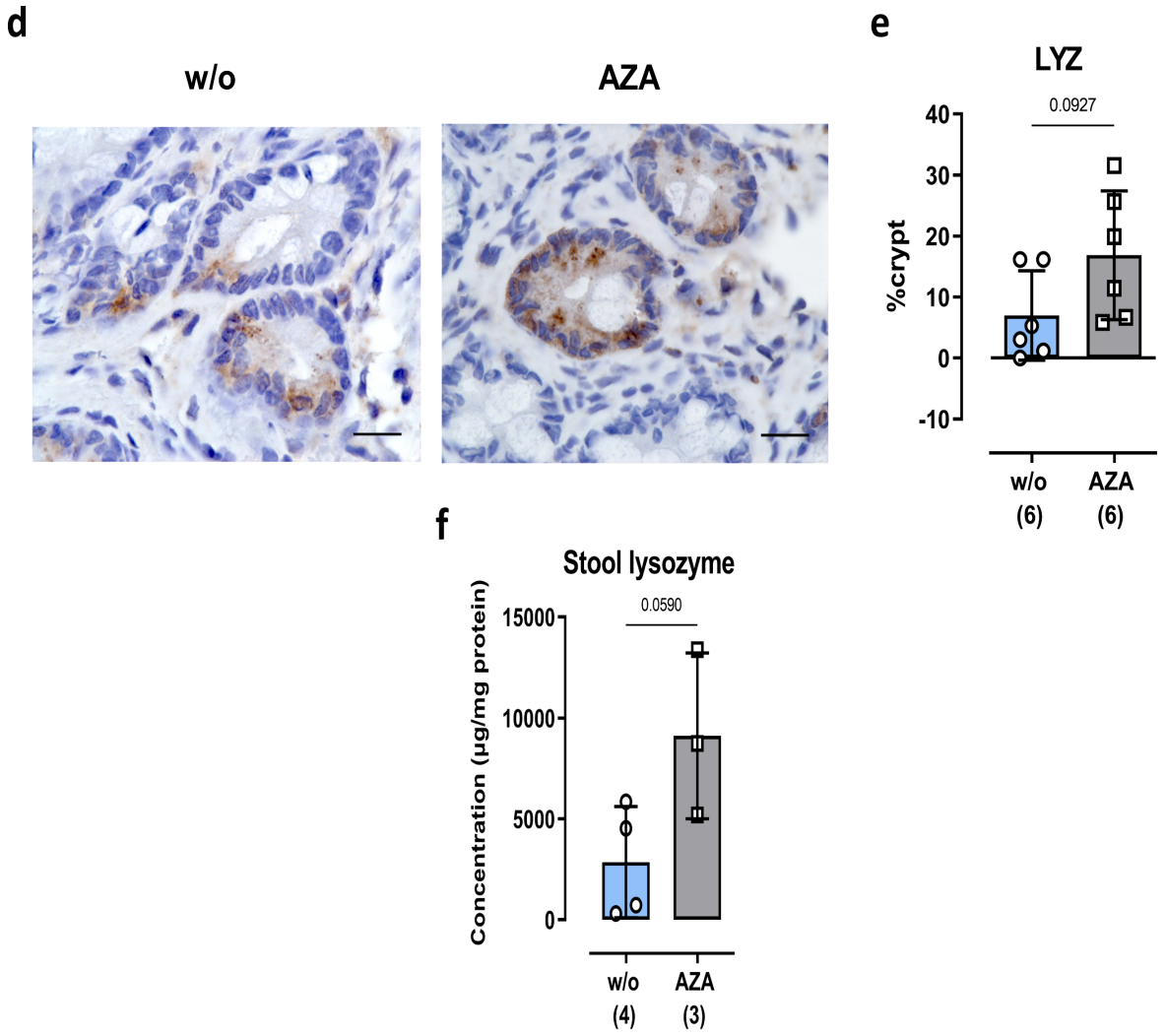

Figure 10. Levels of Paneth cells markers in CD patients treated with AZA compared to CD controls. mRNA expression of (a) *LYZ*, (b) *DEFA5* and (c) *DEFA6* in ileal samples from CD patients. (d) Microscopic images of IHC staining of LYZ in ileal samples from CD patients. (e) Intensity of the staining per crypt was measured using ImageJ software. (f) Lysozyme level was measured in fecal samples from CD patients treated or not treated with AZA by ELISA. (a, e, f) Unpaired t test with Welch's correction; (b, c) Mann-Whitney test; results are shown as (a, e, f) mean ± SD, (b, c) median with interquartile range. *$p < 0.05$. *LYZ*: lysozyme; *DEFA5*, 6: alpha-defensin 5, 6; w/o: non-AZA treated patients.

Beside the immunomodulatory effect of AZA, a novel target was unraveled by boosting PC antimicrobial repertoire. The next set of experiments was dedicated to determining if this impact is a direct one or if it comes secondary to changes in immune cells.

4.3 Azathioprine suppresses cell proliferation and drives cell differentiation of intestinal epithelial cells

To examine whether AZA induces alterations in PC differentiation and functions, various intestinal epithelial cell lines were tested. First, MODE-K cells, a murine small intestinal epithelial cell line, were treated with a series of AZA concentrations ranging from 1 mM and 0.1 µM for 3 days (Fig. 11a). While 1 µM AZA resulted in a slight decrease in cell viability reaching an average of 95%, a significant loss was evident staring from 10 µM and down to 1 mM (Fig. 11b). However, a significant decline in cell numbers was observed in 1 µM AZA-treated cells with an average of 0.26×10^6 per ml compared to control (0.91×10^6 per ml) (Fig. 11c). This suppression in cellular proliferation was associated with heightened cellular respiration in AZA-treated cells, indicating high cell viability (Fig. 11d). Interestingly, a significant increase in *Lyz1* mRNA expression was detected in AZA-treated cells compared to cells treated with DMSO (Fig. 11e). Based on the findings presented in Figure 11c,d, AZA was hypothesized to block cell proliferation and hence boost mitochondrial respiration, leading to improved cell differentiation. To test this, MODE-K cells were treated with the uncoupling agent DNP (2,4-dinitrophenol), an inhibitor of mitochondrial OXPHOS, in the presence or absence of AZA (Fig. 11f). Introducing AZA impacted cellular proliferation as observed in cells treated with DNP or cells treated only with AZA (Fig. 11g). While mRNA level of *Lyz1* was intensely decreased in cells treated with DNP only, a moderate increase was detected in DNP+AZA treated cells (Fig. 11h).

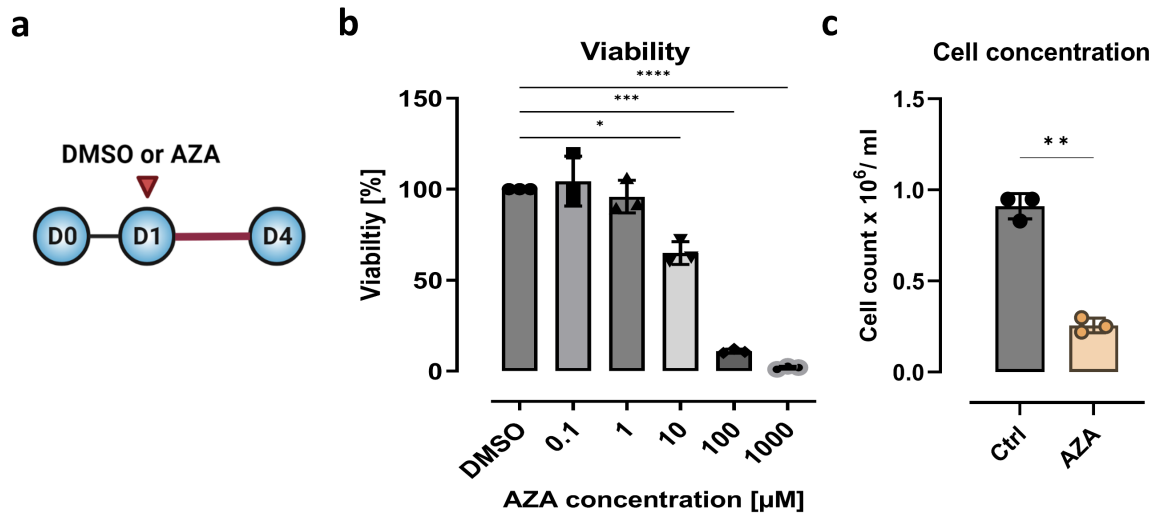

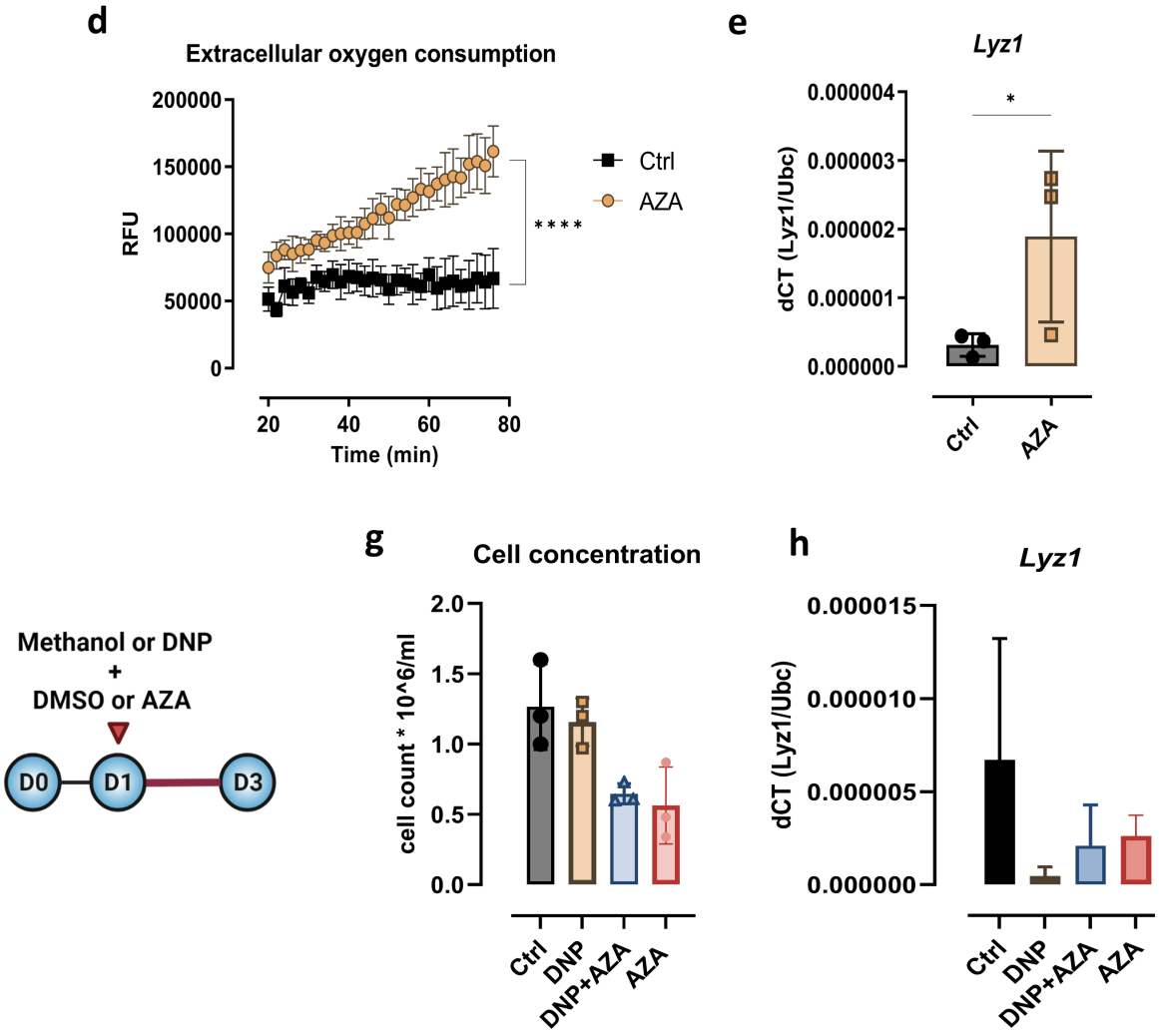

Figure 11. Effect of AZA on MODE-K cells *in vitro*. (a) Overnight-incubated MODE-K cells were treated with either AZA or DMSO for 3 days. (b) Neutral red assay was performed to determine viability of cells treated with DMSO or serial AZA concentrations (0.1 – 1000 µM). (c) Viable cell numbers of DMSO or 1 µM AZA-treated cells were counted by trypan blue exclusion. (d) Mitochondrial bioenergetics were measured in DMSO or AZA-treated MODE-K cells using MitoXpress Xtra Oxygen Consumption Assay. (e) mRNA levels of *Lyz1* were measured in DMSO or AZA-treated MODE-K cells. (f) Mitochondrial dysfunction was induced in MODE-K cells by adding DNP for 2 days in the presence or absence of AZA (1µM). Subsequently, (g) cells were counted and mRNA expression of *Lyz1* was measured *via* qPCR (h). All experiments were repeated three times. (b) One-way ANOVA with Dunnett's multiple comparisons test; (c, e) paired t test; (d) Two-way ANOVA with Dunnett's multiple comparisons test; results are shown as (b, c, e, g, h) mean ± SD and (d) mean ± SEM. *$p < 0.05$, ***$p < 0.001$, ****$p < 0.0001$. DMSO: dimethyl sulfoxide; DNP: dinitrophenol; RFU: relative fluorescence units.

As previously reported, mitochondrial OXPHOS is the main driver of cell differentiation in the intestinal crypt (Sünderhauf et al., 2021). Moreover, mitochondrial mutations were reported to be associated with CD and PC impairment (Jackson et al., 2020; Khaloian et al., 2020). Cells isolated from mice that carry mutation in mitochondrial *ATP8* gene displayed loss of OXPHOS function and hence produced less ATP that was compensated by higher glycolysis in comparison to wild-type (WT) B6 mice (Hirose et al., 2017). ileal samples harvested from these mice exhibited a decrease in the numbers of Lyz + cells in ileal crypts (Fig. 12a, b). In contrast, ileal mucin 2 (Muc2) levels were not impacted by mitochondrial mutation (Fig. 12c, d). These observations clearly emphasized the role of mitochondria in PC development and function which was modulated by AZA.

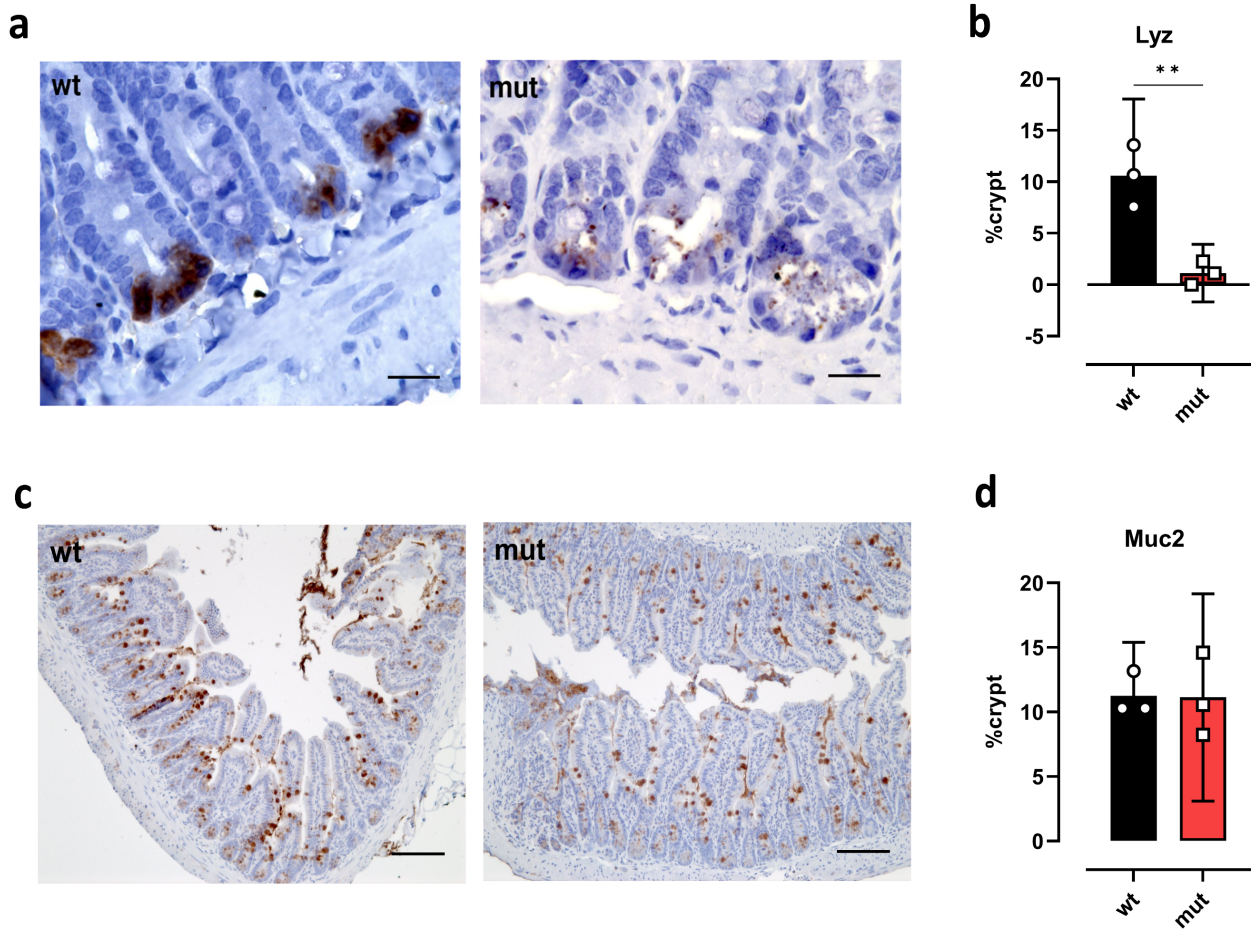

Figure 12. Effect of mitochondrial impairment on PC development. (a, c) Immunohistochemistry staining of ileal sections from wt and mut mice with Lyz and Muc2 antibodies. (b, d) levels of Lyz and Muc2 in ileal crypts were measured using ImageJ software. Data are (b) mean ± SD and (d) median with interquartile range; (b) Unpaired t test and (d) Mann Whitney test. $^{**}p < 0.01$. Lyz: lysozyme; Muc2: mucin 2.

Next, the effect of AZA was examined on other intestinal epithelial cell lines, HT-29 and Caco-2. The reason for choosing these cells is that despite the fact that they have colonic origins, *LYZ* is highly expressed on mRNA levels. Additionally, they exhibit two major phenotypes that characterize differentiated IECs. While HT-29 display secretory phenotype, Caco-2 mimic absorptive enterocytes (Ferraretto et al., 2018). A series of different AZA concentrations (0.1-1000 μM) was tested in both cell lines and viability was determined by neutral red assay (Fig. 13a, 14a). A decline in cell viability was observed in both cell lines from 10 μM to 1 mM as shown by neutral red assay (Fig. 13a, 14a).

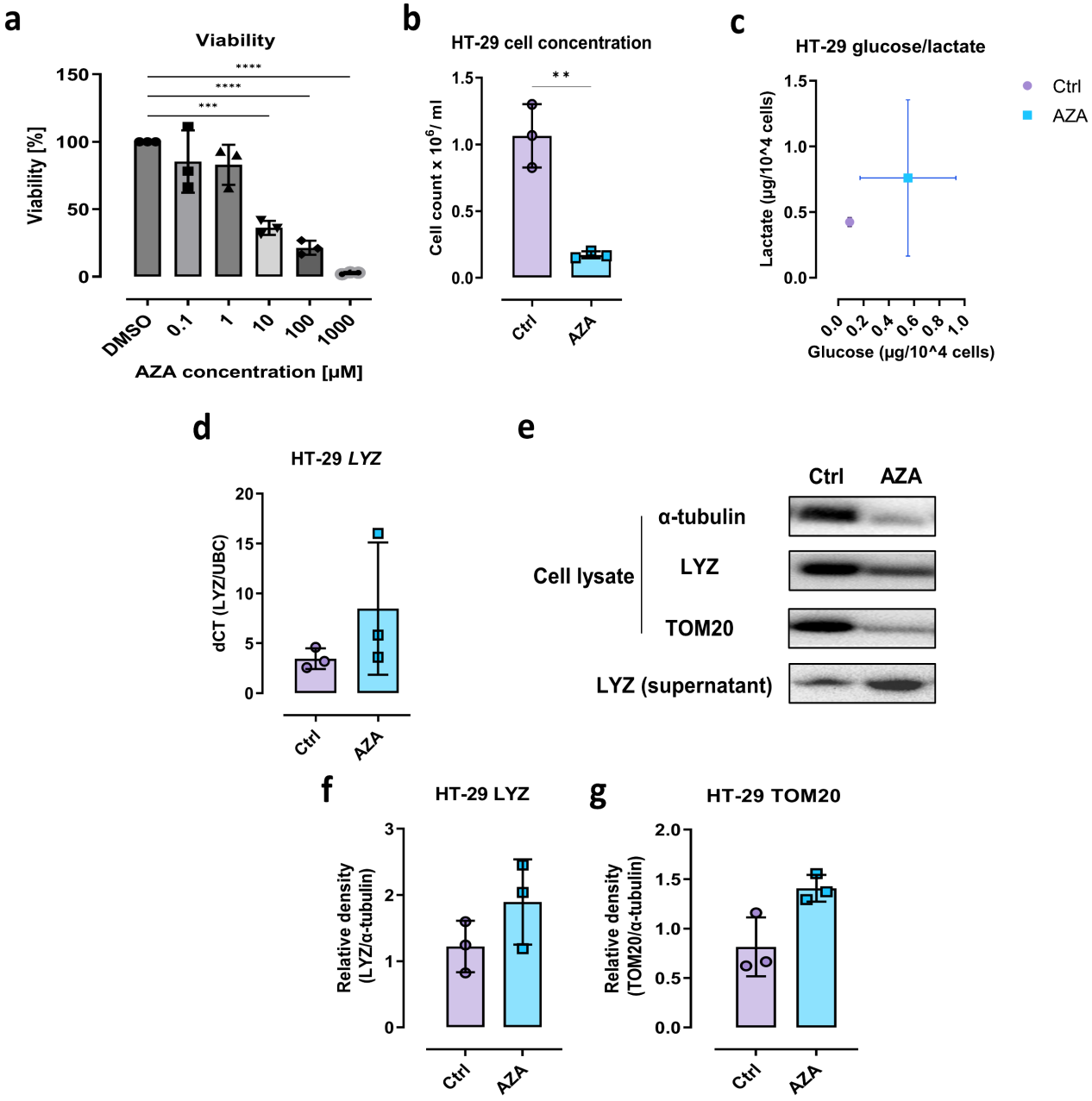

Figure 13. Effect of AZA on colonic HT-29. (a) Neutral red assay was performed to determine viability of HT-29 treated with DMSO or serial AZA concentrations (0.1 – 1000 µM) for 3 days. In another set of experiments, cells were treated with either 10 µM AZA or DMSO for 3 days. Cells were counted on day 3 (b) and (c) levels of D-glucose and L-lactate were measured in the supernatants. (d) mRNA expression of *LYZ* was measured in DMSO or AZA-treated cells. (e) Western blot was performed to measure protein levels of α-tubulin, LYZ (in cell lysate and supernatant) and TOM20. (f, g) Relative density of both LYZ and TOM20 were analyzed relative to α-tubulin. All experiments were repeated three times. (a) One-way ANOVA with Dunnett's multiple comparisons test; (b, d, f, g) paired t test; results are shown as (b, c, e, g, h) mean ± SD and (d) mean ± SEM. ***p* < 0.01, ****p* < 0.001, *****p* < 0.0001. LYZ: lysozyme; TOM20: translocase of outer membrane 20.

However, the response to 10 µM AZA varied greatly between both cell lines. While AZA-treated HT-29 showed a great loss of proliferative activity (Fig. 13b), Caco2 cells were not affected significantly by the drug (Fig. 14b).

Additionally, it was found that AZA treatment caused a change in the metabolic processes in HT-29 cells, as demonstrated by decreased glucose consumption and lactate production (Fig. 13c). qPCR analysis showed contrasting results between both cell lines. *LYZ* mRNA was upregulated in AZA-treated HT-29 (Fig. 13d). Similarly, LYZ was increased in cell lysate and supernatant of AZA-treated HT-29 on protein level (Fig. 13e, f).

Nevertheless, Caco-2 treated with AZA exhibited the opposite on mRNA level with no detection of LYZ protein intra or extracellularly (Fig. 14d). Additionally, levels of lactate and glucose did not exhibit major alterations in AZA-treated Caco-2 cells (Fig. 14c). Cellular differentiation relies mainly on mitochondrial OXPHOS for energy generation (Sünderhauf et al., 2021). A rise in mitochondrial marker, TOM20 was observed in AZA-treated HT-29 (Fig. 13e,g), while Caco-2 did not exhibit the same effect (Fig. 14e,f).

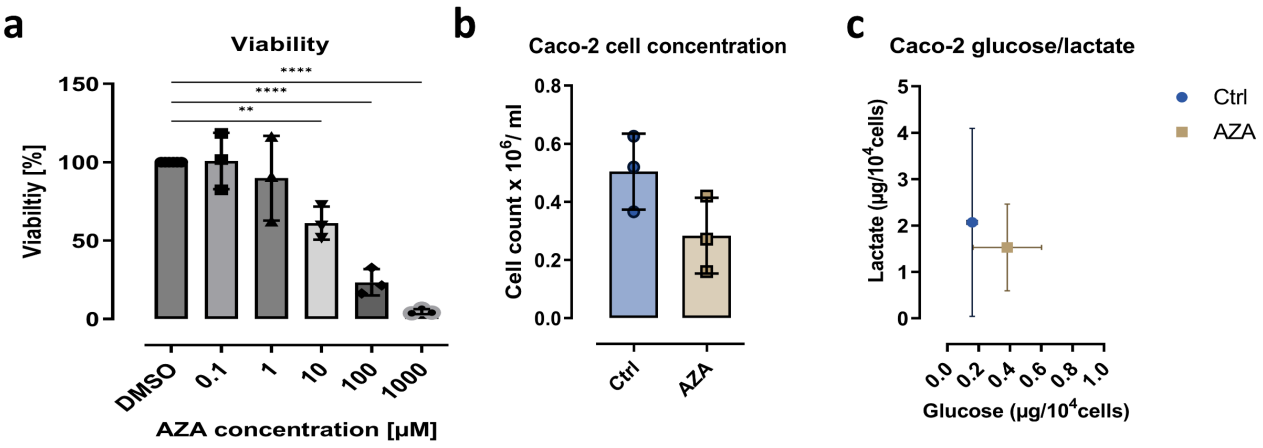

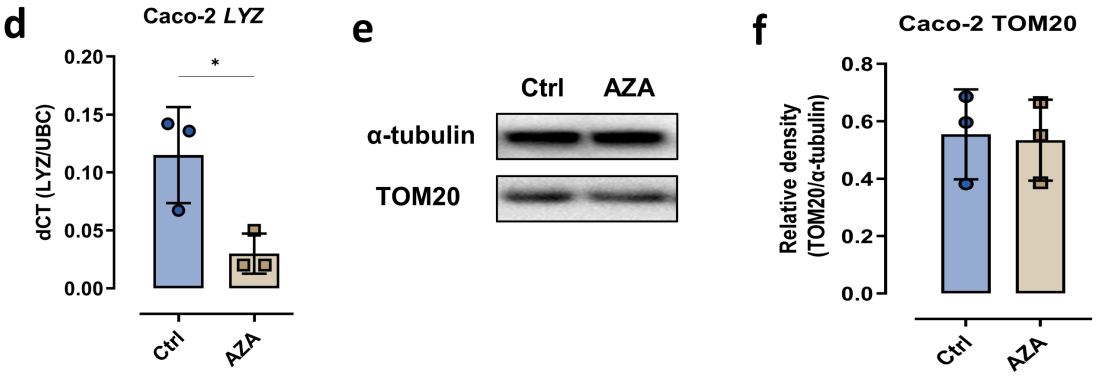

Figure 14. Effect of AZA on colonic Caco-2. (a) Neutral red assay was performed to determine viability of HT-29 treated with DMSO or serial AZA concentrations (0.1 – 1000 µM) for 3 days. In another set of experiments, cells were treated with either 10 µM AZA or DMSO for 3 days. Cells were counted on day 3 (b) and (c) levels of D-glucose and L-lactate were measured in the supernatants. (d) mRNA expression of *LYZ* was measured in DMSO or AZA-treated cells. (e) Western blot was performed to measure protein levels of α-tubulin and TOM20. (f) Relative density of TOM20 were analyzed relative to α-tubulin. All experiments were repeated three times. (a) One-way ANOVA with Dunnett's multiple comparisons test; (b, d, f) Paired t test; results are shown as mean ± SD. *$p < 0.05$, **$p < 0.01$, ***$p < 0.001$, ****$p < 0.0001$. LYZ: lysozyme; TOM20: translocase of outer membrane 20.

Differences in the expression of AZA-metabolizing enzymes were expected to be behind the high variance observed between intestinal epithelial cell lines in response to AZA treatment. Indeed, mRNA level of *HPRT1* was highly upregulated in Caco-2 cells followed by MODE-K cells (Fig. 15a). HT-29 cells exhibited the lowest expression of *HPRT1.* On the other hand, *TPMT* levels were lowest in MODE-K (Fig. 15b). While *XDH* was not detectable in Caco-2 cells, high levels were found in MODE-K compared to HT-29 (Fig. 15c).

In brief, AZA induced metabolic alterations in MODE-K and HT-29. This was associated with improved cell differentiation accompanied by increased LYZ expression and diminished cell proliferation. Nonetheless, 2D-cell lines don't fully recapitulate the *in-vivo* intestinal condition. A more complex system that contains different epithelial cells present in intestinal crypts was needed to verify these findings.

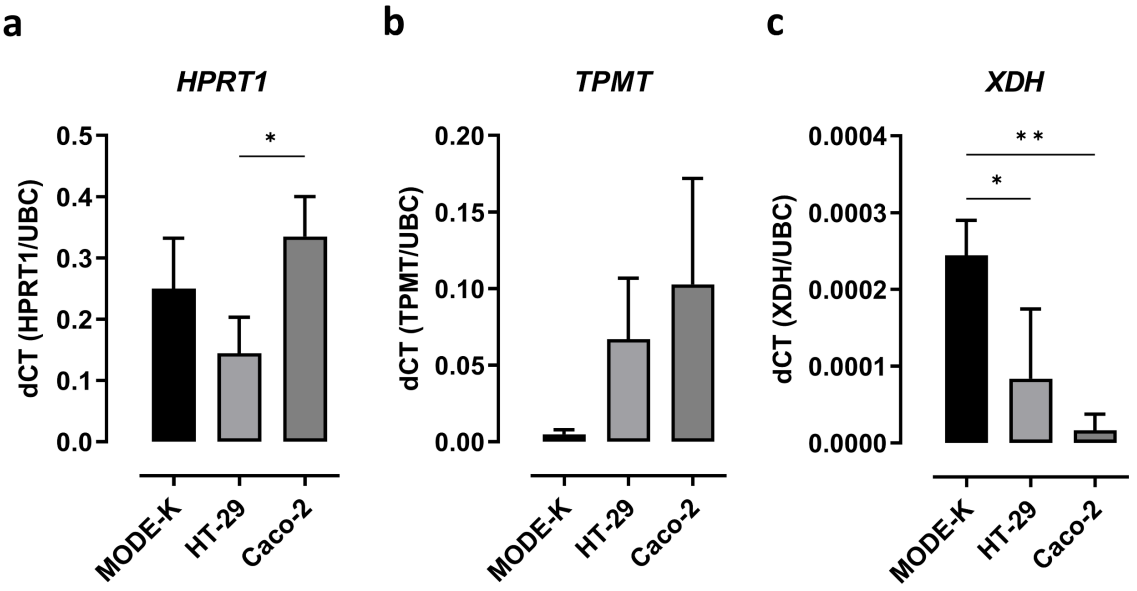

Figure 15. Expression levels of AZA-metabolizing enzymes in intestinal cell lines. qPCR was performed to measure mRNA expression of *HPRT1* (a), *TPMT* (b) and *XDH* (c) in MODE-K, HT-29 and Caco-2 cells. Statistical differences were detected by Tukey's multiple comparisons test. Data are mean ± SD. *$p < 0.05$, **$p < 0.01$. *HPRT1:* hypoxanthine phosphoribosyltransferase *1; TPMT:* thiopurine S-methyltransferase*; XDH:* xanthine dehydrogenase.

4.4 Azathioprine tips the differentiation towards secretory lineage in SI 3D-organoids

In the previous experiments, AZA demonstrated anti-proliferative and AMPs upregulating activities. However, the question remains of whether AZA impacts other IECs. Organoid system represents a suitable model to study this matter as it contains a wide range of IECs, such as enterocytes, goblet cells and PCs. Microscopically, wt organoids treated with 1 µM AZA for 3 days were morphologically distinct from controls (Fig. 16a,b). Small and rounded structures were associated with AZA treatment (Fig. 16b). Notably, diameter of AZA-treated wt organoids was around 103 µm while DMSO-treated group exhibited longer width, 153 µm (Fig. 16c). Differentiation was heightened in AZA-treated organoids as demonstrated in the increased expression of *Lyz1*, *Defa3* and *Muc2,* and the downregulation of *Lgr5* (Fig. 16d-g). AZA induced a slight upregulation of *Atoh1* expression and a decrease in *Hes1* gene (Fig. 16i,j). An additional indication that AZA amplifies differentiation over proliferation is the severe loss of *Ki67* expression in AZA-treated organoids (Fig. 16h). Metabolic markers such as D-glucose and L-lactate were measured in the supernatants of AZA-treated organoids. Diminished proliferation was associated with low glucose consumption and lactate production (Fig. 16k).

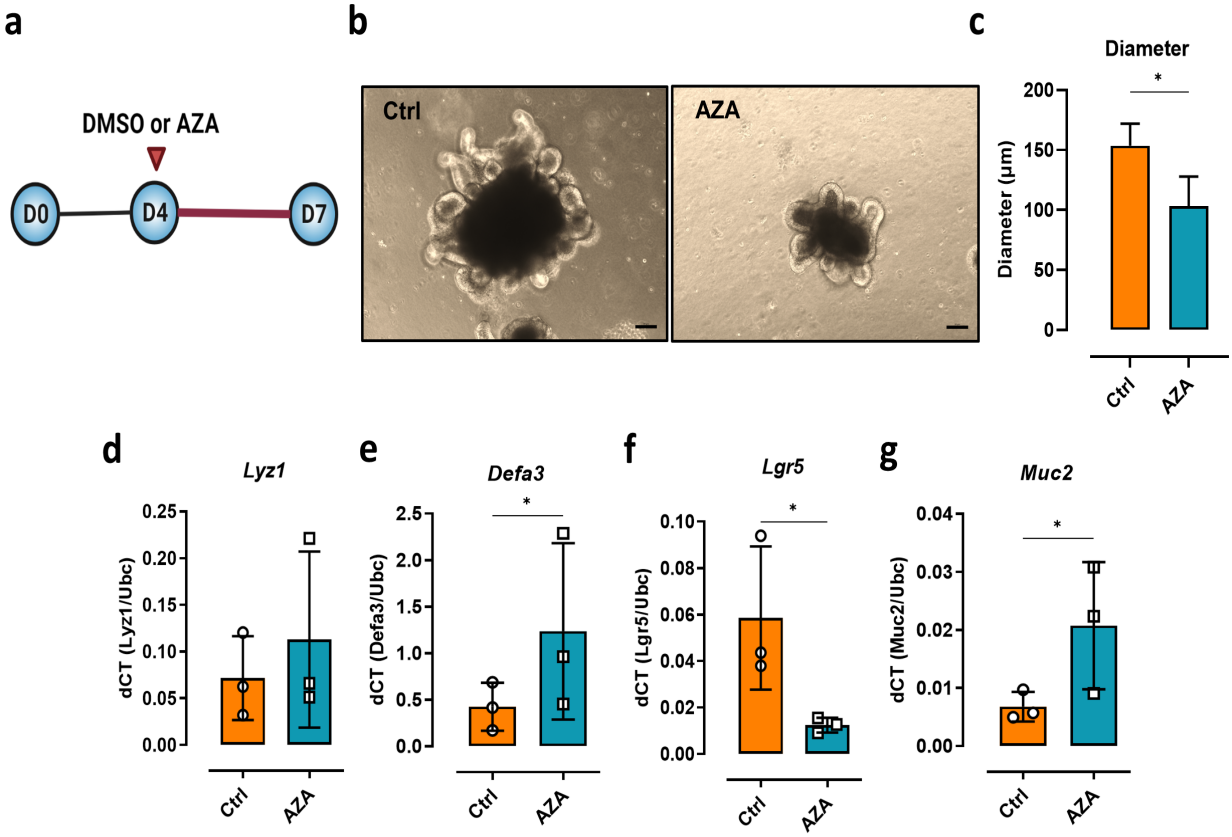

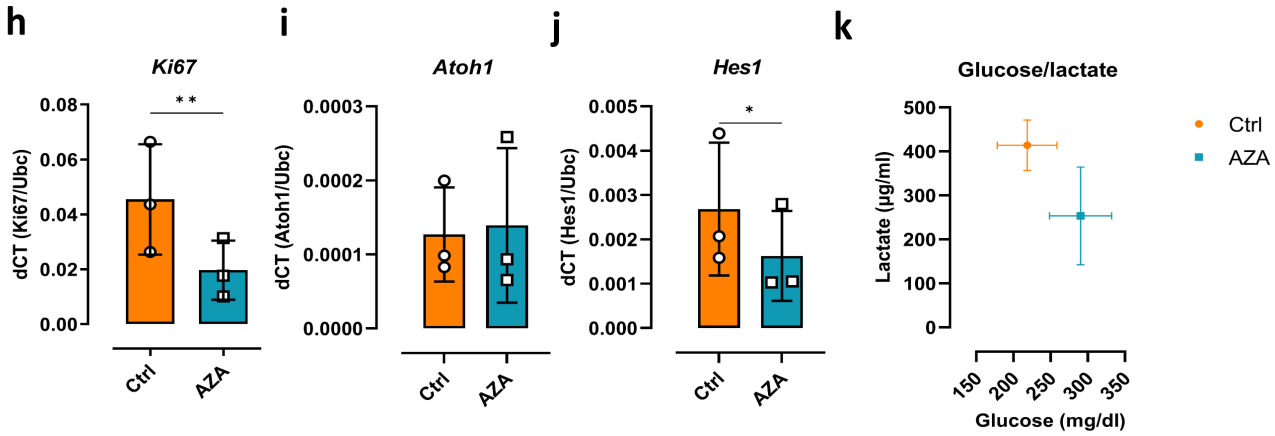

Figure 16. Effect of AZA on small intestinal organoids. (a) C57Bl/6 SI organoids were maintained on standard medium for 4 days. Consequently, DMSO or AZA (1 µM) was introduced on day 4 for 3 days. (b) Microscopic appearance of SI organoids treated with DMSO or AZA. (c) Diameter of DMSO and AZA-treated organoids was measured using Zeiss ZEN software. mRNA expression of *Lyz1* (d), *Defa3* (e), *Lgr5* (f), *Muc2* (g) in DMSO and AZA-treated organoids. Expression of *Ki67* (h), *Atoh1* (i), *Hes1* (j) were measured in ctrl and AZA-treated organoids via qPCR. (k) Glucose and lactate levels were measured in the supernatants of SI organoids. Statistical differences were detected by paired t test. Data are mean ± SD. *$p < 0.05$, **$p < 0.01$. *Lyz1*: lysozyme 1; *Defa3*: alpha-defensin 3; *Muc2*: mucin 2; *Atoh1*: Atonal BHLH Transcription Factor 1; *Hes1*: Hairy and enhancer of split-1.

Several publications reported that PCs highly express CD24 (Baghdadi and Kim, 2022; Sato et al., 2011). Flow cytometry analysis revealed a drastic decrease in the viability of AZA-treated organoids (Fig. 17b). By gating for living cells with high side scatter (SSC) and positive CD24 expression (Fig. 17a, 28), a significant increase in the percentage of this population in AZA-treated organoids (Fig. 17c).

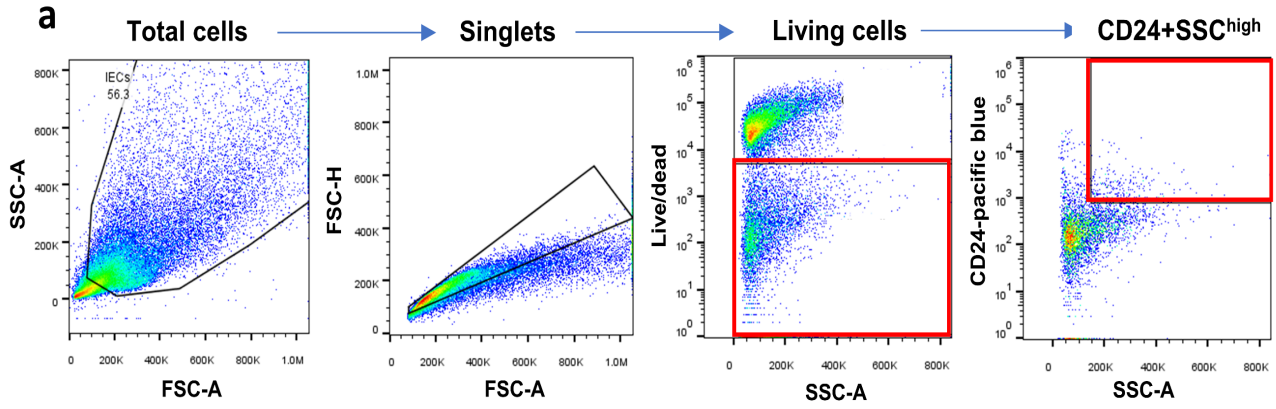

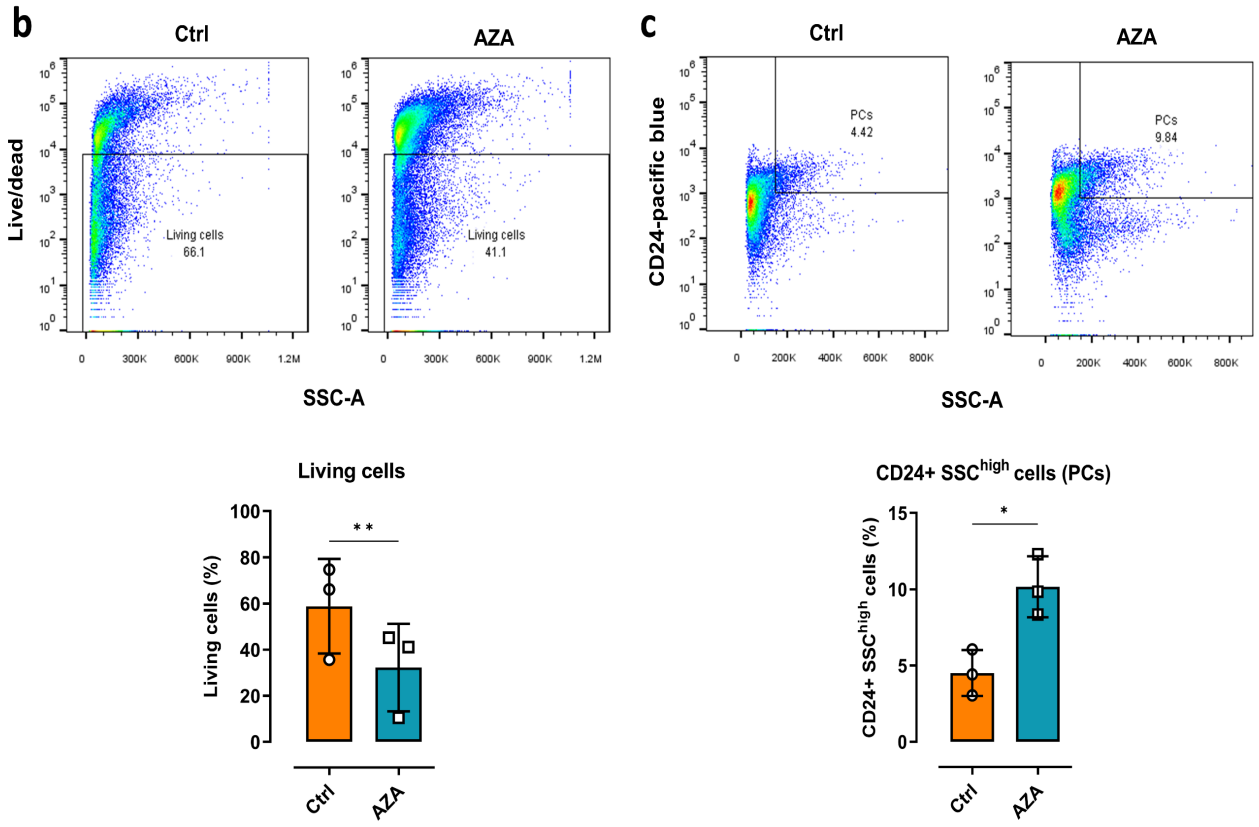

Figure 17. Flow cytometry of B6 SI organoids. (a) Gating strategy of single cell suspension generated from SI organoids treated with DMSO or AZA for 3 days. Dot plots and percentages of living cells (b) and CD24+ SSC^{high} (b) were measured using Flowjo software. Statistical differences were detected by unpaired t test. Data are mean ± SD. *$p < 0.05$, **$p < 0.01$. FSC: forward scatter; SSC: side scatter.

These results clearly demonstrated that differentiation to secretory cells like PCs was heightened by AZA administration in the absence of immune cells, the main targets of AZA, as observed with intestinal organoids. Importantly, these changes were associated with metabolic and mitochondrial alterations. Since CD patients were reported to exhibit mitochondrial impairment causing the emergence of dysfunctional PCs (Alula et al., 2021; Khaloian et al., 2020), it was speculated that AZA could overcome mitochondrial malfunction and restore PC normal capacity. Therefore, the next experiments were performed to evaluate the interconnection between AZA and mitochondria.

4.5 Azathioprine restores aberrant PC functions

4.5.1 Mitochondrial dysfunction in IECs is accompanied by loss of PC in 3D SI organoids

It has been previously established that the main driving force behind cell differentiation in the intestinal crypt is mitochondrial OXPHOS (Sünderhauf et al., 2021). As shown in Fig. 12, *ATP8*-mut mice showed evidence of PC impairment in the ileum. To investigate the impact of AZA on mitochondria, small intestinal organoids were generated from *ATP8*-mut mice. ATP8 mutant organoids were compared to WT organoids that have the same nuclear background (Fig. 18a). Morphologically, no difference was observed between *ATP8* mutant and WT organoids (Fig. 18b). qPCR analysis revealed a moderate decrease in *Lyz1* and a severe reduction in *Defa3* in *ATP8* mutant organoids (Fig. 18c,d). mRNA levels of *Lgr5* and *Ki67* did not significantly differ compared to WT organoids (Fig. 18e,f).

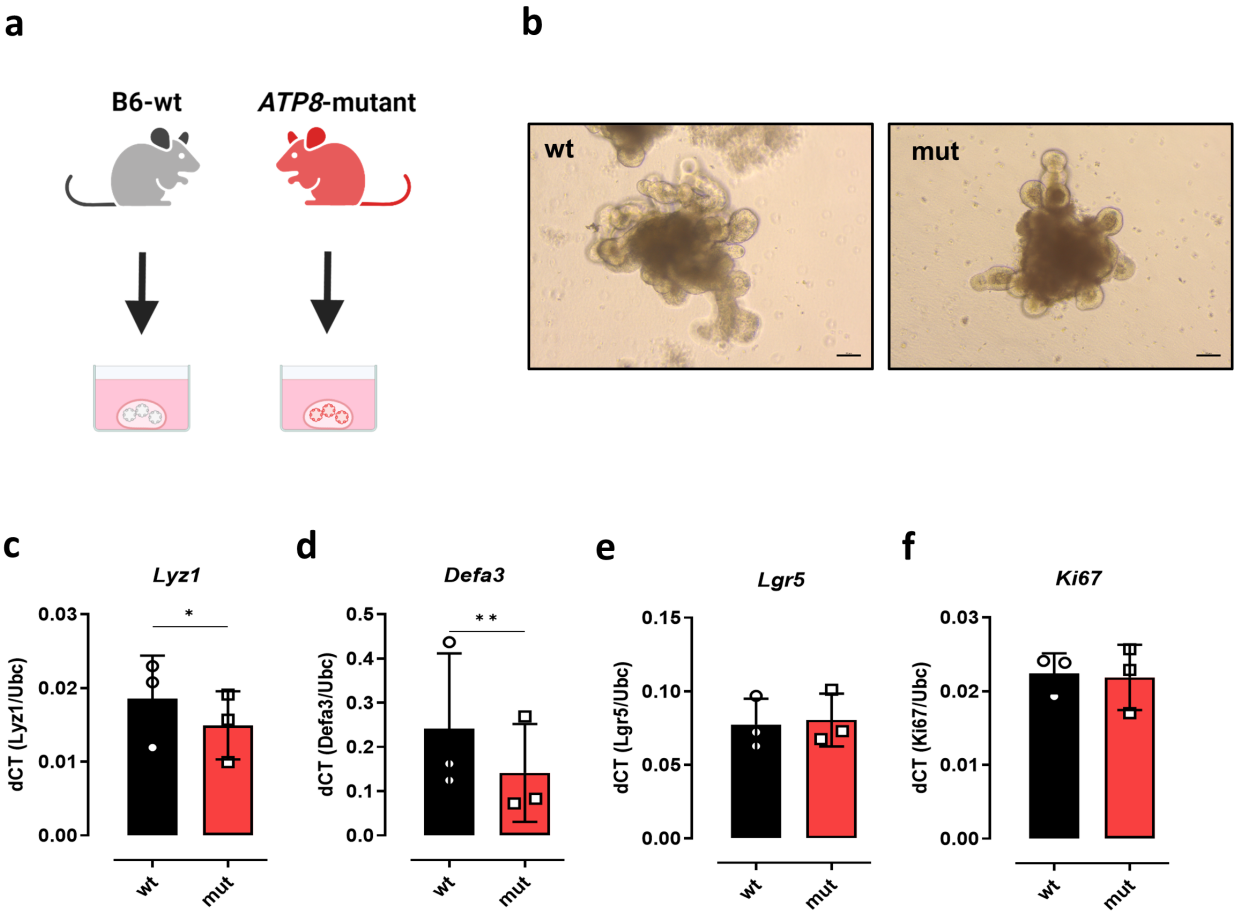

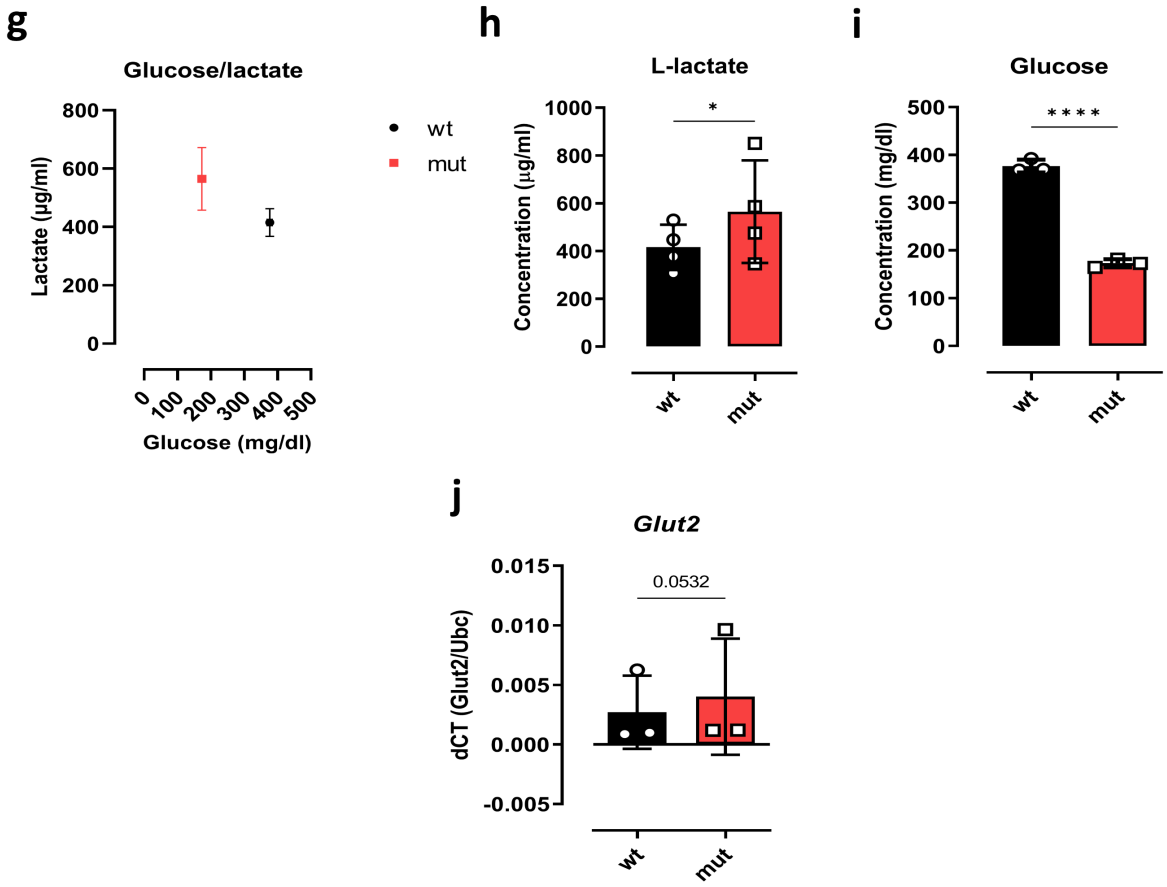

Figure 18. Characterization of ATP8-mutant SI organoids . (a) SI organoids were generated from wt and ATP8-mutant mice. (b) Microscopic appearance of wt and ATP8-mut SI organoids. mRNA expression of PC markers; *Lyz1* (c) and *Defa3* (d) in wt and mut SI organoids. (e, f) mRNA levels of *Lgr5* and *Ki67* were measured by qPCR in wt and mut SI organoids. (g, h, i) Levels of metabolic markers (lactate and glucose) were measured in the supernatants of intestinal organoids and Glut2 mRNA level (j) was measured by qPCR. Statistical differences were detected by paired t test. Data are mean ± SD. **p* < 0.05, ***p* < 0.01, *****p*< 0.0001. *Lyz1*: lysozyme 1; *Defa3*: alpha-defensin 3; *Glut2:* glucose transporter 2.

ATP8 mutant organoids exhibited an enhanced glycolytic metabolism as demonstrated by higher glucose consumption and higher lactate levels in their supernatant (Fig. 18g-i). Additionally, an upregulation of *Glut2* mRNA, a glucose transporter mainly present at the basolateral epithelium (Zietek et al., 2015), was found in *ATP8* mutant organoids (Fig. 18j).

4.5.2 AZA treatment improves PC function in SI 3D organoids

Subsequently, AZA was tested if it would reverse PC abnormality associated with mitochondrial dysfunction. *ATP8* mutant SI organoids were kept under standard medium for 4 days. Subsequently, medium was exchanged with either DMSO or 1 µM AZA-containing medium and organoids were incubated for 3 days (Fig. 19a). Similar to what was observed with wt organoids, AZA treatment influenced the size and shape of ATP8 mutant organoids reaching around 117 µm in diameter while control organoids` diameter was 176 µm (Fig. 19b,c). A rise in the mRNA expression of different PC markers (*Lyz1* and *Defa3*) was observed with AZA-treated ATP8 mut organoids (Fig. 19d,e). Further, protein level of lysozyme increased in AZA-treated organoids as demonstrated in Fig. 19g,h. *Atoh1* expression was moderately increased in AZA-treated organoids, while a comparable level of *Hes1* was found between both treatment groups (Fig. 19i,j). *Ki67* was downregulated, and level of lactate was decreased in AZA-treated organoids (Fig. 19f,k). On the other hand, levels of glucose did not greatly differ between the two groups (Fig. 19k).

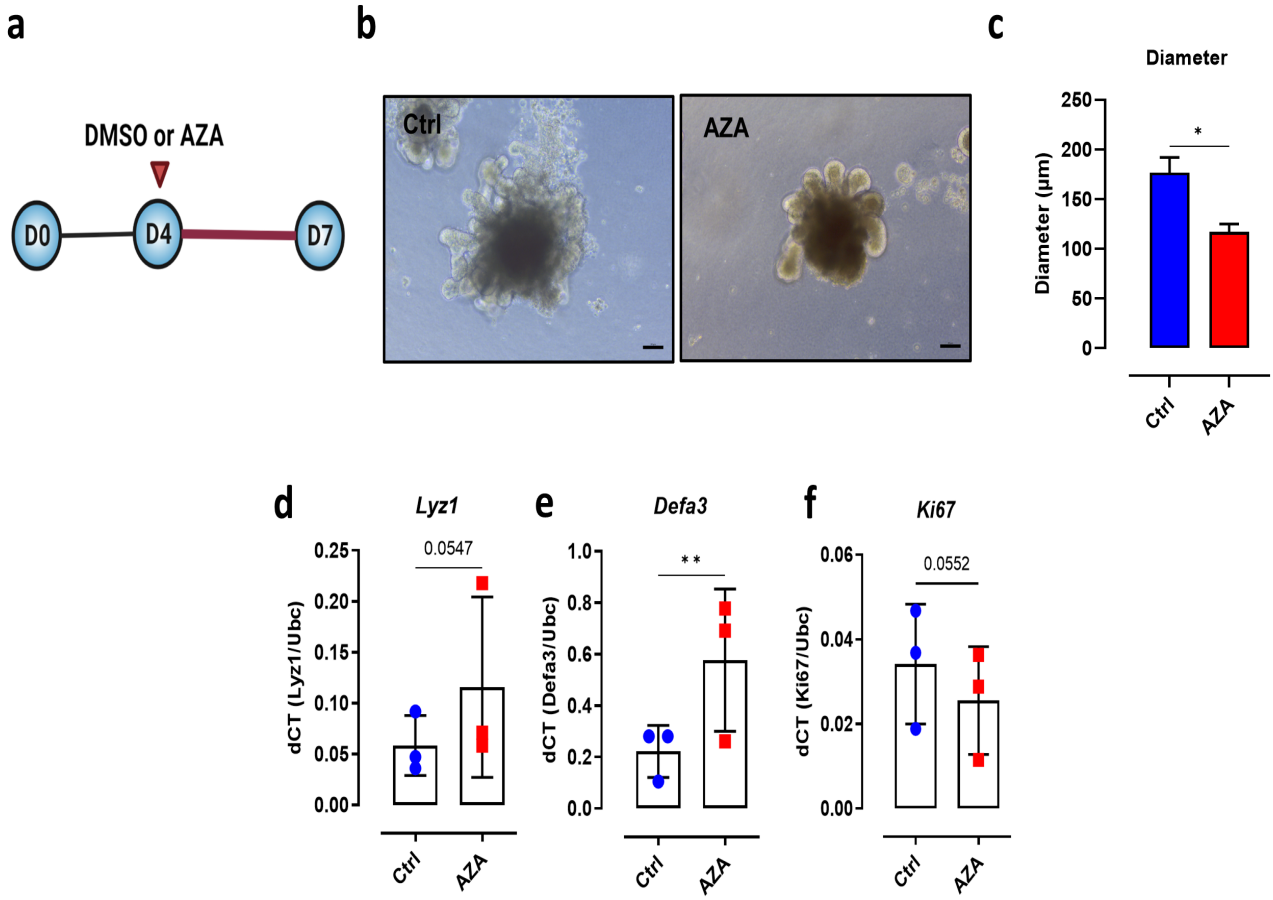

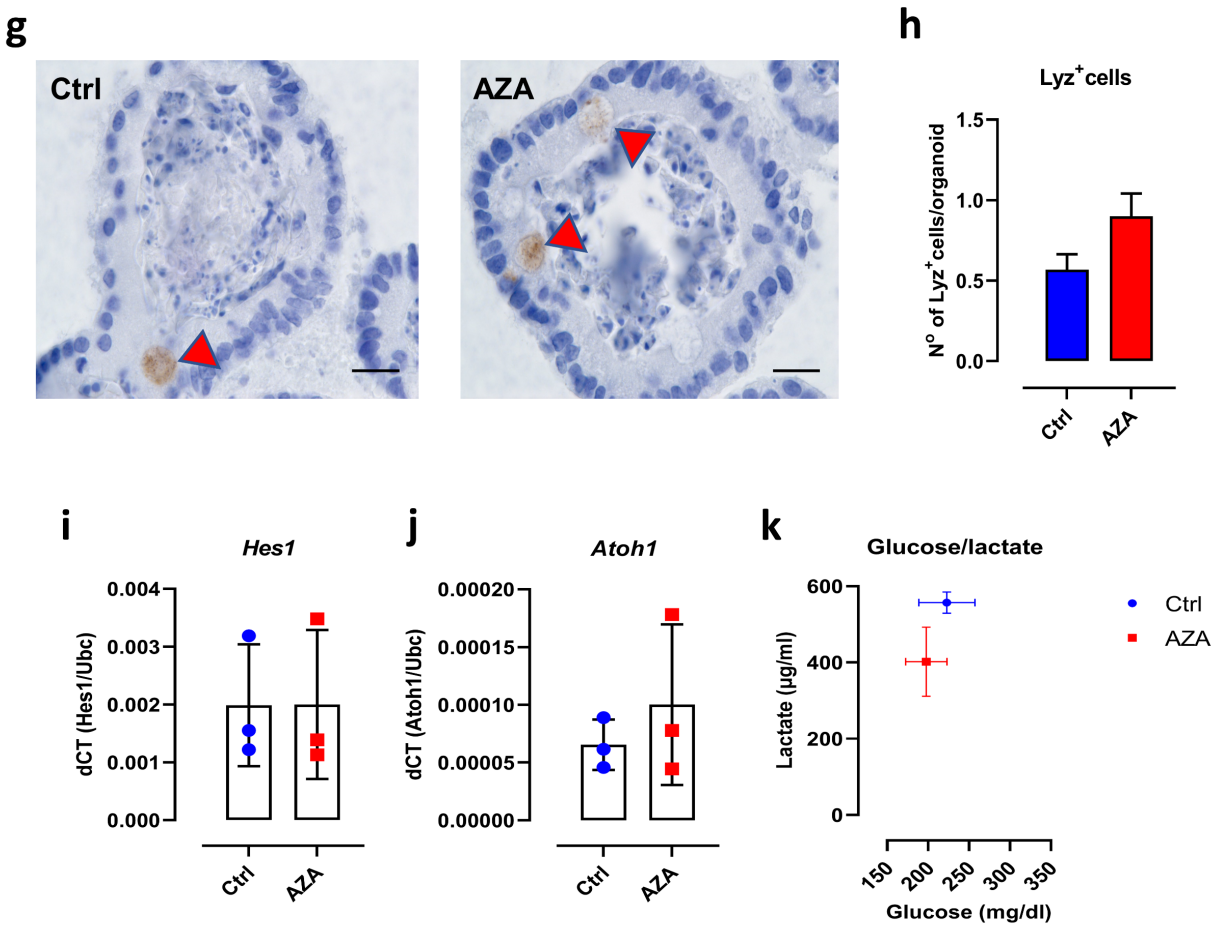

Figure 19. Effect of AZA on intestinal organoids with mitochondrial impairment. (a) ATP8 mutant SI organoids were maintained on standard medium for 4 days. Consequently, DMSO or AZA was introduced on day 4 at a concentration of 1µM for 3 days. (b) Microscopic appearance of SI organoids treated with DMSO or AZA. (c) Diameter of DMSO and AZA-treated organoids. mRNA expression of *Lyz1* (d), *Defa3* (e) and *Ki67* (f) in DMSO and AZA-treated organoids. (g) Immunohistochemistry staining of paraffin-embedded organoids with Lyz antibody. (h) Numbers of LyzC positive cells were counted in both ctrl and AZA-treated organoids using ImageJ software. mRNA levels of *Atoh1* (i), *Hes1* (j) were measured in ctrl and AZA-treated organoids via qPCR. (k) Glucose and lactate levels were measured in the supernatants of SI organoids. Statistical differences were detected by paired t test Data are mean ± SD. *$p < 0.05$, **$p < 0.01$. *Lyz1*: lysozyme 1; *Defa3*: alpha-defensin 3; *Atoh1*: Atonal BHLH Transcription Factor 1; *Hes1*: Hairy and enhancer of split-1.

Deleterious effects induced by mitochondrial mutation were resolved by AZA treatment. AZA-treated ATP8 mutant organoids exhibited elevated numbers of PCs and decreased lactate production. These findings corroborate the previous observation of enhanced mitochondrial respiration in AZA-treated MODE-K cells. One important facet of mitochondrial functions is the regulation of lipid metabolism (Vamecq et al., 2012). Mounting evidence suggests an altered lipid profile in CD

patients which is linked to PC impairment (Liu et al., 2021). Thus, the connection between diet-induced obesity and PCs was examined.

4.6 Accumulation of triglycerides is evident in CD patients

CD patients were found to have dysregulated metabolism with elevation of metabolites like lactate (Hove et al., 2009; Jansson et al., 2009). Other reports emphasized on the altered lipid profiles in IBD patients (Koutroubakis et al., 2001; Sappati Biyyani et al., 2010; Scoville et al., 2018). Similarly, a significant rise in triglyceride (TG) levels was observed in CD patients compared to healthy subjects (mean ± SD: 58.66 ± 16.68 vs. 23.75 ± 4.76 mg/dL, $p<0.0001$) (Fig. 20a). Female patients showed greater concentrations of TG than male patients (mean ± SD: 63.65 ± 5.54 vs. 51.42 ± 16.03 mg/dL) (Fig. 20b,c).

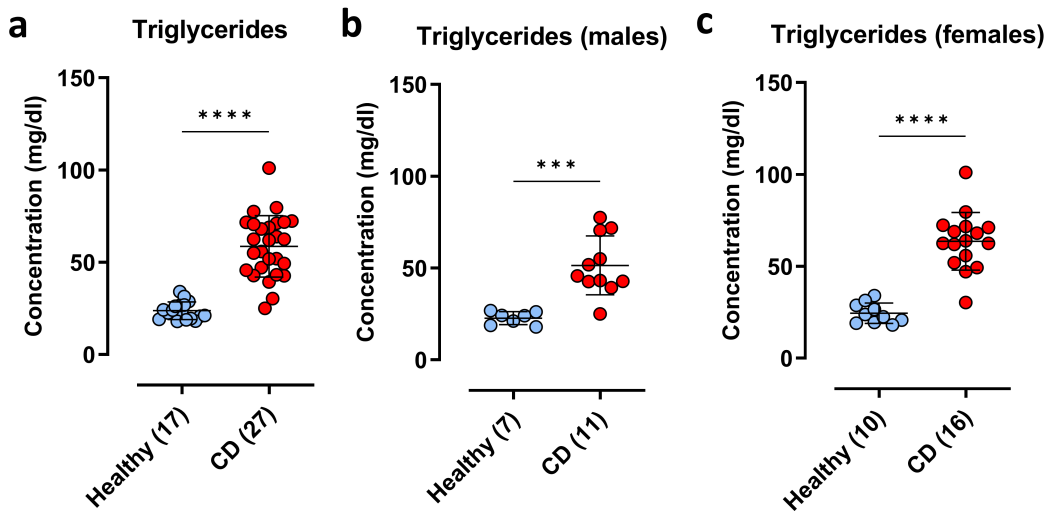

Figure 20. Serum triglyceride levels in patients with Crohn`s disease. (a) Levels of triglycerides were measured in CD patients and healthy controls. Readings were further divided based on gender; (b) males and (c) females. Statistical differences were detected by unpaired t test. Data are mean ± SD. ***$p < 0.001$, ****$p< 0.0001$.

It may be hypothesized that these findings might be attributable to mitochondrial impairment observed in IBD patients (Sünderhauf et al., 2021). Several inhibitors of mitochondrial OXPHOS induced TG accumulation and increased glucose uptake (Vankoningsloo et al., 2005). The next experiments were dedicated to examine diet-induced hypertriglyceridemia role in PC dysregulation.

4.7 Thermoneutral housing negatively affects Paneth cells

Several studies pointed out that PCs are highly sensitive towards diet-induced obesity (Hodin et al., 2011; Liu et al., 2021). Ambient temperature is a major contributing factor to energy expenditure and weight gain (Moellering and Smith, 2012). Nevertheless, this significant risk is usually overlooked in the design of most obesity mouse models. Giles *et al.* reported a model in which thermoneutral housing aggravated diet-induced non-alcoholic fatty liver disease (NAFLD) (Giles et al., 2017). To functionally characterize whether high TG levels impact PC differentiation and function, the obesity model described by (Giles et al., 2017) was used. C57BL6/J mice were divided into four groups; (1) chow diet-fed mice housed at 22°C, (2) chow diet-fed mice housed at 30°C, (3) HFD-fed mice housed at 22°C and (4) HFD-fed mice housed at 30°C (Fig. 21a). The whole experiment lasted for 6 weeks.

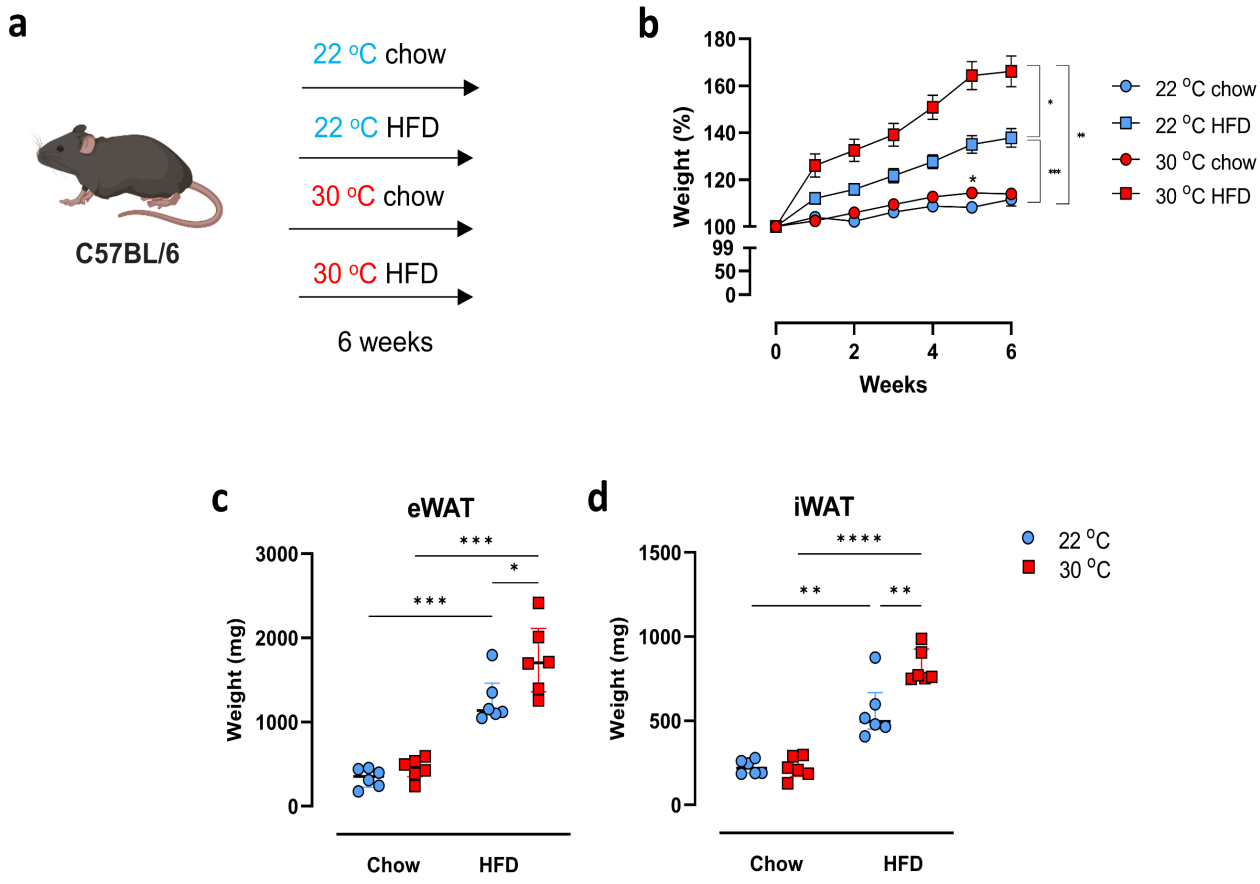

Figure 21. Effect of dietary modification and housing condition on obesity. (a) C57BL6/J mice were maintained on chow diet or HFD at either 22°C or 30°C for 6 weeks. (b) Weight gain was weekly monitored and mass of eWAT (c) and iWAT (d) was measured on the last day of the experiment. Significant differences were detected by performing two-way ANOVA. Results are shown as (b) mean ± SD; (c, d) median with interquartile range. *$p < 0.05$, **$p < 0.01$, ***$p < 0.001$, ****$p < 0.0001$. eWAT: epididymal white adipose tissue; iWAT: inguinal adipose tissue.

The highest weight gain was observed with HFD-fed mice housed at 30°C reaching an average of 166% in week 6 (Fig. 21b). In comparison to HFD-fed mice placed at 30°C, housing at 22°C resulted in a significantly lower body weight (mean: 138%). Interestingly, to a lesser extent, a similar difference could be seen in chow diet-fed animals between week 2 and 5. Moreover, changes observed with chow diet-fed mice reached a statistical significance in week 5 (Fig. 21b). Weights of different white adipose tissue (WAT), such as epididymal and inguinal WAT (eWAT and iWAT) showed similar findings to what observed with body weight (Fig. 21c,d).

Around 155 metabolites were identified in the serum of chow and HFD-fed mice through NMR spectroscopy analysis (detailed concentrations of each metabolite are listed in Table. 19,20). Principal component analysis (PCA) showed distinct metabolomics profiles based on diet type (Fig. 22a). When HFD mice were stratified according to housing conditions, a clear demarcation was also observed. In contrast, a large overlap was present between 22°C and 30°C housed chow-fed mice. Partial least squares discriminant analysis (PLS-DA) confirmed that data could be discriminated by dietary intake in combination with housing temperature (Fig. 22b).

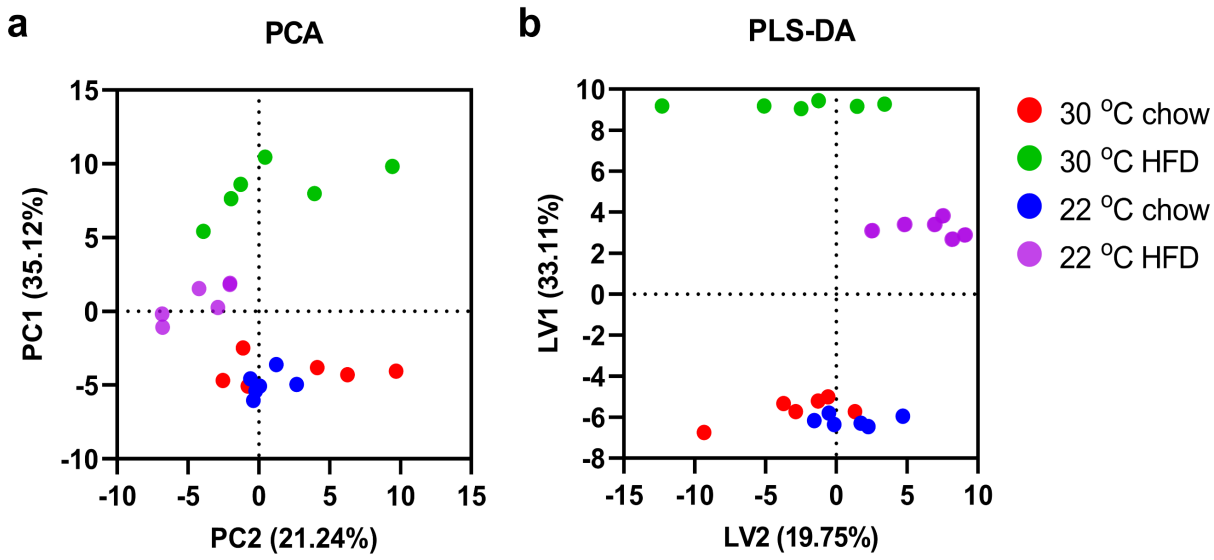

Figure 22. PCA (a) and PLS-DA (b) plots of the metabolome of mouse serum. ^{1}H-NMR metabolomic profiles of 30°C chow (red), 30°C HFD (green), 22°C chow (blue) and 22°C HFD (purple). The amount of variance is shown on each axis. (a) PCA: principal component analysis; PC: principle component; (b) PLS -DA: partial least squares discriminant analysis; LV: latent variable. Measurements and analysis were performed by Dr. Franziska Schmelter from the Institute of Nutritional Medicine, University Hospital Schleswig-Holstein, Campus Lubeck, Germany.

Differences in individual serum lipid metabolites were examined between the groups. In general, the highest concentrations of several metabolites were found in HFD-fed, 30°C group (phospholipid levels of IDL: 9.39± 0.316 mg/dL; cholesterol: 283.8 ± 8.12; triglycerides: 142.3 ± 8.68; triglyceride levels of LDL: 21.06±1.96; LDL: 146.2 ± 11.98) (Fig. 23 and Table 19). Notably, we observed metabolic alterations in chow diet- fed mice housed at 30°C in comparison with 22°C. Specifically, LDL-particles were upregulated in the former group (600.73 ± 69.16 vs. 516 ± 53.59 mg/dL, $p< 0.001$, Table. 19)

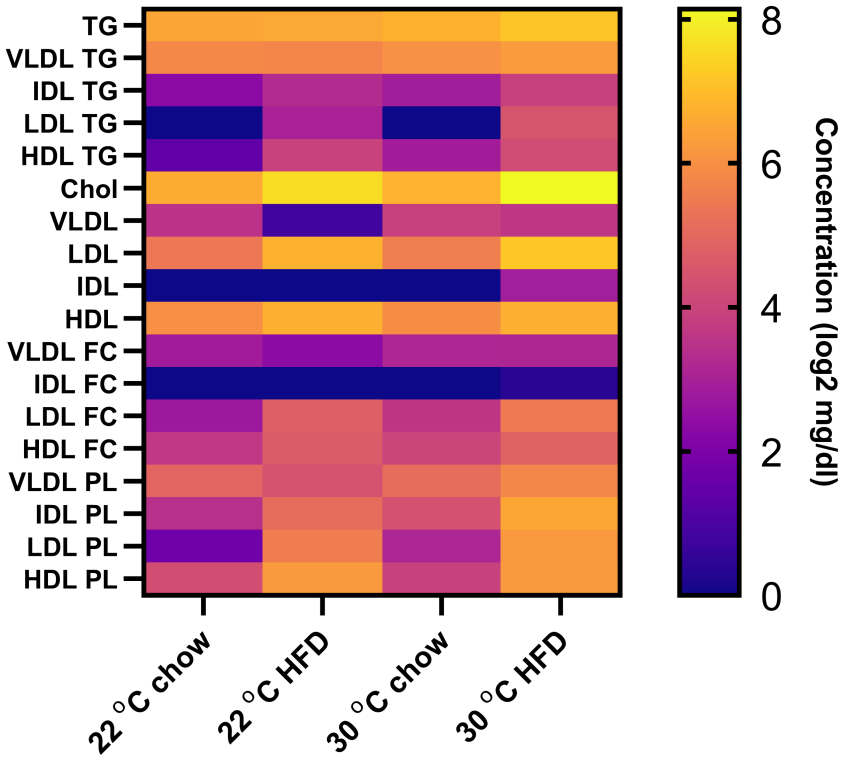

Figure 23. Serum lipid profiles of mice fed with either chow or HFD diet and housed under different housing temperature. Heat map of selected metabolite levels which was measured by ^{1}H-NMR. For each metabolite, the log2-median value was used. Yellow represents maximum levels and blue represents minimum levels. Detailed concentrations and statistical difference are shown in table 19, 20. TG: triglycerides; VLDL: very low density lipoprotein; IDL: intermediate lipoprotein; LDL: low density lipoprotein; HDL: high density lipoprotein; Chol: cholesterol; FC: free cholesterol; PL: phospholipids. Measurements and analysis were performed by Dr. Franziska Schmelter from the Institute of Nutritional Medicine, University Hospital Schleswig-Holstein, Campus Lubeck, Germany.

To examine the effect of observed dyslipidemia on PCs, ileal mRNA expression of *Lyz1* and *Defa3* was examined by qPCR. Chow diet-fed mice housed at 30°C displayed significantly lower levels of *Lyz1* in comparison to their counterparts at 22°C (Fig. 24a). On the other hand, thermoneutral-housed mice exhibited an upregulation in ileal *Defa3* expression regardless of dietary intake (Fig. 24b). H&E staining of ileal sections revealed mild and focal mucosal accumulation of inflammatory cells in HFD-fed mice (Fig. 24c).

Numbers of PC were the lowest in HFD-fed animals at 22°C, averaging around two cells per crypt (Fig. 24d). Ileum of HFD-fed mice at 30°C registered slightly higher numbers compared to 22°C, reaching an average of three PCs per crypt. Further, the levels of PCs were comparable in CD-fed groups with all animals exceeding three cells per crypt.

More pronounced findings were detected in IHC evaluation of ileal Lyz protein which is mainly expressed by PCs (Fig. 24e,f)**.** HFD-fed, 22°C group showed a severe loss of Lyz+ cells, reaching around 5% of ileal crypt. Interestingly, when compared to chow diet- fed group housed at 22°C, CD-fed mice placed at 30°C displayed significantly lower levels of Lyz protein.

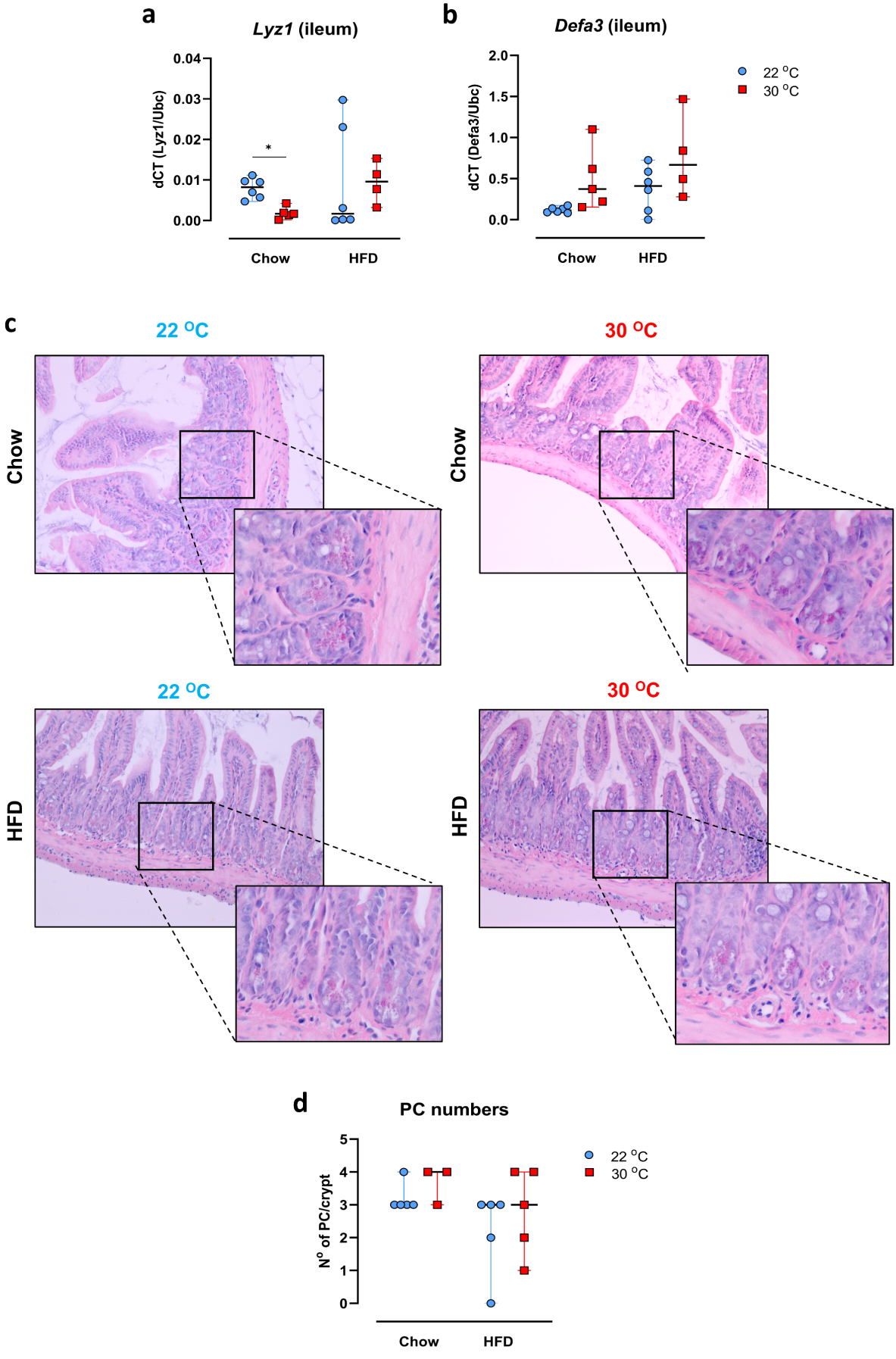
a
Lyz1 (ileum)
dCT (Lyz1/Ubc)
0.04
0.03
0.02
0.01
0.00
*
Chow
HFD
b
Defa3 (ileum)
dCT (Defa3/Ubc)
2.0
1.5
1.0
0.5
0.0
22 °C
30 °C
Chow
HFD
c
22 °C
30 °C
Chow
HFD
22 °C
30 °C
HFD
d
PC numbers
N° of PC/crypt
5
4
3
2
1
0
22 °C
30 °C
Chow
HFD

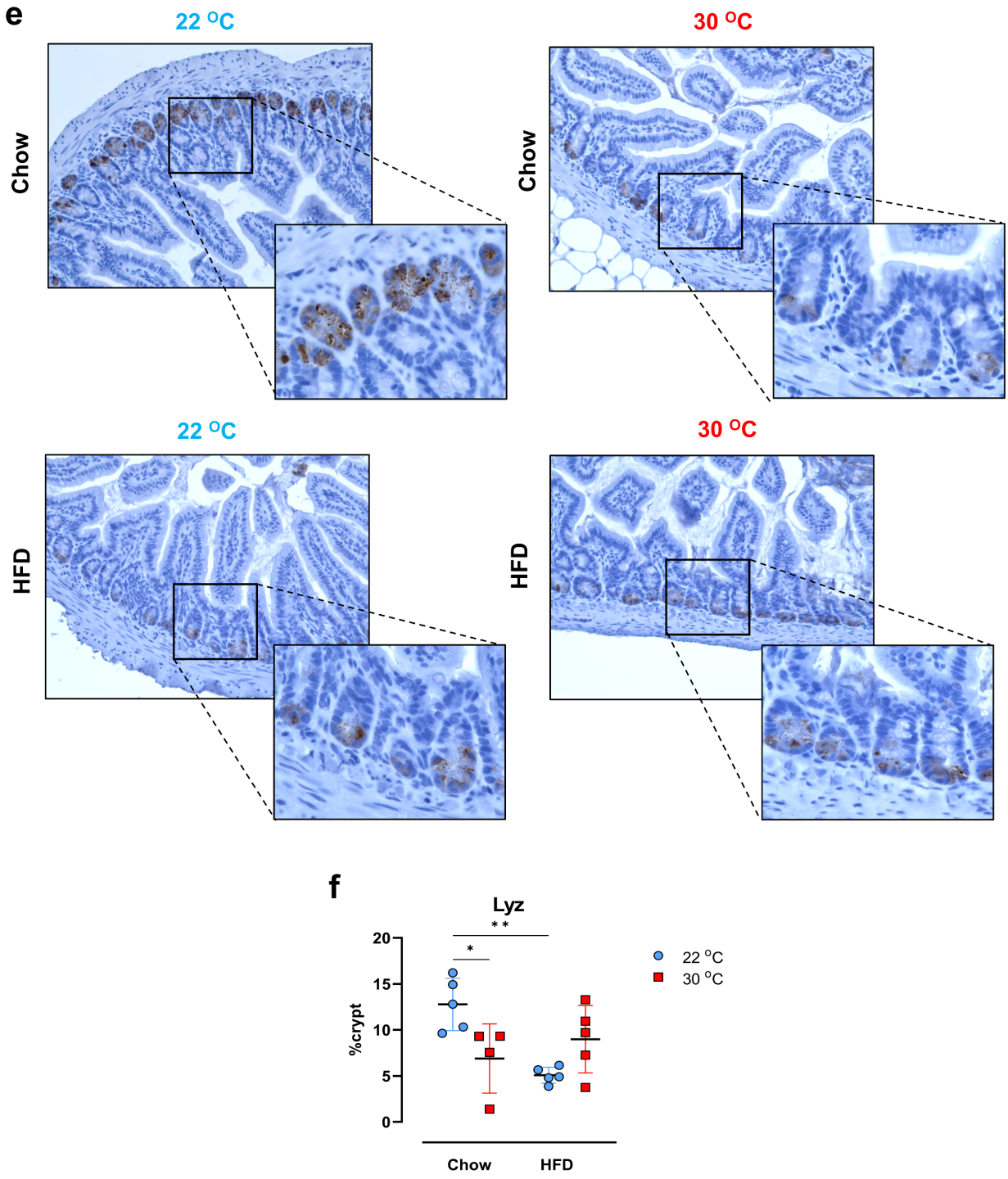

Figure 24. Effect of dietary modification and housing condition on PCs. Ileal mRNA expression of *Lyz1* (a) and *Defa3* (b) was measured via qPCR. (c) H&E staining of paraffin-embedded ileal sections. (d) Numbers of PCs per crypt were counted using ImageJ software. (e) Immunohistochemistry staining of paraffin-embedded ileum with Lyz antibody. (f) Levels of Lyz were measured in ileal crypts using ImageJ software. (a, b, f) Two-stage linear step-up procedure of Benjamini, Krieger and Yekutieli; (d) Holm-Šídák's multiple comparisons test; results are shown as (a, b, d) median with range and (f) mean ± SD. *$p < 0.05$, ***$p < 0.001$. Lyz: lysozyme; *Defa3*: alpha defensin 3; PC: Paneth cell.

To mimic the *in vivo* findings, B6 SI organoids were either treated with DMSO (0.3% v/v) or 30 µM palmitic acid (PA) for 7 days. PA is one of the major fatty acids present in HFD used in the animal study and it is known to induce negative modulation of IECs (Beyaz et al., 2016; Gori et al., 2020). Organoid numbers and morphology were unaffected by PA treatment (Fig. 25a,b). Similarly, PA-treated organoids exhibited comparable mRNA levels of AMPs: *Lyz1* and *Defa3* to control (Fig. 25c,d). On the other hand, *Lgr5* was slightly raised under PA treatment, indicating higher proliferative status (Fig. 25e).

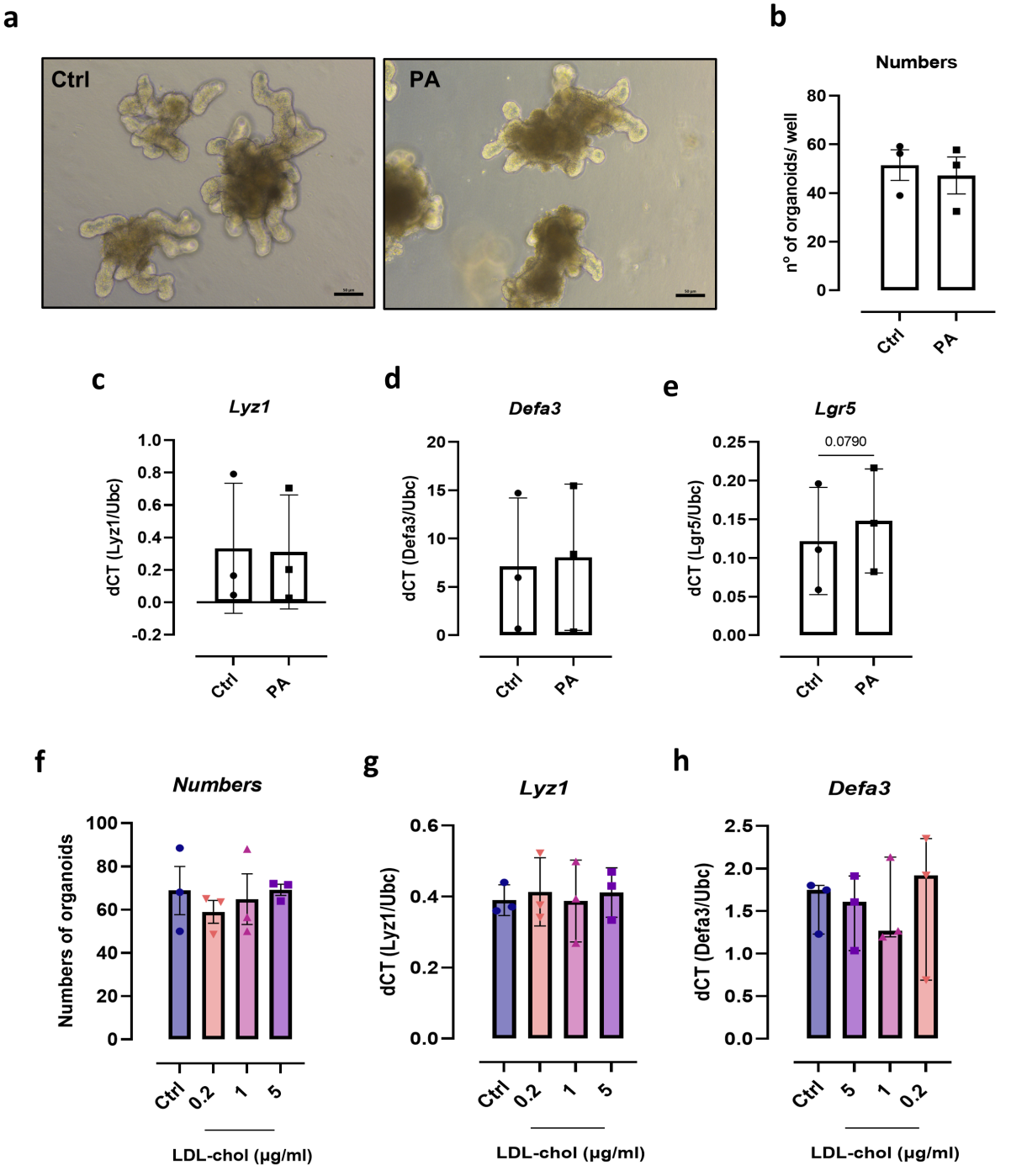

Figure 25. Effect of lipid moieties on SI organoids. B6 organoids were treated with either DMSO or PA (30 µM) for 7 days. (a) Microscopic appearance of DMSO or PA-treated organoids on day7. (b) Numbers of organoids were counted and (c, d, e) mRNA expression of *Lyz1*, *Defa3, Lgr5* was measured via qPCR. SI organoids were treated with 150 mM NaCl, 0.01% EDTA or LDL-chol (0.2, 1 and 5 µg/ml) for 7 days. (f) Numbers of organoids were counted and (g, h) mRNA expression of *Lyz1* and *Defa3* was measured via qPCR. (c,d,e) Statistical differences were detected by paired t test Data are shown as mean ± SD. PA: palmitic acid; LDL-chol: low density lipoprotein- cholesterol; *Lyz*: lysozyme; *Defa3*: alpha defensin 3.

In another set of experiments, 3D-organoids were treated with different concentrations of low density lipoprotein-cholesterol (LDL-chol) (0.2, 1 and 5 µg/ml) for 7 days. Overexpression of LDL receptor caused downregulation of PC-related genes (Meoli et al., 2019). Similar to what was observed with PA, changes in numbers or expression of PC-associated markers were minimal in LDL-chol-treated organoids compared to controls (Fig. 25 f-h).

Dyslipidemia induced by short-term intake of HFD along with thermoneutral housing severely affected AMPs repertoire without the appearance of noticeable clinical manifestations. This is an indication that the downregulation in AMPs in CD patients does not come secondary to intestinal inflammation. Since AZA induced changes in glucose/lactate ratio and improved PC differentiation *in vitro*, it was speculated that lipid metabolites are influenced by AZA therapy.

4.8 Cholesterol and LDL-6 subfraction were significantly downregulated by azathioprine treatment

Subsequently, it was assessed if AZA possesses lipid-lowering activity by examining CD patients' sera. Metabolites of patients who received AZA in the period between 2017-2022 were compared to those who were not treated with the drug via NMR analysis. Overall, levels of various major lipid metabolites, including cholesterol, very low density (VLDL), low density (LDL), intermediate (IDL) and high density (HDL) lipoproteins were comparable between the two groups (Fig. 26a, Table 21,22). Free cholesterol concentration in LDL subfraction 6 (LDL-6 FC) was exceptionally reduced in AZA-treated patients (mean ± SEM: 5.67 ± 2.01 vs. 7.15 ± 2.86 mg/dL, $p < 0.05$) (Fig. 26b, Table 21,22).

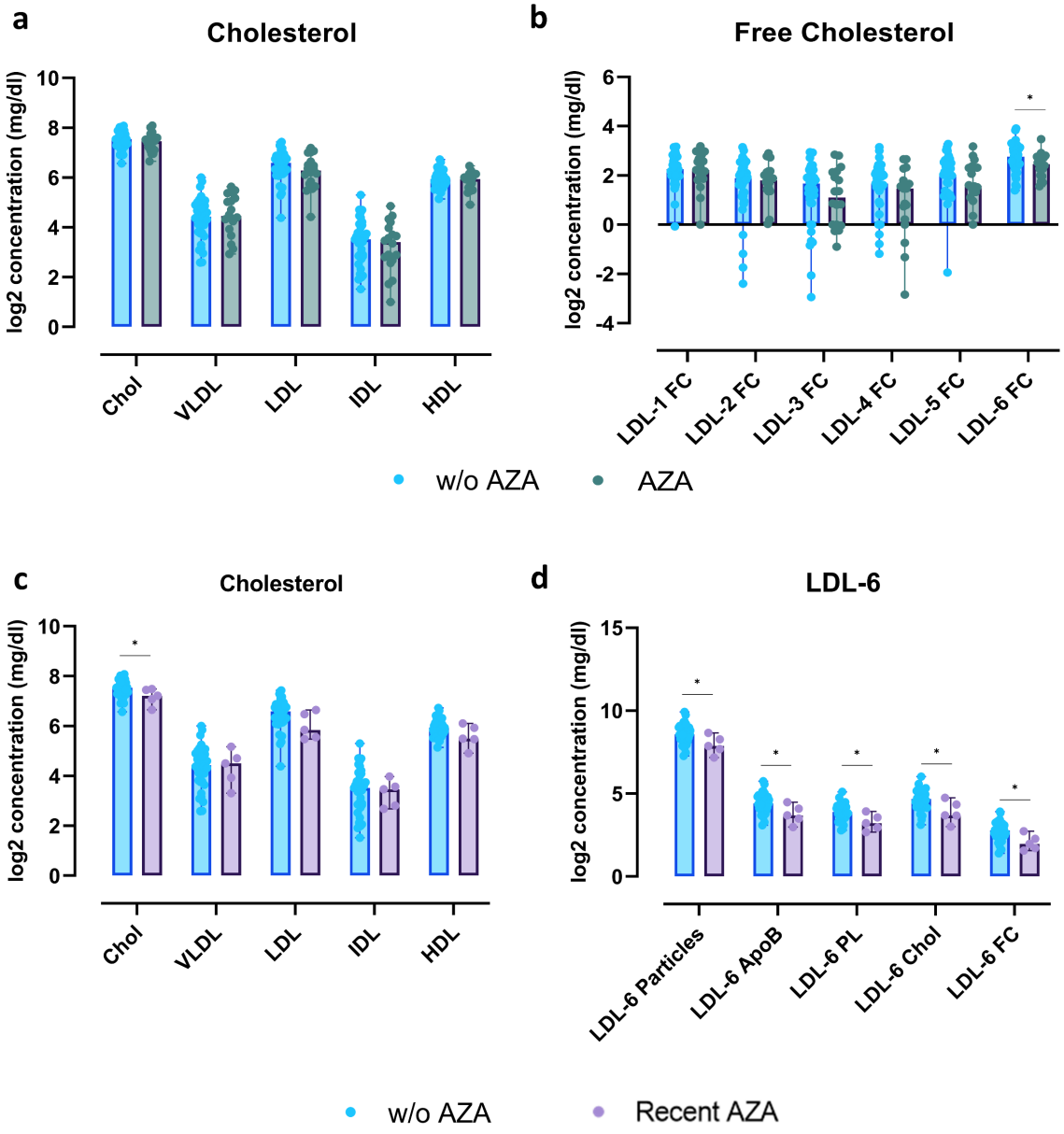

Figure 26. Serum lipid profiles of patients with Crohn`s disease. (a,b) Levels of various metabolites were measured by ^{1}H-NMR in the serum of AZA treated and control CD patients. Lipoproteins (c) and LDL-6 subfraction (d) were determined in patients who recently received AZA and compared to non-AZA treated counterparts. Significant differences were detected by performing multiple Mann-Whitney tests. Data are shown as median with range. *p < 0.05. VLDL: very low density lipoprotein; IDL: intermediate lipoprotein; LDL: low density lipoprotein; HDL: high density lipoprotein; Chol: cholesterol; FC: free cholesterol; PL: phospholipids. Detailed concentrations and comparison tests could be found in Table 21, 22. Measurements and analysis were performed by Dr. Franziska Schmelter from the Institute of Nutritional Medicine, University Hospital Schleswig-Holstein, Campus Lubeck, Germany.

By only comparing patients currently on AZA regimen to non-AZA-treated ones, more significant variances were detected. Specifically, diminished concentrations of cholesterol were found in the sera of the former group (mean ± SD:147.8 ± 31.93 vs. 190.1 ± 44.74 mg/dL, $p < 0.05$) (Fig. 26c). Likewise, different lipid moieties in LDL-6, such as LDL-6 FC, phospholipids (LDL-6 PL), apolipoprotein B (LDL-6 ApoB) and cholesterol (LDL-6 Chol) were decreased in patients recently treated with AZA (Fig. 26d). These findings indirectly showed that AZA rescuing effects in the intestine might be explained through the regulation of lipid metabolism.

5. Discussion

5.1 Ileal compartment is highly affected by azathioprine therapy

AZA belongs to a wide spectrum of drugs used in the management of IBD and specifically CD (Baumgart and Sandborn, 2012). Further, AZA is often prescribed in several autoimmune diseases such as Behçet syndrome, autoimmune hepatitis and Bullous pemphigoid ("Azathioprine: Drug information - UpToDate," 2022). The immunosuppressive effects of AZA were heavily investigated with slight focus on IECs (Winkelstein, 1979). Hence, the question was how AZA, an orally administered drug will impact the development and the metabolism of IECs. The first evidence collected is the high expression of AZA-metabolizing enzymes in terminal ileum. Interestingly, correlation analysis revealed a positive correlation between ileal *HPRT1* expression and PC markers, *LYZ* and *DEFA6*. HPRT is an important catalyst in the process of the formation of active AZA metabolites (Gearry and Barclay, 2005). Enzymatic activity of HPRT is a useful indicator of AZA cytotoxic side effects such as leukopenia (Ding et al., 2012). Moreover, patients with HPRT deficiency respond to AZA ineffectively (Derijks and Wong, 2009). Several gut bacterial species like *E.coli* and *Bacteroides thetaiotaomicron* were reported to possess the capability of metabolizing AZA by releasing HPRT (Lazarević et al., 2022).

PCs play a crucial role in the maintenance of mucosal immunity (Cray et al., 2021). Disrupted PC function and reduced levels of AMPs were associated with ileal CD (Wehkamp and Stange, 2020). Several PC markers were upregulated in AZA-treated CD patients. On the other hand, the only study which addressed this question found no influence of AZA on mRNA expression of ileal AMPs (Kübler et al., 2009). The patients recruited for this study were experiencing clinical relapse and the authors reported increased expression of both *DEFA5* and *DEFA6* in severely inflamed ileal tissue. One can argue that the observations made by Kübler *et al.* are rather due to the inflammatory status associated with active disease which might have masked the real effects of AZA. Further, this study made no statement about the time at which AZA was introduced nor the duration of the therapy.

Based on these observations, it was postulated that AZA specifically targets pathways involved in proliferation and differentiation. This hypothesis was reinforced by *in vitro* experiments. Using different cell lines and SI organoids, AZA treatment improved

differentiation towards secretory cell lineage and dampened proliferation. Two independent studies showed similar findings in several epithelial cell lines (Khare et al., 2019; Schroll et al., 2005).

AZA is a considerably slow-acting drug as the first signs of clinical improvement might take several months (Espín and García-Fernández, 2022). There is no clear explanation of this phenomenon that makes some physicians favor using other rapidly acting medications. Ben-Horin *et al.* proposed an explanation based on T cell perspective (Ben-Horin et al., 2009). The authors suggested that AZA-late response is owing to a long gap between the initiation of AZA therapy and proapoptotic effect. T cells with arrested cell cycle were found to retain their effector capacity that causes tissue damage. On the other hand, enhanced epithelial differentiation was evident only after three days of AZA introduction in intestinal organoids. The intestinal physiology is quite complex and the turnover of cells such as PCs takes weeks (Stappenbeck, 2009). Further, despite its vitality in modeling intestinal health and disease, organoid system still does not fully mimic the *in vivo* scenario.

Interestingly, contrasting variations were found between MODE-K and HT29 on the one hand and Caco-2 cells on the other in response to AZA. Different reasons could explain this disparity. First, activity of AZA-metabolizing enzymes might vary between cell lines. In the present study, mRNA levels of *HPRT1*, *TPMT* and *XDH* greatly varied between cell lines. AZA dosage adjustment is recommended for patients with TPMT deficiency (Yang et al., 2019). Another explanation is the different physiological nature of intestinal cell lines. Collett *et al.* revealed that drug transport is strongly related to transepithelial electrical resistance (TEER) (Collett et al., 1996). While HT29 monolayer exhibited TEER equivalent to that of the intestine, Caco-2 required calcium chelation to reach *in vivo* TEER.

One of the mechanisms by which AZA induces apoptosis is targeting Rac1 (Tiede et al., 2003). Mutations in Rac1 impacted intestinal epithelial differentiation and proliferation (Cheung et al., 2016; Stappenbeck and Gordon, 2000). As previously mentioned in the introduction section, PC autophagy plays an important role in the pathogenesis of CD. Through autophagy, engulfed misfolded proteins, damaged organelles, and invading bacteria by phagophores form what is known as autophagosomes which would eventually lead to the activation of innate immunity

(Yang and Shen, 2021). Similarly, Hooper *et al* suggested that AZA exerts its effect by targeting mTORC1, a major regulator of autophagy, in macrophages (Hooper et al., 2019).

5.2 Azathioprine induces changes in host metabolism

The observations regarding AZA impact on the balance between cellular differentiation and proliferation were associated with metabolic alterations. Decreased glycolysis and heightened mitochondrial OXPHOS were evident in AZA-treated cells. The effect of AZA on host metabolism is largely undefined, let alone the intestinal metabolism. Riegel *et al.* explored carbohydrate metabolism in rat hepatocytes after intraperitoneal injection of AZA for 2 weeks (Riegel et al., 1990). They concluded that liver glucose and lactate were comparable to that of their control counterparts. Nonetheless, liver glycogen was significantly decreased in AZA-treated animals. Specifically, glycogen formation was diminished in hepatocytes of AZA-treated group when pyruvate used as a substrate but not in the presence of the NEAA, serine. Pyruvate is an important metabolite, sitting at the crossroads of major metabolic pathways namely glycolysis and gluconeogenesis (Gropper and Smith, 2012). The aforementioned study comes in agreement with our data, indicating that AZA is targeting pathways involved in glucose metabolism.

5.2.1 Impaired OXPHOS-induced PC dysfunction is restored by AZA therapy

Mitochondria exert leverage in the stemness and differentiation of IECs. This role is could clearly be spotted upon mitochondrial impairment associated with IBD. Khaloian *et al.* reported that inducing mitochondrial dysfunction by ISC-specific deletion of mitochondrial chaperone Hsp60 resulted in reduced stemness and the development of abnormal PCs (Khaloian et al., 2020). Further, mitochondrial dysfunction linked to ablation of prohibitin 1 in IECs preceded spontaneous ileitis with abnormalities in PCs functions (Jackson et al., 2020). Alula *et al* demonstrated that PCs of CD patients displayed mitochondrial deformities in comparison with non-IBD controls (Alula et al., 2021). These changes were not exclusive to patients with active disease but interestingly involved inactive CD (Alula et al., 2021). Accumulation of mutations in mitochondrial DNA eventually results in a wide range of pathological disorders (Taylor and Turnbull, 2005). This is due to the vestigial nature of mitochondrial DNA repair system which make it more susceptible to harmful damages (Tuppen et al., 2010).

Grieves *et al* elucidated how mitochondrial mutations spread in all cells along colonic crypt from one mutated ISC (Greaves et al., 2006).

Mitochondrial ATP synthase, a rotatory complex, contains 17 protein subunits and consists of a membrane-extrinsic F1 catalytic and membrane-embedded Fo domains, which are connected by a peripheral and central stalk Consistent with the previous studies, mutation in mitochondrial *ATP8* gene influenced PCs differentiation in both ileum and SI organoids. Polymorphisms in mitochondrial ATP8 are linked to GIT pathologies such as irritable bowel disease (Wang et al., 2013). PCs tightly regulate gut microbiota composition through MyD88 pathway (Salzman et al., 2010; Vaishnava et al., 2008). This could explain previous findings when changes was reported in the microbial communities of ATP8 mut mice (Hirose et al., 2017). Accumulating data linked altered host mitochondrial functions and dysbiosis in CD (Jackson and Theiss, 2019; Mottawea et al., 2016).

To compensate for the defect in energy generation, *ATP8* mut organoids exhibited changes in their metabolic phenotype as demonstrated by increased glucose uptake and high lactate production. Aerobic glycolysis gives rise to pyruvate which is mainly converted to lactate at the expense of entering the TCA cycle (Urbauer et al., 2021). ISC expansion was not impacted by mitochondrial mutation as seen with the unaltered *Lgr5* expression. Heightened lactate production might have contributed to the maintenance of ISCs. Loss of lactate dehydrogenase which catalyzes pyruvate conversion to lactate reduced ISC expansion in *Drosophila* (Dan Wang et al., 2021). Another indication of the increased glucose uptake in *ATP8* mut organoids is the upregulation of the glucose transporter, *Glut2* on mRNA levels. Glut2 was found to be localized at the basolateral side of the epithelium in SI organoids (Zietek et al., 2015). Despite that Glut2 drives glucose exit into the circulation, the presence of a gradient across the membrane changes the direction to glucose import into the cells (Zietek et al., 2015). Given that organoid is a closed system, it is assumed the existence of a gradient that activates Glut2.

Contrary to what was observed with boosted mitochondrial respiration in AZA-treated cells, the majority of publications state that AZA causes hepatic mitochondrial injury and ATP depletion (Lee and Farrell, 2001; Tapner et al., 2004). One explanation for this toxic effect is the high AZA concentration used in these studies. Mitochondrial

injury was observed with a dosage of above 100 µM which exceeds the standard therapeutic doses (1.5-2.5 mg/kg body weight). Exceptionally, Khare *et al* reported a decrease in intracellular reactive oxygen species (ROS) in AZA-treated intestinal cells exposed to mitochondrial stress (Khare et al., 2019). In Khare *et al* and the present study, a maximum concentration of 10 µM was used. Taken together, these reported variations might be due to cell-specific effect and targeting of highly proliferative cells.

5.2.2 CD-associated dyslipidemia might be corrected by AZA

HFD-induced obesity was found to have deleterious effects on PCs which comes in line with various studies (Beyaz et al., 2016; Hodin et al., 2011; Liu et al., 2021). However, most of these reports focused on the long-term effects of western diet. Liu *et al.* showed that 8-week intake of HFD induced negative impact on PC numbers and morphology (Liu et al., 2021). However, in the present study, aberrant PCs were detected as early as 6 weeks of HFD intake. This early impact could be attributable to the higher fat content used in our experiments. While the diet used by Liu *et al.* contained 40% fat content, it was higher in our study reaching 60%. Moreover, mice, which also exhibited diminished PCs, were fed 60% fat diet for 14 months in the study by (Beyaz et al., 2016). The alterations observed were accompanied by negligible intestinal inflammation, indicating that gut injury is probably secondary to diet-induced changes in intestinal epithelium.

On the other hand, treating intestinal organoids with PA or LDL didn't result in loss of AMPs on mRNA level as observed *in vivo.* These observations come in line with what was reported by (Filippello et al., 2022). Despite using high concentration of PA (0.5 mM) which resulted in decreased viability, mRNA expression of PC markers: *Lyz1* and *Sox9* was unaltered in intestinal organoids. Treatment of organoids with 30 µM PA for 3-4 weeks induced the accumulation of Lgr5+ ISCs as reported by (Beyaz et al., 2016). However, the authors didn't address the functional status of PCs in this model. A similar upregulation of *Lgr5* mRNA was observed in the present study which might indirectly indicate the heightened self-renewal of ISC at the expense of differentiation. Another hypothesis is that PCs might be incapable of metabolizing lipids. Beumer et al., 2022 reported that lipid metabolism is linked to BMP activation which reaches its peak at the tip of the intestinal villi where enterocytes reside. Further, A study using single-cell RNA sequencing (RNA-seq) recently found that enterocytes in SI organoids do not express many apolipoproteins markers (Fujii et al., 2018).

Ambient temperature is a major understated factor that plays an important role in intestinal physiology (de Moraes et al., 2021; Giles et al., 2017; Wang et al., 2022; Xing et al., 2022). For example, incubation of Caco-2/HT-29 co-culture at 40°C or 42°C disrupted barrier integrity and increased permeability (Lian et al., 2021). Independent of dietary intake, mice housed at 30°C exhibited low levels of ileal Lyz protein. This could be a valid explanation of the high intestinal permeability observed by Giles *et al.* in animals housed in a similar conditions (Giles et al., 2017). Defective PCs induce gut dysbiosis and incite the growth of invasive pathogenic bacteria which compromise intestinal permeability (Burger et al., 2018).

Metabolically, cholesterol concentrations were highly in Tn-housed mice. Liu *et al.* proposed that the accumulation of secondary bile acids in the terminal ileum is behind the western diet-induced PC dysfunction (Liu et al., 2021). Liver cholesterol is the source of primary bile acids which are later converted to secondary bile acids by bacteria such as *Clostridium* spp in the terminal ileum (Chiang and Li, 2009). In another study, inhibition of the phospholipid-remodeling enzyme, Lpcat3, which was associated with accelerated cholesterol biosynthesis, resulted in a reduction in the number of Lyz+ PCs (Wang et al., 2018).

AZA-treated patients were found to have lower accumulation of cholesterol and lipid moieties conjugated to LDL-6. LDL-6, which belongs to dense LDL, is known to be a potent atherogenic LDL subclass (Marz et al., 1993; Winkler et al., 2003a, 2003b). Nam *et al.* approached this premise in patients with glioblastoma (Nam et al., 2021). Downregulation of proteins involved in cholesterol biosynthesis, including LDLR, FDFT1, EPHA2 was observed in cells treated with AZA (Nam et al., 2021). Conversely, combing cyclosporine and steroids with AZA therapy did not induce changes in the lipid profiles of patients who underwent renal transplantation (Akman et al., 2007).

5.3 Limitations

One of the biggest challenges in this study is the collection of human samples. The onset and duration of AZA therapy could not be verified in all patients. Additionally, since IBD management usually includes combination therapy, it can be argued that the ameliorating effects observed in AZA-treated patients might be due to synergistic effect. Nonetheless, the real impact of AZA on PCs was clearly evident when *in vitro*

assessment was performed. Duration of AZA therapy usually takes months but the positive effects were observed after only 3 days in the present study. A longer treatment period that can mimic *in vivo* scenario could not be implemented due to the drawbacks associated with cell culture models. Therefore, an animal study is still needed to validate these findings.

In vitro models of human intestine don't fully recapitulate *in vivo* physiology in different aspects such as oxygen levels and metabolism. While partial pressure of oxygen (pO_2) is around 32 mmHg (~5%) in the small intestine, the pO_2 at the sea level ranges between 140–150 mmHg (~21%) (Konjar et al., 2021). Additionally, an oxygen gradient was reported to exist along the intestinal crypt-villus axis with pO_2 of 22 mm Hg (3%) at the villus tip and around 59 mmHg (8%) at the crypt base (Fisher et al., 2013). Moreover, metabolic composition of intestinal lumen and blood is far more complex than that of commercially available cell culture media. These variations play crucial role in intestinal epithelium differentiation and regeneration.

5.4 Conclusion

In conclusion, mitochondria are essential for maintaining PC development and function. Metabolic alterations define cell fate within the intestinal crypt. In mt-*Atp8* mutant mice, the steady-state metabolism is shifted towards glycolysis at the expense of mitochondrial OXPHOS. As a consequence, levels of AMPs were decreased in the ileal compartment of these mice which is likely behind the changes observed in their gut microbiota. CD patients exhibited similar characteristics which have been linked to mitochondrial impairment. Interestingly, AZA was found to reverse this impairment through metabolic modulation (Fig. 27). AZA induced changes in IECs with specific effect towards PCs by targeting mitochondrial OXPHOS and glycolysis pathways. Changes in lipid profile were found to be associated with CD. Indeed, metabolic alterations induced by dietary modifications negatively altered PC functions. Indirect evidence indicated that AZA overcomes PC dysfunction capacity through lipid-lowering activity.

This study clearly revealed an unexplored aspect of AZA mechanism of action. This will open the way to a better refinement of CD therapy according to patients' needs. In that respect, further investigations are needed to pinpoint the pathways targeted by AZA. The active metabolites of AZA are diverse and the question still remains whether

these molecules possess unique features and moreover, more studies are required to elucidate if the AZA-induced changes observed in PCs are reflected on gut microbiota and lipid metabolism.

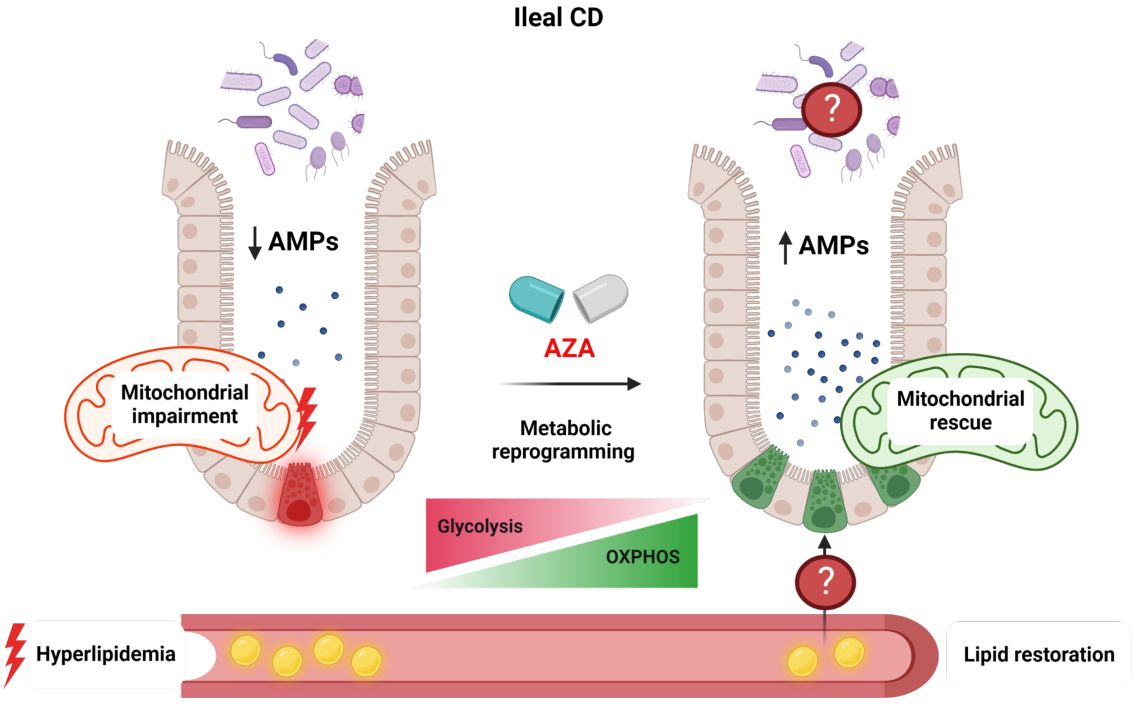

Figure 27. A schematic description of the impact of AZA on intestinal metabolism and PC function. Designed with Biorender.com

6. References

A-Rahim, Yousif I; Farrell, R.J., 2021. Overview of azathioprine and mercaptopurine use in inflammatory bowel disease - UpToDate [WWW Document]. URL https://www.uptodate.com/contents/overview-of-azathioprine-and-mercaptopurine-use-in-inflammatory-bowel-disease?search=crohn disease &topicRef=4069&source=related_link (accessed 7.26.21).

Akman, B., Uyar, M., Afsar, B., Sezer, S., Ozdemir, F.N., Haberal, M., 2007. Lipid Profile During Azathioprine or Mycophenolate Mofetil Combinations With Cyclosporine and Steroids. Transplant. Proc. 39, 135–137. https://doi.org/10.1016/J.TRANSPROCEED.2006.10.210

Alatab, S., Sepanlou, S.G., Ikuta, K., Vahedi, H., Bisignano, C., Safiri, S., Sadeghi, A., Nixon, M.R., Abdoli, A., Abolhassani, H., Alipour, V., Almadi, M.A.H., Almasi-Hashiani, A., Anushiravani, A., Arabloo, J., Atique, S., Awasthi, A., Badawi, A., Baig, A.A.A., Bhala, N., Bijani, A., Biondi, A., Borzì, A.M., Burke, K.E., Carvalho, F., Daryani, A., Dubey, M., Eftekhari, A., Fernandes, E., Fernandes, J.C., Fischer, F., Haj-Mirzaian, Arvin, Haj-Mirzaian, Arya, Hasanzadeh, A., Hashemian, M., Hay, S.I., Hoang, C.L., Househ, M., Ilesanmi, O.S., Balalami, N.J., James, S.L., Kengne, A.P., Malekzadeh, M.M., Merat, S., Meretoja, T.J., Mestrovic, T., Mirrakhimov, E.M., Mirzaei, H., Mohammad, K.A., Mokdad, A.H., Monasta, L., Negoi, I., Nguyen, T.H., Nguyen, C.T., Pourshams, A., Poustchi, H., Rabiee, M., Rabiee, N., Ramezanzadeh, K., Rawaf, D.L., Rawaf, S., Rezaei, N., Robinson, S.R., Ronfani, L., Saxena, S., Sepehrimanesh, M., Shaikh, M.A., Sharafi, Z., Sharif, M., Siabani, S., Sima, A.R., Singh, J.A., Soheili, A., Sotoudehmanesh, R., Suleria, H.A.R., Tesfay, B.E., Tran, B., Tsoi, D., Vacante, M., Wondmieneh, A.B., Zarghi, A., Zhang, Z.J., Dirac, M., Malekzadeh, R., Naghavi, M., 2020. The global, regional, and national burden of inflammatory bowel disease in 195 countries and territories, 1990–2017: a systematic analysis for the Global Burden of Disease Study 2017. Lancet Gastroenterol. Hepatol. 5, 17–30. https://doi.org/10.1016/S2468-1253(19)30333-4/ATTACHMENT/5AA708E8-7CFF-4F76-9A08-991638178EC5/MMC1.PDF

Alula, K.M., Jackson, D.N., Smith, A.D., Kim, D.S., Turner, K., Odstrcil, E., Kaipparettu, B.A., Dassopoulos, T., Venuprasad, K., Feagins, L.A., Theiss, A.L., 2021. Targeting Mitochondrial Damage as a Therapeutic for Ileal Crohn's Disease. Cells 10. https://doi.org/10.3390/CELLS10061349

Amre, D.K., MacK, D.R., Morgan, K., Israel, D., Lambrette, P., Costea, I., Krupoves, A., Fegury, H., Dong, J., Grimard, G., Deslandres, C., Levy, E., Seidman, E.G., 2009. Interleukin 10 (IL-10) gene variants and susceptibility for paediatric onset Crohn's disease. Aliment. Pharmacol. Ther. 29, 1025–1031. https://doi.org/10.1111/J.1365-2036.2009.03953.X

Ananthakrishnan, A.N., 2015. Epidemiology and risk factors for IBD. Nat. Rev. Gastroenterol. Hepatol. 12, 205–217. https://doi.org/10.1038/NRGASTRO.2015.34

Ananthakrishnan, A.N., Khalili, H., Konijeti, G.G., Higuchi, L.M., De Silva, P., Fuchs, C.S., Willett, W.C., Richter, J.M., Chan, A.T., 2014. Long-term intake of dietary fat and risk of ulcerative colitis and Crohn's disease. Gut 63, 776–784. https://doi.org/10.1136/GUTJNL-2013-305304

Andoh, A., Fujiyama, Y., Bamba, T., Hosoda, S., 1993. Differential cytokine regulation of complement C3, C4, and factor B synthesis in human intestinal epithelial cell line, Caco-2. J Immunol. 151, 4239–47.

Andoh, A., Fujiyama, Y., Sumiyoshi, K., Bamba, T., 1996. Local secretion of complement C3 in the exocrine pancreas: Ductal epithelial cells as a possible biosynthetic site. Gastroenterology 110, 1919–1925. https://doi.org/10.1053/gast.1996.v110.pm8964419

Aniwan, S., Harmsen, W.S., Tremaine, W.J., Loftus, E. V., 2019. Incidence of inflammatory bowel disease by race and ethnicity in a population-based inception cohort from 1970 through 2010. Therap. Adv. Gastroenterol. 12. https://doi.org/10.1177/1756284819827692

Armbruster, N.S., Stange, E.F., Wehkamp, J., 2017. In the Wnt of Paneth Cells: Immune-Epithelial Crosstalk in Small Intestinal Crohn's Disease. Front. Immunol. 8, 1204. https://doi.org/10.3389/FIMMU.2017.01204

Arrieta, M.C., Madsen, K., Doyle, J., Meddings, J., 2009. Reducing small intestinal permeability attenuates colitis in the IL10 gene-deficient mouse. Gut 58, 41–48. https://doi.org/10.1136/GUT.2008.150888

Atreya, R., Siegmund, B., 2021. Location is important: differentiation between ileal and colonic Crohn's disease. Nat. Rev. Gastroenterol. Hepatol. 2021 188 18, 544–558. https://doi.org/10.1038/s41575-021-00424-6

Azathioprine: Drug information - UpToDate [WWW Document], n.d. URL https://www.uptodate.com/contents/azathioprine-drug-information?topicRef=4056&source=see_link (accessed 10.5.21).

Baghdadi, M.B., Kim, T.H., 2022. Analysis of mouse intestinal organoid culture with conditioned media isolated from mucosal enteric glial cells. STAR Protoc. 3. https://doi.org/10.1016/J.XPRO.2022.101351

Barnes, Edward L., Loftus, E. V., Kappelman, M.D., 2021. Effects of Race and Ethnicity on Diagnosis and Management of Inflammatory Bowel Diseases. Gastroenterology 160, 677–689. https://doi.org/10.1053/J.GASTRO.2020.08.064

Barnes, Edward L, Nowell, W.B., Venkatachalam, S., Dobes, A., Kappelman, M.D., 2021. Racial and Ethnic Distribution of Inflammatory Bowel Disease in the United States. Inflamm. Bowel Dis. https://doi.org/10.1093/IBD/IZAB219

Barreau, F., Madre, C., Meinzer, U., Berrebi, D., Dussaillant, M., Merlin, F., Eckmann, L., Karin, M., Sterkers, G., Bonacorsi, S., Lesuffleur, T., Hugot, J.P., 2010. Nod2 regulates the host response towards microflora by modulating T cell function and epithelial permeability in mouse Peyer's patches. Gut 59, 207–217. https://doi.org/10.1136/GUT.2008.171546

Bastide, P., Darido, C., Pannequin, J., Kist, R., Robine, S., Marty-Double, C., Bibeau, F., Scherer, G., Joubert, D., Hollande, F., Blache, P., Jay, P., 2007. Sox9 regulates cell proliferation and is required for Paneth cell differentiation in the intestinal epithelium. J. Cell Biol. 178, 635–648. https://doi.org/10.1083/JCB.200704152

Baumgart, D.C., Sandborn, W.J., 2012. Crohn's disease. Lancet (London, England) 380, 1590–1605. https://doi.org/10.1016/S0140-6736(12)60026-9

Beisner, J., Teltschik, Z., MJ, O., Tiemessen, M., Staal, F., Wang, G., Gersemann, M., Perminow, G., Vatn, M., Schwab, M., Stange, E., Wehkamp, J., 2014. TCF-1-mediated Wnt signaling regulates Paneth cell innate immune defense effectors HD-5 and -6: Implications for Crohn's disease. Am. J. Physiol. - Gastrointest. Liver Physiol. 307, 487–498. https://doi.org/10.1152/AJPGI.00347.2013/ASSET/IMAGES/LARGE/ZH301714674000009.JPEG

Bel, S., Pendse, M., Wang, Y., Li, Y., Ruhn, K.A., Hassell, B., Leal, T., Winter, S.E., Xavier, R.J., Hooper, L. V., 2017. Paneth cells secrete lysozyme via secretory autophagy during bacterial infection of the intestine. Science 357, 1047. https://doi.org/10.1126/SCIENCE.AAL4677

Ben-Horin, S., Goldstein, I., Fudim, E., Picard, O., Yerushalmi, Z., Barshack, I., Bank, I., Goldschmid, Y., Bar Meir, S., Mayer, L., Chowers, Y., 2009. Early preservation of effector functions followed by eventual T cell memory depletion: a model for the delayed onset of the effect of thiopurines. Gut 58, 396–403. https://doi.org/10.1136/GUT.2008.157339

Betteridge, J.D., Armbruster, S.P., Maydonovitch, C., Veerappan, G.R., 2013. Inflammatory bowel disease prevalence by age, gender, race, and geographic location in the U.S. military health care population. Inflamm. Bowel Dis. 19, 1421–1427. https://doi.org/10.1097/MIB.0B013E318281334D

Beumer, J., Clevers, H., 2020. Cell fate specification and differentiation in the adult mammalian intestine. Nat. Rev. Mol. Cell Biol. https://doi.org/10.1038/s41580-020-0278-0

Beumer, J., Puschhof, J., Yengej, F.Y., Zhao, L., Martinez-Silgado, A., Blotenburg, M., Begthel, H., Boot, C., van Oudenaarden, A., Chen, Y.G., Clevers, H., 2022. BMP gradient along the intestinal villus axis controls zonated enterocyte and goblet cell states. Cell Rep. 38, 110438. https://doi.org/10.1016/J.CELREP.2022.110438

Beyaz, S., Mana, M.D., Roper, J., Kedrin, D., Saadatpour, A., Hong, S.J., Bauer-Rowe, K.E., Xifaras, M.E., Akkad, A., Arias, E., Pinello, L., Katz, Y., Shinagare, S., Abu-Remaileh, M., Mihaylova, M.M., Lamming, D.W., Dogum, R., Guo, G., Bell, G.W., Selig, M., Nielsen, G.P., Gupta, N., Ferrone, C.R., Deshpande, V., Yuan, G.C., Orkin, S.H., Sabatini, D.M., Yilmaz, Ö.H., 2016. High-fat diet enhances stemness and tumorigenicity of intestinal progenitors. Nat. 2016 5317592 531, 53–58. https://doi.org/10.1038/nature17173

Böttcher, A., Büttner, M., Tritschler, S., Sterr, M., Aliluev, A., Oppenländer, L., Burtscher, I., Sass, S., Irmler, M., Beckers, J., Ziegenhain, C., Enard, W., Schamberger, A.C., Verhamme, F.M., Eickelberg, O., Theis, F.J., Lickert, H., 2021. Non-canonical Wnt/PCP signalling regulates intestinal stem cell lineage priming towards enteroendocrine and Paneth cell fates. Nat. Cell Biol. 2021 231 23, 23–31. https://doi.org/10.1038/s41556-020-00617-2

Brem, R., Karran, P., 2012. Multiple forms of DNA Damage Caused by UVA Photoactivation of DNA 6-Thioguanine. Photochem. Photobiol. 88, 5–13.

https://doi.org/10.1111/J.1751-1097.2011.01043.X

Brooke, B., Hoffmann, D., Swarbrick, E., 1969. Azathioprine for Crohn's disease. Lancet (London, England) 2, 612–614. https://doi.org/10.1016/S0140-6736(69)90325-0

Bry, L., Falk, P., Huttner, K., Ouellette, A., Midtvedt, T., Gordon, J.I., 1994. Paneth cell differentiation in the developing intestine of normal and transgenic mice. Proc. Natl. Acad. Sci. U. S. A. 91, 10335. https://doi.org/10.1073/PNAS.91.22.10335

Burger, E., Araujo, A., López-Yglesias, A., Rajala, M.W., Geng, L., Levine, B., Hooper, L. V., Burstein, E., Yarovinsky, F., 2018. Loss of Paneth Cell Autophagy Causes Acute Susceptibility to Toxoplasma gondii-Mediated Inflammation. Cell Host Microbe 23, 177-190.e4. https://doi.org/10.1016/J.CHOM.2018.01.001

Burisch, J., Munkholm, P., 2015. The epidemiology of inflammatory bowel disease. Scand. J. Gastroenterol. 50, 942–951. https://doi.org/10.3109/00365521.2015.1014407

Cadwell, K., Patel, K.K., Komatsu, M., Virgin IV, H.W., Stappenbeck, T.S., 2009. A common role for Atg16L1, Atg5, and Atg7 in small intestinal Paneth cells and Crohn's disease. Autophagy 5, 250. https://doi.org/10.4161/AUTO.5.2.7560

Caprilli, R., 2008. Why does Crohn's disease usually occur in terminal ileum? J. Crohn's Colitis 2, 352–356. https://doi.org/10.1016/J.CROHNS.2008.06.001

Cara CJ, Pena AS, Sans M, Rodrigo L, Guerrero-Esteo M, Hinojosa J, García-Paredes J, G.L., 2004. Reviewing the mechanism of action of thiopurine drugs: towards a new paradigm in clinical practice. Med Sci Monit 10, RA247-54.

Caruso, R., Lo, B.C., Núñez, G., 2020. Host–microbiota interactions in inflammatory bowel disease. Nat. Rev. Immunol. 2020 207 20, 411–426. https://doi.org/10.1038/s41577-019-0268-7

Chande, N., Townsend, C., Parker, C., MacDonald, J., 2016. Azathioprine or 6-mercaptopurine for induction of remission in Crohn's disease. Cochrane database Syst. Rev. 10. https://doi.org/10.1002/14651858.CD000545.PUB5

Chen, G., Ran, X., Li, B., Li, Y., He, D., Huang, B., Fu, S., Liu, J., Wang, W., 2018. Sodium Butyrate Inhibits Inflammation and Maintains Epithelium Barrier Integrity in a TNBS-induced Inflammatory Bowel Disease Mice Model. EBioMedicine 30, 317–325. https://doi.org/10.1016/j.ebiom.2018.03.030

Cheung, E.C., Lee, P., Ceteci, F., Nixon, C., Blyth, K., Sansom, O.J., Vousden, K.H., 2016. Opposing effects of TIGAR- and RAC1-derived ROS on Wnt-driven proliferation in the mouse intestine. Genes Dev. 30, 52. https://doi.org/10.1101/GAD.271130.115

Chevalier, G., Laveissière, A., Desachy, G., Barnich, N., Sivignon, A., Maresca, M., Nicoletti, C., Di Pasquale, E., Martinez-Medina, M., Simpson, K.W., Yajnik, V., Sokol, H., Adegbamigbe, T., Ahmad, T., Arnott, I., Bouhnik, Y., Carbonnel, F., Colombel, J.F., Doherty, G., Cummings, J.R.F., Hébuterne, X., Herfarth, H., Kevans, D., de Chambrun, G.P., Nachury, M., Nancey, S., Roblin, X., Tremelling, M.A.W., Plassais, J., Strozzi, F., Cervino, A., Morra, R., Bonny, C.,

2021. Blockage of bacterial FimH prevents mucosal inflammation associated with Crohn's disease. Microbiome 9. https://doi.org/10.1186/S40168-021-01135-5

Chiang, J.Y.L., Li, T., 2009. Regulation of Bile Acid and Cholesterol Metabolism by PPARs. PPAR Res. 2009. https://doi.org/10.1155/2009/501739

Chileveru, H.R., Lim, S.A., Chairatana, P., Wommack, A.J., Chiang, I.L., Nolan, E.M., 2015. Visualizing Attack of Escherichia coli by the Antimicrobial Peptide Human Defensin 5. Biochemistry 54, 1767. https://doi.org/10.1021/BI501483Q

Chu, H., Pazgier, M., Jung, G., Nuccio, S.P., Castillo, P.A., De Jong, M.F., Winter, M.G., Winter, S.E., Wehkamp, J., Shen, B., Salzman, N.H., Underwood, M.A., Tsolis, R.M., Young, G.M., Lu, W., Lehrer, R.I., Bäumler, A.J., Bevins, C.L., 2012. Human α-defensin 6 promotes mucosal innate immunity through self-assembled peptide nanonets. Science 337, 477–481. https://doi.org/10.1126/SCIENCE.1218831

Collett, A., Sims, E., Walker, D., He, Y.L., Ayrton, J., Rowland, M., Warhurst, G., 1996. Comparison of HT29-18-C1 and Caco-2 cell lines as models for studying intestinal paracellular drug absorption. Pharm. Res. 13, 216–221. https://doi.org/10.1023/A:1016082829111

Colten, H.R., Borsos, T., Rapp, H.J., 1966. In vitro synthesis of the first component of complement by guinea pig small intestine. Proc. Natl. Acad. Sci. U. S. A. 56, 1158–1163. https://doi.org/10.1073/PNAS.56.4.1158

Coward, S., Clement, F., Benchimol, E.I., Bernstein, C.N., Avina-Zubieta, J.A., Bitton, A., Carroll, M.W., Hazlewood, G., Jacobson, K., Jelinski, S., Deardon, R., Jones, J.L., Kuenzig, M.E., Leddin, D., McBrien, K.A., Murthy, S.K., Nguyen, G.C., Otley, A.R., Panaccione, R., Rezaie, A., Rosenfeld, G., Peña-Sánchez, J.N., Singh, H., Targownik, L.E., Kaplan, G.G., 2019. Past and Future Burden of Inflammatory Bowel Diseases Based on Modeling of Population-Based Data. Gastroenterology 156, 1345-1353.e4. https://doi.org/10.1053/J.GASTRO.2019.01.002

Cray, P., Sheahan, B.J., Dekaney, C.M., 2021. Secretory Sorcery: Paneth Cell Control of Intestinal Repair and Homeostasis. Cell. Mol. Gastroenterol. Hepatol. 12, 1239. https://doi.org/10.1016/J.JCMGH.2021.06.006

Cuffari, C., Hunt, S., Bayless, T.M., 2000. Enhanced bioavailability of azathioprine compared to 6-mercaptopurine therapy in inflammatory bowel disease: correlation with treatment efficacy. Aliment. Pharmacol. Ther. 14, 1009–1014. https://doi.org/10.1046/J.1365-2036.2000.00812.X

de Moraes, L.R., Delicato, M.E.A., da Silva Cruz, A., da Silva, H.T.F.N.P., de Vasconcelos Alves, C.V.B., Campos, D.B., Saraiva, E.P., da Costa, F.P., Guerra, R.R., 2021. Methionine supplementing effects on intestine, liver and uterus morphology, and on positivity and expression of Calbindin-D28k and TRPV6 epithelial calcium carriers in laying quail in thermoneutral conditions and under thermal stress. PLoS One 16, e0245615. https://doi.org/10.1371/JOURNAL.PONE.0245615

De Souza, H.S.P., Fiocchi, C., 2016. Immunopathogenesis of IBD: current state of

the art. Nat. Rev. Gastroenterol. Hepatol. 13, 13–27. https://doi.org/10.1038/NRGASTRO.2015.186

Dean, L., 2020. Azathioprine Therapy and TPMT and NUDT15 Genotype. Med. Genet. Summ.

Derer, S., Brethack, A.K., Pietsch, C., Jendrek, S.T., Nitzsche, T., Bokemeyer, A., Hov, J.R., Schäffler, H., Bettenworth, D., Grassl, G.A., Sina, C., 2020. Inflammatory Bowel Disease–associated GP2 Autoantibodies Inhibit Mucosal Immune Response to Adherent-invasive Bacteria. Inflamm. Bowel Dis. 26, 1856–1868. https://doi.org/10.1093/IBD/IZAA069

Deretic, V., Master, S., Singh, S., 2008. Autophagy Gives a Nod and a Wink to the Inflammasome and Paneth Cells in Crohn's Disease. Dev. Cell 15, 641. https://doi.org/10.1016/J.DEVCEL.2008.10.009

Derijks, L., Wong, D., 2009. Pharmacogenetics of Thiopurines in Inflammatory Bowel Disease. Curr. Pharm. Des. 16, 145–154. https://doi.org/10.2174/138161210790112773

Dharmasiri, S., Garrido-Martin, E.M., Harris, R.J., Bateman, A.C., Collins, J.E., Cummings, J.R.F., Sanchez-Elsner, T., 2021. Human Intestinal Macrophages Are Involved in the Pathology of Both Ulcerative Colitis and Crohn Disease. Inflamm. Bowel Dis. 27, 1641–1652. https://doi.org/10.1093/IBD/IZAB029

Ding, L., Zhang, F. Bin, Liu, H., Gao, X., Bi, H.C., Wang, X.D., Chen, B.L., Zhang, Y., Zhao, L.Z., Zhong, G.P., Hu, P.J., Chen, M.H., Huang, M., 2012. Hypoxanthine guanine phosphoribosyltransferase activity is related to 6-thioguanine nucleotide concentrations and thiopurine-induced leukopenia in the treatment of inflammatory bowel disease. Inflamm. Bowel Dis. 18, 63–73. https://doi.org/10.1002/IBD.21676

Dooley, T., Curto, E., Reddy, S., Davis, R., Lambert, G., Wilborn, T., Elson, C., 2004. Regulation of gene expression in inflammatory bowel disease and correlation with IBD drugs: screening by DNA microarrays. Inflamm. Bowel Dis. 10, 1–14. https://doi.org/10.1097/00054725-200401000-00001

Doron, I., Mesko, M., Li, X. V., Kusakabe, T., Leonardi, I., Shaw, D.G., Fiers, W.D., Lin, W.Y., Bialt-DeCelie, M., Román, E., Longman, R.S., Pla, J., Wilson, P.C., Iliev, I.D., 2021. Mycobiota-induced IgA antibodies regulate fungal commensalism in the gut and are dysregulated in Crohn's disease. Nat. Microbiol. 6, 1493–1504. https://doi.org/10.1038/S41564-021-00983-Z

Durand, A., Donahue, B., Peignon, G., Letourneur, F., Cagnard, N., Slomianny, C., Perret, C., Shroyer, N.F., Romagnolo, B., 2012. Functional intestinal stem cells after Paneth cell ablation induced by the loss of transcription factor Math1 (Atoh1). Proc. Natl. Acad. Sci. U. S. A. 109, 8965–8970. https://doi.org/10.1073/PNAS.1201652109/-/DCSUPPLEMENTAL

Duricova, D., Burisch, J., Jess, T., Gower-Rousseau, C., Lakatos, P.L., 2014. Age-related differences in presentation and course of inflammatory bowel disease: An update on the population-based literature. J. Crohn's Colitis 8, 1351–1361. https://doi.org/10.1016/J.CROHNS.2014.05.006/2/8-11-1351-F2.JPEG

El-Yazigi, A., Wahab, F.A., 1993. Pharmacokinetics of Azathioprine After Repeated

Oral and Single Intravenous Administration. J. Clin. Pharmacol. 33, 522–526. https://doi.org/10.1002/J.1552-4604.1993.TB04698.X

Elion, G., 1989. The purine path to chemotherapy. Science 244, 41–47. https://doi.org/10.1126/SCIENCE.2649979

ELION, G., CALLAHAN, S., HITCHINGS, G., RUNDLES, R., 1960. The metabolism of 2-amino-6-[(1-methyl-4-nitro-5-imidazolyl)thio]purine (B.W. 57-323) in man. Cancer Chemother Rep 47–52.

Ericksen, B., Wu, Z., Lu, W., Lehrer, R.I., 2005. Antibacterial Activity and Specificity of the Six Human α-Defensins. Antimicrob. Agents Chemother. 49, 269. https://doi.org/10.1128/AAC.49.1.269-275.2005

Erickson, A.R., Cantarel, B.L., Lamendella, R., Darzi, Y., Mongodin, E.F., Pan, C., Shah, M., Halfvarson, J., Tysk, C., Henrissat, B., Raes, J., Verberkmoes, N.C., Fraser, C.M., Hettich, R.L., Jansson, J.K., 2012. Integrated Metagenomics/Metaproteomics Reveals Human Host-Microbiota Signatures of Crohn's Disease. PLoS One 7. https://doi.org/10.1371/JOURNAL.PONE.0049138

Espín, S., García-Fernández, A.J., 2022. Azathioprine. Encycl. Toxicol. Third Ed. 347–350. https://doi.org/10.1016/B978-0-12-386454-3.00470-X

Farin, H.F., Van Es, J.H., Clevers, H., 2012. Redundant sources of Wnt regulate intestinal stem cells and promote formation of Paneth cells. Gastroenterology 143. https://doi.org/10.1053/J.GASTRO.2012.08.031

Ferraretto, A., Bottani, M., De Luca, P., Cornaghi, L., Arnaboldi, F., Maggioni, M., Fiorilli, A., Donetti, E., 2018. Morphofunctional properties of a differentiated Caco2/HT-29 co-culture as an in vitro model of human intestinal epithelium. Biosci. Rep. 38. https://doi.org/10.1042/BSR20171497

Feuerstein, J.D., Cheifetz, A.S., 2017. Crohn Disease: Epidemiology, Diagnosis, and Management. Mayo Clin. Proc. 92, 1088–1103. https://doi.org/10.1016/J.MAYOCP.2017.04.010

Filippello, A., Di Mauro, S., Scamporrino, A., Torrisi, S.A., Leggio, G.M., Di Pino, A., Scicali, R., Di Marco, M., Malaguarnera, R., Purrello, F., Piro, S., 2022. Molecular Effects of Chronic Exposure to Palmitate in Intestinal Organoids: A New Model to Study Obesity and Diabetes. Int. J. Mol. Sci. 23. https://doi.org/10.3390/IJMS23147751/S1

Fisher, E.M., Khan, M., Salisbury, R., Kuppusamy, P., 2013. Noninvasive monitoring of small intestinal oxygen in a rat model of chronic mesenteric ischemia. Cell Biochem. Biophys. 67, 451–459. https://doi.org/10.1007/S12013-013-9611-Y

Fowler, E. V., Doecke, J., Simms, L.A., Zhao, Z.Z., Webb, P.M., Hayward, N.K., Whiteman, D.C., Florin, T.H., Montgomery, G.W., Cavanaugh, J.A., Radford-Smith, G.L., 2008. ATG16L1 T300A shows strong associations with disease subgroups in a large Australian IBD population: further support for significant disease heterogeneity. Am. J. Gastroenterol. 103, 2519–2526. https://doi.org/10.1111/J.1572-0241.2008.02023.X

French, H., Mark Dalzell, A., Srinivasan, R., El-Matary, W., 2011. Relapse Rate

Following Azathioprine Withdrawal in Maintaining Remission for Crohn's Disease: A Meta-Analysis. Dig. Dis. Sci. 2011 567 56, 1929–1936. https://doi.org/10.1007/S10620-011-1671-5

Fujii, M., Matano, M., Toshimitsu, K., Takano, A., Mikami, Y., Nishikori, S., Sugimoto, S., Sato, T., 2018. Human Intestinal Organoids Maintain Self-Renewal Capacity and Cellular Diversity in Niche-Inspired Culture Condition. Cell Stem Cell 23, 787-793.e6. https://doi.org/10.1016/J.STEM.2018.11.016

Fujino, S., Andoh, A., Bamba, S., Ogawa, A., Hata, K., Araki, Y., Bamba, T., Fujiyama, Y., 2003. Increased expression of interleukin 17 in inflammatory bowel disease. Gut 52, 65–70. https://doi.org/10.1136/GUT.52.1.65

Garabedian, E.M., Roberts, L.J.J., McNevin, M.S., Gordon, J.I., 1997. Examining the Role of Paneth Cells in the Small Intestine by Lineage Ablation in Transgenic Mice. J. Biol. Chem. 272, 23729–23740. https://doi.org/10.1074/JBC.272.38.23729

Gassler, N., 2017. Paneth cells in intestinal physiology and pathophysiology. World J. Gastrointest. Pathophysiol. 8, 150. https://doi.org/10.4291/WJGP.V8.I4.150

Gaudino, S.J., Beaupre, M., Lin, X., Joshi, P., Rathi, S., McLaughlin, P.A., Kempen, C., Mehta, N., Eskiocak, O., Yueh, B., Blumberg, R.S., van der Velden, A.W.M., Shroyer, K.R., Bialkowska, A.B., Beyaz, S., Kumar, P., 2021. IL-22 receptor signaling in Paneth cells is critical for their maturation, microbiota colonization, Th17-related immune responses, and anti-Salmonella immunity. Mucosal Immunol. 14, 389–401. https://doi.org/10.1038/S41385-020-00348-5

Gearry, R.B., Barclay, M.L., 2005. Azathioprine and 6-mercaptopurine pharmacogenetics and metabolite monitoring in inflammatory bowel disease. J. Gastroenterol. Hepatol. 20, 1149–1157. https://doi.org/10.1111/J.1440-1746.2005.03832.X

Gearry, R.B., Day, A.S., Barclay, M.L., Leong, R.W., Sparrow, M.P., 2010. Azathioprine and allopurinol: A two-edged interaction. J. Gastroenterol. Hepatol. 25, 653–655. https://doi.org/10.1111/J.1440-1746.2010.06254.X

Geremia, A., Biancheri, P., Allan, P., Corazza, G.R., Di Sabatino, A., 2014. Innate and adaptive immunity in inflammatory bowel disease. Autoimmun. Rev. 13, 3–10. https://doi.org/10.1016/J.AUTREV.2013.06.004

Gibson, P.R., 2004. Increased gut permeability in Crohn's disease: is TNF the link? Gut 53, 1724. https://doi.org/10.1136/GUT.2004.047092

Giles, D.A., Moreno-Fernandez, M.E., Stankiewicz, T.E., Graspeuntner, S., Cappelletti, M., Wu, D., Mukherjee, R., Chan, C.C., Lawson, M.J., Klarquist, J., Sünderhauf, A., Softic, S., Kahn, C.R., Stemmer, K., Iwakura, Y., Aronow, B.J., Karns, R., Steinbrecher, K.A., Karp, C.L., Sheridan, R., Shanmukhappa, S.K., Reynaud, D., Haslam, D.B., Sina, C., Rupp, J., Hogan, S.P., Divanovic, S., 2017. Thermoneutral housing exacerbates nonalcoholic fatty liver disease in mice and allows for sex-independent disease modeling. Nat. Med. 2017 237 23, 829–838. https://doi.org/10.1038/nm.4346

Gjuladin-Hellon, T., Iheozor-Ejiofor, Z., Gordon, M., Akobeng, A., 2019. Azathioprine and 6-mercaptopurine for maintenance of surgically-induced remission in

Crohn's disease. Cochrane database Syst. Rev. 8. https://doi.org/10.1002/14651858.CD010233.PUB3

Gori, M., Altomare, A., Cocca, S., Solida, E., Ribolsi, M., Carotti, S., Rainer, A., Francesconi, M., Morini, S., Cicala, M., Guarino, M.P.L., 2020. Palmitic Acid Affects Intestinal Epithelial Barrier Integrity and Permeability In Vitro. Antioxidants 2020, Vol. 9, Page 417 9, 417. https://doi.org/10.3390/ANTIOX9050417

Greaves, L.C., Preston, S.L., Tadrous, P.J., Taylor, R.W., Barron, M.J., Oukrif, D., Leedham, S.J., Deheragoda, M., Sasieni, P., Novelli, M.R., Jankowski, J.A.Z., Turnbull, D.M., Wright, N.A., McDonald, S.A.C., 2006. Mitochondrial DNA mutations are established in human colonic stem cells, and mutated clones expand by crypt fission. Proc. Natl. Acad. Sci. U. S. A. 103, 714. https://doi.org/10.1073/PNAS.0505903103

Gren, S.T., Grip, O., 2016. Role of Monocytes and Intestinal Macrophages in Crohn's Disease and Ulcerative Colitis. Inflamm. Bowel Dis. 22, 1992–1998. https://doi.org/10.1097/MIB.0000000000000824

Greuter, T., Manser, C., Pittet, V., Vavricka, S.R., Biedermann, L., 2020. Gender Differences in Inflammatory Bowel Disease. Digestion 101 Suppl 1, 98–104. https://doi.org/10.1159/000504701

Gropper, S., Smith, J., 2012. Advanced Nutrition and Human Metabolism.

Gullberg, E., Söderholm, J.D., 2006. Peyer's Patches and M Cells as Potential Sites of the Inflammatory Onset in Crohn's Disease. Ann N Y Acad Sci. 1072, 218–232. https://doi.org/10.1196/ANNALS.1326.028

Guzman, J.R., Conlin, V.S., Jobin, C., 2013. Diet, Microbiome, and the Intestinal Epithelium: An Essential Triumvirate? Biomed Res. Int. 2013, 12. https://doi.org/10.1155/2013/425146

Harbord, M., Annese, V., Vavricka, S.R., Allez, M., Acosta, M.B. de, Boberg, K.M., Burisch, J., Martine, D.V., De Vries, A.M., Dick, A.D., Juillerat, P., Karlsen, T.H., Koutroubakis, I., Lakatos, P.L., Orchard, T., Papay, P., Raine, T., Reinshagen, M., Thaci, D., Tilg, H., Carbonnel, F., Gottfried, N., Christoph, H., Peter, B., Emil, B., Krznaric, Z., Brankica, M.S., Martin, B., Thomas, D., Torben, K., Karin, K., Pia, M., Britta, S., Tamas, M., Paolo, G., Lie, H.M., Jaroslaw, K., Edyta, Z., Mircea, D.M., Alexander, P., Njegica, J., Dino, T., David, D., Javier, G., Eugeni, D.M., Hans, S., Ferhat, C.A., 2016. The First European Evidence-based Consensus on Extra-intestinal Manifestations in Inflammatory Bowel Disease. J. Crohn's Colitis 10, 239–254. https://doi.org/10.1093/ECCO-JCC/JJV213

Harwig, S.S.L., Tan, L., Qu, X.D., Cho, Y., Eisenhauer, P.B., Lehrer, R.I., 1995. Bactericidal properties of murine intestinal phospholipase A2. J. Clin. Invest. 95, 603. https://doi.org/10.1172/JCI117704

Heida, F.H., Beyduz, G., Bulthuis, M.L.C., Kooi, E.M.W., Bos, A.F., Timmer, A., Hulscher, J.B.F., 2016. Paneth cells in the developing gut: when do they arise and when are they immune competent? Pediatr. Res. 2016 802 80, 306–310. https://doi.org/10.1038/pr.2016.67

Helbig, K.L., Nothnagel, M., Hampe, J., Balschun, T., Nikolaus, S., Schreiber, S.,

Franke, A., Nöthlings, U., 2012. A case-only study of gene-environment interaction between genetic susceptibility variants in NOD2 and cigarette smoking in Crohn's disease aetiology. BMC Med. Genet. 13, 14. https://doi.org/10.1186/1471-2350-13-14

Hirose, M., Künstner, A., Schilf, P., Sünderhauf, A., Rupp, J., Jöhren, O., Schwaninger, M., Sina, C., Baines, J.F., Ibrahim, S.M., 2017. Mitochondrial gene polymorphism is associated with gut microbial communities in mice. Sci. Reports 2017 71 7, 1–9. https://doi.org/10.1038/s41598-017-15377-7

Hodges, P., Kelly, P., 2020. Inflammatory bowel disease in Africa: what is the current state of knowledge? Int. Health 12, 222–230. https://doi.org/10.1093/INTHEALTH/IHAA005

Hodgson, H.J.F., Potter, B.J., Jewell, D.P., 1977. C3 metabolism in ulcerative colitis and Crohn's disease. Clin. Exp. Immunol. 28, 490.

Hodin, C.M., Verdam, F.J., Grootjans, J., Rensen, S.S., Verheyen, F.K., Dejong, C.H.C., Buurman, W.A., Greve, J.W., Lenaerts, K., 2011. Reduced Paneth cell antimicrobial protein levels correlate with activation of the unfolded protein response in the gut of obese individuals. J. Pathol. 225, 276–284. https://doi.org/10.1002/PATH.2917

Hooper, K.M., Casanova, V., Kemp, S., Staines, K.A., Satsangi, J., Barlow, P.G., Henderson, P., Stevens, C., 2019. The Inflammatory Bowel Disease Drug Azathioprine Induces Autophagy via mTORC1 and the Unfolded Protein Response Sensor PERK. Inflamm. Bowel Dis. 25, 1481–1496. https://doi.org/10.1093/IBD/IZZ039

Hove, H., Nordgaard-Andersen, I., Mortensen, P.B., 2009. Faecal DL-Lactate Concentration in 100 Gastrointestinal Patients. https://doi.org/10.3109/00365529409090473 29, 255–259. https://doi.org/10.3109/00365529409090473

Imhann, F., Vich Vila, A., Bonder, M.J., Fu, J., Gevers, Di., Visschedijk, M.C., Spekhorst, L.M., Alberts, R., Franke, L., Van Dullemen, H.M., Ter Steege, R.W.F., Huttenhower, C., Dijkstra, G., Xavier, R.J., Festen, E.A.M., Wijmenga, C., Zhernakova, A., Weersma, R.K., 2018. Interplay of host genetics and gut microbiota underlying the onset and clinical presentation of inflammatory bowel disease. Gut 67, 108–119. https://doi.org/10.1136/GUTJNL-2016-312135

Irvine, E.J., Marshall, J.K., 2000. Increased intestinal permeability precedes the onset of Crohn's disease in a subject with familial risk. Gastroenterology 119, 1740–1744. https://doi.org/10.1053/gast.2000.20231

Jackson, D.N., Panopoulos, M., Neumann, W.L., Turner, K., Cantarel, B.L., Thompson-Snipes, L., Dassopoulos, T., Feagins, L.A., Souza, R.F., Mills, J.C., Blumberg, R.S., Venuprasad, K., Thompson, W.E., Theiss, A.L., 2020. Mitochondrial dysfunction during loss of prohibitin 1 triggers Paneth cell defects and ileitis. Gut 69, 1928–1938. https://doi.org/10.1136/GUTJNL-2019-319523

Jackson, D.N., Theiss, A.L., 2019. Gut bacteria signaling to mitochondria in intestinal inflammation and cancer. https://doi.org/10.1080/19490976.2019.1592421 11, 285–304. https://doi.org/10.1080/19490976.2019.1592421

Jain, U., Otley, A.R., Van Limbergen, J., Stadnyk, A.W., 2014. The complement system in inflammatory bowel disease. Inflamm. Bowel Dis. 20, 1628–1637. https://doi.org/10.1097/MIB.0000000000000056

Jansson, J., Willing, B., Lucio, M., Fekete, A., Dicksved, J., Halfvarson, J., Tysk, C., Schmitt-Kopplin, P., 2009. Metabolomics reveals metabolic biomarkers of Crohn's disease. PLoS One 4. https://doi.org/10.1371/JOURNAL.PONE.0006386

Jardé, T., Chan, W.H., Rossello, F.J., Kaur Kahlon, T., Theocharous, M., Kurian Arackal, T., Flores, T., Giraud, M., Richards, E., Chan, E., Kerr, G., Engel, R.M., Prasko, M., Donoghue, J.F., Abe, S. ichi, Phesse, T.J., Nefzger, C.M., McMurrick, P.J., Powell, D.R., Daly, R.J., Polo, J.M., Abud, H.E., 2020. Mesenchymal Niche-Derived Neuregulin-1 Drives Intestinal Stem Cell Proliferation and Regeneration of Damaged Epithelium. Cell Stem Cell 27, 646-662.e7. https://doi.org/10.1016/J.STEM.2020.06.021

Karran, P., 2006. Thiopurines, DNA damage, DNA repair and therapy-related cancer. Br. Med. Bull. 79–80, 153–170. https://doi.org/10.1093/BMB/LDL020

Kaser, A., Lee, A.H., Franke, A., Glickman, J.N., Zeissig, S., Tilg, H., Nieuwenhuis, E.E.S., Higgins, D.E., Schreiber, S., Glimcher, L.H., Blumberg, R.S., 2008. XBP1 links ER stress to intestinal inflammation and confers genetic risk for human inflammatory bowel disease. Cell 134, 743. https://doi.org/10.1016/J.CELL.2008.07.021

Khademi, Z., Milajerdi, A., Larijani, B., Esmaillzadeh, A., 2021. Dietary Intake of Total Carbohydrates, Sugar and Sugar-Sweetened Beverages, and Risk of Inflammatory Bowel Disease: A Systematic Review and Meta-Analysis of Prospective Cohort Studies. Front. Nutr. 8, 707795. https://doi.org/10.3389/FNUT.2021.707795

Khaloian, S., Rath, E., Hammoudi, N., Gleisinger, E., Blutke, A., Giesbertz, P., Berger, E., Metwaly, A., Waldschmitt, N., Allez, M., Haller, D., 2020. Mitochondrial impairment drives intestinal stem cell transition into dysfunctional Paneth cells predicting Crohn's disease recurrence. Gut 69, 1939–1951. https://doi.org/10.1136/GUTJNL-2019-319514

Khare, V., Krnjic, A., Frick, A., Gmainer, C., Asboth, M., Jimenez, K., Lang, M., Baumgartner, M., Evstatiev, R., Gasche, C., 2019. Mesalamine and azathioprine modulate junctional complexes and restore epithelial barrier function in intestinal inflammation. Sci. Reports 2019 91 9, 1–11. https://doi.org/10.1038/s41598-019-39401-0

Klockars, M., Reitamo, S., Reitamo, J.J., Moller, C., 1977. Immunohistochemical identification of lysozyme in intestinal lesions in ulcerative colitis and Crohn's disease. Gut 18, 377. https://doi.org/10.1136/GUT.18.5.377

Konjar, Š., Pavšič, M., Veldhoen, M., 2021. Regulation of Oxygen Homeostasis at the Intestinal Epithelial Barrier Site. Int. J. Mol. Sci. 2021, Vol. 22, Page 9170 22, 9170. https://doi.org/10.3390/IJMS22179170

Koslowski, M.J., Kübler, I., Chamaillard, M., Schaeffeler, E., Reinisch, W., Wang, G., Beisner, J., Teml, A., Peyrin-Biroulet, L., Winter, S., Herrlinger, K.R., Rutgeerts,

P., Vermeire, S., Cooney, R., Fellermann, K., Jewell, D., Bevins, C.L., Schwab, M., Stange, E.F., Wehkamp, J., 2009. Genetic Variants of Wnt Transcription Factor TCF-4 (TCF7L2) Putative Promoter Region Are Associated with Small Intestinal Crohn's Disease. PLoS One 4, 4496. https://doi.org/10.1371/JOURNAL.PONE.0004496

Koutroubakis, I.E., Malliaraki, N., Vardas, E., Ganotakis, E., Margioris, A.N., Manousos, O.N., Kouroumalis, E.A., 2001. Increased levels of lipoprotein (a) in Crohn's disease: a relation to thrombosis? Eur. J. Gastroenterol. Hepatol. 13, 1415–1419. https://doi.org/10.1097/00042737-200112000-00004

Kübler, I., Koslowski, M., Gersemann, M., Fellermann, K., Beisner, J., Becker, S., Rothfuss, K., Herrlinger, K., Stange, E., Wehkamp, J., 2009. Influence of standard treatment on ileal and colonic antimicrobial defensin expression in active Crohn's disease. Aliment. Pharmacol. Ther. 30, 621–633. https://doi.org/10.1111/J.1365-2036.2009.04070.X

Kundu, B., Khare, S.K., 1999. Progress in Drug Research, in: Progress in Drug Research. p. 18.

Kuo, W.T., Shen, L., Zuo, L., Shashikanth, N., Ong, M.L.D.M., Wu, L., Zha, J., Edelblum, K.L., Wang, Yitang, Wang, Yingmin, Nilsen, S.P., Turner, J.R., 2019. Inflammation-induced Occludin Downregulation Limits Epithelial Apoptosis by Suppressing Caspase 3 Expression. Gastroenterology 157, 1323. https://doi.org/10.1053/J.GASTRO.2019.07.058

Lala, S., Ogura, Y., Osborne, C., Hor, S.Y., Bromfield, A., Davies, S., Ogunbiyi, O., Nuñez, G., Keshav, S., 2003. Crohn's disease and the NOD2 gene: a role for paneth cells. Gastroenterology 125, 47–57. https://doi.org/10.1016/S0016-5085(03)00661-9

Lazarević, S., Đanic, M., Al-Salami, H., Mooranian, A., Mikov, M., 2022. Gut Microbiota Metabolism of Azathioprine: A New Hallmark for Personalized Drug-Targeted Therapy of Chronic Inflammatory Bowel Disease. Front. Pharmacol. 13, 1147. https://doi.org/10.3389/FPHAR.2022.879170/BIBTEX

Lee, A.U., Farrell, G.C., 2001. Mechanism of azathioprine-induced injury to hepatocytes: roles of glutathione depletion and mitochondrial injury. J. Hepatol. 35, 756–764. https://doi.org/10.1016/S0168-8278(01)00196-9

Lee, J.C., Lee, H.Y., Kim, T.K., Kim, M.S., Park, Y.M., Kim, J., Park, K., Kweon, M.N., Kim, S.H., Bae, J.W., Hur, K.Y., Lee, M.S., 2017. Obesogenic diet-induced gut barrier dysfunction and pathobiont expansion aggravate experimental colitis. PLoS One 12. https://doi.org/10.1371/JOURNAL.PONE.0187515

Lees, C.W., Barrett, J.C., Parkes, M., Satsangi, J., 2011. New IBD genetics: common pathways with other diseases. Gut 60, 1739–1753. https://doi.org/10.1136/GUT.2009.199679

Levy, E., Rizwan, Y., Thibault, L., Lepage, G., Brunet, S., Bouthillier, L., Seidman, E., 2000. Altered lipid profile, lipoprotein composition, and oxidant and antioxidant status in pediatric Crohn disease. Am. J. Clin. Nutr. 71, 807–815. https://doi.org/10.1093/AJCN/71.3.807

Lewin, K., 1969. The Paneth cell in disease. Gut 10, 804–811. https://doi.org/10.1136/GUT.10.10.804

Lian, P., Braber, S., Varasteh, S., Wichers, H.J., Folkerts, G., 2021. Hypoxia and heat stress affect epithelial integrity in a Caco-2/HT-29 co-culture. Sci. Reports 2021 111 11, 1–14. https://doi.org/10.1038/s41598-021-92574-5

Lichtenstein, G., Loftus, E., Isaacs, K., Regueiro, M., Gerson, L., Sands, B., 2018. Correction: ACG Clinical Guideline: Management of Crohn's Disease in Adults. Am. J. Gastroenterol. 113, 1101. https://doi.org/10.1038/S41395-018-0120-X

Liu, T.C., Kern, J.T., Jain, U., Sonnek, N.M., Xiong, S., Simpson, K.F., VanDussen, K.L., Winkler, E.S., Haritunians, T., Malique, A., Lu, Q., Sasaki, Y., Storer, C., Diamond, M.S., Head, R.D., McGovern, D.P.B., Stappenbeck, T.S., 2021. Western diet induces Paneth cell defects through microbiome alterations and farnesoid X receptor and type I interferon activation. Cell Host Microbe 29, 988-1001.e6. https://doi.org/10.1016/J.CHOM.2021.04.004

Liu, T.C., Kern, J.T., VanDussen, K.L., Xiong, S., Kaiko, G.E., Wilen, C.B., Rajala, M.W., Caruso, R., Holtzman, M.J., Gao, F., McGovern, D.P.B., Nunez, G., Head, R.D., Stappenbeck, T.S., 2018. Interaction between smoking and ATG16L1T300A triggers Paneth cell defects in Crohn's disease. J. Clin. Invest. 128, 5110–5122. https://doi.org/10.1172/JCI120453

Lo, C.H., Lochhead, P., Khalili, H., Song, M., Tabung, F.K., Burke, K.E., Richter, J.M., Giovannucci, E.L., Chan, A.T., Ananthakrishnan, A.N., 2020. Dietary Inflammatory Potential and Risk of Crohn's Disease and Ulcerative Colitis. Gastroenterology 159, 873. https://doi.org/10.1053/J.GASTRO.2020.05.011

Lu, R., Zhang, Y. guo, Xia, Y., Zhang, J., Kaser, A., Blumberg, R., Sun, J., 2021. Paneth Cell Alertness to Pathogens Maintained by Vitamin D Receptors. Gastroenterology 160, 1269–1283. https://doi.org/10.1053/J.GASTRO.2020.11.015

Mahid, S.S., Minor, K.S., Soto, R.E., Hornung, C.A., Galandiuk, S., 2006. Smoking and inflammatory bowel disease: a meta-analysis. Mayo Clin. Proc. 81, 1462–1471. https://doi.org/10.4065/81.11.1462

Mallow, E.B., Harris, A., Salzman, N., Russell, J.P., DeBerardinis, R.J., Ruchelli, E., Bevins, C.L., 1996. Human Enteric Defensins: GENE STRUCTURE AND DEVELOPMENTAL EXPRESSION. J. Biol. Chem. 271, 4038–4045. https://doi.org/10.1074/JBC.271.8.4038

Martini, E., Krug, S.M., Siegmund, B., Neurath, M.F., Becker, C., 2017. Mend Your Fences: The Epithelial Barrier and its Relationship With Mucosal Immunity in Inflammatory Bowel Disease. Cell. Mol. Gastroenterol. Hepatol. 4, 33–46. https://doi.org/10.1016/J.JCMGH.2017.03.007

Marz, W., Baumstark, M.W., Scharnagl, H., Ruzicka, V., Buxbaum, S., Herwig, J., Pohl, T., Russ, A., Schaaf, L., Berg, A., Bohles, H.J., Usadel, K.H., Gross, W., 1993. Accumulation of "small dense" low density lipoproteins (LDL) in a homozygous patients with familial defective apolipoprotein B-100 results from heterogenous interaction of LDL subfractions with the LDL receptor. J. Clin. Invest. 92, 2922. https://doi.org/10.1172/JCI116915

Marzo, M., Felice, C., Pugliese, D., Andrisani, G., Mocci, G., Armuzzi, A., Guidi, L., 2015. Management of perianal fistulas in Crohn's disease: An up-to-date review. World J. Gastroenterol. 21, 1394. https://doi.org/10.3748/WJG.V21.I5.1394

Mastroianni, J.R., Costales, J.K., Zaksheske, J., Selsted, M.E., Salzman, N.H., Ouellette, A.J., 2012. Alternative Luminal Activation Mechanisms for Paneth Cell α-Defensins. J. Biol. Chem. 287, 11205. https://doi.org/10.1074/JBC.M111.333559

Matsumoto, N., Satyam, A., Geha, M., Lapchak, P.H., Dalle Lucca, J.J., Tsokos, M.G., Tsokos, G.C., 2017. C3a Enhances the Formation of Intestinal Organoids through C3aR1. Front. Immunol. 8. https://doi.org/10.3389/FIMMU.2017.01046

Mayberry, J.F., Lobo, A., Ford, A.C., Thomas, A., 2013. NICE clinical guideline (CG152): the management of Crohn's disease in adults, children and young people. Aliment. Pharmacol. Ther. 37, 195–203. https://doi.org/10.1111/APT.12102

MCCOLLISTER, R.J., GILBERT, W.R., ASHTON, D.M., WYNGAARDEN, J.B., 1964. Pseudofeedback Inhibition of Purine Synthesis by 6-Mercaptopurine Ribonucleotide and Other Purine Analogues. J. Biol. Chem. 239, 1560–1563. https://doi.org/10.1016/S0021-9258(18)91353-0

Meconi, S., Vercellone, A., Levillain, F., Payré, B., Al Saati, T., Capilla, F., Desreumaux, P., Darfeuille-michaud, A., Altare, F., 2007. Adherent-invasive Escherichia coli isolated from Crohn's disease patients induce granulomas in vitro. Cell. Microbiol. 9, 1252–1261. https://doi.org/10.1111/J.1462-5822.2006.00868.X

Meoli, L., Ben-Zvi, D., Panciotti, C., Kvas, S., Pizarro, P., Munoz, R., Stylopoulos, N., 2019. Intestine-Specific Overexpression of LDLR Enhances Cholesterol Excretion and Induces Metabolic Changes in Male Mice. Endocrinology 160, 744. https://doi.org/10.1210/EN.2018-00098

Mhanna, M., Gharaibeh, M., Rashid, M., Sharab, A., Shehab, M., Zihlif, M., 2019. TPMT Genotype and Adverse Effects of Azathioprine among Jordanian Group. Curr. Drug Metab. 20, 889–897. https://doi.org/10.2174/1389200220666191021100953

Miao, Q., Yan, L., Zhou, Y., Li, Y., Zou, Y., Wang, L., Bai, Y., Zhang, J., 2021. Association of genetic variants in TPMT, ITPA, and NUDT15 with azathioprine-induced myelosuppression in southwest china patients with autoimmune hepatitis. Sci. Reports 2021 111 11, 1–8. https://doi.org/10.1038/s41598-021-87095-0

Moellering, D.R., Smith, D.L., 2012. Ambient Temperature and Obesity. Curr. Obes. Rep. 1, 26. https://doi.org/10.1007/S13679-011-0002-7

Moller, F.T., Andersen, V., Wohlfahrt, J., Jess, T., 2015. Familial risk of inflammatory bowel disease: a population-based cohort study 1977-2011. Am. J. Gastroenterol. 110, 564–571. https://doi.org/10.1038/AJG.2015.50

Mottawea, W., Chiang, C.K., Mühlbauer, M., Starr, A.E., Butcher, J., Abujamel, T., Deeke, S.A., Brandel, A., Zhou, H., Shokralla, S., Hajibabaei, M., Singleton, R., Benchimol, E.I., Jobin, C., Mack, D.R., Figeys, D., Stintzi, A., 2016. Altered

intestinal microbiota-host mitochondria crosstalk in new onset Crohn's disease. Nat. Commun. 7. https://doi.org/10.1038/NCOMMS13419

Mukherjee, S., Hooper, L. V., 2015. Antimicrobial defense of the intestine. Immunity 42, 28–39. https://doi.org/10.1016/J.IMMUNI.2014.12.028

Nakamura, K., Yokoi, Y., Fukaya, R., Ohira, S., Shinozaki, R., Nishida, T., Kikuchi, M., Ayabe, T., 2020. Expression and Localization of Paneth Cells and Their α-Defensins in the Small Intestine of Adult Mouse. Front. Immunol. 11. https://doi.org/10.3389/FIMMU.2020.570296/FULL

Nakata, T., Shimizu, H., Nagata, S., Ito, G., Fujii, S., Suzuki, K., Kawamoto, A., Ishibashi, F., Kuno, R., Anzai, S., Murano, T., Mizutani, T., Oshima, S., Tsuchiya, K., Nakamura, T., Hozumi, K., Watanabe, M., Okamoto, R., 2017. Indispensable role of Notch ligand-dependent signaling in the proliferation and stem cell niche maintenance of APC-deficient intestinal tumors. Biochem. Biophys. Res. Commun. 482, 1296–1303. https://doi.org/10.1016/J.BBRC.2016.12.031

Nam, H.J., Kim, Y.E., Moon, B.S., Kim, H.Y., Jung, D., Choi, S., Jang, J.W., Nam, D.H., Cho, H., 2021. Azathioprine antagonizes aberrantly elevated lipid metabolism and induces apoptosis in glioblastoma. iScience 24. https://doi.org/10.1016/J.ISCI.2021.102238

Neurath, M.F., 2014. Cytokines in inflammatory bowel disease. Nat. Rev. Immunol. 14, 329–342. https://doi.org/10.1038/NRI3661

Novak, E.A., Mollen, K.P., 2015. Mitochondrial dysfunction in inflammatory bowel disease. Front. Cell Dev. Biol. 3, 62. https://doi.org/10.3389/FCELL.2015.00062/BIBTEX

Ogura, Y., Bonen, D.K., Inohara, N., Nicolae, D.L., Chen, F.F., Ramos, R., Britton, H., Moran, T., Karaliuskas, R., Duerr, R.H., Achkar, J.P., Brant, S.R., Bayless, T.M., Kirschner, B.S., Hanauer, S.B., Nũez, G., Cho, J.H., 2001. A frameshift mutation in NOD2 associated with susceptibility to Crohn's disease. Nat. 2001 4116837 411, 603–606. https://doi.org/10.1038/35079114

Ogura, Y., Lala, S., Xin, W., Smith, E., Dowds, T.A., Chen, F.F., Zimmermann, E., Tretiakova, M., Cho, J.H., Hart, J., Greenson, J.K., Keshav, S., Nuñez, G., 2003. Expression of NOD2 in Paneth cells: a possible link to Crohn's ileitis. Gut 52, 1591–1597. https://doi.org/10.1136/GUT.52.11.1591

Ohno, M., Hasegawa, M., Hayashi, A., Caballero-Flores, G., Alteri, C.J., Lawley, T.D., Kamada, N., Núñez, G., Inohara, N., 2020. Lipopolysaccharide O structure of adherent and invasive Escherichia coli regulates intestinal inflammation via complement C3. PLoS Pathog. 16. https://doi.org/10.1371/JOURNAL.PPAT.1008928

Os, E.C. Van, Zins, B.J., Sandborn, W.J., Mays, D.C., Tremaine, W.J., Mahoney, D.W., Zinsmeister, A.R., Lipsky, J.J., 1996. Azathioprine pharmacokinetics after intravenous, oral, delayed release oral and rectal foam administration. Gut 39, 63–68. https://doi.org/10.1136/GUT.39.1.63

Ott, N.R.| G.& H., Schölmerich, C., Nat, J., 2013. Extraintestinal manifestations and complications in IBD. Nat. Rev. Gastroenterol. Hepatol. 2013 1010 10, 585–595.

https://doi.org/10.1038/nrgastro.2013.117

Ouellette, A.J., 2006. Paneth cell alpha-defensin synthesis and function. Curr. Top. Microbiol. Immunol. 306, 1–25. https://doi.org/10.1007/3-540-29916-5_1

Palmela, C., Chevarin, C., Xu, Z., Torres, J., Sevrin, G., Hirten, R., Barnich, N., Ng, S.C., Colombel, J.F., 2018. Adherent-invasive Escherichia coli in inflammatory bowel disease. Gut 67, 574–587. https://doi.org/10.1136/GUTJNL-2017-314903

Paneth, J., 1887. Ueber die secernirenden Zellen des Dünndarm-Epithels. Arch. für mikroskopische Anat. 1887 31, 113–191. https://doi.org/10.1007/BF02955706

Pararasa, C., Zhang, N., Tull, T.J., Chong, M.H.A., Siu, J.H.Y., Guesdon, W., Chavele, K.M., Sanderson, J.D., Langmead, L., Kok, K., Spencer, J., Vossenkamper, A., 2019. Reduced CD27−IgD− B cells in blood and raised CD27−IgD− B cells in gut-associated lymphoid tissue in inflammatory bowel disease. Front. Immunol. 10, 361. https://doi.org/10.3389/FIMMU.2019.00361/FULL

Park, D., Fergusson, A., Ford, L., Berg, J., Mansur, A.H., 2009. Side effects from azathioprine in a patient with thiopurine S-methyl transferase deficiency. Respir. Med. CME 2, 102–105. https://doi.org/10.1016/J.RMEDC.2008.10.005

Park, J., Cheon, J.H., 2021. Incidence and Prevalence of Inflammatory Bowel Disease across Asia. Yonsei Med. J. 62, 99. https://doi.org/10.3349/YMJ.2021.62.2.99

Parkes, G.C., Whelan, K., Lindsay, J.O., 2014. Smoking in inflammatory bowel disease: impact on disease course and insights into the aetiology of its effect. J. Crohns. Colitis 8, 717–725. https://doi.org/10.1016/J.CROHNS.2014.02.002

Pellegrinet, L., Rodilla, V., Liu, Z., Chen, S., Koch, U., Espinosa, L., Kaestner, K.H., Kopan, R., Lewis, J., Radtke, F., 2011. Dll1- and dll4-mediated notch signaling are required for homeostasis of intestinal stem cells. Gastroenterology 140, 1230-1240.e7. https://doi.org/10.1053/J.GASTRO.2011.01.005

Peppercorn, M.A., Cheifetz, A.S., n.d. Definitions, epidemiology, and risk factors for inflammatory bowel disease - UpToDate [WWW Document]. URL https://www.uptodate.com/contents/definitions-epidemiology-and-risk-factors-for-inflammatory-bowel-disease (accessed 3.2.22).

Peppercorn, M.A., Kane, S. V, n.d. Clinical manifestations, diagnosis, and prognosis of Crohn disease in adults - UpToDate [WWW Document]. URL https://www.uptodate.com/contents/clinical-manifestations-diagnosis-and-prognosis-of-crohn-disease-in-adults?topicRef=4066&source=related_link (accessed 3.24.22).

Pollard, J.D., Hartung, H.P., Hughes, R.A.C., 2005. Principles of Immunotherapy. Peripher. Neuropathy 1, 635–648. https://doi.org/10.1016/B978-0-7216-9491-7.50031-4

Poppe, D., Tiede, I., Fritz, G., Becker, C., Bartsch, B., Wirtz, S., Strand, D., Tanaka, S., Galle, P.R., Bustelo, X.R., Neurath, M.F., 2006. Azathioprine Suppresses Ezrin-Radixin-Moesin-Dependent T Cell-APC Conjugation through Inhibition of Vav Guanosine Exchange Activity on Rac Proteins. J. Immunol. 176, 640.

https://doi.org/10.4049/JIMMUNOL.176.1.640

Potter, B.J., Hodgson, H.J.F., Mee, A.S., Jewell, D.P., 1979. Clq metabolism in ulcerative colitis and Crohn's disease. Gut 20, 1012–1019. https://doi.org/10.1136/GUT.20.11.1012

Preisker, S., Brethack, A.K., Bokemeyer, A., Bettenworth, D., Sina, C., Derer, S., 2019. Crohn's Disease Patients in Remission Display an Enhanced Intestinal IgM^+ B Cell Count in Concert with a Strong Activation of the Intestinal Complement System. Cells 8. https://doi.org/10.3390/CELLS8010078

Rath, E., Haller, D., 2022. Intestinal epithelial cell metabolism at the interface of microbial dysbiosis and tissue injury. Mucosal Immunol. 15, 595–604. https://doi.org/10.1038/S41385-022-00514-X

Repetto, G., del Peso, A., Zurita, J.L., 2008. Neutral red uptake assay for the estimation of cell viability/cytotoxicity. Nat. Protoc. 2008 37 3, 1125–1131. https://doi.org/10.1038/nprot.2008.75

Richens, E.R., Thorp, C.M., Bland, P.W., Hall, N.D., 1982. Circulating immune complexes in Crohn's disease. Dig. Dis. Sci. 1982 272 27, 129–138. https://doi.org/10.1007/BF01311706

Riegel, W., Stephan, E., Balle, C., Heidland, A., Hörl, W.H., 1990. Effect of cyclosporin A, azathioprine, and prednisolone on carbohydrate metabolism of rat hepatocytes. Transpl. Int. 1990 31 3, 2–7. https://doi.org/10.1007/BF00333193

Ripollés Piquer, B., Nazih, H., Bourreille, A., Segain, J.P., Huvelin, J.M., Galmiche, J.P., Bard, J.M., 2006. Altered lipid, apolipoprotein, and lipoprotein profiles in inflammatory bowel disease: consequences on the cholesterol efflux capacity of serum using Fu5AH cell system. Metabolism. 55, 980–988. https://doi.org/10.1016/J.METABOL.2006.03.006

Rizzello, F., Spisni, E., Giovanardi, E., Imbesi, V., Salice, M., Alvisi, P., Valerii, M.C., Gionchetti, P., 2019. Implications of the Westernized Diet in the Onset and Progression of IBD. Nutrients 11. https://doi.org/10.3390/NU11051033

Roda, G., Chien Ng, S., Kotze, P.G., Argollo, M., Panaccione, R., Spinelli, A., Kaser, A., Peyrin-Biroulet, L., Danese, S., 2020. Crohn's disease. Nat. Rev. Dis. Prim. 2020 61 6, 1–19. https://doi.org/10.1038/s41572-020-0156-2

Rodríguez-Colman, M.J., Schewe, M., Meerlo, M., Stigter, E., Gerrits, J., Pras-Raves, M., Sacchetti, A., Hornsveld, M., Oost, K.C., Snippert, H.J., Verhoeven-Duif, N., Fodde, R., Burgering, B.M.T., 2017. Interplay between metabolic identities in the intestinal crypt supports stem cell function. Nat. 2017 5437645 543, 424–427. https://doi.org/10.1038/nature21673

Rogler, G., Singh, A., Kavanaugh, A., Rubin, D.T., 2021. Extraintestinal Manifestations of Inflammatory Bowel Disease: Current Concepts, Treatment, and Implications for Disease Management. Gastroenterology 161, 1118. https://doi.org/10.1053/J.GASTRO.2021.07.042

Ross, J., 2014. Colour Analysis Tools in ... Using the Colour Deconvolution plugin in ImageJ [WWW Document]. URL https://cupdf.com/document/colour-analysis-

tools-in-using-the-colour-deconvolution-plugin-in-imagej-jacqui.html?page=1 (accessed 6.1.22).

Rui, M., Fei, Z., Wang, Y., Shi, F., Meng, R., Shang, Y., Ma, A., Li, H., 2021. Will the Inducing and Maintaining Remission of Non-biological Agents and Biological Agents Differ for Crohn's Disease? The Evidence From the Network Meta-Analysis. Front. Med. 8. https://doi.org/10.3389/FMED.2021.679258

Rumbo, M., Schiffrin, E.J., 2005. Ontogeny of intestinal epithelium immune functions: developmental and environmental regulation. Cell. Mol. Life Sci. 62, 1288–1296. https://doi.org/10.1007/S00018-005-5033-3

Sahasranaman, S., Howard, D., Roy, S., 2008. Clinical pharmacology and pharmacogenetics of thiopurines. Eur. J. Clin. Pharmacol. 2008 648 64, 753–767. https://doi.org/10.1007/S00228-008-0478-6

SALSER, J.S., HUTCHISON, D.J., BALIS, M.E., 1960. Studies on the Mechanism of Action of 6-Mercaptopurine in Cell-free Preparations. J. Biol. Chem. 235, 429–432. https://doi.org/10.1016/S0021-9258(18)69541-9

Salzman, N.H., Hung, K., Haribhai, D., Chu, H., Karlsson-Sjöberg, J., Amir, E., Teggatz, P., Barman, M., Hayward, M., Eastwood, D., Stoel, M., Zhou, Y., Sodergren, E., Weinstock, G.M., Bevins, C.L., Williams, C.B., Bos, N.A., 2010. Enteric defensins are essential regulators of intestinal microbial ecology. Nat. Immunol. 11, 76. https://doi.org/10.1038/NI.1825

Sankaran-Walters, S., Hart, R., Dills, C., 2017. Guardians of the Gut: Enteric Defensins. Front. Microbiol. 8, 647. https://doi.org/10.3389/FMICB.2017.00647

Sappati Biyyani, R.S.R., Putka, B.S., Mullen, K.D., 2010. Dyslipidemia and lipoprotein profiles in patients with inflammatory bowel disease. J. Clin. Lipidol. 4, 478–482. https://doi.org/10.1016/J.JACL.2010.08.021

Sato, T., Van Es, J.H., Snippert, H.J., Stange, D.E., Vries, R.G., Van Den Born, M., Barker, N., Shroyer, N.F., Van De Wetering, M., Clevers, H., 2011. Paneth cells constitute the niche for Lgr5 stem cells in intestinal crypts. Nature 469, 415. https://doi.org/10.1038/NATURE09637

Sato, T., Vries, R.G., Snippert, H.J., Van De Wetering, M., Barker, N., Stange, D.E., Van Es, J.H., Abo, A., Kujala, P., Peters, P.J., Clevers, H., 2009. Single Lgr5 stem cells build crypt-villus structures in vitro without a mesenchymal niche. Nature 459, 262–265. https://doi.org/10.1038/NATURE07935

Satsangi, J., Silverberg, M.S., Vermeire, S., Colombel, J.F., 2006. The Montreal classification of inflammatory bowel disease: controversies, consensus, and implications. Gut 55, 749. https://doi.org/10.1136/GUT.2005.082909

Savarino, E., Bodini, G., Dulbecco, P., Assandri, L., Bruzzone, L., Mazza, F., Frigo, A., Fazio, V., Marabotto, E., Savarino, V., 2013. Adalimumab is more effective than azathioprine and mesalamine at preventing postoperative recurrence of Crohn's disease: a randomized controlled trial. Am. J. Gastroenterol. 108, 1731–1742. https://doi.org/10.1038/AJG.2013.287

Schroll, S., Sarlette, A., Ahrens, K., Manns, M.P., Göke, M., 2005. Effects of azathioprine and its metabolites on repair mechanisms of the intestinal

epithelium in vitro. Regul. Pept. 131, 1–11. https://doi.org/10.1016/J.REGPEP.2005.03.001

Schwalbe, G., 1872. Beiträge zur Kenntniss der Drüsen in den Darmwandungen, in's Besondere der Brunner'schen Drüsen. Arch. für mikroskopische Anat. 8, 92–140.

Schwartz, D.A., Loftus, E. V., Tremaine, W.J., Panaccione, R., Harmsen, W.S., Zinsmeister, A.R., Sandborn, W.J., 2002. The natural history of fistulizing Crohn's disease in Olmsted County, Minnesota. Gastroenterology 122, 875–880. https://doi.org/10.1053/GAST.2002.32362

Schwärzler, J., Mayr, L., Vich Vila, A., Grabherr, F., Niederreiter, L., Philipp, M., Grander, C., Meyer, M., Jukic, A., Tröger, S., Enrich, B., Przysiecki, N., Tschurtschenthaler, M., Sommer, F., Kronberger, I., Koch, J., Hilbe, R., Hess, M.W., Oberhuber, G., Sprung, S., Ran, Q., Koch, R., Effenberger, M., Kaneider, N.C., Wieser, V., Keller, M.A., Weersma, R.K., Aden, K., Rosenstiel, P., Blumberg, R.S., Kaser, A., Tilg, H., Adolph, T.E., 2022. PUFA-Induced Metabolic Enteritis as a Fuel for Crohn's Disease. Gastroenterology 162, 1690–1704. https://doi.org/10.1053/J.GASTRO.2022.01.004

Scoville, E.A., Allaman, M.M., Adams, D.W., Motley, A.K., Peyton, S.C., Ferguson, S.L., Horst, S.N., Williams, C.S., Beaulieu, D.B., Schwartz, D.A., Wilson, K.T., Coburn, L.A., 2019. Serum Polyunsaturated Fatty Acids Correlate with Serum Cytokines and Clinical Disease Activity in Crohn's Disease. Sci. Rep. 9. https://doi.org/10.1038/S41598-019-39232-Z

Scoville, E.A., Allaman, M.M., Brown, C.T., Motley, A.K., Horst, S.N., Williams, C.S., Koyama, T., Zhao, Z., Adams, D.W., Beaulieu, D.B., Schwartz, D.A., Wilson, K.T., Coburn, L.A., 2018. Alterations in Lipid, Amino Acid, and Energy Metabolism Distinguish Crohn's Disease from Ulcerative Colitis and Control Subjects by Serum Metabolomic Profiling. Metabolomics 14. https://doi.org/10.1007/S11306-017-1311-Y

Severs, M., Spekhorst, L.M., Mangen, M.J.J., Dijkstra, G., Löwenberg, M., Hoentjen, F., Van Der Meulen-De Jong, A.E., Pierik, M., Ponsioen, C.Y., Bouma, G., Van Der Woude, J.C., Van Der Valk, M.E., Romberg-Camps, M.J.L., Clemens, C.H.M., Van De Meeberg, P., Mahmmod, N., Jansen, J., Jharap, B., Weersma, R.K., Oldenburg, B., Festen, E.A.M., Fidder, H.H., 2018. Sex-Related Differences in Patients With Inflammatory Bowel Disease: Results of 2 Prospective Cohort Studies. Inflamm. Bowel Dis. 24, 1298–1306. https://doi.org/10.1093/IBD/IZY004

Shroyer, N.F., Helmrath, M.A., Wang, V.Y.C., Antalffy, B., Henning, S.J., Zoghbi, H.Y., 2007. Intestine-specific ablation of mouse atonal homolog 1 (Math1) reveals a role in cellular homeostasis. Gastroenterology 132, 2478–2488. https://doi.org/10.1053/J.GASTRO.2007.03.047

Shroyer, N.F., Wallis, D., Venken, K.J.T., Bellen, H.J., Zoghbi, H.Y., 2005. Gfi1 functions downstream of Math1 to control intestinal secretory cell subtype allocation and differentiation. Genes Dev. 19, 2412–2417. https://doi.org/10.1101/GAD.1353905

Simpson, K.W., Dogan, B., Rishniw, M., Goldstein, R.E., Klaessig, S., McDonough,

P.L., German, A.J., Yates, R.M., Russell, D.G., Johnson, S.E., Berg, D.E., Harel, J., Bruant, G., McDonough, S.P., Schukken, Y.H., 2006. Adherent and Invasive Escherichia coli Is Associated with Granulomatous Colitis in Boxer Dogs. Infect. Immun. 74, 4778. https://doi.org/10.1128/IAI.00067-06

Sina, C., Kemper, C., Derer, S., 2018. The intestinal complement system in inflammatory bowel disease: Shaping intestinal barrier function. Semin. Immunol. 37, 66–73. https://doi.org/10.1016/J.SMIM.2018.02.008

Socha-Banasiak, A., Sputa-Grzegrzółka, P., Grzegrzółka, J., Pacześ, K., Dzięgiel, P., Sordyl, B., Romanowicz, H., Czkwianianc, E., 2021. Metallothioneins in Inflammatory Bowel Diseases: Importance in Pathogenesis and Potential Therapy Target. Can. J. Gastroenterol. Hepatol. 2021. https://doi.org/10.1155/2021/6665697

Soh, H., Im, J.P., Han, K., Park, S., Hong, S.W., Moon, J.M., Kang, E.A., Chun, J., Lee, H.J., Kim, J.S., 2020. Crohn's disease and ulcerative colitis are associated with different lipid profile disorders: a nationwide population-based study. Aliment. Pharmacol. Ther. 51, 446–456. https://doi.org/10.1111/APT.15562

Stappenbeck, T., Gordon, J.I., 2000. Rac1 mutations produce aberrant epithelial differentiation in the developing and adult mouse small intestine. Development 127, 2629–2642. https://doi.org/10.1242/DEV.127.12.2629

Stappenbeck, T.S., 2009. Paneth Cell Development, Differentiation, and Function: New Molecular Cues. Gastroenterology. https://doi.org/10.1053/j.gastro.2009.05.013

Starr, A.E., Deeke, S.A., Ning, Z., Chiang, C.-K., Zhang, X., Mottawea, W., Singleton, R., Benchimol, E.I., Wen, M., Mack, D.R., Stintzi, A., Figeys, D., 2017. Proteomic analysis of ascending colon biopsies from a paediatric inflammatory bowel disease inception cohort identifies protein biomarkers that differentiate Crohn's disease from UC. Gut 66, 1573–1583. https://doi.org/10.1136/GUTJNL-2015-310705

Steponaitiene, R., Kupcinskas, J., Survilaite, S., Varkalaite, G., Jonaitis, L., Kiudelis, G., Denapiene, G., Valantinas, J., Skieceviciene, J., Kupcinskas, L., 2016. TPMT and ITPA genetic variants in Lithuanian inflammatory bowel disease patients: Prevalence and azathioprine-related side effects. Adv. Med. Sci. 61, 135–140. https://doi.org/10.1016/J.ADVMS.2015.09.008

Su, D., Nie, Y., Zhu, A., Chen, Z., Wu, P., Zhang, L., Luo, M., Sun, Q., Cai, L., Lai, Y., Xiao, Z., Duan, Z., Zheng, S., Wu, G., Hu, R., Tsukamoto, H., Lugea, A., Liu, Z., Pandol, S.J., Han, Y.P., 2016. Vitamin D Signaling through Induction of Paneth Cell Defensins Maintains Gut Microbiota and Improves Metabolic Disorders and Hepatic Steatosis in Animal Models. Front. Physiol. 7. https://doi.org/10.3389/FPHYS.2016.00498

Sun, X., Chalmers, L., Fu, X., Zhao, M., 2012. A Molecular Link Between Interleukin 22 and Intestinal Mucosal Wound Healing. Adv. wound care 1, 231–237. https://doi.org/10.1089/WOUND.2011.0334

Sünderhauf, A., Hicken, M., Schlichting, H., Skibbe, K., Ragab, M., Raschdorf, A., Hirose, M., Schäffler, H., Bokemeyer, A., Bettenworth, D., Savitt, A.G., Perner,

S., Ibrahim, S., Peerschke, E.I., Ghebrehiwet, B., Derer, S., Sina, C., 2021. Loss of Mucosal p32/gC1qR/HABP1 Triggers Energy Deficiency and Impairs Goblet Cell Differentiation in Ulcerative Colitis. Cell. Mol. Gastroenterol. Hepatol. 12, 229–250. https://doi.org/10.1016/J.JCMGH.2021.01.017

Suzuki, K., Fukui, H., Kayahara, T., Sawada, M., Seno, H., Hiai, H., Kageyama, R., Okano, H., Chiba, T., 2005. Hes1-deficient mice show precocious differentiation of Paneth cells in the small intestine. Biochem. Biophys. Res. Commun. 328, 348–352. https://doi.org/10.1016/J.BBRC.2004.12.174

Swidsinski, A., Loening-Baucke, V., Bengmark, S., Lochs, H., Dörffel, Y., 2007. Azathioprine and mesalazine-induced effects on the mucosal flora in patients with IBD colitis. Inflamm. Bowel Dis. 13, 51–56. https://doi.org/10.1002/IBD.20003

Tapner, M.J., Jones, B.E., Wu, W.M., Farrell, G.C., 2004. Toxicity of low dose azathioprine and 6-mercaptopurine in rat hepatocytes. Roles of xanthine oxidase and mitochondrial injury. J. Hepatol. 40, 454–463. https://doi.org/10.1016/J.JHEP.2003.11.024

Tay, B.S., Lilley, R.M.C., Murray, A.W., Atkinson, M.R., 1969. Inhibition of phosphoribosyl pyrophosphate amidotransferase from Ehrlich ascites-tumour cells by thiopurine nucleotides. Biochem. Pharmacol. 18, 936–938. https://doi.org/10.1016/0006-2952(69)90069-0

Taylor, R.W., Turnbull, D.M., 2005. MITOCHONDRIAL DNA MUTATIONS IN HUMAN DISEASE. Nat. Rev. Genet. 6, 389. https://doi.org/10.1038/NRG1606

Tiede, I., Fritz, G., Strand, S., Poppe, D., Dvorsky, R., Strand, D., Lehr, H.A., Wirtz, S., Becker, C., Atreya, R., Mudter, J., Hildner, K., Bartsch, B., Holtmann, M., Blumberg, R., Walczak, H., Iven, H., Galle, P.R., Ahmadian, M.R., Neurath, M.F., 2003. CD28-dependent Rac1 activation is the molecular target of azathioprine in primary human CD4+ T lymphocytes. J. Clin. Invest. 111, 1133. https://doi.org/10.1172/JCI16432

Timmer, A., Patton, P.H., Chande, N., McDonald, J.W., MacDonald, J.K., Group, C.I., 2016. Azathioprine and 6-mercaptopurine for maintenance of remission in ulcerative colitis. Cochrane Database Syst. Rev. 2016. https://doi.org/10.1002/14651858.CD000478.PUB4

Todorov, H., Kollar, B., Bayer, F., Brandão, I., Mann, A., Mohr, J., Pontarollo, G., Formes, H., Stauber, R., Kittner, J.M., Endres, K., Watzer, B., Nockher, W.A., Sommer, F., Gerber, S., Reinhardt, C., 2020. α-Linolenic Acid-Rich Diet Influences Microbiota Composition and Villus Morphology of the Mouse Small Intestine. Nutrients 12. https://doi.org/10.3390/NU12030732

Torres, J., Mehandru, S., Colombel, J.F., Peyrin-Biroulet, L., 2017. Crohn's disease. Lancet (London, England) 389, 1741–1755. https://doi.org/10.1016/S0140-6736(16)31711-1

Tschurtschenthaler, M., Adolph, T.E., Ashcroft, J.W., Niederreiter, L., Bharti, R., Saveljeva, S., Bhattacharyya, J., Flak, M.B., Shih, D.Q., Fuhler, G.M., Parkes, M., Kohno, K., Iwawaki, T., van der Woude, C.J., Harding, H.P., Smith, A.M., Peppelenbosch, M.P., Targan, S.R., Ron, D., Rosenstiel, P., Blumberg, R.S.,

Kaser, A., 2017. Defective ATG16L1-mediated removal of IRE1α drives Crohn's disease–like ileitis. J. Exp. Med. 214, 401. https://doi.org/10.1084/JEM.20160791

Tuppen, H.A.L., Blakely, E.L., Turnbull, D.M., Taylor, R.W., 2010. Mitochondrial DNA mutations and human disease. Biochim. Biophys. Acta - Bioenerg. https://doi.org/10.1007/s13762-018-1717-8

Turpin, W., Lee, S.H., Raygoza Garay, J.A., Madsen, K.L., Meddings, J.B., Bedrani, L., Power, N., Espin-Garcia, O., Xu, W., Smith, M.I., Griffiths, A.M., Moayyedi, P., Turner, D., Seidman, E.G., Steinhart, A.H., Marshall, J.K., Jacobson, K., Mack, D., Huynh, H., Bernstein, C.N., Paterson, A.D., Abreu, M., Beck, P., Croitoru, K., Dieleman, L., Feagan, B., Griffiths, A., Guttman, D., Kaplan, G., Krause, D.O., Madsen, K., Marshall, J., Ropeleski, M., Seidman, E., Silverberg, M., Snapper, S., Stadnyk, A., Steinhart, H., Surette, M., Walters, T., Vallance, B., Aumais, G., Bitton, A., Cino, M., Critch, J., Denson, L., Deslandres, C., El-Matary, W., Herfarth, H., Higgins, P., Hyams, J., McGrath, J., Otley, A., Panancionne, R., Baldassano, R., Hedin, C., Hussey, S., Hyams, H., Keljo, D., Kevans, D., Lees, C., Murthy, S., Panaccione, R., Parekh, N., Plamondon, S., Radford-Smith, G., Rosh, J., Rubin, D., Schultz, M., Siegel, C., 2020. Increased Intestinal Permeability Is Associated With Later Development of Crohn's Disease. Gastroenterology 159, 2092-2100.e5. https://doi.org/10.1053/J.GASTRO.2020.08.005

Urbauer, E., Rath, E., Haller, D., 2021. Mitochondrial Metabolism in the Intestinal Stem Cell Niche—Sensing and Signaling in Health and Disease. Front. Cell Dev. Biol. 8, 1520. https://doi.org/10.3389/FCELL.2020.602814/BIBTEX

Vaishnava, S., Behrendt, C.L., Ismail, A.S., Eckmann, L., Hooper, L. V., 2008. Paneth cells directly sense gut commensals and maintain homeostasis at the intestinal host-microbial interface. Proc. Natl. Acad. Sci. U. S. A. 105, 20858–20863. https://doi.org/10.1073/PNAS.0808723105/SUPPL_FILE/0808723105SI.PDF

Vamecq, J., Dessein, A.-F., Fontaine, M., Briand, G., Porchet, N., Latruffe, N., Andreolotti, P., Cherkaoui-Malki, M., 2012. Mitochondrial dysfunction and lipid homeostasis. Curr. Drug Metab. 13, 1388–1400. https://doi.org/10.2174/138920012803762792

van Furth, R., Gassmann, A., Diesselhoff-Den Dulk, M., 1975. The effect of azathioprine (Imuran) on the cell cycle of promonocytes and the production of monocytes in the bone marrow. J. Exp. Med. 141, 531–546. https://doi.org/10.1084/JEM.141.3.531

Van Heel, D.A., Ghosh, S., Hunt, K.A., Mathew, C.G., Forbes, A., Jewell, D.P., Playford, R.J., 2005. Synergy between TLR9 and NOD2 innate immune responses is lost in genetic Crohn's disease. Gut 54, 1553. https://doi.org/10.1136/GUT.2005.065888

Van Leuven, S.I., Hezemans, R., Levels, J.H., Snoek, S., Stokkers, P.C., Hovingh, G.K., Kastelein, J.J.P., Stroes, E.S., De Groot, E., Hommes, D.W., 2007. Enhanced atherogenesis and altered high density lipoprotein in patients with Crohn's disease. J. Lipid Res. 48, 2640–2646.

https://doi.org/10.1194/jlr.M700176-JLR200

Van Scoik, K., Johnson, C., Porter, W., 1985. The pharmacology and metabolism of the thiopurine drugs 6-mercaptopurine and azathioprine. Drug Metab. Rev. 16, 157–174. https://doi.org/10.3109/03602538508991433

Vankoningsloo, S., Piens, M., Lecocq, C., Gilson, A., De Pauw, A., Renard, P., Demazy, C., Houbion, A., Raes, M., Arnould, T., 2005. Mitochondrial dysfunction induces triglyceride accumulation in 3T3-L1 cells: Role of fatty acid β-oxidation and glucose. J. Lipid Res. 46, 1133–1149. https://doi.org/10.1194/jlr.M400464-JLR200

Vavricka, S.R., Brun, L., Ballabeni, P., Pittet, V., Prinz Vavricka, B.M., Zeitz, J., Rogler, G., Schoepfer, A.M., 2011. Frequency and risk factors for extraintestinal manifestations in the Swiss inflammatory bowel disease cohort. Am. J. Gastroenterol. 106, 110–119. https://doi.org/10.1038/AJG.2010.343

Verma, A., Pittala, S., Alhozeel, B., Shteinfer-Kuzmine, A., Ohana, E., Gupta, R., Chung, J.H., Shoshan-Barmatz, V., 2022. The role of the mitochondrial protein VDAC1 in inflammatory bowel disease: a potential therapeutic target. Mol. Ther. 30, 726–744. https://doi.org/10.1016/j.ymthe.2021.06.024

Vester-Andersen, M.K., Mirsepasi-Lauridsen, H.C., Prosberg, M. V., Mortensen, C.O., Träger, C., Skovsen, K., Thorkilgaard, T., Nøjgaard, C., Vind, I., Krogfelt, K.A., Sørensen, N., Bendtsen, F., Petersen, A.M., 2019. Increased abundance of proteobacteria in aggressive Crohn's disease seven years after diagnosis. Sci. Reports 2019 91 9, 1–10. https://doi.org/10.1038/s41598-019-49833-3

Vich Vila, A., Imhann, F., Collij, V., Jankipersadsing, S.A., Gurry, T., Mujagic, Z., Kurilshikov, A., Bonder, M.J., Jiang, X., Tigchelaar, E.F., Dekens, J., Peters, V., Voskuil, M.D., Visschedijk, M.C., van Dullemen, H.M., Keszthelyi, D., Swertz, M.A., Franke, L., Alberts, R., Festen, E.A.M., Dijkstra, G., Masclee, A.A.M., Hofker, M.H., Xavier, R.J., Alm, E.J., Fu, J., Wijmenga, C., Jonkers, D.M.A.E., Zhernakova, A., Weersma, R.K., 2018. Gut microbiota composition and functional changes in inflammatory bowel disease and irritable bowel syndrome. Sci. Transl. Med. 10. https://doi.org/10.1126/SCITRANSLMED.AAP8914

Vidal, K., Grosjean, I., Revillard, J.P., Gespach, C., Kaiserlian, D., 1993. Immortalization of mouse intestinal epithelial cells by the SV40-large T gene: Phenotypic and immune characterization of the MODE-K cell line. J. Immunol. Methods 166, 63–73. https://doi.org/10.1016/0022-1759(93)90329-6

Wagner, J., Maksimovic, J., Farries, G., Sim, W.H., Bishop, R.F., Cameron, D.J., Catto-Smith, A.G., Kirkwood, C.D., 2013. Bacteriophages in gut samples from pediatric Crohn's disease patients: metagenomic analysis using 454 pyrosequencing. Inflamm. Bowel Dis. 19, 1598–1608. https://doi.org/10.1097/MIB.0B013E318292477C

Wang, A., Keita, Å. V., Phan, V., McKay, C.M., Schoultz, I., Lee, J., Murphy, M.P., Fernando, M., Ronaghan, N., Balce, D., Yates, R., Dicay, M., Beck, P.L., Macnaughton, W.K., Söderholm, J.D., McKay, D.M., 2014. Targeting mitochondria-derived reactive oxygen species to reduce epithelial barrier dysfunction and colitis. Am. J. Pathol. https://doi.org/10.1016/j.ajpath.2014.05.019

Wang, B., Rong, X., Palladino, E.N.D., Wang, J., Fogelman, A.M., Martín, M.G., Alrefai, W.A., Ford, D.A., Tontonoz, P., 2018. Phospholipid remodeling and cholesterol availability regulate intestinal stemness and tumorigenesis. Cell Stem Cell 22, 206. https://doi.org/10.1016/J.STEM.2017.12.017

Wang, B., Zhang, S. qin, Dong, J. li, Li, Y., Jin, Y. xiao, Xiao, H. wen, Wang, H. chao, Fan, S. jun, Cui, M., 2022. Ambient temperature structures the gut microbiota of zebrafish to impact the response to radioactive pollution. Environ. Pollut. 293. https://doi.org/10.1016/J.ENVPOL.2021.118539

Wang, Dan, Odle, J., Liu, Y., 2021. Metabolic Regulation of Intestinal Stem Cell Homeostasis. Trends Cell Biol. 31, 325–327. https://doi.org/10.1016/J.TCB.2021.02.001

Wang, D., Peregrina, K., Dhima, E., Lin, E.Y., Mariadason, J.M., Augenlicht, L.H., 2011. Paneth cell marker expression in intestinal villi and colon crypts characterizes dietary induced risk for mouse sporadic intestinal cancer. Proc. Natl. Acad. Sci. U. S. A. 108, 10272–10277. https://doi.org/10.1073/PNAS.1017668108/-/DCSUPPLEMENTAL

Wang, D, Zhao, X.J., Cui, X.F., Li, L.Z., Zhang, H.J., 2021. Correlation of serum lipid profile and disease activity in patients with inflammatory bowel disease. Zhonghua nei ke za zhi 60, 834–836. https://doi.org/10.3760/CMA.J.CN112138-20200930-00847

Wang, W.F., Li, X., Guo, M.Z., Chen, J. De, Yang, Y.S., Peng, L.H., Wang, Y.H., Zhang, C.Y., Li, H.H., 2013. Mitochondrial ATP 6 and 8 polymorphisms in irritable bowel syndrome with diarrhea. World J. Gastroenterol. 19, 3847. https://doi.org/10.3748/WJG.V19.I24.3847

Wehkamp, J., Chu, H., Shen, B., Feathers, R.W., Kays, R.J., Lee, S.K., Bevins, C.L., 2006. Paneth cell antimicrobial peptides: Topographical distribution and quantification in human gastrointestinal tissues. FEBS Lett. 580, 5344–5350. https://doi.org/10.1016/J.FEBSLET.2006.08.083

Wehkamp, J., Harder, J., Weichenthal, M., Schwab, M., Schäffeler, E., Schlee, M., Herrlinger, K.R., Stallmach, A., Noack, F., Fritz, P., Schröder, J.M., Bevins, C.L., Fellermann, K., Stange, E.F., 2004. NOD2 (CARD15) mutations in Crohn's disease are associated with diminished mucosal alpha-defensin expression. Gut 53, 1658–1664. https://doi.org/10.1136/GUT.2003.032805

Wehkamp, J., Salzman, N.H., Porter, E., Nuding, S., Weichenthal, M., Petras, R.E., Shen, B., Schaeffeler, E., Schwab, M., Linzmeier, R., Feathers, R.W., Chu, H., Lima, H., Fellermann, K., Ganz, T., Stange, E.F., Bevins, C.L., 2005. Reduced Paneth cell α-defensins in ileal Crohn's disease. Proc. Natl. Acad. Sci. U. S. A. 102, 18129. https://doi.org/10.1073/PNAS.0505256102

Wehkamp, J., Stange, E.F., 2020. An Update Review on the Paneth Cell as Key to Ileal Crohn's Disease. Front. Immunol. https://doi.org/10.3389/fimmu.2020.00646

Wiens, M.E., Smith, J.G., 2017. α-Defensin HD5 Inhibits Human Papillomavirus 16 Infection via Capsid Stabilization and Redirection to the Lysosome. MBio 8. https://doi.org/10.1128/MBIO.02304-16

Willing, B.P., Dicksved, J., Halfvarson, J., Andersson, A.F., Lucio, M., Zheng, Z., Järnerot, G., Tysk, C., Jansson, J.K., Engstrand, L., 2010. A Pyrosequencing Study in Twins Shows That Gastrointestinal Microbial Profiles Vary With Inflammatory Bowel Disease Phenotypes. Gastroenterology 139, 1844-1854.e1. https://doi.org/10.1053/J.GASTRO.2010.08.049

Wilson, C.L., Ouellette, A.J., Satchell, D.P., Ayabe, T., López-Boado, Y.S., Stratman, J.L., Hultgren, S.J., Matrisian, L.M., Parks, W.C., 1999. Regulation of intestinal alpha-defensin activation by the metalloproteinase matrilysin in innate host defense. Science 286, 113–117. https://doi.org/10.1126/SCIENCE.286.5437.113

Winkelstein, A., 1979. The effects of azathioprine and 6 MP on immunity. J. Immunopharmacol. 1, 429–454. https://doi.org/10.3109/08923977909040545

Winkler, K., Konrad, T., Füllert, S., Friedrich, I., Destani, R., Baumstark, M.W., Krebs, K., Wieland, H., März, W., 2003a. Pioglitazone reduces atherogenic dense LDL particles in nondiabetic patients with arterial hypertension: a double-blind, placebo-controlled study. Diabetes Care 26, 2588–2594. https://doi.org/10.2337/DIACARE.26.9.2588

Winkler, K., Wetzka, B., Hoffmann, M.M., Friedrich, I., Kinner, M., Baumstark, M.W., Zahradnik, H.P., Wieland, H., März, W., 2003b. Triglyceride-rich lipoproteins are associated with hypertension in preeclampsia. J. Clin. Endocrinol. Metab. 88, 1162–1166. https://doi.org/10.1210/JC.2002-021160

Wu, A., Yu, B., Zhang, K., Xu, Z., Wu, D., He, J., Luo, J., Luo, Y., Yu, J., Zheng, P., Che, L., Mao, X., Huang, Z., Wang, L., Zhao, J., Chen, D., 2020. Transmissible gastroenteritis virus targets Paneth cells to inhibit the self-renewal and differentiation of Lgr5 intestinal stem cells via Notch signaling. Cell Death Dis. 11. https://doi.org/10.1038/S41419-020-2233-6

Xing, S., Chen, S., Zhao, Y., Luo, Y., Yu, B., He, J., Huang, Z., Zheng, P., Mao, X., Luo, J., Yan, H., Yu, J., 2022. Effects of High Ambient Temperature on Small Intestinal Morphology and Colonic Microbiota in Weaned Piglets. Anim. an Open Access J. from MDPI 12. https://doi.org/10.3390/ANI12141743

Xu, C., Wang, A., Marin, M., Honnen, W., Ramasamy, S., Porter, E., Subbian, S., Pinter, A., Melikyan, G.B., Lu, W., Chang, T.L., 2021. Human Defensins Inhibit SARS-CoV-2 Infection by Blocking Viral Entry. Viruses 13. https://doi.org/10.3390/V13071246

Xu, P., Elamin, E., Elizalde, M., Bours, P.P.H.A., Pierik, M.J., Masclee, A.A.M., Jonkers, D.M.A.E., 2019. Modulation of Intestinal Epithelial Permeability by Plasma from Patients with Crohn's Disease in a Three-dimensional Cell Culture Model. Sci. Rep. 9. https://doi.org/10.1038/S41598-018-38322-8

Yamamoto, S., Ma, X., 2009. Role of Nod2 in the development of Crohn's disease. Microbes Infect. 11, 912. https://doi.org/10.1016/J.MICINF.2009.06.005

Yang, E., Shen, J., 2021. The roles and functions of Paneth cells in Crohn's disease: A critical review. Cell Prolif. 54. https://doi.org/10.1111/CPR.12958

Yang, J., Wang, P., Qin, Z., Jia, M., Zhang, C., Tian, X., Zheng, Y., Zhang, A., Zhang, X., Liu, S., 2019. NUDT15 and TPMT Genetic Polymorphisms Are

Related to Azathioprine Intolerance in Chinese Patients with Rheumatic Diseases. Genet. Test. Mol. Biomarkers 23, 751–757. https://doi.org/10.1089/GTMB.2018.0313

Yilmaz, Ö.H., Katajisto, P., Lamming, D.W., Gültekin, Y., Bauer-Rowe, K.E., Sengupta, S., Birsoy, K., Dursun, A., Onur Yilmaz, V., Selig, M., Nielsen, G.P., Mino-Kenudson, M., Zukerberg, L.R., Bhan, A.K., Deshpande, V., Sabatini, D.M., 2012. mTORC1 in the Paneth cell niche couples intestinal stem cell function to calorie intake. Nature 486, 490. https://doi.org/10.1038/NATURE11163

Yu, S., Balasubramanian, I., Laubitz, D., Tong, K., Bandyopadhyay, S., Lin, X., Flores, J., Singh, R., Liu, Y., Macazana, C., Zhao, Y., Béguet-Crespel, F., Patil, K., Midura-Kiela, M.T., Wang, D., Yap, G.S., Ferraris, R.P., Wei, Z., Bonder, E.M., Häggblom, M.M., Zhang, L., Douard, V., Verzi, M.P., Cadwell, K., Kiela, P.R., Gao, N., 2020. Paneth cell-derived lysozyme defines the composition of mucolytic microbiota and the inflammatory tone of the intestine. Immunity 53, 398. https://doi.org/10.1016/J.IMMUNI.2020.07.010

Yu, S., Tong, K., Zhao, Y., Balasubramanian, I., Yap, G.S., Ferraris, R.P., Bonder, E.M., Verzi, M.P., Gao, N., 2018. Paneth Cell Multipotency Induced by Notch Activation following Injury. Cell Stem Cell 23, 46-59.e5. https://doi.org/10.1016/J.STEM.2018.05.002

Zaltman, C., Parra, R.S., Sassaki, L.Y., Santana, G.O., de Lourdes Abreu Ferrari, M., Miszputen, S.J., Amarante, H.M.B.S., Kaiser, R.L., Flores, C., Catapani, W.R., Parente, J.M.L., Bafutto, M., Ramos, O., Gonçalves, C.D., Guimaraes, I.M., da Rocha, J.J.R., Feitosa, M.R., Feres, O., Saad-Hossne, R., Penna, F.G.C., Cunha, P.F.S., Gomes, T.N.F., Nones, R.B., Faria, M.A.G., Dias Parente, M.P.P., Scotton, A.S., Caratin, R.F., Senra, J., Chebli, J.M., 2021. Real-world disease activity and sociodemographic, clinical and treatment characteristics of moderate-to-severe inflammatory bowel disease in Brazil. World J. Gastroenterol. 27, 208. https://doi.org/10.3748/WJG.V27.I2.208

Zeng, L., Hu, S., Chen, P., Wei, W., Tan, Y., 2017. Macronutrient Intake and Risk of Crohn's Disease: Systematic Review and Dose–Response Meta-Analysis of Epidemiological Studies. Nutrients 9. https://doi.org/10.3390/NU9050500

Zhang, J., Ye, J., Ren, Y., Zuo, J., Dai, W., He, Y., Tan, M., Song, W., Yuan, Y., 2018. Intracellular activation of complement C3 in Paneth cells improves repair of intestinal epithelia during acute injury. Immunotherapy 10, 1325–1336. https://doi.org/10.2217/IMT-2018-0122

Zhou, H., Zhou, S.Y., Gillilland, M., Li, J.Y., Lee, A., Gao, J., Zhang, G., Xu, X., Owyang, C., 2020. Bile acid toxicity in Paneth cells contributes to gut dysbiosis induced by high-fat feeding. JCI Insight 5. https://doi.org/10.1172/JCI.INSIGHT.138881

Zietek, T., Rath, E., Haller, D., Daniel, H., 2015. Intestinal organoids for assessing nutrient transport, sensing and incretin secretion. Sci. Rep. 5. https://doi.org/10.1038/SREP16831

7. Appendix

7.1 Supplementary material

Table 14. Clinical characteristics of CD patients used for qPCR analysis.

Total number of patients	21			
AZA therapy n (%)	-AZA 9 (50%)		+ AZA 12 (50%)	
Remission n (%)	5 (55.6%)		9 (75%)	
Active n (%)	4 (44.4%)		3 (25%)	
Gender n (%)	3 males (33.3%)	6 females (66.7%)	4 males (33.3%)	8 females (66.7%)
Age Mean ± SD	38.3 ± 9.5		38.3 ± 7.7	
Disease pattern n (%)				
Ileocolitis	6 (66.7%)		8 (66.7%)	
Ileitis	1 (11.1%)		1 (8.3%)	
Colitis	2 (22.2%)		2 (16.7%)	
Proctitis	-		1 (8.3%)	

Table 15. Clinical characteristics of CD patients used for IHC analysis.

Total number of patients	12			
AZA therapy n (%)	-AZA 6 (50%)		+ AZA 6 (50%)	
Remission n (%)	5 (83.3%)		6 (100%)	
Active n (%)	1 (16.7%)		0 (0%)	
Gender n (%)	1 male (16.7%)	5 females (83.3%)	2 males (33.3%)	4 females (66.7%)
Age Mean ± SD	39 ± 14.2		33.3 ± 12	
Disease pattern n (%)				
Ileocolitis	2 (33.3%)		5 (83.3%)	
Ileitis	-		-	
Colitis	2 (33.3%)		1 (16.7%)	
Not defined	2 (33.3%)		-	

Table 16. Clinical characteristics of CD patients used for ELISA.

Total number of patients	7			
AZA therapy n (%)	-AZA 4 (57.1%)		+ AZA 3 (42.9%)	
Remission n (%)	4 (100%)		2 (66.7%)	
Active n (%)	0 (0%)		1 (33.3%)	
Gender n (%)	3 males (0%)	1 female (100%)	0 males (0%)	3 females (100%)
Age Mean ± SD	36.3 ± 12.3		44.7 ± 18.4	
Disease pattern n (%)				
Ileocolitis	2 (50%)		3 (100%)	
Ileitis	2 (50%)		-	
Colitis	-		-	

Table 17. Clinical characteristics of human serum samples for triglycerides.

Total number of samples	**44**			
Diagnosis n (%)	Healthy 17 (37.8%)		CD 27 (62.2%)	
Remission n (%)	-		27(100%)	
Active n (%)	-		0 (0%)	
Gender n (%)	7 males (41.2%)	10 females (58.8%)	11 males (40.7%)	16 females (59.3%)
Age Mean ± SD	29.7 ± 7		42 ± 16.1	
Disease pattern n (%)				
Ileocolitis	-		7 (25.9%)	
Ileitis	-		7 (25.9%)	
Colitis	-		13 (48.1%)	

Table 18. Clinical characteristics of CD patients used for NMR analysis.

Total number of patients	**58**			
AZA therapy n (%)	-AZA 40 (57.1%)		+ AZA 18 (42.9%)	
Gender n (%)	16 males (40%)	24 females (60%)	9 males (50%)	9 females (50%)
Age Mean ± SD	41.6 ± 14.5		41.8 ± 14.4	

Table 19. List of serum metabolites detected in obesity mouse model.

	Chow 30°C		**HFD 30°C**		**Chow 22°C**		**HFD 22°C**	
Metabolite	Average	SEM	Average	SEM	Average	SEM	Average	SEM
Ethanol	1.03	0.27	0.27	0.19	1.62	0.22	0.73	0.13
Trimethylamine-N-oxide	0.11	0.02	0.04	0.03	0.13	0.01	0.07	0.03
2-Aminobutyric acid	0.00	0.00	0.00	0.00	0.00	0.00	0.00	0.00
Alanine	0.54	0.04	0.64	0.05	0.60	0.04	0.62	0.05
Asparagine	0.01	0.01	0.04	0.02	0.00	0.00	0.00	0.00
Creatine	0.09	0.01	0.04	0.01	0.09	0.01	0.07	0.01
Creatinine	0.06	0.00	0.07	0.01	0.05	0.01	0.06	0.00
Glutamic acid	0.19	0.01	0.21	0.01	0.24	0.02	0.23	0.01
Glutamine	0.49	0.02	0.55	0.03	0.58	0.04	0.56	0.03
Glycine	0.44	0.02	0.47	0.03	0.44	0.02	0.44	0.03
Histidine	0.06	0.02	0.08	0.03	0.06	0.03	0.07	0.02
Isoleucine	0.12	0.02	0.09	0.01	0.11	0.01	0.10	0.01
Leucine	0.21	0.01	0.19	0.02	0.21	0.01	0.21	0.02
Lysine	0.23	0.08	0.29	0.06	0.13	0.06	0.15	0.07
Methionine	0.02	0.01	0.03	0.01	0.03	0.01	0.02	0.01
N,N-Dimethylglycine	0.00	0.00	0.00	0.00	0.00	0.00	0.00	0.00
Ornithine	0.05	0.01	0.09	0.02	0.03	0.01	0.07	0.02
Phenylalanine	0.14	0.01	0.13	0.02	0.17	0.01	0.15	0.01
Proline	0.21	0.07	0.16	0.10	0.10	0.06	0.14	0.09
Sarcosine	0.00	0.00	0.00	0.00	0.00	0.00	0.01	0.00
Threonine	0.00	0.00	0.00	0.00	0.00	0.00	0.00	0.00

Tyrosine	0.08	0.01	0.09	0.01	0.09	0.01	0.09	0.01
Valine	0.31	0.02	0.29	0.01	0.32	0.02	0.31	0.02
Acetic acid	0.36	0.05	0.13	0.02	0.27	0.02	0.10	0.01
Citric acid	0.07	0.05	0.17	0.07	0.09	0.04	0.17	0.05
Formic acid	0.04	0.01	0.03	0.00	0.03	0.01	0.03	0.01
Lactic acid	6.83	0.70	5.12	0.52	6.90	0.39	5.12	0.35
Succinic acid	0.06	0.02	0.05	0.01	0.05	0.01	0.05	0.01
Choline	0.26	0.07	0.39	0.11	0.15	0.02	0.34	0.10
2-Oxoglutaric acid	0.02	0.01	0.01	0.01	0.01	0.01	0.01	0.01
3-Hydroxybutyric acid	0.38	0.08	0.46	0.10	0.21	0.04	0.20	0.05
Acetoacetic acid	0.00	0.00	0.00	0.00	0.00	0.00	0.00	0.00
Acetone	0.03	0.01	0.04	0.01	0.01	0.00	0.01	0.00
Pyruvic acid	0.19	0.01	0.14	0.01	0.15	0.00	0.14	0.01
D-Galactose	0.00	0.00	0.00	0.00	0.00	0.00	0.00	0.00
Glucose	14.17	1.08	16.67	0.84	14.33	0.67	17.83	0.60
Glycerol	0.60	0.16	0.57	0.20	0.50	0.04	0.51	0.15
Dimethylsulfone	0.01	0.00	0.00	0.00	0.01	0.00	0.00	0.00
Ca-EDTA	0.00	0.00	0.00	0.00	0.00	0.00	0.00	0.00
K-EDTA	0.00	0.00	0.00	0.00	0.00	0.00	0.00	0.00
TG	111.45	13.11	142.33	8.68	91.48	4.16	95.65	9.23
Chol	109.56	2.62	283.81	8.12	96.80	4.27	194.61	5.56
LDL	52.84	6.58	146.22	11.98	44.28	3.52	110.35	3.61
HDL	58.46	3.93	100.04	7.58	62.60	3.53	102.26	2.46
ApoA1	79.57	7.78	149.97	7.44	74.99	4.55	145.21	5.25
ApoA2	14.81	2.85	14.65	2.81	19.42	2.26	25.90	3.44
ApoB100	43.13	2.34	125.91	8.00	37.32	3.62	79.92	5.35
LDL/HDL	0.91	0.11	1.49	0.13	0.74	0.10	1.09	0.05
ApoB100/ApoA1	0.58	0.07	0.86	0.10	0.51	0.08	0.55	0.03
ApoB Particles	784.23	42.52	2289.36	145.44	678.53	65.76	1453.27	97.34
VLDL Particles	99.67	21.07	36.33	12.93	75.62	7.05	18.27	7.77
IDL Particles	3.00	2.54	65.26	17.34	0.00	0.00	3.84	3.84
LDL Particles	600.73	69.13	1851.19	79.31	516.33	53.59	1234.85	48.61
LDL-1 Particles	91.85	33.26	736.88	40.86	74.21	19.03	309.24	43.41
LDL-2 Particles	336.50	42.31	581.08	105.55	339.47	25.25	551.93	45.68
LDL-3 Particles	13.61	10.65	86.42	46.89	0.00	0.00	59.90	24.92
LDL-4 Particles	0.00	0.00	0.00	0.00	0.00	0.00	0.00	0.00
LDL-5 Particles	108.80	33.80	187.66	70.95	101.97	15.02	132.77	45.95
LDL-6 Particles	355.18	47.20	517.68	165.24	393.79	33.86	420.96	56.58
VLDL TG	70.77	11.07	74.07	6.51	60.32	6.07	53.15	7.81
IDL TG	7.79	1.88	15.29	1.68	5.66	0.75	9.26	1.48
LDL TG	0.78	0.44	21.06	1.95	0.47	0.47	7.50	1.23
HDL TG	5.58	1.83	19.66	2.37	3.12	1.15	12.17	3.54
VLDL	16.79	4.07	14.99	4.12	11.93	1.17	2.41	1.10
IDL	0.19	0.19	7.92	2.97	0.00	0.00	0.17	0.17
LDL	52.84	6.58	146.22	11.98	44.28	3.52	110.35	3.61
HDL	58.46	3.93	100.04	7.58	62.60	3.53	102.26	2.46

VLDL FC	9.32	1.43	10.44	1.45	7.57	0.49	4.67	0.88
IDL FC	0.00	0.00	1.42	0.64	0.00	0.00	0.00	0.00
LDL FC	13.17	2.28	44.45	3.95	7.33	1.23	26.98	1.42
HDL FC	14.90	1.26	26.05	1.79	12.49	0.54	23.81	0.75
VLDL PL	21.96	3.39	29.99	3.08	19.71	1.48	13.99	1.95
IDL PL	2.18	0.69	9.39	0.32	0.97	0.33	3.68	0.45
LDL PL	26.62	3.04	76.42	5.54	21.67	1.90	54.07	1.40
HDL PL	72.18	4.54	126.81	9.08	76.72	4.28	125.89	4.32
HDL ApoA1	107.73	7.71	184.68	11.99	106.87	5.29	182.64	4.72
HDL ApoA2	16.56	2.75	17.65	2.81	21.46	2.31	27.97	3.52
VLDL ApoB	5.48	1.16	2.00	0.71	4.16	0.39	1.01	0.43
IDL ApoB	0.16	0.14	3.59	0.95	0.00	0.00	0.21	0.21
LDL ApoB	33.04	3.80	101.81	4.36	28.40	2.95	67.91	2.67
VLDL-1 TG	61.06	7.77	66.72	6.22	62.73	4.55	58.99	6.35
VLDL-2 TG	7.31	2.06	10.32	0.28	3.18	1.18	2.27	0.62
VLDL-3 TG	2.01	1.38	0.00	0.00	0.02	0.02	0.00	0.00
VLDL-4 TG	1.41	0.96	0.00	0.00	0.55	0.32	0.00	0.00
VLDL-5 TG	4.73	0.29	5.09	0.30	5.18	0.32	5.52	0.19
VLDL-1 Chol	14.21	1.93	19.78	1.18	12.93	0.54	11.63	0.76
VLDL-2 Chol	2.66	0.77	5.28	0.84	1.19	0.42	0.52	0.18
VLDL-3 Chol	0.86	0.55	0.30	0.30	0.00	0.00	0.00	0.00
VLDL-4 Chol	0.95	0.52	3.91	2.16	0.20	0.15	0.00	0.00
VLDL-5 Chol	2.43	0.26	3.10	0.37	2.68	0.13	2.86	0.23
VLDL-1 FC	3.53	0.72	5.64	0.41	3.32	0.24	3.07	0.27
VLDL-2 FC	0.84	0.33	0.02	0.02	0.20	0.09	0.00	0.00
VLDL-3 FC	0.81	0.35	0.03	0.03	0.23	0.10	0.00	0.00
VLDL-4 FC	0.44	0.25	0.29	0.25	0.09	0.09	0.00	0.00
VLDL-5 FC	2.81	0.17	4.21	0.23	2.95	0.08	2.86	0.14
VLDL-1 PL	9.24	1.45	11.92	0.95	9.26	0.55	7.92	0.67
VLDL-2 PL	2.02	0.62	2.68	0.37	1.11	0.41	0.32	0.12
VLDL-3 PL	1.08	0.64	0.00	0.00	0.25	0.17	0.00	0.00
VLDL-4 PL	1.24	0.48	0.38	0.38	0.60	0.28	0.00	0.00
VLDL-5 PL	3.21	0.29	4.01	0.31	3.38	0.13	3.58	0.23
LDL-1 TG	0.00	0.00	5.89	1.03	0.00	0.00	0.42	0.42
LDL-2 TG	0.18	0.18	4.20	0.74	0.00	0.00	1.56	0.46
LDL-3 TG	2.01	0.19	5.56	0.34	2.05	0.09	3.43	0.26
LDL-4 TG	0.00	0.00	0.00	0.00	0.00	0.00	0.00	0.00
LDL-5 TG	0.47	0.21	3.51	1.08	0.15	0.15	0.71	0.40
LDL-6 TG	4.15	0.47	3.52	1.23	4.07	0.37	3.22	0.36
LDL-1 Chol	10.26	3.66	80.76	4.35	8.05	2.22	33.71	4.61
LDL-2 Chol	36.67	4.41	61.53	11.54	37.25	2.90	58.97	5.27
LDL-3 Chol	0.87	0.84	5.38	3.50	0.00	0.00	4.50	2.15
LDL-4 Chol	0.00	0.00	0.00	0.00	0.00	0.00	0.00	0.00
LDL-5 Chol	8.28	2.89	11.27	4.34	7.73	1.12	10.32	3.46
LDL-6 Chol	21.30	3.15	35.80	10.86	24.67	2.33	26.87	3.73
LDL-1 FC	1.78	0.82	22.49	1.55	1.05	0.54	8.51	1.39

LDL-2 FC	10.91	1.28	19.66	3.44	11.12	0.73	18.83	1.47
LDL-3 FC	1.00	0.42	4.67	1.61	0.00	0.00	4.25	0.83
LDL-4 FC	0.11	0.11	0.00	0.00	0.00	0.00	0.02	0.02
LDL-5 FC	2.31	0.99	3.91	1.13	1.92	0.22	3.39	0.91
LDL-6 FC	4.09	0.85	8.77	2.45	5.04	0.50	6.95	0.74
LDL-1 PL	5.46	1.95	41.62	2.17	4.48	1.10	17.39	2.37
LDL-2 PL	17.77	2.14	30.45	5.78	17.94	1.33	28.96	2.61
LDL-3 PL	0.66	0.50	3.49	2.01	0.00	0.00	2.77	1.29
LDL-4 PL	0.00	0.00	0.00	0.00	0.00	0.00	0.00	0.00
LDL-5 PL	4.80	1.53	6.36	2.16	4.44	0.59	5.77	1.74
LDL-6 PL	13.20	1.73	20.56	4.89	14.95	1.12	16.59	1.61
LDL-1 ApoB	5.05	1.83	40.53	2.25	4.08	1.05	17.01	2.39
LDL-2 ApoB	18.51	2.33	31.96	5.81	18.67	1.39	30.35	2.51
LDL-3 ApoB	0.75	0.59	4.75	2.58	0.00	0.00	3.30	1.37
LDL-4 ApoB	0.00	0.00	0.00	0.00	0.00	0.00	0.00	0.00
LDL-5 ApoB	5.98	1.86	10.32	3.90	5.61	0.83	7.30	2.53
LDL-6 ApoB	19.53	2.60	28.47	9.09	21.66	1.86	23.15	3.11
HDL-1 TG	3.09	1.02	11.88	1.21	1.34	0.60	7.23	2.15
HDL-2 TG	2.24	0.47	5.10	0.33	2.31	0.22	4.58	0.71
HDL-3 TG	1.88	0.30	4.90	0.28	2.16	0.19	4.01	0.55
HDL-4 TG	0.38	0.19	1.87	0.77	0.11	0.11	0.14	0.09
HDL-1 Chol	25.12	2.45	64.10	3.21	23.43	1.43	50.12	4.05
HDL-2 Chol	15.30	1.03	25.31	2.74	17.40	1.00	28.14	1.01
HDL-3 Chol	7.49	1.79	10.36	2.55	9.77	0.99	15.84	2.00
HDL-4 Chol	0.97	0.97	0.00	0.00	0.42	0.42	0.16	0.16
HDL-1 FC	5.96	0.52	11.87	0.93	4.66	0.29	10.48	0.61
HDL-2 FC	2.13	0.43	2.86	0.56	2.29	0.23	4.05	0.35
HDL-3 FC	0.33	0.21	0.56	0.26	0.18	0.09	1.46	0.35
HDL-4 FC	0.00	0.00	0.00	0.00	0.00	0.00	0.00	0.00
HDL-1 PL	33.74	3.09	76.07	3.69	31.45	1.82	61.86	4.73
HDL-2 PL	22.01	1.37	36.00	3.53	25.60	1.48	40.05	1.50
HDL-3 PL	12.09	2.38	19.33	3.70	16.15	1.54	25.06	3.10
HDL-4 PL	2.82	2.01	0.00	0.00	2.15	0.73	1.29	1.29
HDL-1 ApoA1	61.36	5.39	126.33	6.69	55.25	2.41	103.23	7.91
HDL-2 ApoA1	15.67	1.21	24.42	1.90	17.41	1.16	28.67	1.07
HDL-3 ApoA1	18.66	3.11	25.91	5.14	22.76	2.14	36.83	3.46
HDL-4 ApoA1	3.72	2.10	0.00	0.00	0.55	0.55	0.00	0.00
HDL-1 ApoA2	4.22	0.42	7.37	0.50	4.09	0.30	7.49	0.63
HDL-2 ApoA2	3.81	0.36	5.81	0.71	4.71	0.35	7.33	0.36
HDL-3 ApoA2	4.30	1.06	6.06	1.53	6.25	0.64	9.41	1.34
HDL-4 ApoA2	0.52	0.52	0.00	0.00	0.19	0.19	0.00	0.00
Concentrations are in mg/dL								

Table 20. Tukey's multiple comparisons test of NMR metabolites in obesity mouse model.

Metabolite	Mean Diff	Summary	Adjusted P Value
Ethanol			
Chow 30°C vs. HFD 30°C	0.7533	ns	>0.9999
Chow 30°C vs. Chow 22°C	-0.5917	ns	>0.9999
HFD 30°C vs. HFD 22°C	-0.4617	ns	>0.9999
Chow 22°C vs. HFD 22°C	0.8833	ns	>0.9999
Trimethylamine-N-oxide			
Chow 30°C vs. HFD 30°C	0.06500	ns	>0.9999
Chow 30°C vs. Chow 22°C	-0.01667	ns	>0.9999
HFD 30°C vs. HFD 22°C	-0.02667	ns	>0.9999
Chow 22°C vs. HFD 22°C	0.05500	ns	>0.9999
2-Aminobutyric acid			
Chow 30°C vs. HFD 30°C	0.000	ns	>0.9999
Chow 30°C vs. Chow 22°C	0.000	ns	>0.9999
HFD 30°C vs. HFD 22°C	0.000	ns	>0.9999
Chow 22°C vs. HFD 22°C	0.000	ns	>0.9999
Alanine			
Chow 30°C vs. HFD 30°C	-0.09833	ns	>0.9999
Chow 30°C vs. Chow 22°C	-0.05500	ns	>0.9999
HFD 30°C vs. HFD 22°C	0.02333	ns	>0.9999
Chow 22°C vs. HFD 22°C	-0.02000	ns	>0.9999
Asparagine			
Chow 30°C vs. HFD 30°C	-0.02833	ns	>0.9999
Chow 30°C vs. Chow 22°C	0.01000	ns	>0.9999
HFD 30°C vs. HFD 22°C	0.03833	ns	>0.9999
Chow 22°C vs. HFD 22°C	0.000	ns	>0.9999
Creatine			
Chow 30°C vs. HFD 30°C	0.04833	ns	>0.9999
Chow 30°C vs. Chow 22°C	0.001667	ns	>0.9999
HFD 30°C vs. HFD 22°C	-0.03167	ns	>0.9999
Chow 22°C vs. HFD 22°C	0.01500	ns	>0.9999
Creatinine			
Chow 30°C vs. HFD 30°C	-0.01000	ns	>0.9999
Chow 30°C vs. Chow 22°C	0.006667	ns	>0.9999
HFD 30°C vs. HFD 22°C	0.008333	ns	>0.9999
Chow 22°C vs. HFD 22°C	-0.008333	ns	>0.9999
Glutamic acid			
Chow 30°C vs. HFD 30°C	-0.01833	ns	>0.9999
Chow 30°C vs. Chow 22°C	-0.05000	ns	>0.9999
HFD 30°C vs. HFD 22°C	-0.01833	ns	>0.9999
Chow 22°C vs. HFD 22°C	0.01333	ns	>0.9999
Glutamine			
Chow 30°C vs. HFD 30°C	-0.05167	ns	>0.9999
Chow 30°C vs. Chow 22°C	-0.08667	ns	>0.9999
HFD 30°C vs. HFD 22°C	-0.01000	ns	>0.9999
Chow 22°C vs. HFD 22°C	0.02500	ns	>0.9999
Glycine			
Chow 30°C vs. HFD 30°C	-0.02167	ns	>0.9999
Chow 30°C vs. Chow 22°C	0.003333	ns	>0.9999

HFD 30°C vs. HFD 22°C	0.02667	ns	>0.9999
Chow 22°C vs. HFD 22°C	0.001667	ns	>0.9999
Histidine			
Chow 30°C vs. HFD 30°C	-0.02000	ns	>0.9999
Chow 30°C vs. Chow 22°C	-0.003333	ns	>0.9999
HFD 30°C vs. HFD 22°C	0.008333	ns	>0.9999
Chow 22°C vs. HFD 22°C	-0.008333	ns	>0.9999
Isoleucine			
Chow 30°C vs. HFD 30°C	0.03000	ns	>0.9999
Chow 30°C vs. Chow 22°C	0.01333	ns	>0.9999
HFD 30°C vs. HFD 22°C	-0.01333	ns	>0.9999
Chow 22°C vs. HFD 22°C	0.003333	ns	>0.9999
Leucine			
Chow 30°C vs. HFD 30°C	0.01833	ns	>0.9999
Chow 30°C vs. Chow 22°C	-0.003333	ns	>0.9999
HFD 30°C vs. HFD 22°C	-0.02333	ns	>0.9999
Chow 22°C vs. HFD 22°C	-0.001667	ns	>0.9999
Lysine			
Chow 30°C vs. HFD 30°C	-0.05333	ns	>0.9999
Chow 30°C vs. Chow 22°C	0.1000	ns	>0.9999
HFD 30°C vs. HFD 22°C	0.1417	ns	>0.9999
Chow 22°C vs. HFD 22°C	-0.01167	ns	>0.9999
Methionine			
Chow 30°C vs. HFD 30°C	-0.01000	ns	>0.9999
Chow 30°C vs. Chow 22°C	-0.006667	ns	>0.9999
HFD 30°C vs. HFD 22°C	0.008333	ns	>0.9999
Chow 22°C vs. HFD 22°C	0.005000	ns	>0.9999
N.N-Dimethylglycine			
Chow 30°C vs. HFD 30°C	0.000	ns	>0.9999
Chow 30°C vs. Chow 22°C	0.000	ns	>0.9999
HFD 30°C vs. HFD 22°C	0.000	ns	>0.9999
Chow 22°C vs. HFD 22°C	0.000	ns	>0.9999
Ornithine			
Chow 30°C vs. HFD 30°C	-0.03667	ns	>0.9999
Chow 30°C vs. Chow 22°C	0.02167	ns	>0.9999
HFD 30°C vs. HFD 22°C	0.01500	ns	>0.9999
Chow 22°C vs. HFD 22°C	-0.04333	ns	>0.9999
Phenylalanine			
Chow 30°C vs. HFD 30°C	0.01167	ns	>0.9999
Chow 30°C vs. Chow 22°C	-0.02667	ns	>0.9999
HFD 30°C vs. HFD 22°C	-0.01667	ns	>0.9999
Chow 22°C vs. HFD 22°C	0.02167	ns	>0.9999
Proline			
Chow 30°C vs. HFD 30°C	0.05000	ns	>0.9999
Chow 30°C vs. Chow 22°C	0.1150	ns	>0.9999
HFD 30°C vs. HFD 22°C	0.02500	ns	>0.9999
Chow 22°C vs. HFD 22°C	-0.04000	ns	>0.9999
Sarcosine			
Chow 30°C vs. HFD 30°C	0.000	ns	>0.9999
Chow 30°C vs. Chow 22°C	-0.003333	ns	>0.9999
HFD 30°C vs. HFD 22°C	-0.006667	ns	>0.9999
Chow 22°C vs. HFD 22°C	-0.003333	ns	>0.9999
Threonine			
Chow 30°C vs. HFD 30°C	0.000	ns	>0.9999

Chow 30°C vs. Chow 22°C	0.000	ns	>0.9999
HFD 30°C vs. HFD 22°C	0.000	ns	>0.9999
Chow 22°C vs. HFD 22°C	0.000	ns	>0.9999
Tyrosine			
Chow 30°C vs. HFD 30°C	-0.008333	ns	>0.9999
Chow 30°C vs. Chow 22°C	-0.005000	ns	>0.9999
HFD 30°C vs. HFD 22°C	-0.005000	ns	>0.9999
Chow 22°C vs. HFD 22°C	-0.008333	ns	>0.9999
Valine			
Chow 30°C vs. HFD 30°C	0.02333	ns	>0.9999
Chow 30°C vs. Chow 22°C	-0.006667	ns	>0.9999
HFD 30°C vs. HFD 22°C	-0.02667	ns	>0.9999
Chow 22°C vs. HFD 22°C	0.003333	ns	>0.9999
2-Hydroxybutyric acid			
Chow 30°C vs. HFD 30°C	-0.06000	ns	>0.9999
Chow 30°C vs. Chow 22°C	0.02667	ns	>0.9999
HFD 30°C vs. HFD 22°C	0.02500	ns	>0.9999
Chow 22°C vs. HFD 22°C	-0.06167	ns	>0.9999
Acetic acid			
Chow 30°C vs. HFD 30°C	0.2283	ns	>0.9999
Chow 30°C vs. Chow 22°C	0.08667	ns	>0.9999
HFD 30°C vs. HFD 22°C	0.02833	ns	>0.9999
Chow 22°C vs. HFD 22°C	0.1700	ns	>0.9999
Citric acid			
Chow 30°C vs. HFD 30°C	-0.1017	ns	>0.9999
Chow 30°C vs. Chow 22°C	-0.01833	ns	>0.9999
HFD 30°C vs. HFD 22°C	0.003333	ns	>0.9999
Chow 22°C vs. HFD 22°C	-0.08000	ns	>0.9999
Formic acid			
Chow 30°C vs. HFD 30°C	0.008333	ns	>0.9999
Chow 30°C vs. Chow 22°C	0.01500	ns	>0.9999
HFD 30°C vs. HFD 22°C	0.003333	ns	>0.9999
Chow 22°C vs. HFD 22°C	-0.003333	ns	>0.9999
Lactic acid			
Chow 30°C vs. HFD 30°C	1.717	ns	0.9998
Chow 30°C vs. Chow 22°C	-0.06667	ns	>0.9999
HFD 30°C vs. HFD 22°C	0.000	ns	>0.9999
Chow 22°C vs. HFD 22°C	1.783	ns	0.9997
Succinic acid			
Chow 30°C vs. HFD 30°C	0.01167	ns	>0.9999
Chow 30°C vs. Chow 22°C	0.01000	ns	>0.9999
HFD 30°C vs. HFD 22°C	-0.006667	ns	>0.9999
Chow 22°C vs. HFD 22°C	-0.005000	ns	>0.9999
Choline			
Chow 30°C vs. HFD 30°C	-0.1350	ns	>0.9999
Chow 30°C vs. Chow 22°C	0.1017	ns	>0.9999
HFD 30°C vs. HFD 22°C	0.04667	ns	>0.9999
Chow 22°C vs. HFD 22°C	-0.1900	ns	>0.9999
2-Oxoglutaric acid			
Chow 30°C vs. HFD 30°C	0.01167	ns	>0.9999
Chow 30°C vs. Chow 22°C	0.01000	ns	>0.9999
HFD 30°C vs. HFD 22°C	-0.001667	ns	>0.9999
Chow 22°C vs. HFD 22°C	0.000	ns	>0.9999
3-Hydroxybutyric acid			

Chow 30°C vs. HFD 30°C	-0.07833	ns	>0.9999
Chow 30°C vs. Chow 22°C	0.1717	ns	>0.9999
HFD 30°C vs. HFD 22°C	0.2517	ns	>0.9999
Chow 22°C vs. HFD 22°C	0.001667	ns	>0.9999
Acetoacetic acid			
Chow 30°C vs. HFD 30°C	0.000	ns	>0.9999
Chow 30°C vs. Chow 22°C	0.000	ns	>0.9999
HFD 30°C vs. HFD 22°C	0.000	ns	>0.9999
Chow 22°C vs. HFD 22°C	0.000	ns	>0.9999
Acetone			
Chow 30°C vs. HFD 30°C	-0.01333	ns	>0.9999
Chow 30°C vs. Chow 22°C	0.01667	ns	>0.9999
HFD 30°C vs. HFD 22°C	0.03167	ns	>0.9999
Chow 22°C vs. HFD 22°C	0.001667	ns	>0.9999
Pyruvic acid			
Chow 30°C vs. HFD 30°C	0.04500	ns	>0.9999
Chow 30°C vs. Chow 22°C	0.03167	ns	>0.9999
HFD 30°C vs. HFD 22°C	-0.001667	ns	>0.9999
Chow 22°C vs. HFD 22°C	0.01167	ns	>0.9999
D-Galactose			
Chow 30°C vs. HFD 30°C	0.000	ns	>0.9999
Chow 30°C vs. Chow 22°C	0.000	ns	>0.9999
HFD 30°C vs. HFD 22°C	0.000	ns	>0.9999
Chow 22°C vs. HFD 22°C	0.000	ns	>0.9999
Glucose			
Chow 30°C vs. HFD 30°C	-2.500	ns	0.9993
Chow 30°C vs. Chow 22°C	-0.1667	ns	>0.9999
HFD 30°C vs. HFD 22°C	-1.167	ns	>0.9999
Chow 22°C vs. HFD 22°C	-3.500	ns	0.9981
Glycerol			
Chow 30°C vs. HFD 30°C	0.03000	ns	>0.9999
Chow 30°C vs. Chow 22°C	0.1050	ns	>0.9999
HFD 30°C vs. HFD 22°C	0.06333	ns	>0.9999
Chow 22°C vs. HFD 22°C	-0.01167	ns	>0.9999
Dimethylsulfone			
Chow 30°C vs. HFD 30°C	0.008333	ns	>0.9999
Chow 30°C vs. Chow 22°C	0.005000	ns	>0.9999
HFD 30°C vs. HFD 22°C	0.003333	ns	>0.9999
Chow 22°C vs. HFD 22°C	0.006667	ns	>0.9999
Ca-EDTA			
Chow 30°C vs. HFD 30°C	0.000	ns	>0.9999
Chow 30°C vs. Chow 22°C	0.000	ns	>0.9999
HFD 30°C vs. HFD 22°C	0.000	ns	>0.9999
Chow 22°C vs. HFD 22°C	0.000	ns	>0.9999
K-EDTA			
Chow 30°C vs. HFD 30°C	0.000	ns	>0.9999
Chow 30°C vs. Chow 22°C	0.000	ns	>0.9999
HFD 30°C vs. HFD 22°C	0.000	ns	>0.9999
Chow 22°C vs. HFD 22°C	0.000	ns	>0.9999
TG			
Chow 30°C vs. HFD 30°C	-30.88	ns	0.4107
Chow 30°C vs. Chow 22°C	19.97	ns	0.7498
HFD 30°C vs. HFD 22°C	46.68	ns	0.0903
Chow 22°C vs. HFD 22°C	-4.167	ns	0.9968

Chol			
Chow 30°C vs. HFD 30°C	-174.3	****	<0.0001
Chow 30°C vs. Chow 22°C	12.76	ns	0.9196
HFD 30°C vs. HFD 22°C	89.20	****	<0.0001
Chow 22°C vs. HFD 22°C	-97.81	****	<0.0001
LDL			
Chow 30°C vs. HFD 30°C	-93.38	****	<0.0001
Chow 30°C vs. Chow 22°C	8.557	ns	0.9737
HFD 30°C vs. HFD 22°C	35.87	ns	0.2760
Chow 22°C vs. HFD 22°C	-66.07	**	0.0053
HDL			
Chow 30°C vs. HFD 30°C	-41.58	ns	0.1597
Chow 30°C vs. Chow 22°C	-4.137	ns	0.9969
HFD 30°C vs. HFD 22°C	-2.218	ns	0.9995
Chow 22°C vs. HFD 22°C	-39.66	ns	0.1940
ApoA1			
Chow 30°C vs. HFD 30°C	-70.40	**	0.0024
Chow 30°C vs. Chow 22°C	4.578	ns	0.9958
HFD 30°C vs. HFD 22°C	4.762	ns	0.9952
Chow 22°C vs. HFD 22°C	-70.22	**	0.0025
ApoA2			
Chow 30°C vs. HFD 30°C	0.1583	ns	>0.9999
Chow 30°C vs. Chow 22°C	-4.607	ns	0.9957
HFD 30°C vs. HFD 22°C	-11.25	ns	0.9431
Chow 22°C vs. HFD 22°C	-6.480	ns	0.9882
ApoB100			
Chow 30°C vs. HFD 30°C	-82.78	***	0.0002
Chow 30°C vs. Chow 22°C	5.813	ns	0.9914
HFD 30°C vs. HFD 22°C	45.99	ns	0.0980
Chow 22°C vs. HFD 22°C	-42.61	ns	0.1433
LDL/HDL			
Chow 30°C vs. HFD 30°C	-0.5817	ns	>0.9999
Chow 30°C vs. Chow 22°C	0.1733	ns	>0.9999
HFD 30°C vs. HFD 22°C	0.4050	ns	>0.9999
Chow 22°C vs. HFD 22°C	-0.3500	ns	>0.9999
ApoB100/ApoA1			
Chow 30°C vs. HFD 30°C	-0.2883	ns	>0.9999
Chow 30°C vs. Chow 22°C	0.06167	ns	>0.9999
HFD 30°C vs. HFD 22°C	0.3117	ns	>0.9999
Chow 22°C vs. HFD 22°C	-0.03833	ns	>0.9999
ApoB Particles			
Chow 30°C vs. HFD 30°C	-1505	****	<0.0001
Chow 30°C vs. Chow 22°C	105.7	****	<0.0001
HFD 30°C vs. HFD 22°C	836.1	****	<0.0001
Chow 22°C vs. HFD 22°C	-774.7	****	<0.0001
VLDL Particles			
Chow 30°C vs. HFD 30°C	63.34	**	0.0084
Chow 30°C vs. Chow 22°C	24.06	ns	0.6246
HFD 30°C vs. HFD 22°C	18.07	ns	0.8028
Chow 22°C vs. HFD 22°C	57.35	*	0.0215
IDL Particles			
Chow 30°C vs. HFD 30°C	-62.26	*	0.0100
Chow 30°C vs. Chow 22°C	2.998	ns	0.9988
HFD 30°C vs. HFD 22°C	61.41	*	0.0115

Chow 22°C vs. HFD 22°C	-3.843	ns	0.9975
LDL Particles			
Chow 30°C vs. HFD 30°C	-1250	****	<0.0001
Chow 30°C vs. Chow 22°C	84.41	***	0.0001
HFD 30°C vs. HFD 22°C	616.3	****	<0.0001
Chow 22°C vs. HFD 22°C	-718.5	****	<0.0001
LDL-1 Particles			
Chow 30°C vs. HFD 30°C	-645.0	****	<0.0001
Chow 30°C vs. Chow 22°C	17.63	ns	0.8141
HFD 30°C vs. HFD 22°C	427.6	****	<0.0001
Chow 22°C vs. HFD 22°C	-235.0	****	<0.0001
LDL-2 Particles			
Chow 30°C vs. HFD 30°C	-244.6	****	<0.0001
Chow 30°C vs. Chow 22°C	-2.968	ns	0.9988
HFD 30°C vs. HFD 22°C	29.16	ns	0.4627
Chow 22°C vs. HFD 22°C	-212.5	****	<0.0001
LDL-3 Particles			
Chow 30°C vs. HFD 30°C	-72.80	**	0.0016
Chow 30°C vs. Chow 22°C	13.61	ns	0.9043
HFD 30°C vs. HFD 22°C	26.52	ns	0.5458
Chow 22°C vs. HFD 22°C	-59.90	*	0.0146
LDL-4 Particles			
Chow 30°C vs. HFD 30°C	0.000	ns	>0.9999
Chow 30°C vs. Chow 22°C	0.000	ns	>0.9999
HFD 30°C vs. HFD 22°C	0.000	ns	>0.9999
Chow 22°C vs. HFD 22°C	0.000	ns	>0.9999
LDL-5 Particles			
Chow 30°C vs. HFD 30°C	-78.86	***	0.0005
Chow 30°C vs. Chow 22°C	6.833	ns	0.9863
HFD 30°C vs. HFD 22°C	54.89	*	0.0308
Chow 22°C vs. HFD 22°C	-30.81	ns	0.4128
LDL-6 Particles			
Chow 30°C vs. HFD 30°C	-162.5	****	<0.0001
Chow 30°C vs. Chow 22°C	-38.61	ns	0.2149
HFD 30°C vs. HFD 22°C	96.73	****	<0.0001
Chow 22°C vs. HFD 22°C	-27.17	ns	0.5252
VLDL TG			
Chow 30°C vs. HFD 30°C	-3.302	ns	0.9984
Chow 30°C vs. Chow 22°C	10.45	ns	0.9537
HFD 30°C vs. HFD 22°C	20.92	ns	0.7219
Chow 22°C vs. HFD 22°C	7.173	ns	0.9842
IDL TG			
Chow 30°C vs. HFD 30°C	-7.500	ns	0.9820
Chow 30°C vs. Chow 22°C	2.128	ns	0.9996
HFD 30°C vs. HFD 22°C	6.027	ns	0.9905
Chow 22°C vs. HFD 22°C	-3.602	ns	0.9979
LDL TG			
Chow 30°C vs. HFD 30°C	-20.28	ns	0.7409
Chow 30°C vs. Chow 22°C	0.3083	ns	>0.9999
HFD 30°C vs. HFD 22°C	13.55	ns	0.9054
Chow 22°C vs. HFD 22°C	-7.032	ns	0.9851
HDL TG			
Chow 30°C vs. HFD 30°C	-14.08	ns	0.8953
Chow 30°C vs. Chow 22°C	2.457	ns	0.9993

HFD 30°C vs. HFD 22°C	7.490	ns	0.9821
Chow 22°C vs. HFD 22°C	-9.050	ns	0.9691
VLDL			
Chow 30°C vs. HFD 30°C	1.802	ns	0.9997
Chow 30°C vs. Chow 22°C	4.863	ns	0.9949
HFD 30°C vs. HFD 22°C	12.58	ns	0.9225
Chow 22°C vs. HFD 22°C	9.522	ns	0.9643
IDL			
Chow 30°C vs. HFD 30°C	-7.732	ns	0.9803
Chow 30°C vs. Chow 22°C	0.1900	ns	>0.9999
HFD 30°C vs. HFD 22°C	7.757	ns	0.9801
Chow 22°C vs. HFD 22°C	-0.1650	ns	>0.9999
LDL			
Chow 30°C vs. HFD 30°C	-93.38	****	<0.0001
Chow 30°C vs. Chow 22°C	8.557	ns	0.9737
HFD 30°C vs. HFD 22°C	35.87	ns	0.2760
Chow 22°C vs. HFD 22°C	-66.07	**	0.0053
HDL			
Chow 30°C vs. HFD 30°C	-41.58	ns	0.1597
Chow 30°C vs. Chow 22°C	-4.137	ns	0.9969
HFD 30°C vs. HFD 22°C	-2.218	ns	0.9995
Chow 22°C vs. HFD 22°C	-39.66	ns	0.1940
VLDL FC			
Chow 30°C vs. HFD 30°C	-1.117	ns	>0.9999
Chow 30°C vs. Chow 22°C	1.755	ns	0.9998
HFD 30°C vs. HFD 22°C	5.765	ns	0.9916
Chow 22°C vs. HFD 22°C	2.893	ns	0.9989
IDL FC			
Chow 30°C vs. HFD 30°C	-1.417	ns	0.9999
Chow 30°C vs. Chow 22°C	0.000	ns	>0.9999
HFD 30°C vs. HFD 22°C	1.417	ns	0.9999
Chow 22°C vs. HFD 22°C	0.000	ns	>0.9999
LDL FC			
Chow 30°C vs. HFD 30°C	-31.28	ns	0.3988
Chow 30°C vs. Chow 22°C	5.845	ns	0.9913
HFD 30°C vs. HFD 22°C	17.48	ns	0.8181
Chow 22°C vs. HFD 22°C	-19.65	ns	0.7591
HDL FC			
Chow 30°C vs. HFD 30°C	-11.15	ns	0.9445
Chow 30°C vs. Chow 22°C	2.418	ns	0.9994
HFD 30°C vs. HFD 22°C	2.240	ns	0.9995
Chow 22°C vs. HFD 22°C	-11.33	ns	0.9420
VLDL PL			
Chow 30°C vs. HFD 30°C	-8.033	ns	0.9780
Chow 30°C vs. Chow 22°C	2.248	ns	0.9995
HFD 30°C vs. HFD 22°C	16.01	ns	0.8540
Chow 22°C vs. HFD 22°C	5.725	ns	0.9918
IDL PL			
Chow 30°C vs. HFD 30°C	-7.212	ns	0.9839
Chow 30°C vs. Chow 22°C	1.210	ns	>0.9999
HFD 30°C vs. HFD 22°C	5.708	ns	0.9919
Chow 22°C vs. HFD 22°C	-2.713	ns	0.9991
LDL PL			
Chow 30°C vs. HFD 30°C	-49.80	ns	0.0614

Chow 30°C vs. Chow 22°C	4.958	ns	0.9946
HFD 30°C vs. HFD 22°C	22.35	ns	0.6782
Chow 22°C vs. HFD 22°C	-32.41	ns	0.3666
HDL PL			
Chow 30°C vs. HFD 30°C	-54.63	*	0.0320
Chow 30°C vs. Chow 22°C	-4.538	ns	0.9959
HFD 30°C vs. HFD 22°C	0.9133	ns	>0.9999
Chow 22°C vs. HFD 22°C	-49.18	ns	0.0664
HDL ApoA1			
Chow 30°C vs. HFD 30°C	-76.95	***	0.0007
Chow 30°C vs. Chow 22°C	0.8600	ns	>0.9999
HFD 30°C vs. HFD 22°C	2.047	ns	0.9996
Chow 22°C vs. HFD 22°C	-75.76	***	0.0009
HDL ApoA2			
Chow 30°C vs. HFD 30°C	-1.085	ns	>0.9999
Chow 30°C vs. Chow 22°C	-4.893	ns	0.9948
HFD 30°C vs. HFD 22°C	-10.32	ns	0.9552
Chow 22°C vs. HFD 22°C	-6.515	ns	0.9880
VLDL ApoB			
Chow 30°C vs. HFD 30°C	3.483	ns	0.9981
Chow 30°C vs. Chow 22°C	1.322	ns	0.9999
HFD 30°C vs. HFD 22°C	0.9917	ns	>0.9999
Chow 22°C vs. HFD 22°C	3.153	ns	0.9986
IDL ApoB			
Chow 30°C vs. HFD 30°C	-3.423	ns	0.9982
Chow 30°C vs. Chow 22°C	0.1633	ns	>0.9999
HFD 30°C vs. HFD 22°C	3.375	ns	0.9983
Chow 22°C vs. HFD 22°C	-0.2117	ns	>0.9999
LDL ApoB			
Chow 30°C vs. HFD 30°C	-68.77	**	0.0033
Chow 30°C vs. Chow 22°C	4.640	ns	0.9956
HFD 30°C vs. HFD 22°C	33.90	ns	0.3258
Chow 22°C vs. HFD 22°C	-39.52	ns	0.1968
VLDL-1 TG			
Chow 30°C vs. HFD 30°C	-5.667	ns	0.9921
Chow 30°C vs. Chow 22°C	-1.673	ns	0.9998
HFD 30°C vs. HFD 22°C	7.730	ns	0.9803
Chow 22°C vs. HFD 22°C	3.737	ns	0.9977
VLDL-2 TG			
Chow 30°C vs. HFD 30°C	-3.007	ns	0.9988
Chow 30°C vs. Chow 22°C	4.132	ns	0.9969
HFD 30°C vs. HFD 22°C	8.048	ns	0.9779
Chow 22°C vs. HFD 22°C	0.9100	ns	>0.9999
VLDL-3 TG			
Chow 30°C vs. HFD 30°C	2.013	ns	0.9996
Chow 30°C vs. Chow 22°C	1.990	ns	0.9996
HFD 30°C vs. HFD 22°C	0.000	ns	>0.9999
Chow 22°C vs. HFD 22°C	0.02333	ns	>0.9999
VLDL-4 TG			
Chow 30°C vs. HFD 30°C	1.413	ns	0.9999
Chow 30°C vs. Chow 22°C	0.8600	ns	>0.9999
HFD 30°C vs. HFD 22°C	0.000	ns	>0.9999
Chow 22°C vs. HFD 22°C	0.5533	ns	>0.9999
VLDL-5 TG			

Chow 30°C vs. HFD 30°C	-0.3600	ns	>0.9999
Chow 30°C vs. Chow 22°C	-0.4533	ns	>0.9999
HFD 30°C vs. HFD 22°C	-0.4317	ns	>0.9999
Chow 22°C vs. HFD 22°C	-0.3383	ns	>0.9999
VLDL-1 Chol			
Chow 30°C vs. HFD 30°C	-5.573	ns	0.9924
Chow 30°C vs. Chow 22°C	1.283	ns	>0.9999
HFD 30°C vs. HFD 22°C	8.148	ns	0.9771
Chow 22°C vs. HFD 22°C	1.292	ns	>0.9999
VLDL-2 Chol			
Chow 30°C vs. HFD 30°C	-2.618	ns	0.9992
Chow 30°C vs. Chow 22°C	1.468	ns	0.9999
HFD 30°C vs. HFD 22°C	4.760	ns	0.9952
Chow 22°C vs. HFD 22°C	0.6733	ns	>0.9999
VLDL-3 Chol			
Chow 30°C vs. HFD 30°C	0.5517	ns	>0.9999
Chow 30°C vs. Chow 22°C	0.8550	ns	>0.9999
HFD 30°C vs. HFD 22°C	0.3033	ns	>0.9999
Chow 22°C vs. HFD 22°C	0.000	ns	>0.9999
VLDL-4 Chol			
Chow 30°C vs. HFD 30°C	-2.965	ns	0.9988
Chow 30°C vs. Chow 22°C	0.7483	ns	>0.9999
HFD 30°C vs. HFD 22°C	3.910	ns	0.9973
Chow 22°C vs. HFD 22°C	0.1967	ns	>0.9999
VLDL-5 Chol			
Chow 30°C vs. HFD 30°C	-0.6700	ns	>0.9999
Chow 30°C vs. Chow 22°C	-0.2517	ns	>0.9999
HFD 30°C vs. HFD 22°C	0.2317	ns	>0.9999
Chow 22°C vs. HFD 22°C	-0.1867	ns	>0.9999
VLDL-1 FC			
Chow 30°C vs. HFD 30°C	-2.107	ns	0.9996
Chow 30°C vs. Chow 22°C	0.2100	ns	>0.9999
HFD 30°C vs. HFD 22°C	2.568	ns	0.9992
Chow 22°C vs. HFD 22°C	0.2517	ns	>0.9999
VLDL-2 FC			
Chow 30°C vs. HFD 30°C	0.8233	ns	>0.9999
Chow 30°C vs. Chow 22°C	0.6417	ns	>0.9999
HFD 30°C vs. HFD 22°C	0.01500	ns	>0.9999
Chow 22°C vs. HFD 22°C	0.1967	ns	>0.9999
VLDL-3 FC			
Chow 30°C vs. HFD 30°C	0.7767	ns	>0.9999
Chow 30°C vs. Chow 22°C	0.5833	ns	>0.9999
HFD 30°C vs. HFD 22°C	0.03167	ns	>0.9999
Chow 22°C vs. HFD 22°C	0.2250	ns	>0.9999
VLDL-4 FC			
Chow 30°C vs. HFD 30°C	0.1500	ns	>0.9999
Chow 30°C vs. Chow 22°C	0.3567	ns	>0.9999
HFD 30°C vs. HFD 22°C	0.2933	ns	>0.9999
Chow 22°C vs. HFD 22°C	0.08667	ns	>0.9999
VLDL-5 FC			
Chow 30°C vs. HFD 30°C	-1.407	ns	0.9999
Chow 30°C vs. Chow 22°C	-0.1417	ns	>0.9999
HFD 30°C vs. HFD 22°C	1.355	ns	0.9999
Chow 22°C vs. HFD 22°C	0.09000	ns	>0.9999

VLDL-1 PL			
Chow 30°C vs. HFD 30°C	-2.683	ns	0.9991
Chow 30°C vs. Chow 22°C	-0.02667	ns	>0.9999
HFD 30°C vs. HFD 22°C	4.000	ns	0.9972
Chow 22°C vs. HFD 22°C	1.343	ns	0.9999
VLDL-2 PL			
Chow 30°C vs. HFD 30°C	-0.6600	ns	>0.9999
Chow 30°C vs. Chow 22°C	0.9100	ns	>0.9999
HFD 30°C vs. HFD 22°C	2.365	ns	0.9994
Chow 22°C vs. HFD 22°C	0.7950	ns	>0.9999
VLDL-3 PL			
Chow 30°C vs. HFD 30°C	1.078	ns	>0.9999
Chow 30°C vs. Chow 22°C	0.8267	ns	>0.9999
HFD 30°C vs. HFD 22°C	0.000	ns	>0.9999
Chow 22°C vs. HFD 22°C	0.2517	ns	>0.9999
VLDL-4 PL			
Chow 30°C vs. HFD 30°C	0.8617	ns	>0.9999
Chow 30°C vs. Chow 22°C	0.6450	ns	>0.9999
HFD 30°C vs. HFD 22°C	0.3800	ns	>0.9999
Chow 22°C vs. HFD 22°C	0.5967	ns	>0.9999
VLDL-5 PL			
Chow 30°C vs. HFD 30°C	-0.8067	ns	>0.9999
Chow 30°C vs. Chow 22°C	-0.1717	ns	>0.9999
HFD 30°C vs. HFD 22°C	0.4317	ns	>0.9999
Chow 22°C vs. HFD 22°C	-0.2033	ns	>0.9999
LDL-1 TG			
Chow 30°C vs. HFD 30°C	-5.892	ns	0.9911
Chow 30°C vs. Chow 22°C	0.000	ns	>0.9999
HFD 30°C vs. HFD 22°C	5.472	ns	0.9928
Chow 22°C vs. HFD 22°C	-0.4200	ns	>0.9999
LDL-2 TG			
Chow 30°C vs. HFD 30°C	-4.012	ns	0.9971
Chow 30°C vs. Chow 22°C	0.1833	ns	>0.9999
HFD 30°C vs. HFD 22°C	2.632	ns	0.9992
Chow 22°C vs. HFD 22°C	-1.563	ns	0.9998
LDL-3 TG			
Chow 30°C vs. HFD 30°C	-3.558	ns	0.9980
Chow 30°C vs. Chow 22°C	-0.04333	ns	>0.9999
HFD 30°C vs. HFD 22°C	2.133	ns	0.9996
Chow 22°C vs. HFD 22°C	-1.382	ns	0.9999
LDL-4 TG			
Chow 30°C vs. HFD 30°C	0.000	ns	>0.9999
Chow 30°C vs. Chow 22°C	0.000	ns	>0.9999
HFD 30°C vs. HFD 22°C	0.000	ns	>0.9999
Chow 22°C vs. HFD 22°C	0.000	ns	>0.9999
LDL-5 TG			
Chow 30°C vs. HFD 30°C	-3.038	ns	0.9987
Chow 30°C vs. Chow 22°C	0.3233	ns	>0.9999
HFD 30°C vs. HFD 22°C	2.802	ns	0.9990
Chow 22°C vs. HFD 22°C	-0.5600	ns	>0.9999
LDL-6 TG			
Chow 30°C vs. HFD 30°C	0.6267	ns	>0.9999
Chow 30°C vs. Chow 22°C	0.08333	ns	>0.9999
HFD 30°C vs. HFD 22°C	0.3050	ns	>0.9999

Chow 22°C vs. HFD 22°C	0.8483	ns	>0.9999
LDL-1 Chol			
Chow 30°C vs. HFD 30°C	-70.50	**	0.0024
Chow 30°C vs. Chow 22°C	2.217	ns	0.9995
HFD 30°C vs. HFD 22°C	47.05	ns	0.0864
Chow 22°C vs. HFD 22°C	-25.67	ns	0.5730
LDL-2 Chol			
Chow 30°C vs. HFD 30°C	-24.86	ns	0.5989
Chow 30°C vs. Chow 22°C	-0.5767	ns	>0.9999
HFD 30°C vs. HFD 22°C	2.562	ns	0.9992
Chow 22°C vs. HFD 22°C	-21.72	ns	0.6976
LDL-3 Chol			
Chow 30°C vs. HFD 30°C	-4.513	ns	0.9959
Chow 30°C vs. Chow 22°C	0.8667	ns	>0.9999
HFD 30°C vs. HFD 22°C	0.8767	ns	>0.9999
Chow 22°C vs. HFD 22°C	-4.503	ns	0.9960
LDL-4 Chol			
Chow 30°C vs. HFD 30°C	0.000	ns	>0.9999
Chow 30°C vs. Chow 22°C	0.000	ns	>0.9999
HFD 30°C vs. HFD 22°C	0.000	ns	>0.9999
Chow 22°C vs. HFD 22°C	0.000	ns	>0.9999
LDL-5 Chol			
Chow 30°C vs. HFD 30°C	-2.987	ns	0.9988
Chow 30°C vs. Chow 22°C	0.5583	ns	>0.9999
HFD 30°C vs. HFD 22°C	0.9500	ns	>0.9999
Chow 22°C vs. HFD 22°C	-2.595	ns	0.9992
LDL-6 Chol			
Chow 30°C vs. HFD 30°C	-14.50	ns	0.8870
Chow 30°C vs. Chow 22°C	-3.367	ns	0.9983
HFD 30°C vs. HFD 22°C	8.928	ns	0.9703
Chow 22°C vs. HFD 22°C	-2.203	ns	0.9995
LDL-1 FC			
Chow 30°C vs. HFD 30°C	-20.71	ns	0.7283
Chow 30°C vs. Chow 22°C	0.7333	ns	>0.9999
HFD 30°C vs. HFD 22°C	13.98	ns	0.8973
Chow 22°C vs. HFD 22°C	-7.460	ns	0.9823
LDL-2 FC			
Chow 30°C vs. HFD 30°C	-8.757	ns	0.9719
Chow 30°C vs. Chow 22°C	-0.2167	ns	>0.9999
HFD 30°C vs. HFD 22°C	0.8350	ns	>0.9999
Chow 22°C vs. HFD 22°C	-7.705	ns	0.9805
LDL-3 FC			
Chow 30°C vs. HFD 30°C	-3.668	ns	0.9978
Chow 30°C vs. Chow 22°C	1.003	ns	>0.9999
HFD 30°C vs. HFD 22°C	0.4200	ns	>0.9999
Chow 22°C vs. HFD 22°C	-4.252	ns	0.9966
LDL-4 FC			
Chow 30°C vs. HFD 30°C	0.1100	ns	>0.9999
Chow 30°C vs. Chow 22°C	0.1100	ns	>0.9999
HFD 30°C vs. HFD 22°C	-0.01833	ns	>0.9999
Chow 22°C vs. HFD 22°C	-0.01833	ns	>0.9999
LDL-5 FC			
Chow 30°C vs. HFD 30°C	-1.603	ns	0.9998

Chow 30°C vs. Chow 22°C	0.3900	ns	>0.9999
HFD 30°C vs. HFD 22°C	0.5183	ns	>0.9999
Chow 22°C vs. HFD 22°C	-1.475	ns	0.9999
LDL-6 FC			
Chow 30°C vs. HFD 30°C	-4.677	ns	0.9955
Chow 30°C vs. Chow 22°C	-0.9500	ns	>0.9999
Chow 30°C vs. HFD 22°C	-2.860	ns	0.9990
Chow 22°C vs. HFD 22°C	-1.910	ns	0.9997
LDL-1 PL			
Chow 30°C vs. HFD 30°C	-36.16	ns	0.2691
Chow 30°C vs. Chow 22°C	0.9800	ns	>0.9999
HFD 30°C vs. HFD 22°C	24.23	ns	0.6190
Chow 22°C vs. HFD 22°C	-12.91	ns	0.9170
LDL-2 PL			
Chow 30°C vs. HFD 30°C	-12.68	ns	0.9209
Chow 30°C vs. Chow 22°C	-0.1733	ns	>0.9999
HFD 30°C vs. HFD 22°C	1.492	ns	0.9999
Chow 22°C vs. HFD 22°C	-11.02	ns	0.9462
LDL-3 PL			
Chow 30°C vs. HFD 30°C	-2.832	ns	0.9990
Chow 30°C vs. Chow 22°C	0.6583	ns	>0.9999
HFD 30°C vs. HFD 22°C	0.7217	ns	>0.9999
Chow 22°C vs. HFD 22°C	-2.768	ns	0.9991
LDL-4 PL			
Chow 30°C vs. HFD 30°C	0.000	ns	>0.9999
Chow 30°C vs. Chow 22°C	0.000	ns	>0.9999
HFD 30°C vs. HFD 22°C	0.000	ns	>0.9999
Chow 22°C vs. HFD 22°C	0.000	ns	>0.9999
LDL-5 PL			
Chow 30°C vs. HFD 30°C	-1.560	ns	0.9998
Chow 30°C vs. Chow 22°C	0.3683	ns	>0.9999
HFD 30°C vs. HFD 22°C	0.5950	ns	>0.9999
Chow 22°C vs. HFD 22°C	-1.333	ns	0.9999
LDL-6 PL			
Chow 30°C vs. HFD 30°C	-7.362	ns	0.9829
Chow 30°C vs. Chow 22°C	-1.758	ns	0.9998
HFD 30°C vs. HFD 22°C	3.970	ns	0.9972
Chow 22°C vs. HFD 22°C	-1.633	ns	0.9998
LDL-1 ApoB			
Chow 30°C vs. HFD 30°C	-35.48	ns	0.2856
Chow 30°C vs. Chow 22°C	0.9700	ns	>0.9999
HFD 30°C vs. HFD 22°C	23.52	ns	0.6415
Chow 22°C vs. HFD 22°C	-12.93	ns	0.9167
LDL-2 ApoB			
Chow 30°C vs. HFD 30°C	-13.45	ns	0.9073
Chow 30°C vs. Chow 22°C	-0.1633	ns	>0.9999
HFD 30°C vs. HFD 22°C	1.605	ns	0.9998
Chow 22°C vs. HFD 22°C	-11.69	ns	0.9367
LDL-3 ApoB			
Chow 30°C vs. HFD 30°C	-4.005	ns	0.9972
Chow 30°C vs. Chow 22°C	0.7483	ns	>0.9999
HFD 30°C vs. HFD 22°C	1.458	ns	0.9999
Chow 22°C vs. HFD 22°C	-3.295	ns	0.9984

LDL-4 ApoB			
Chow 30°C vs. HFD 30°C	0.000	ns	>0.9999
Chow 30°C vs. Chow 22°C	0.000	ns	>0.9999
HFD 30°C vs. HFD 22°C	0.000	ns	>0.9999
Chow 22°C vs. HFD 22°C	0.000	ns	>0.9999
LDL-5 ApoB			
Chow 30°C vs. HFD 30°C	-4.340	ns	0.9964
Chow 30°C vs. Chow 22°C	0.3733	ns	>0.9999
HFD 30°C vs. HFD 22°C	3.020	ns	0.9988
Chow 22°C vs. HFD 22°C	-1.693	ns	0.9998
LDL-6 ApoB			
Chow 30°C vs. HFD 30°C	-8.937	ns	0.9702
Chow 30°C vs. Chow 22°C	-2.123	ns	0.9996
HFD 30°C vs. HFD 22°C	5.318	ns	0.9934
Chow 22°C vs. HFD 22°C	-1.495	ns	0.9998
HDL-1 TG			
Chow 30°C vs. HFD 30°C	-8.792	ns	0.9715
Chow 30°C vs. Chow 22°C	1.745	ns	0.9998
HFD 30°C vs. HFD 22°C	4.648	ns	0.9956
Chow 22°C vs. HFD 22°C	-5.888	ns	0.9911
HDL-2 TG			
Chow 30°C vs. HFD 30°C	-2.853	ns	0.9990
Chow 30°C vs. Chow 22°C	-0.06333	ns	>0.9999
HFD 30°C vs. HFD 22°C	0.5150	ns	>0.9999
Chow 22°C vs. HFD 22°C	-2.275	ns	0.9995
HDL-3 TG			
Chow 30°C vs. HFD 30°C	-3.015	ns	0.9988
Chow 30°C vs. Chow 22°C	-0.2800	ns	>0.9999
HFD 30°C vs. HFD 22°C	0.8833	ns	>0.9999
Chow 22°C vs. HFD 22°C	-1.852	ns	0.9997
HDL-4 TG			
Chow 30°C vs. HFD 30°C	-1.485	ns	0.9999
Chow 30°C vs. Chow 22°C	0.2700	ns	>0.9999
HFD 30°C vs. HFD 22°C	1.733	ns	0.9998
Chow 22°C vs. HFD 22°C	-0.02167	ns	>0.9999
HDL-1 Chol			
Chow 30°C vs. HFD 30°C	-38.98	ns	0.2074
Chow 30°C vs. Chow 22°C	1.688	ns	0.9998
HFD 30°C vs. HFD 22°C	13.98	ns	0.8973
Chow 22°C vs. HFD 22°C	-26.69	ns	0.5403
HDL-2 Chol			
Chow 30°C vs. HFD 30°C	-10.02	ns	0.9588
Chow 30°C vs. Chow 22°C	-2.105	ns	0.9996
HFD 30°C vs. HFD 22°C	-2.827	ns	0.9990
Chow 22°C vs. HFD 22°C	-10.74	ns	0.9499
HDL-3 Chol			
Chow 30°C vs. HFD 30°C	-2.868	ns	0.9989
Chow 30°C vs. Chow 22°C	-2.277	ns	0.9995
HFD 30°C vs. HFD 22°C	-5.482	ns	0.9928
Chow 22°C vs. HFD 22°C	-6.073	ns	0.9903
HDL-4 Chol			
Chow 30°C vs. HFD 30°C	0.9717	ns	>0.9999
Chow 30°C vs. Chow 22°C	0.5567	ns	>0.9999
HFD 30°C vs. HFD 22°C	-0.1583	ns	>0.9999

Chow 22°C vs. HFD 22°C	0.2567	ns	>0.9999
HDL-1 FC			
Chow 30°C vs. HFD 30°C	-5.913	ns	0.9910
Chow 30°C vs. Chow 22°C	1.302	ns	>0.9999
HFD 30°C vs. HFD 22°C	1.388	ns	0.9999
Chow 22°C vs. HFD 22°C	-5.827	ns	0.9914
HDL-2 FC			
Chow 30°C vs. HFD 30°C	-0.7283	ns	>0.9999
Chow 30°C vs. Chow 22°C	-0.1600	ns	>0.9999
HFD 30°C vs. HFD 22°C	-1.198	ns	>0.9999
Chow 22°C vs. HFD 22°C	-1.767	ns	0.9998
HDL-3 FC			
Chow 30°C vs. HFD 30°C	-0.2333	ns	>0.9999
Chow 30°C vs. Chow 22°C	0.1550	ns	>0.9999
HFD 30°C vs. HFD 22°C	-0.8950	ns	>0.9999
Chow 22°C vs. HFD 22°C	-1.283	ns	>0.9999
HDL-4 FC			
Chow 30°C vs. HFD 30°C	0.000	ns	>0.9999
Chow 30°C vs. Chow 22°C	0.000	ns	>0.9999
HFD 30°C vs. HFD 22°C	0.000	ns	>0.9999
Chow 22°C vs. HFD 22°C	0.000	ns	>0.9999
HDL-1 PL			
Chow 30°C vs. HFD 30°C	-42.34	ns	0.1474
Chow 30°C vs. Chow 22°C	2.282	ns	0.9995
HFD 30°C vs. HFD 22°C	14.22	ns	0.8926
Chow 22°C vs. HFD 22°C	-30.40	ns	0.4248
HDL-2 PL			
Chow 30°C vs. HFD 30°C	-13.99	ns	0.8972
Chow 30°C vs. Chow 22°C	-3.593	ns	0.9979
HFD 30°C vs. HFD 22°C	-4.050	ns	0.9971
Chow 22°C vs. HFD 22°C	-14.44	ns	0.8881
HDL-3 PL			
Chow 30°C vs. HFD 30°C	-7.245	ns	0.9837
Chow 30°C vs. Chow 22°C	-4.067	ns	0.9970
HFD 30°C vs. HFD 22°C	-5.728	ns	0.9918
Chow 22°C vs. HFD 22°C	-8.907	ns	0.9705
HDL-4 PL			
Chow 30°C vs. HFD 30°C	2.820	ns	0.9990
Chow 30°C vs. Chow 22°C	0.6717	ns	>0.9999
HFD 30°C vs. HFD 22°C	-1.293	ns	>0.9999
Chow 22°C vs. HFD 22°C	0.8550	ns	>0.9999
HDL-1 ApoA1			
Chow 30°C vs. HFD 30°C	-64.97	**	0.0064
Chow 30°C vs. Chow 22°C	6.113	ns	0.9901
HFD 30°C vs. HFD 22°C	23.11	ns	0.6546
Chow 22°C vs. HFD 22°C	-47.98	ns	0.0771
HDL-2 ApoA1			
Chow 30°C vs. HFD 30°C	-8.742	ns	0.9720
Chow 30°C vs. Chow 22°C	-1.737	ns	0.9998
HFD 30°C vs. HFD 22°C	-4.253	ns	0.9966
Chow 22°C vs. HFD 22°C	-11.26	ns	0.9429
HDL-3 ApoA1			
Chow 30°C vs. HFD 30°C	-7.253	ns	0.9836
Chow 30°C vs. Chow 22°C	-4.103	ns	0.9969

HFD 30°C vs. HFD 22°C	-10.92	ns	0.9476
Chow 22°C vs. HFD 22°C	-14.07	ns	0.8956
HDL-4 ApoA1			
Chow 30°C vs. HFD 30°C	3.715	ns	0.9977
Chow 30°C vs. Chow 22°C	3.168	ns	0.9986
HFD 30°C vs. HFD 22°C	0.000	ns	>0.9999
Chow 22°C vs. HFD 22°C	0.5467	ns	>0.9999
HDL-1 ApoA2			
Chow 30°C vs. HFD 30°C	-3.152	ns	0.9986
Chow 30°C vs. Chow 22°C	0.1267	ns	>0.9999
HFD 30°C vs. HFD 22°C	-0.1267	ns	>0.9999
Chow 22°C vs. HFD 22°C	-3.405	ns	0.9982
HDL-2 ApoA2			
Chow 30°C vs. HFD 30°C	-2.003	ns	0.9996
Chow 30°C vs. Chow 22°C	-0.9000	ns	>0.9999
HFD 30°C vs. HFD 22°C	-1.512	ns	0.9998
Chow 22°C vs. HFD 22°C	-2.615	ns	0.9992
HDL-3 ApoA2			
Chow 30°C vs. HFD 30°C	-1.762	ns	0.9998
Chow 30°C vs. Chow 22°C	-1.957	ns	0.9997
HFD 30°C vs. HFD 22°C	-3.350	ns	0.9983
Chow 22°C vs. HFD 22°C	-3.155	ns	0.9986
HDL-4 ApoA2			
Chow 30°C vs. HFD 30°C	0.5183	ns	>0.9999
Chow 30°C vs. Chow 22°C	0.3300	ns	>0.9999
HFD 30°C vs. HFD 22°C	0.000	ns	>0.9999
Chow 22°C vs. HFD 22°C	0.1883	ns	>0.9999

Table 21. List of serum metabolites detected in the serum of CD patients

	Ctrl		AZA		Recent AZA	
Metabolite	Average	SEM	Average	SEM	Average	SEM
Ethanol	0.0068	0.0068	0.0000	0.0000	0.0000	0.0000
Trimethylamine-N-oxide	0.0000	0.0000	0.0044	0.0044	0.0160	0.0160
2-Aminobutyric acid	0.0000	0.0000	0.0000	0.0000	0.0000	0.0000
Alanine	0.4443	0.0164	0.4672	0.0218	0.4360	0.0484
Asparagine	0.0122	0.0062	0.0300	0.0096	0.0120	0.0120
Creatine	0.0254	0.0038	0.0261	0.0043	0.0220	0.0102
Creatinine	0.0830	0.0035	0.0950	0.0134	0.1220	0.0475
Glutamic acid	0.0841	0.0169	0.0694	0.0171	0.0480	0.0240
Glutamine	0.6500	0.0150	0.6783	0.0307	0.6540	0.0284
Glycine	0.3327	0.0158	0.3461	0.0368	0.2880	0.0292
Histidine	0.0792	0.0041	0.0728	0.0046	0.0720	0.0058
Isoleucine	0.0595	0.0037	0.0617	0.0065	0.0580	0.0107
Leucine	0.1014	0.0050	0.1194	0.0108	0.1080	0.0146
Lysine	0.1714	0.0132	0.1744	0.0218	0.1920	0.0166
Methionine	0.0043	0.0024	0.0061	0.0042	0.0100	0.0100
N,N-Dimethylglycine	0.0003	0.0003	0.0011	0.0008	0.0040	0.0024
Ornithine	0.0273	0.0053	0.0328	0.0084	0.0300	0.0167

Metabolite	Average	SEM	Average	SEM	Average	SEM
Phenylalanine	0.0678	0.0034	0.0717	0.0054	0.0740	0.0081
Proline	0.1559	0.0299	0.1594	0.0394	0.1100	0.0473
Sarcosine	0.0005	0.0004	0.0000	0.0000	0.0000	0.0000
Threonine	0.0859	0.0148	0.0961	0.0234	0.0560	0.0349
Tyrosine	0.0541	0.0030	0.0572	0.0031	0.0580	0.0037
Valine	0.2195	0.0081	0.2333	0.0192	0.2100	0.0207
2-Hydroxybutyric acid	0.0062	0.0062	0.0139	0.0139	0.0000	0.0000
Acetic acid	0.0084	0.0035	0.0061	0.0024	0.0080	0.0049
Citric acid	0.1203	0.0104	0.1367	0.0116	0.1480	0.0128
Formic acid	0.0049	0.0016	0.0028	0.0019	0.0040	0.0040
Lactic acid	2.8162	0.2737	3.1944	0.4823	2.5000	0.3347
Succinic acid	0.0068	0.0041	0.0033	0.0020	0.0080	0.0058
Choline	0.0000	0.0000	0.0000	0.0000	0.0000	0.0000
2-Oxoglutaric acid	0.0000	0.0000	0.0000	0.0000	0.0000	0.0000
3-Hydroxybutyric acid	0.0786	0.0231	0.0900	0.0411	0.1620	0.1123
Acetoacetic acid	0.0092	0.0044	0.0394	0.0234	0.0700	0.0602
Acetone	0.0249	0.0057	0.0256	0.0071	0.0260	0.0093
Pyruvic acid	0.0908	0.0118	0.0717	0.0090	0.0480	0.0171
D-Galactose	0.0000	0.0000	0.0000	0.0000	0.0000	0.0000
Glucose	5.1000	0.2326	5.0172	0.3882	4.7800	0.1497
Glycerol	0.0105	0.0081	0.0433	0.0310	0.0560	0.0560
Dimethyl sulfone	0.0035	0.0012	0.1444	0.1224	0.0020	0.0020
TG	169.3803	18.8290	174.7500	25.1259	136.9540	29.4849
Chol	190.1014	7.3551	176.1378	10.9732	147.7780	14.2803
LDL	94.2341	5.8478	81.7433	8.2322	67.5400	11.3606
HDL	61.1908	2.5669	58.9950	3.3783	49.9300	6.7796
ApoA1	157.9189	4.8588	159.6089	7.1561	139.1080	17.9814
ApoA2	35.0905	0.9199	36.2117	1.8537	30.0840	2.6340
ApoB100	81.1457	4.0044	74.1183	5.3131	63.0340	8.1835
LDL/HDL	1.6181	0.1231	1.4111	0.1370	1.4680	0.3016
ApoB100/ApoA1	0.5311	0.0323	0.4756	0.0343	0.4900	0.0879
ApoB Particles	1475.4538	72.8078	1347.6800	96.6023	1146.1800	148.7776
VLDL Particles	172.5892	13.2185	184.5322	18.3142	171.0880	35.1433
IDL Particles	95.3078	6.3182	91.9922	9.8409	85.4480	10.0213
LDL Particles	1188.8892	66.0431	1028.8044	89.6929	848.7880	128.6723
LDL-1 Particles	178.6470	8.6301	176.2200	13.3664	159.1560	4.3159
LDL-2 Particles	133.4916	9.6295	130.0406	12.2613	114.9040	6.6268
LDL-3 Particles	114.6692	11.1458	96.3100	17.1651	85.7040	21.7341
LDL-4 Particles	132.2486	15.2919	109.9656	20.6364	104.4940	36.9659
LDL-5 Particles	225.9519	17.7029	196.3561	30.0151	161.3340	35.0825
LDL-6 Particles	424.7481	28.9352	354.5750	33.8515	259.3980	44.8767
VLDL TG	113.5341	13.0169	118.1511	17.8480	89.2960	22.0579
IDL TG	22.1451	3.7417	23.4789	5.2257	14.7640	5.6524
LDL TG	20.3311	1.1525	20.1950	1.9468	17.1020	1.4129
HDL TG	14.5505	0.9737	16.3017	1.7684	14.4740	2.5619

VLDL	24.0954	2.2002	25.8272	3.1262	22.0000	4.5020
IDL	12.5711	1.2797	11.5267	1.7112	10.4240	1.7160
LDL	94.2341	5.8478	81.7433	8.2322	67.5400	11.3606
HDL	61.1908	2.5669	58.9950	3.3783	49.9300	6.7796
VLDL FC	11.0584	0.8815	11.5678	1.2485	10.0780	2.1909
IDL FC	3.7157	0.3655	3.3889	0.4437	3.0320	0.5173
LDL FC	25.6332	1.6820	22.6322	2.3102	19.3400	3.1395
HDL FC	11.8830	0.8241	11.7233	0.9762	10.2520	1.5262
VLDL PL	27.1686	2.1410	29.0472	3.3402	24.9180	5.5221
IDL PL	9.1922	0.9009	9.1011	1.2217	6.2400	1.6617
LDL PL	56.3670	2.8144	50.3161	4.0298	43.0780	5.4965
HDL PL	91.6711	3.3760	91.6922	4.2611	80.4400	10.5092
HDL ApoA1	160.7057	5.2298	162.9972	7.3921	141.8660	18.5035
HDL ApoA2	35.4481	0.8862	36.4261	1.8947	30.3280	2.5106
VLDL ApoB	9.4922	0.7270	10.1489	1.0073	9.4080	1.9330
IDL ApoB	5.2416	0.3475	5.0583	0.5412	4.6980	0.5512
LDL ApoB	65.3876	3.6321	56.5811	4.9327	46.6800	7.0769
VLDL-1 TG	59.4068	8.5677	57.7706	9.8072	43.3020	11.3126
VLDL-2 TG	18.9027	2.3199	21.3033	3.7819	14.6220	4.9604
VLDL-3 TG	15.3414	1.6662	17.6589	2.9351	12.7440	4.3739
VLDL-4 TG	11.1843	0.8718	11.8289	1.3057	11.2580	2.8828
VLDL-5 TG	2.9651	0.1872	3.0111	0.2250	3.4960	0.3155
VLDL-1 Chol	9.1162	1.2566	9.4078	1.4375	7.3160	1.3862
VLDL-2 Chol	3.8041	0.4258	4.5128	0.7538	2.8560	0.8195
VLDL-3 Chol	4.4746	0.3982	5.1278	0.7112	3.9860	1.0814
VLDL-4 Chol	5.5551	0.4499	5.7083	0.6549	5.8420	1.2471
VLDL-5 Chol	1.6281	0.1485	1.6956	0.1431	2.0440	0.2244
VLDL-1 FC	4.1054	0.5488	3.9433	0.5554	3.0840	0.7050
VLDL-2 FC	1.5000	0.1925	1.8300	0.3109	1.2040	0.3800
VLDL-3 FC	2.0435	0.2323	2.2139	0.3121	1.7800	0.4952
VLDL-4 FC	1.8768	0.2007	2.0494	0.2693	2.2760	0.4636
VLDL-5 FC	0.6992	0.0766	0.8239	0.0809	0.9680	0.1038
VLDL-1 PL	9.7695	1.3514	9.8072	1.5548	7.5300	1.8078
VLDL-2 PL	4.8873	0.5058	5.4594	0.8394	3.9220	1.1116
VLDL-3 PL	5.0973	0.4292	5.7072	0.7396	4.6200	1.2210
VLDL-4 PL	5.2703	0.3755	5.6617	0.5431	5.6200	1.1168
VLDL-5 PL	1.9862	0.1578	2.1406	0.1672	2.5080	0.2803
LDL-1 TG	5.7438	0.5526	5.8839	0.6961	5.3960	0.7703
LDL-2 TG	2.0903	0.1300	2.2294	0.2246	1.8920	0.1367
LDL-3 TG	2.3773	0.1182	2.2989	0.1259	2.2120	0.1441
LDL-4 TG	2.1827	0.1687	2.2311	0.2946	2.0340	0.2534
LDL-5 TG	2.9422	0.2045	2.9356	0.4355	2.2060	0.3087
LDL-6 TG	5.6943	0.3909	5.0856	0.5951	3.8600	0.6417
LDL-1 Chol	17.1254	0.9820	16.9061	1.6425	14.7420	0.4487
LDL-2 Chol	12.5346	1.0294	11.7767	1.4575	9.9740	0.7359
LDL-3 Chol	9.8978	1.1626	8.0889	1.7156	6.4240	2.2839

LDL-4 Chol	10.9554	1.3854	8.7061	1.7880	8.2080	3.2941
LDL-5 Chol	16.6427	1.4582	14.4250	2.2586	11.7060	2.9108
LDL-6 Chol	27.4492	1.8770	22.3500	2.2836	16.1600	3.2939
LDL-1 FC	5.1024	0.3115	4.9983	0.5304	4.3920	0.1915
LDL-2 FC	3.8232	0.3394	3.8117	0.4186	3.1080	0.2011
LDL-3 FC	3.1776	0.3493	2.7878	0.5097	1.9640	0.5624
LDL-4 FC	3.4086	0.3369	2.6739	0.4640	2.4640	0.7826
LDL-5 FC	4.5459	0.3434	3.8167	0.5216	3.2200	0.7679
LDL-6 FC	7.1522	0.4707	5.6339	0.4612	4.3180	0.6580
LDL-1 PL	10.5241	0.4871	10.5906	0.8138	9.5980	0.3512
LDL-2 PL	7.3368	0.5183	6.9856	0.7303	6.0760	0.3540
LDL-3 PL	6.1600	0.5867	5.2372	0.8999	4.6180	1.1053
LDL-4 PL	6.6168	0.7257	5.4022	0.9663	5.1300	1.7363
LDL-5 PL	9.4565	0.7139	8.4056	1.1723	7.0680	1.4180
LDL-6 PL	15.8895	0.9333	13.2983	1.1153	10.0800	1.5592
LDL-1 ApoB	9.8251	0.4745	9.6922	0.7349	8.7540	0.2388
LDL-2 ApoB	7.3414	0.5297	7.1517	0.6741	6.3200	0.3635
LDL-3 ApoB	6.3065	0.6130	5.2967	0.9443	4.7120	1.1945
LDL-4 ApoB	7.2735	0.8410	6.0478	1.1353	5.7460	2.0337
LDL-5 ApoB	12.4268	0.9737	10.7989	1.6508	8.8720	1.9295
LDL-6 ApoB	23.3603	1.5913	19.5011	1.8617	14.2680	2.4673
HDL-1 TG	5.0986	0.4673	5.7089	0.7998	4.8220	1.2722
HDL-2 TG	2.5976	0.2048	2.8867	0.3376	2.6520	0.4063
HDL-3 TG	2.9903	0.2121	3.3917	0.3863	3.1040	0.4253
HDL-4 TG	4.2473	0.2650	4.8150	0.4464	4.3780	0.6064
HDL-1 Chol	20.5262	1.6553	18.7189	2.1237	15.3420	3.6746
HDL-2 Chol	9.5051	0.5369	9.1678	0.6249	7.6760	1.0213
HDL-3 Chol	11.0511	0.4247	10.9606	0.6271	9.5760	1.0915
HDL-4 Chol	19.0132	0.8854	18.8133	1.2462	16.1420	1.8236
HDL-1 FC	4.5008	0.4106	4.2478	0.4979	3.3300	0.7709
HDL-2 FC	2.0770	0.1446	2.0583	0.1674	1.7780	0.2609
HDL-3 FC	2.3705	0.1238	2.2528	0.2151	1.7900	0.3825
HDL-4 FC	3.6457	0.2029	3.4617	0.3228	2.9920	0.5967
HDL-1 PL	26.5873	2.1386	25.6433	2.4675	22.1540	4.8560
HDL-2 PL	16.0730	0.8359	15.9061	1.0499	13.9140	1.8083
HDL-3 PL	19.7130	0.6832	19.7556	1.0863	17.5660	2.0504
HDL-4 PL	29.3919	1.0233	29.5394	1.3521	26.5060	2.6397
HDL-1 ApoA1	32.8246	3.0724	33.2850	3.5586	27.9660	7.1235
HDL-2 ApoA1	23.1835	0.9366	23.6917	1.3585	20.4040	3.4468
HDL-3 ApoA1	29.9959	1.0886	30.7861	1.6335	27.0820	3.3927
HDL-4 ApoA1	74.2076	2.6530	75.3589	3.6780	66.3120	6.6292
Metabolite	Average	SEM	Average	SEM	Average	SEM
HDL-1 ApoA2	3.8292	0.3036	3.9911	0.3647	3.1920	0.7314
HDL-2 ApoA2	4.7203	0.2064	4.8389	0.3630	4.0700	0.4634
HDL-3 ApoA2	7.5857	0.2466	7.7956	0.5815	6.7020	0.5751
HDL-4 ApoA2	19.0435	0.8297	19.4644	1.0847	16.1860	1.4125

Concentrations are in mg/dL

Table 22. Multiple Mann-Whitney tests between control and AZA-treated CD patients

	AZA vs. Ctrl			Recent AZA vs. Ctrl		
	Predicted (LS) mean diff	Summary	*P* Value	Predicted (LS) mean diff.	Summary	*P* Value
Ethanol	-0.7432	ns	>0.999999	-0.5676	ns	>0.999999
Trimethylamine-N-oxide	1.528	ns	0.327273	4.200	ns	0.119048
2-Aminobutyric acid	0.000	ns	>0.999999	0.000	ns	>0.999999
Alanine	5.450	ns	0.240174	-0.3405	ns	0.962221
Asparagine	7.061	*	0.027039	1.476	ns	>0.999999
Creatine	2.271	ns	0.623231	-1.476	ns	0.814462
Creatinine	0.4955	ns	0.917654	0.3405	ns	0.958836
Glutamic acid	-2.849	ns	0.531768	-4.314	ns	0.469665
Glutamine	4.418	ns	0.341917	0.9081	ns	0.887796
Glycine	-0.1239	ns	0.982257	-6.243	ns	0.298326
Histidine	-5.120	ns	0.260504	-3.292	ns	0.567874
Isoleucine	-0.08258	ns	0.989054	-0.5676	ns	0.933453
Leucine	6.359	ns	0.167492	4.200	ns	0.485785
Lysine	0.08258	ns	0.989334	0.6811	ns	0.916395
Methionine	0.8671	ns	0.897480	2.384	ns	0.409944
N.N-Dimethylglycine	2.312	ns	0.246884	7.832	ns	0.033101
Ornithine	2.188	ns	0.622862	1.022	ns	0.858194
Phenylalanine	2.932	ns	0.524441	4.654	ns	0.435865
Proline	0.4129	ns	0.929295	-2.838	ns	0.629736
Sarcosine	-1.486	ns	0.551515	-1.135	ns	>0.999999
Threonine	1.445	ns	0.749845	-3.632	ns	0.533852
Tyrosine	1.610	ns	0.726365	2.611	ns	0.674030
Valine	0.1239	ns	0.982242	-2.043	ns	0.740938
2-Hydroxybutyric acid	0.8258	ns	0.775758	-0.5676	ns	>0.999999
Acetic acid	-0.4955	ns	0.902979	2.270	ns	0.685173
Citric acid	2.725	ns	0.559184	4.200	ns	0.488687
Formic acid	-2.725	ns	0.456086	-0.5676	ns	0.903793
Lactic acid	7.226	ns	0.117507	0.2270	ns	0.977036
Succinic acid	-0.5781	ns	0.873140	4.427	ns	0.470863
Choline	0.000	ns	>0.999999	0.000	ns	>0.999999
2-Oxoglutaric acid	0.000	ns	>0.999999	0.000	ns	>0.999999
3-Hydroxybutyric acid	-0.2065	ns	0.965450	4.768	ns	0.406149

Acetoacetic acid	4.170	ns	0.233048	8.854	*	0.040848
Acetone	2.932	ns	0.518916	4.541	ns	0.439716
Pyruvic acid	-1.899	ns	0.684336	-8.854	ns	0.131838
D-Galactose	0.000	ns	>0.999999	0.000	ns	>0.999999
Glucose	0.1652	ns	0.975184	-1.589	ns	0.799244
Glycerol	1.693	ns	0.390738	3.178	ns	0.226481
Dimethylsulfone	4.129	ns	0.265022	-1.249	ns	0.873182
TG	1.321	ns	0.783018	-2.611	ns	0.678380
Chol	-5.203	ns	0.265004	-12.37	ns	0.032887
LDL	-5.450	ns	0.242559	-9.649	ns	0.104264
HDL	-1.404	ns	0.766325	-8.968	ns	0.131997
ApoA1	3.468	ns	0.460241	-6.243	ns	0.304342
ApoA2	1.074	ns	0.824261	-10.56	ns	0.073392
ApoB100	-4.707	ns	0.313989	-9.422	ns	0.113290
LDL/HDL	-4.088	ns	0.380437	-2.270	ns	0.712439
ApoB100/ApoA1	-3.345	ns	0.473610	-2.838	ns	0.643747
ApoB Particles	-4.707	ns	0.313989	-9.422	ns	0.113290
VLDL Particles	3.221	ns	0.493408	0.5676	ns	0.940021
IDL Particles	-1.652	ns	0.728963	-1.249	ns	0.850736
LDL Particles	-6.524	ns	0.160522	-10.56	ns	0.073392
LDL-1 Particles	-0.7432	ns	0.879981	-5.335	ns	0.382953
LDL-2 Particles	-0.3303	ns	0.950427	-2.157	ns	0.734571
LDL-3 Particles	-4.790	ns	0.303258	-5.789	ns	0.340188
LDL-4 Particles	-3.592	ns	0.441185	-3.178	ns	0.601969
LDL-5 Particles	-5.203	ns	0.265004	-7.605	ns	0.206859
LDL-6 Particles	-6.607	ns	0.155191	-12.37	*	0.032887
VLDL TG	1.610	ns	0.732007	-3.405	ns	0.573924
IDL TG	0.6607	ns	0.894013	-4.427	ns	0.472161
LDL TG	-0.5368	ns	0.911256	-5.449	ns	0.364504
HDL TG	4.129	ns	0.378067	1.022	ns	0.880355
VLDL	2.477	ns	0.599956	-0.3405	ns	0.969991
IDL	-2.395	ns	0.612397	-2.611	ns	0.678380
LDL	-5.450	ns	0.242559	-9.649	ns	0.104264
HDL	-1.404	ns	0.766325	-8.968	ns	0.131997
VLDL FC	2.106	ns	0.653314	-1.930	ns	0.763193
IDL FC	-1.528	ns	0.745718	-2.724	ns	0.653943
LDL FC	-4.377	ns	0.349695	-8.059	ns	0.179718
HDL FC	0.3303	ns	0.950427	-3.973	ns	0.520492
VLDL PL	2.065	ns	0.663235	-2.157	ns	0.734571
IDL PL	-0.5781	ns	0.904880	-6.470	ns	0.284526
LDL PL	-6.029	ns	0.195383	-9.649	ns	0.104264
HDL PL	1.817	ns	0.702404	-5.789	ns	0.342291
HDL ApoA1	3.386	ns	0.471159	-5.789	ns	0.342291
HDL ApoA2	0.4542	ns	0.925363	-10.78	ns	0.066891
VLDL ApoB	3.262	ns	0.484717	0.5676	ns	0.940021
IDL ApoB	-1.693	ns	0.718929	-1.249	ns	0.850736

LDL ApoB	-6.524	ns	0.159346	-10.56	ns	0.073392
VLDL-1 TG	0.9910	ns	0.838121	-2.157	ns	0.734571
VLDL-2 TG	1.652	ns	0.728963	-3.065	ns	0.623809
VLDL-3 TG	2.643	ns	0.575418	-2.384	ns	0.706290
VLDL-4 TG	2.477	ns	0.599956	0.7946	ns	0.910129
VLDL-5 TG	1.899	ns	0.686235	8.059	ns	0.179718
VLDL-1 Chol	2.106	ns	0.653565	-0.3405	ns	0.964408
VLDL-2 Chol	2.767	ns	0.554078	-3.292	ns	0.597211
VLDL-3 Chol	2.973	ns	0.527788	-2.384	ns	0.706290
VLDL-4 Chol	0.2065	ns	0.968120	0.7946	ns	0.910129
VLDL-5 Chol	2.808	ns	0.548334	7.378	ns	0.219734
VLDL-1 FC	0.9084	ns	0.848539	-2.497	ns	0.683523
VLDL-2 FC	4.088	ns	0.380476	-1.362	ns	0.826654
VLDL-3 FC	2.808	ns	0.551355	-1.476	ns	0.821312
VLDL-4 FC	4.129	ns	0.375592	5.562	ns	0.357851
VLDL-5 FC	5.409	ns	0.244224	8.286	ns	0.164910
VLDL-1 PL	1.652	ns	0.725609	-1.249	ns	0.844092
VLDL-2 PL	1.899	ns	0.685973	-2.611	ns	0.673333
VLDL-3 PL	2.767	ns	0.554074	-1.930	ns	0.763193
VLDL-4 PL	2.560	ns	0.584566	2.157	ns	0.734571
VLDL-5 PL	3.923	ns	0.400178	8.059	ns	0.178332
LDL-1 TG	2.147	ns	0.647169	1.249	ns	0.850736
LDL-2 TG	3.345	ns	0.473858	-2.724	ns	0.657704
LDL-3 TG	-1.115	ns	0.813873	-2.043	ns	0.741332
LDL-4 TG	0.8671	ns	0.855510	-1.135	ns	0.857038
LDL-5 TG	-3.386	ns	0.468395	-7.378	ns	0.219832
LDL-6 TG	-5.038	ns	0.280723	-11.24	ns	0.055220
LDL-1 Chol	0.000	ns	>0.999999	-4.881	ns	0.423879
LDL-2 Chol	-1.982	ns	0.673265	-4.881	ns	0.423812
LDL-3 Chol	-4.459	ns	0.340355	-5.789	ns	0.342231
LDL-4 Chol	-4.253	ns	0.360574	-3.859	ns	0.526319
LDL-5 Chol	-4.914	ns	0.290836	-7.605	ns	0.205376
LDL-6 Chol	-7.350	ns	0.112988	-12.15	*	0.036649
LDL-1 FC	-0.04129	ns	0.996457	-3.178	ns	0.603154
LDL-2 FC	0.000	ns	>0.999999	-5.449	ns	0.366684
LDL-3 FC	-3.510	ns	0.452081	-6.470	ns	0.282208
LDL-4 FC	-6.524	ns	0.159080	-6.016	ns	0.320874
LDL-5 FC	-5.038	ns	0.278686	-7.719	ns	0.195857
LDL-6 FC	-9.125	*	0.047267	-13.39	*	0.018878
LDL-1 PL	0.6607	ns	0.890531	-3.746	ns	0.541248
LDL-2 PL	-1.404	ns	0.769396	-3.746	ns	0.545527
LDL-3 PL	-4.748	ns	0.307548	-5.562	ns	0.360085
LDL-4 PL	-4.707	ns	0.311870	-4.200	ns	0.493286
LDL-5 PL	-4.955	ns	0.286771	-7.378	ns	0.219848
LDL-6 PL	-7.185	ns	0.121500	-12.83	*	0.026281

LDL-1 ApoB	-0.7020	ns	0.883165	-5.335	ns	0.382953
LDL-2 ApoB	-0.3303	ns	0.946910	-2.157	ns	0.729687
LDL-3 ApoB	-4.790	ns	0.303258	-5.789	ns	0.340188
LDL-4 ApoB	-3.551	ns	0.446482	-3.178	ns	0.601969
LDL-5 ApoB	-5.203	ns	0.265004	-7.605	ns	0.206859
LDL-6 ApoB	-6.607	ns	0.155191	-12.37	ns	0.032887
HDL-1 TG	2.890	ns	0.536545	-2.043	ns	0.739860
HDL-2 TG	2.932	ns	0.530701	2.157	ns	0.731583
HDL-3 TG	4.129	ns	0.375645	1.930	ns	0.760019
HDL-4 TG	4.914	ns	0.290640	1.703	ns	0.792119
HDL-1 Chol	-1.486	ns	0.752768	-6.924	ns	0.250835
HDL-2 Chol	-1.693	ns	0.718953	-8.286	ns	0.165093
HDL-3 Chol	0.4542	ns	0.925411	-5.789	ns	0.342291
HDL-4 Chol	-0.7845	ns	0.869465	-6.243	ns	0.302382
HDL-1 FC	0.04129	ns	0.996460	-5.449	ns	0.364451
HDL-2 FC	0.2890	ns	0.953954	-3.746	ns	0.539323
HDL-3 FC	-1.528	ns	0.745685	-7.265	ns	0.224869
HDL-4 FC	-2.973	ns	0.524858	-6.243	ns	0.300375
HDL-1 PL	-0.08258	ns	0.992914	-5.108	ns	0.404287
HDL-2 PL	0.4129	ns	0.936290	-4.200	ns	0.496031
HDL-3 PL	-0.1239	ns	0.981990	-6.016	ns	0.322977
HDL-4 PL	-0.7432	ns	0.879981	-6.243	ns	0.304342
HDL-1 ApoA1	1.363	ns	0.772785	-3.065	ns	0.620773
HDL-2 ApoA1	3.056	ns	0.516196	-6.243	ns	0.304342
HDL-3 ApoA1	1.610	ns	0.732002	-5.789	ns	0.342291
HDL-4 ApoA1	0.7432	ns	0.876817	-5.562	ns	0.360078
HDL-1 ApoA2	2.890	ns	0.536547	-4.200	ns	0.493452
HDL-2 ApoA2	0.5368	ns	0.911598	-6.470	ns	0.284516
HDL-3 ApoA2	-0.7020	ns	0.883481	-5.789	ns	0.340187
HDL-4 ApoA2	1.280	ns	0.786460	-7.151	ns	0.234992

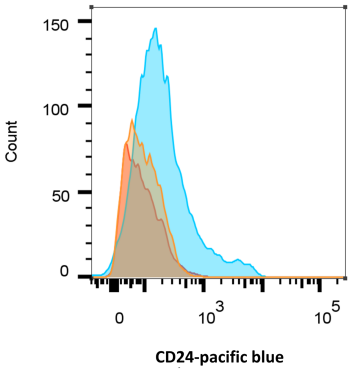

	Sample Name	Subset Name	Count
	Unstained	*cells*	*3924*
	Isotype Ctrl	*cells*	*3121*
	Stained	*cells*	*7881*

Figure 28. Flow cytometry of SI organoids. Cell suspension from B6 SI organoids was either stained with anti-mouse CD24 antibody- pacific blue or its isotype control.

7.2 Acknowledgment

Words cannot express my gratitude to Prof. Dr. Stefanie Derer for the useful comments, remarks, ideas and engagement that significantly improved this study. I owe her a lot for always being there when I needed her support, reviewing my progress constantly and guiding me through my PhD studies.

An immense thank you to Prof. Dr. Christian Sina for giving me the opportunity to work at the Institute of Nutritional medicine and for all the guidance, support and outstanding feedback.

I am deeply indebted to Prof. Dr. Senad Divanovic for his unwavering support throughout the last 4 years. It has been an amazing experience to work with his group in Cincinnati Children's Hospital. He and his group. Traci, Michelle, Maria, Jarren, Pablo and Kei made me feel at home from day one of my visit and still continue to give me their full endorsement whenever needed. I am also grateful to Prof. Dr. Jan Rupp for insightful ideas and fruitful discussions that greatly enhanced this project.

Every result described in this thesis was accomplished with the help and support of fellow lab mates. Maren Hicken, Heidi Schlichting, Annika Sünderhauf and Ann-Kathrin Brethack significantly contributed and assisted me at every stage of this research project. I have learned a lot from their experience with different laboratory methods. Thanks should also go to Daniel Margis, who assisted me with the *in vitro* assessment of AZA. I would like to extend my sincere thanks to Dr. Franziska Schmelter for sharing her NMR data with me and conducting metabolomic analysis. I am also grateful to Dr. Larissa Almeida for offering invaluable advice and support in flow cytometry. I would be remiss in not mentioning Lea Kubetzko, Annika Raschdorf, Dr. Anna Kordowski and Vivian Lelleck.

I want to give my deepest appreciation to Prof. Dr. Saleh Ibrahim and Dr. Misa Hirose for their unlimited support especially with mt-Atp8 mice. From University Hospital Regensburg. I would like to thank Dr. Hauke Tews and Dr. Patricia Mester for providing me with human biopsies which greatly enhanced this project.

Finally, I would like to acknowledge with gratitude Ülkü, my parents, Gouman and Gamal and my brother, Mohanad for their unhesitating support and encouragement through good times and bad times.

7.3 Publications

- Thiel A-L, **Ragab M**, Wagner AE, Divanovic S, Derer S and Sina C (2020) Purification and Functional Characterization of the Chloroform/Methanol-Soluble Protein 3 (CM3) From Triticum aestivum in Drosophila melanogaster. Front. Nutr. 7:607937. doi: 10.3389/fnut.2020.607937

- Sünderhauf. A., Hicken. M., Schlichting. H., Skibbe. K., **Ragab. M.**, Raschdorf. A., Hirose. M., Schäffler. H., Bokemeyer. A., Bettenworth. D., Savitt. A. G.. Perner. S., Ibrahim. S., Peerschke. E. I., Ghebrehiwet. B., Derer. S., & Sina. C. (2021). Loss of Mucosal p32/gC1qR/HABP1 Triggers Energy Deficiency and Impairs Goblet Cell Differentiation in Ulcerative Colitis. Cellular and molecular gastroenterology and hepatology. 12(1). 229–250. https://doi.org/10.1016/j.jcmgh.2021.01.017

- Skibbe. K., Brethack. A. K., Sünderhauf. A., **Ragab. M.**, Raschdorf. A., Hicken. M., Schlichting. H., Preira. J., Brandt. J., Castven. D., Föh. B., Pagel. R., Marquardt. J. U., Sina. C., & Derer. S. (2021). Colorectal Cancer Progression Is Potently Reduced by a Glucose-Free. High-Protein Diet: Comparison to Anti-EGFR Therapy. Cancers. 13(22). 5817. https://doi.org/10.3390/cancers13225817

- Link CWM, Rau CN, Udoye CC, **Ragab M**, Korkmaz RÜ, Comdühr S, Clauder A-K, Lindemann T, Frehse B, Hofmann K, Almeida LN, Laumonnier Y, Beidaq AE, Finkelman FD and Manz RA (2020) IL-2-Agonist-Induced IFN-γ Exacerbates Systemic Anaphylaxis in Food Allergen-Sensitized Mice. Front. Immunol. 11:596772. doi: 10.3389/fimmu.2020.596772

- Schmelter. F., Föh. B., Mallagaray. A., Rahmöller. J., Ehlers. M., Lehrian. S., von Kopylow. V., Künsting. I., Lixenfeld. A. S.. Martin. E., **Ragab. M.,** Meyer-Saraei. R., Kreutzmann. F., Eitel. I., Taube. S., Käding. N., Jantzen. E., Graf. T., Sina. C., & Günther. U. L. (2021). Metabolic and Lipidomic Markers Differentiate COVID-19 From Non-Hospitalized and Other Intensive Care Patients. Frontiers in molecular biosciences. 8. 737039. https://doi.org/10.3389/fmolb.2021.737039

7.4 Conference contributions

Poster presentations

01/2023 – CAOS: Conference on Advancements in Organoid Sciences. Hamburg. Germany. **Mohab Ragab**, Daniel Margis, Heidi Schlichting. Maren Hicken, Traci E Stankiewicz, Franziska Schmelter, Patricia Mester, Michelle Damen, Jarren Oates, Misa Hirose, Lea Kubetzko, Saleh Ibrahim, Hauke Tews. Senad Divanovic, Christian Sina and Stefanie Derer. Paneth cells and azathioprine in Crohn's disease: revisiting an old drug.

01/2018 – Falk Symposium: Liver-Gut-Microbiome Interactions. Hamburg. Germany. **Mohab Ragab**. Annika Sünderhauf, Kilian von Medem, Florian Bär, René Pagel, Axel Künstner, Christian Sadik, Stefanie Derer, Christian Sina. 12/15-Lipoxygenase deficient mice show exacerbated experimental colitis and alterations in epithelial proliferation

Oral presentations

07/2022 – Meeting of the German research foundation on inflammatory bowel diseases (DACED). Mainz. Germany. **Mohab Ragab**, Daniel Margis, Heidi Schlichting, Maren Hicken, Traci E Stankiewicz, Franziska Schmelter, Patricia Mester, Michelle Damen, Jarren Oates, Misa Hirose, Lea Kubetzko, Saleh Ibrahim. Hauke Tews, Senad Divanovic, Christian Sina and Stefanie Derer. Paneth cells and azathioprine: revisiting an old drug.

7.5 Curriculum vitae

MOHAB RAGAB

Augustenstr. 14a. 23564 Lübeck
+4917658630118
Mohab.Ragab@uksh.de

Date of birth 03/09/1990 **Place of birth** Alexandria, Egypt

Language skills Arabic (Native), English (Fluent), German (Advanced)

Education

Bachelor's degree of Medicine and Surgery (MBBCh) | Faculty of Medicine. Alexandria University. Egypt
2007 – 2014

Master's degree of Infection Biology (M.Sc.) | Lübeck University. Germany
2014 – 2017

Ph.D. thesis | Institute of Nutritional Medicine. UKSH-Lübeck. Germany
2018 – present

Research experience

Internship| Institute for Systemic Inflammation Research. Lübeck University. Germany
10/2015 – 12/2015
The Impact of IL-10 on Murine Monocyte Differentiation

Internship| Department of Microbiology and Infectious diseases. Lübeck University. Germany
01/2016 – 04/2016
The functional importance of CD177 on human neutrophils

M.Sc. Thesis | Lübeck Institute for Experimental Dermatology. Lübeck University. Germany
07/2016 – 03/2017
Prevalence of hepatitis C virus infection in Egyptian patients with rheumatoid arthritis

Graduate Student Researcher | Institute of Nutritional Medicine. UKSH-Lübeck. Germany
2018 – Present
The effect of azathioprine on the metabolic and functional characteristics of Paneth cells in Crohn`s disease patients

Visiting Researcher | Cincinnati Children's Hospital Medical Center. Cincinnati. USA
01/2022 – 04/2022

Skills

- 3D intestinal organoid culture
- 2D cell culture
- Induced Pluripotent Stem (iPS) cell culture
- *in vivo* colitis and obesity models
- ELISA
- Fruit flies model system
- qPCR
- Western Blotting
- Flow Cytometry
- Immunohistochemistry and immunofluorescence